

**UNIVERSITAT POLITÈCNICA DE VALÈNCIA**  
**DEPARTAMENTO DE MÁQUINAS Y MOTORES TÉRMICOS**



# **A CFD STUDY OF CAVITATION IN REAL SIZE DIESEL INJECTORS**

Thesis submitted for the fulfilment of the requirements  
of the “Universitat Politècnica de València” for the degree of  
Doctor of Philosophy

Presented by:  
**Stavroula PATOUNA**

Directed by:  
**Dr. Xandra MARGOT**

Valencia, February 2012



**UNIVERSITAT POLITÈCNICA DE VALÈNCIA**  
**DEPARTAMENTO DE MÁQUINAS Y MOTORES TÉRMICOS**



**A CFD STUDY OF CAVITATION IN  
REAL SIZE DIESEL INJECTORS**

**Para la obtención del grado de DOCTOR**

**Presentada por:**

**Stavroula PATOUNA**

**Dirigida por:**

**Dr. Xandra MARGOT**

**Valencia, Febrero 2012**



*Στους γονείς μου, Αθανασία & Βασίλειο, και στα αδέρφια μου, Αντρέα, Γιώργο και Ευθυμία.*

*Σας ευχαριστώ για την αγάπη σας και τη στήριξή σας!*



## **ABSTRACT**

In Diesel engines, the internal flow characteristics in the fuel injection nozzles, such as the turbulence level and distribution, the cavitation pattern and the velocity profile affect significantly the air-fuel mixture in the spray and subsequently the combustion process. Since the possibility to observe experimentally and measure the flow inside real size Diesel injectors is very limited, Computational Fluid Dynamics (CFD) calculations are generally used to obtain the relevant information.

The work presented within this thesis is focused on the study of cavitation in real size automotive injectors by using a commercial CFD code. It is divided in three major phases, each corresponding to a different complementary objective.

The first objective of the current work is to assess the ability of the cavitation model included in the CFD code to predict cavitating flow conditions. For this, the model is validated for an injector-like study case defined in the literature, and for which experimental data is available in different operating conditions, before and after the start of cavitation. Preliminary studies are performed to analyze the effects on the solution obtained of various numerical parameters of the cavitation model itself and of the solver, and to determine the adequate setup of the model. It may be concluded that overall the cavitation model is able to predict the onset and development of cavitation accurately. Indeed, there is satisfactory agreement between the experimental data of injection rate and choked flow conditions and the corresponding numerical solution.

This study serves as the basis for the physical and numerical understanding of the problem.

Next, using the model configuration obtained from the previous study, unsteady flow calculations are performed for real-size single and multi-hole sac type Diesel injectors, each one with two types of nozzles, tapered and cylindrical. The objective is to validate the model with real automotive cases and to understand in what way some physical factors, such as geometry, operating conditions and needle position affect the inception of cavitation and its development in the nozzle holes. These calculations are made at full needle lift and for various values of injection pressure and back-pressure. The results obtained for injection rate, momentum flux and effective injection velocity at the exit of the nozzles are compared with available CMT-Motores Térmicos in-house experimental data. Also, the cavitation pattern inside the nozzle and its effect on the internal nozzle flow is analyzed. The model predicts with reasonable accuracy the effects of geometry and operating conditions.

Finally, the onset and development of the cavitating flow and its effect on the internal flow and at the nozzle exit of the real size Diesel injectors is studied in relation with the needle movement and position. For this, two types of calculations are performed to analyze the flow during the unsteady regime, some with fixed meshes at various needle lift positions, and others with a moving mesh to simulate the needle aperture and closure motion. The objective is to determine the validity of using one approach or the other to predict the features of the flow during the needle movement phase, especially at the nozzle exit. The methodology developed to fully automate the three-dimensional mesh generation and its motion is explained in detail. The differences in the predicted solutions obtained with the fully transient (moving

mesh) and the pseudo-steady (fixed meshes) simulations are analyzed and the cavitation process characterized during the whole transient of the injection, inside the nozzle and at the exit. It is concluded that the modeling approach chosen may be critical for the prediction of nozzle exit flow conditions, especially if there is cavitation. The calculations with moving mesh boundaries, though slower and more complex, provide valuable information about the transient phase of injection that may not be neglected, especially at low needle lift.



## RESUMEN

Para los motores Diesel, las características del flujo interno en las toberas de los inyectores, tales como el nivel y la distribución de la turbulencia, el nivel de cavitación y el perfil de velocidad, afectan de manera significativa a la mezcla de aire-combustible en los chorros y, por lo tanto, al proceso de la combustión. Puesto que la capacidad de observar experimentalmente y de medir el flujo en el interior de los inyectores Diesel de tamaño real es muy limitada, los cálculos CFD (dinámica de fluidos computacional) se utilizan generalmente para obtener la información relevante.

El trabajo presentado en esta tesis está enfocado al estudio de la cavitación en inyectores reales de automoción, mediante un código comercial CFD. Está dividido en tres fases principales, cada una con un objetivo definido y complementario.

El primer objetivo en este trabajo es evaluar la capacidad de predicción del modelo de cavitación integrado en el código CFD. Para ello, se valida el modelo para un caso de estudio académico bajo distintas condiciones de funcionamiento, con y sin cavitación, comparando con datos experimentales documentados en la bibliografía. En los estudios preliminares llevados a cabo, se prueban diferentes configuraciones numéricas referentes al modelo de cavitación y se estudia su influencia en la solución para determinar la configuración más adecuada. En general, se concluye que el modelo es capaz de predecir el inicio de la cavitación y su desarrollo. Los valores obtenidos de gasto másico y de flujo estrangulado muestran una coincidencia

satisfactoria con los resultados experimentales. Este estudio preliminar sirve de base para la comprensión física y numérica del problema.

Posteriormente, y utilizando la configuración numérica más adecuada obtenida del estudio previo, se procede a realizar cálculos en condiciones no estacionarias para unos inyectores reales mono-orificio y multi-orificio, cada uno con dos tipos de tobera, cilíndrica y cónica. El objetivo es validar el modelo para casos reales de automoción y comprender qué factores físicos, como geometría, condiciones de funcionamiento y levantamiento de aguja, condicionan la formación de la cavitación y su evolución en la tobera. Estos cálculos se hacen a pleno levantamiento de aguja para distintas presiones de inyección y de contra-presión. Los resultados obtenidos de gasto másico, cantidad de movimiento y velocidad efectiva a la salida de las toberas se comparan con datos experimentales disponibles en el grupo de investigación en el que se realiza esta tesis (CMT-Motores Térmicos). Se analiza asimismo la distribución de la cavitación y su efecto en el flujo interno de estos inyectores. Los resultados obtenidos de estos cálculos muestran que se predice bien el efecto de la geometría y de las condiciones de funcionamiento.

En una tercera etapa, el inicio y el desarrollo de la cavitación y su efecto sobre el flujo interno y a la salida de las toberas de tamaño real se estudian en relación con el movimiento y posición de la aguja. Para ello, se efectúan dos tipos de cálculos a fin de analizar el flujo durante el régimen transitorio, unos con mallas fijas a distintos levantamientos de aguja y otros con malla móvil para simular el movimiento de apertura y cierre de la aguja. El objetivo es determinar la validez de uso de ambos métodos para predecir las características del flujo durante el movimiento de la aguja, en particular a la salida de las toberas. Se explica con detalle la metodología desarrollada para

automatizar la generación tridimensional de la malla y su movimiento. Por último, se analizan las diferencias obtenidas en la solución del cálculo transitorio (malla móvil) con el pseudo-estacionario (mallas fijas) y se caracteriza el proceso de cavitación durante toda la fase transitoria de inyección, tanto en el interior de las toberas, como a la salida de las mismas. Se concluye que la decisión de modelar de una u otra manera puede ser crítica para la predicción de las condiciones a la salida de la tobera, especialmente cuando hay presencia de cavitación. El cálculo con malla móvil, aunque bastante más lento y complejo, permite obtener una descripción más detallada y completa del flujo, en particular en las posiciones de bajo levantamiento de la aguja.



## RESUM

Per al motors Diesel, les característiques del flux intern, tals com el nivell i la distribució de la turbulència, el nivell de cavitació i el perfil de velocitat, afecten de manera significativa la barreja d'aire-combustible en els dolls i, per tant, al procés de la combustió. Com que la capacitat experimental d'observar i de mesurar el flux a l'interior dels injectors Diesel de grandària real és molt limitada, els càlculs CDF (dinàmica dels fluids computacional) s'utilitzen generalment per tal d'obtenir la informació rellevant.

El treball presentat en aquesta tesi està enfocat a l'estudi de la cavitació en injectors reals d'automoció, mitjançant un codi comercial CDF, y està dividit en tres fases principals, cada una de elles te un objectiu definit y complementari als altres objectius.

El primer objectiu és avaluar la capacitat de predicció del model de cavitació integrat en el codi CFD. Per a fer-ho, es valida el model per un cas d'estudi acadèmic a distintes condicions de funcionament, amb y sense cavitació, utilitzant dades experimentals documentades en la bibliografia. Als estudis preliminars portats a terme, es proven diferents configuracions numèriques referents al model de cavitació i s'estudia la seua influència a la solució per a determinar la configuració més adequada. Generalment es conclou que el model es és capaç de predir l'inici de la cavitació i el seu desenvolupament. Els valors obtinguts de gast màsic, i de flux estrangulat mostren una coincidència satisfactòria amb resultats experimentals. Aquest estudi preliminar servix de base per la comprensió física i numèrica del problema.

Posteriorment, i utilitzant la configuració numèrica més adequada a l'estudi previ, es procedix a realitzar càlculs estacionaris per a uns injectors reals mono-orifici i multi-orifici, cadascú amb dos tipus de tobera, cilíndrica i cònica. L'objectiu és validar el model per a casos reals que es presenten en automoció i comprendre quins factors físics com la geometria, condicions de funcionament i alçament d'agulla condicionen la formació de la cavitació i la seua evolució en la tobera. Aquests càlculs es fan a ple alçament d'agulla per a diferents pressions d'injecció i de contrapressió. Els resultats obtinguts del gast màsic, quantitat de moviment i velocitat efectiva a l'eixida de les toberes es comparen amb dades experimentals disponibles en el grup d'investigació en el que es realitza la tesi (CMT-Motores Térmicos). S'analitza també la distribució de la cavitació i el seu efecte al flux intern d'aquests injectors. Els resultats obtinguts d'aquests càlculs mostren que es prediu bé l'efecte de la geometria i de les condicions de funcionament.

Per últim, el inici i el desenvolupament de la cavitació i el seu efecte sobre el flux intern i l'eixida dels injectors Diesel de grandària real s'estudien en relació amb el moviment i posició de l'agulla. Així, s'efectuen dos tipus de càlculs per tal d'anilitzar el flux durant el règim transitori, uns amb xarxes fixes a diferents alçaments d'agulla i altres, amb malla mòvil per tal de simular el moviment d'apertura i tancament de l'agulla. L'objectiu és determinar la validesa d'ús d'ambdós mètodes per a predir les característiques del flux durant el moviment transitori de l'agulla, en particular a l'eixida de les toberes. S'explica detalladament la metodologia desenvolupada per tal d'automatitzar la generació tridimensional de la malla i el seu moviment. Per últim, s'analitzen les diferències en la solució del càlcul transitori (malla mòvil) amb el pseudo-estacionari (malles fixes) i es caracteritza el procés de cavitació durant tota la fase transitòria d'injecció, tant en l'interior de les toberes, com a l'eixida de les mateixes. Es conclou

que la decisió de modelar d'una o d'una altra forma pot ser crítica per la predicció de les condicions a l'eixida de la tobera, especialment quan hi ha presència de cavitació. El càlcul amb malla mòvil, encara que prou més lent i complex, permet obtindre una descripció més detallada i completa del flux, particularment a les posicions en las que la agulla es trova a menuts alçaments.



## **ACKNOWLEDGEMENTS**

Firstly, I would like to thank my thesis advisor, Ms. Xandra Margot (PhD), whose encouragement, guidance and invaluable support from the initial to the final level enabled me to develop an understanding of the subject. Furthermore, I am very grateful that she provided the funding and also both freedom and assistance needed to pursue this research work. I would like to thank her also for her patience and understanding during my introduction to the CFD “word”.

I am greatly indebted also to Dr. Sergio Hoyas for his support, especially when many computer problems persisted as well as for his precious indications related with computational resources and other technical equipment.

I would also like to thank Prof. Jean Arrégle and Mr. Oscar de la Garza, for various interesting discussions on the experimental research and on many topics of my interest related with the model validation.

Additionally, I would like to acknowledge the financial support of the CMT-Motores Térmicos. Part of this work has been supported by the Department of Automotive Advanced Technologies of Renault, in the framework of the PREDIT research programme “EMPhASE”.

I would like to thank Dr. Antonio Gil and Dr. Jose Manuel Pastor for their indications on the use of various software applications.

I owe my deepest and sincere gratitude to Mr. Rémi Roussel and Mr. David de Haro Vazquez for their contribution on the CFD simulation during their stage in CMT-Motores Térmicos.

I am indebted to my many student colleagues from the research groups at CMT-Motores Térmicos for providing a stimulating and fun environment in which to learn and grow, as well as assistant in numerous ways: Ms. Mariany Chavez, Mr. Juan Manuel Mompó, Mr. Pablo Fajardo, Mr. Dung Ahn Khuong, Mr. Roberto Navarro Garcia, Mr. Pau Raga Nieto, Mr. Derek Kilian, Mr. Juan Martin, Mr. Michele Bardi.

I would also like to express my appreciation to my family who has encouraged me throughout this project.

Stavroula PATOUNA

February 2012

## **TABLE OF CONTENTS**

<b>ABSTRACT .....</b>	<b>7</b>
<b>RESUMEN .....</b>	<b>11</b>
<b>RESUM .....</b>	<b>15</b>
<b>ACKNOWLEDGEMENTS.....</b>	<b>19</b>
<b>TABLE OF CONTENTS.....</b>	<b>21</b>
<b>LIST OF FIGURES .....</b>	<b>25</b>
<b>LIST OF TABLES .....</b>	<b>33</b>
<b>NOMENCLATURE.....</b>	<b>35</b>
<b>CHAPTER 1. INTRODUCTION .....</b>	<b>37</b>
<b>1.1 Motivation.....</b>	<b>37</b>
<b>1.2 Present Contribution and Objectives.....</b>	<b>39</b>
<b>1.3 Thesis Outline .....</b>	<b>42</b>
<b>CHAPTER 2. LITERATURE SURVEY .....</b>	<b>45</b>
<b>2.1 Introduction .....</b>	<b>45</b>

<b>2.2</b>	<b>Experimental Observations in Cavitating Nozzles.....</b>	<b>46</b>
<b>2.3</b>	<b>Cavitation-Modelling Approaches and Validation .....</b>	<b>67</b>
2.3.1	Barotropic equation approach .....	69
2.3.2	Bubbly mixture approach .....	74
<b>2.4</b>	<b>Studies taking into account needle displacement.....</b>	<b>87</b>
<b>2.5</b>	<b>Summary.....</b>	<b>95</b>
 <b>CHAPTER 3. RESEARCH TOOLS.....</b>		<b>99</b>
<b>3.1</b>	<b>Introduction.....</b>	<b>99</b>
<b>3.2</b>	<b>Numerical Models.....</b>	<b>99</b>
3.2.1	Governing equations for fluid flow .....	100
3.2.2	Equations of moving mesh operations .....	100
3.2.3	Turbulence equations .....	101
3.2.4	Cavitation modelling.....	103
<b>3.3</b>	<b>Experimental Facilities.....</b>	<b>105</b>
3.3.1	Experimental apparatus and operating conditions .....	105
3.3.2	Internal geometry characterization .....	107
<b>3.4</b>	<b>Summary.....</b>	<b>110</b>
 <b>CHAPTER 4. VALIDATION OF THE CAVITATION MODEL WITH AN ACADEMIC STUDY .....</b>		<b>111</b>
<b>4.1</b>	<b>Introduction.....</b>	<b>111</b>
<b>4.2</b>	<b>Computational Domain and Grid Independence Results.....</b>	<b>112</b>
<b>4.3</b>	<b>Turbulence Modelling Study.....</b>	<b>114</b>

<b>4.4</b>	<b>Set-up of Numerical Method</b> .....	<b>117</b>
<b>4.5</b>	<b>Validation Results</b> .....	<b>119</b>
4.5.1	Injection rate results.....	120
4.5.2	Velocity profiles .....	122
4.5.3	Pressure profiles and fields .....	124
<b>4.6</b>	<b>Further Analysis of the Predicted Flow Field Results</b> .....	<b>126</b>
<b>4.7</b>	<b>Summary</b> .....	<b>128</b>
	<b>CHAPTER 5. CAVITATION IN REAL SIZE INJECTORS AT FULL NEEDLE LIFT</b> .....	<b>131</b>
<b>5.1</b>	<b>Introduction</b> .....	<b>131</b>
<b>5.2</b>	<b>Investigated Computational Domains</b> .....	<b>132</b>
<b>5.3</b>	<b>Nozzle flow characterization</b> .....	<b>134</b>
<b>5.4</b>	<b>Validation results</b> .....	<b>135</b>
<b>5.5</b>	<b>Analysis of the Flow Cavitation Pattern</b> .....	<b>141</b>
5.5.1	Predicted flow in single-hole Diesel injectors.....	141
5.5.2	Predicted flow in multi-hole Diesel injectors.....	146
<b>5.6</b>	<b>Summary</b> .....	<b>155</b>
	<b>CHAPTER 6. EFFECT OF THE NEEDLE MOVEMENT ON THE NOZZLE FLOW</b> .....	<b>157</b>
<b>6.1</b>	<b>Introduction</b> .....	<b>157</b>
<b>6.2</b>	<b>Moving mesh strategy</b> .....	<b>157</b>

<b>6.3</b>	<b>Results obtained by Moving Needle Simulations .....</b>	<b>166</b>
6.3.1	Predicted flow in single-hole Diesel injectors .....	166
6.3.2	Predicted flow of multi-hole Diesel injectors.....	174
<b>6.4</b>	<b>Summary.....</b>	<b>188</b>
<b>CHAPTER 7. COMPARATIVE STUDY OF QUASI-STEADY AND MOVING MESH SIMULATIONS .....</b>		<b>193</b>
<b>7.1</b>	<b>Introduction.....</b>	<b>193</b>
<b>7.2</b>	<b>Fixed needle lift strategy .....</b>	<b>194</b>
<b>7.3</b>	<b>Results obtained by Fixed Needle Lift Simulations.....</b>	<b>195</b>
7.3.1	Predicted flow of multi-hole Diesel injectors (symmetry of the injector)....	195
7.3.2	Predicted flow of multi-hole Diesel injectors (whole injector).....	217
<b>7.4</b>	<b>Comparative Analysis of the Cavitating Flow with Fixed and Moving Needle Lift Simulations .....</b>	<b>228</b>
7.4.1	Comparative study of internal flow distribution .....	229
7.4.2	Comparative study of nozzle exit characteristics.....	233
<b>7.5</b>	<b>Summary.....</b>	<b>243</b>
<b>CHAPTER 8. CONCLUSIONS &amp; RECOMMENDATIONS FOR FUTURE WORK .....</b>		<b>247</b>
<b>8.1</b>	<b>Overview .....</b>	<b>247</b>
<b>8.2</b>	<b>Conclusions.....</b>	<b>248</b>
<b>8.3</b>	<b>Recommendations .....</b>	<b>255</b>
 <b>REFERENCES .....</b>		<b>257</b>

## LIST OF FIGURES

Figure 3.1: Configuration of the a) single-hole and b) multi-hole sac-type nozzle. ....	108
Figure 3.2: Silicone moulds characterization of the multi-hole nozzle.....	108
Figure 3.3: Sketch of the multi hole nozzle with main geometric parameters. ....	109
Figure 4.1: Geometry of computation domain and boundary conditions.....	112
Figure 4.2: Visualization of mesh distribution. ....	113
Figure 4.3: Refined locations by a) pressure, b) velocity magnitude. ....	113
Figure 4.4: Predicted velocity profiles obtained with different turbulence models in position v1 and v2 a) at condition without cavitation ( $\Delta p=41$ bar) and b) at choked flow conditions ( $\Delta p=85$ bar). ....	116
Figure 4.5: Injection rate and minimum pressure as a function of nucleus number density ( $\Delta p=85$ bar). ....	119
Figure 4.6: Experimental data from Winklhofer et al. (2001) and predicted injection rate plotted versus the pressure difference, where CC critical conditions. ....	120
Figure 4.7: Volume fraction of vapour distribution with different fluid properties at longitudinal middle plane, $\Delta p=85$ bar. ....	121
Figure 4.8: Predicted volume fraction of vapour fields around critical cavitation at longitudinal middle plane. ....	122
Figure 4.9: Velocity profiles in position v1 and v2 at condition without cavitation ( $\Delta p=41$ bar), with moderate cavitation ( $\Delta p=70$ bar) and at choked flow conditions ( $\Delta p=85$ bar). ....	123

Figure 4.10: a) Pressure distribution (bar) at non cavitating conditions ( $\Delta p=58$ bar), and b) at CC ( $\Delta p=69$ bar).....	125
Figure 4.11: Predicted and experimental pressure profiles at CC conditions. ....	126
Figure 4.12: Velocity magnitude (m/s) and b) volume fraction of vapour fields in perpendicular planes to the flow direction.....	126
Figure 4.13: Distribution of cavitation field obtained by the different turbulence models. ....	127
Figure 5.1: Computational mesh of the single-hole and multi-hole nozzle for the internal flow calculation. ....	133
Figure 5.2: Comparison between experimental and CFD results of flow coefficients for the cylindrical single-hole nozzle (+ Experimental, $\times$ CFD). ....	136
Figure 5.3: Comparison between experimental and CFD results of flow coefficients for the cylindrical multi-hole nozzle (+ Experimental, $\times$ CFD)...	137
Figure 5.4: Effect of pressure drop on discharge and momentum coefficient for single-hole and multi-hole nozzle with a) tapered and b) cylindrical orifices (+ Experimental, $\times$ CFD). ....	140
Figure 5.5: Representative a) volume fraction of vapour and b) velocity field images for different levels of pressure and KN (cylindrical nozzle). Colour scale: volume fraction of vapour: 0-1, velocity magnitude (m/s): 0-300 for $\Delta p=300$ bar, 0-400 for $\Delta p=700$ bar, 0-700 for $\Delta p=1400$ bar. ....	142
Figure 5.6: Volume fraction of vapour distribution with different mesh resolutions.....	143
Figure 5.7: Representative a) volume fraction of vapour and b) velocity images for different level of pressures and KN (tapered nozzle). Colour scale: volume fraction of vapour: 0-1, velocity magnitude (m/s): 0-300 for $\Delta p=300$ bar, 0-400 for $\Delta p=700$ bar, 0-700 for $\Delta p=1400$ bar.....	144

Figure 5.8: Density and axial velocity profiles at the exit of the cylindrical and tapered single hole nozzle for different pressure levels. The legend symbols are the same in all graphs.....	146
Figure 5.9: Representative volume fraction of vapour images of the cylindrical nozzle for different levels of pressure and KN (colour scale: 0-0.5 for the multiple cross-section cuts; 0-1 for the vertical cuts). .....	148
Figure 5.10: Hole outlet measurement locations for the density and velocity profiles.....	149
Figure 5.11: Density profiles at the exit of the cylindrical nozzle for different pressure levels .....	150
Figure 5.12: Density profiles at the exit of the tapered nozzle (the legend for top and bottom figures is the same). .....	151
Figure 5.13: a) Volume fraction and b) velocity distribution in the cylindrical and tapered nozzles (colour scale: 0-1 for the volume fraction of vapour; 0-580 m/s for the velocity magnitude). .....	152
Figure 5.14: Axial velocity profiles at the exit of the tapered and the cylindrical nozzles for different levels of pressure and KN (the legend for the right hand side figures is the same as for the left hand side). .....	154
Figure 6.1: a) Needle at full lift, b) Needle at a low lift. ....	158
Figure 6.2: a) Initial domain at 10 $\mu\text{m}$ needle lift, b) vertices defining the contour; in squares the vertices subject to motion c) patches defined for mesh generation, d) full needle lift mesh after extrusion.....	159
Figure 6.3: Meshes of the moving part obtained by the extrude facility. ....	160
Figure 6.4: Images of the mesh used for the calculation a) general view at full lift, b) close-up at the hole entrance visualizing the coarse (moving) and fine (fixed) region mesh at low and high needle lifts. ....	161
Figure 6.5: Different mesh resolutions (vertical $\times$ horizontal layers) used for the moving mesh part. ....	162

Figure 6.6: Injection rate evolution with different mesh fineness (multi-hole nozzle). .....	162
Figure 6.7: a) Mass flow interpolation between experimental and computational results at fixed needle lifts b) Interpolated points and lift law considered for the calculations versus time. c) CFD Injected mass flow and lift law considered, d) Comparison between CFD and experimental injected mass flow. ....	165
Figure 6.8: Representative images of volume fraction of vapour, velocity magnitude and TKE from top to bottom for a) tapered and b) cylindrical nozzle hole at fully opened needle lift. Color scale: fraction of vapour: 0-1, velocity magnitude (m/s): 0-600, TKE(m <sup>2</sup> /s <sup>2</sup> ): 0-5000. ....	168
Figure 6.9: Predicted volume fraction of vapor field at different needle lifts during the needle valve opening and closing. ....	169
Figure 6.10: Temporal sequence of volume fraction of vapour showing the exit of cavitation cloud at needle closing for the cylindrical nozzle. ....	170
Figure 6.11: Instantaneous results of injection rate, mean velocity, TKE, and volume fraction of vapour at the exit of the nozzle during the simulated injection process. ....	174
Figure 6.12: Sequence of images of predicted cavitation field for the tapered nozzle at 1500/10 bar and very low lifts (about 15 μm). ....	175
Figure 6.13: Predicted cavitation field at different needle lifts for the tapered nozzle during the needle valve opening and closing (1500/50 bar). ....	176
Figure 6.14: Predicted cavitation field at different needle lifts for the cylindrical nozzle during the needle valve opening and closing (1500/50 bar). ....	177
Figure 6.15: Location of nozzle cross-section considered for post-processing in this study. ....	178
Figure 6.16: Instantaneous results of multi-hole nozzle at different section along the nozzle hole for a) cylindrical and b) tapered nozzle (800/50 bar). ....	179

Figure 6.17: Streamlines of the internal flow of a) cylindrical and b) tapered nozzle at low and high lifts (1500/50 bar).....	180
Figure 6.18: Lift curve and % exit area occupied with some vapour (volume fraction of vapour between 0.06 and 1 considered) as a function of time for the cylindrical nozzle.....	181
Figure 6.19: Temporal sequence of volume fraction of vapour showing the exit of cavitation cloud at needle closing for the cylindrical nozzle (1500/10 bar).....	182
Figure 6.20: Instantaneous results of average TKE and volume fraction of vapour at the exit of the cylindrical nozzle.....	185
Figure 6.21: Axial profiles at the examined lifts along a vertical and a horizontal edge for the cylindrical nozzle during the needle opening and closing (1500/50 bar, lifts: 25, 50, 75, 100, 200, 250 $\mu\text{m}$ ).....	187
Figure 6.22: Axial profiles at the examined lifts along a vertical and a horizontal edge for the tapered nozzle during the needle opening and closing (1500/50 bar, lifts: 25, 50, 75, 100, 200, 250 $\mu\text{m}$ ).....	188
Figure 7.1: Injection rate results as a function of lift for the cylindrical and the tapered nozzles in the investigated operating conditions. ....	196
Figure 7.2: Evolution of $C_d$ in function of pressure drop at different needle lifts for a) tapered and b) cylindrical nozzle. ....	197
Figure 7.3: Representative images of volume fraction of vapour of tapered multi-hole nozzles at different needle positions at a) 1500/10 bar, b) 800/10 bar. ....	199
Figure 7.4: Representative images of volume fraction of vapour of cylindrical multi-hole nozzles at different needle positions (1500/10 bar). Same color scale as in Figure 7.3.....	200
Figure 7.5: Representative images of volume fraction of vapour of cylindrical multi-hole nozzles at different needle lifts and operating conditions. ....	201

Figure 7.6: Injection rate as a function of time at 25 $\mu\text{m}$ needle lift, in crosses time instances at which the flow field examined (800/10 bar). .....	202
Figure 7.7: a) volume fraction of vapour and the corresponding b) velocity magnitude fields at different time instances. ....	203
Figure 7.8: Representative images of velocity magnitude of tapered and cylindrical multi-hole nozzles at different needle positions (1500/10 bar)....	205
Figure 7.9: Representative axial velocity profiles of all lifts along the central horizontal and vertical edges for a) the cylindrical nozzle and b) the tapered nozzle (1500/50 bar). ....	207
Figure 7.10: Outlet velocity evolution (area averaged values) as a function of lift for the cylindrical and the tapered nozzles in the investigated operating conditions.....	208
Figure 7.11: Representative images of TKE of tapered and cylindrical multi-hole nozzles at different needle positions (1500/10 bar).....	210
Figure 7.12: Turbulent kinetic energy and turbulent kinetic energy coefficients for the tapered and the cylindrical nozzle. ....	212
Figure 7.13: Rate of change of velocity and TKE in function of lift at the exit of the nozzles.....	214
Figure 7.14: Location of nozzle hole considered for post-processing in this study. ....	215
Figure 7.15: Volume fraction of vapour, TKE, and velocity along the nozzle hole in different lifts (800/50 bar). ....	217
Figure 7.16: Image of the mesh used for the calculations at full lift.....	219
Figure 7.17: Iso-surfaces of volume fraction of vapour in cylindrical and tapered nozzles at low and high needle lift. ....	220
Figure 7.18: Cavitation pattern at a vertical cut for two different times, (cylindrical nozzle, 25 $\mu\text{m}$ needle lift).....	222
Figure 7.19: Injection rate fluctuation in opposite holes (same scale was used in the vertical axis). ....	222

Figure 7.20: Particle tracks of cylindrical and tapered nozzles at low and high needle lift. ....	223
Figure 7.21: Particle tracks at two different instants of the “quasi-steady state” solution. ....	225
Figure 7.22: Variation of the injection rate between the various injection holes at different needle positions for the two series of calculations. ....	227
Figure 7.23: Comparative view of TKE ( $m^2/s^2$ ) at different needle lifts for fixed and transient needle lift analyses, 1500/50 bar (the colour scale is the same in both calculation methods of each lift). ....	231
Figure 7.24: Comparative view of volume fraction of vapour at different needle lifts for fixed and transient needle lift analyses, 1500/50 bar (colour scale: 0-1). ....	232
Figure 7.25: Average instantaneous TKE and volume fraction of vapour at the exit of the nozzle (1500/50 bar), calculated with moving mesh.....	233
Figure 7.26: a) Injection rate at the exit of the nozzle obtained and b) average volume fraction of vapour with different needle lift laws, 1500/50 bar.....	235
Figure 7.27: TKE at different lifts with fixed and moving mesh calculations at 800/50 and 1500/50 bar for a) cylindrical and b) tapered nozzle. ....	237
Figure 7.28: Percentage of area occupied by vapour at the nozzle exit as a function of lift with fixed and moving mesh calculations for different operating conditions. ....	239
Figure 7.29: Injection rate at different lifts with fixed and moving mesh calculations at 800/50 and 1500/50 bar for cylindrical nozzle.....	240
Figure 7.30: Comparison of axial velocity profiles at the exit of the nozzles along a vertical edge obtained by fixed and moving mesh calculations at 25 and 250 $\mu m$ lift. ....	241
Figure 7.31: Comparison of axial velocity profiles at the exit of the nozzles along a horizontal edge obtained by fixed and moving mesh calculations at 25 and 250 $\mu m$ lift. ....	242



## LIST OF TABLES

Table 3.1: Operating conditions investigated at fully opened needle.....	107
Table 3.2: Operating conditions investigated at different needle positions with fixed and moving mesh calculations .....	107
Table 3.3: Dimensions of the cylindrical and tapered single hole-nozzle....	109
Table 3.4: Dimensions of the six holes of the cylindrical and tapered multi hole-nozzle.....	110
Table 4.1: Injection rate results (g/s) obtained for different mesh resolutions. ....	114
Table 4.2: Reference configuration (highlighted) used as basis for parameters variation study and definition of parameters varied: turbulence model, time step, solution algorithm, seed radius, nucleus number.....	115
Table 4.3: a) Fluid properties used for the calculations, b) Fluid properties tested (Peng Kärrholm et al., 2007). ....	117
Table 4.4: Considered combinations of discretization schemes and corresponding injection rate results (UD-upwind differencing-1 <sup>st</sup> order, CD-Central Differencing-2 <sup>nd</sup> order, MARS-Monotone Advection and Reconstruction Scheme-2 <sup>nd</sup> order).....	118
Table 5.1: Cylindrical and tapered nozzle dimensions. ....	132
Table 5.2: Injection rate results for different meshes for cylindrical nozzle (310/10 bar).....	133
Table 5.3: Operating conditions investigated at fully opened needle.....	135
Table 7.1: Cylindrical and tapered nozzle dimensions. ....	209
Table 7.2: Dimensional characterization for cylindrical and tapered nozzle holes.....	218



## NOMENCLATURE

---

CCD	Charge coupled device
CFD	Computational fluid dynamics
$D_i$	Average diameter in the entrance of the orifice
$D_m$	Average diameter in the middle of the orifice
$D_o$	Average diameter in the outlet of the orifice
HEM	Homogeneous Equilibrium Mixture
$L$	Orifice nozzle length
LES	Large eddy simulation
$P_{inj}$	Injection pressure
$P_{back}$	Discharge pressure
$P_{vapor}$	Vapor pressure
$R_a$	Mean upper radius of the nozzle
$R_b$	Mean bottom radius of the nozzle
SMD	Sauter mean diameter
TKE	Turbulent kinetic energy
VCO	Valve covering orifice
VOF	Volume of fluid

---



# CHAPTER 1.

## INTRODUCTION

### 1.1 Motivation

When a liquid is subjected to a pressure below its saturation value at a given temperature, it begins to evaporate. This phenomenon is called 'cavitation' or 'cold boiling', as opposed to boiling due to supplying heat at constant pressure. In the absence of a free surface, the evaporation (and subsequent condensation if the fluid reaches a zone of pressure above the saturation level) can only take place if some kind of seed (or nucleus) is present. While pure liquids can sustain relatively high tensile stresses, almost all commonly encountered liquids in engineering and environmental applications contain some impurities (solid particles or bubbles of dissolved gas) which can act as seeds for cavitation and therefore start the evaporation at saturation pressure.

Cavitation is a phenomenon encountered mainly in liquid pumps and turbines, injection nozzles, throttles, pipes and channels with obstacles, ship propellers. It is also encountered in biology and even in the surrounding nature [1]. In most cases cavitation is undesirable, as it causes performance loss, material damage, vibrations and noise [1, 2]. On the contrary, in engine fuel injection systems, and particularly in Diesel injectors, it is expected that nozzle cavitation will enhance jet turbulence, which in turn will promote fuel

atomization [3, 4]. This is because cavitation, which is known to affect the velocity profiles and the turbulence level, influences the primary break-up of the liquid fuel jet. In addition, the presence of cavitation at the holes exit is expected to favour fuel atomization due to the generation of smaller droplets which vaporise more rapidly, thus enhancing the air-fuel mixture. Especially in the case of common rail injection systems which are designed to operate at very high pressures (up to 1400 bar), the small dimensions of the nozzle holes can lead to extremely high flow velocities of the liquid fuel inside the holes (exceeding 400 m/s). This fact encourages the different cavitation patterns to extend towards the hole exit where they influence the formation of the emerging spray. The improved spray atomization leads to a better combustion process, lower fuel consumption and reduced exhaust gas and particulate emissions. On the other hand, cavitation may be associated with hole-to-hole and cycle-to-cycle spray variations in multi-hole injectors although evidence about this is rather limited [5]. The latter represents an undesirable feature, since it may create spray instabilities. Cavitation can also decrease the flow efficiency (discharge coefficient) due to its effect on the exiting jet, by partially blocking the nozzle exit. Also, the implosion of cavitation bubbles inside the orifice can cause material erosion, thus decreasing the life and performance of the injector. Clearly an optimum amount of cavitation is desirable, and it is important to understand the causes for cavitation generation and development for more efficient automotive nozzle designs. Cavitation inception may be due to “geometric” and “dynamic” factors [6]. Geometric parameters include the type of orifice (valve covered orifice-VCO, sac type), hole entrance curvature, orifice length, ratio of inlet to outlet orifice diameter (taper), and surface roughness. Dynamic parameters can include the imposed pressure gradient, injector needle lift, and needle eccentricity.

## 1.2 Present Contribution and Objectives

In the above context, injector nozzles have a significant effect on the delivery and atomisation of fuel in Diesel automotive engines and the detailed knowledge of the internal flow and cavitation characteristics becomes a prerequisite for the improvement of Diesel engines. However, the small scale of the nozzles and high speed of the fuel injection make direct observation difficult. In fact, the large majority of experimental studies reported refer to scaled-up nozzles [7, 8, 9] although it is recognised that these experiments may not be fully representative of the real size nozzle geometries. Furthermore, the presence of cavitation adds another level of complexity to the problem [10]. As cavitation influences the spray process, its existence, increases uncertainty about the conditions at the nozzle exit. For this reason, cavitation has dominated numerous studies as the key phenomenon connecting internal flow and spray behaviour [11, 12].

The main objective of the present study is to investigate the internal flow and cavitation phenomenon inside real size automotive injectors and to examine its effect on the nozzle exit flow. Because of the difficulties associated with flow measurements and visualisation of the phenomenon inside a real size injector, Computational Fluid Dynamics (CFD) calculations represent a useful tool to provide three dimensional analysis inside the nozzle. This forms the basis of the present investigation. Various studies have appeared in the literature about the simulation of the cavitation inception and development, aiming at assessing the ability of CFD codes to predict the flow behaviour [13, 14, 15, 16, 17]. Many interesting observations concerning the flow inside injectors have resulted from these analyses, bringing useful information to improve injector design and understand spray behaviour. The current study also presents results of a computational fluid dynamics model to predict

cavitation. The cavitation model implemented in a commercial code [18] is based on a simplified form of the more general Rayleigh-Plesset equation [19], which links the rate of change of the bubble radius with the local pressure. Some previous computational studies have examined the nozzle flow and its global effects on spray development [20, 21], but have not coupled the flow inside the nozzle to the spray behaviour. The focus of this thesis is to characterize the effects of various parameters on the two-phase flow properties inside the nozzle and at the nozzle exit of Diesel injectors, with the aim of providing insight for coupling the inner nozzle flow characteristics with spray characteristics. The present study intends to provide physical information, such as flow distribution, discharge coefficient, turbulence quantities, vapour fraction, and velocity distributions at the nozzle exit, which can subsequently be used in spray modelling.

First, an extensive validation was performed using the two-phase nozzle flow data available in the literature, as well as in-house experimental data. In particular, the model has been validated for an academic geometry, consisting in a transparent throttle channel, for which the optical and hydraulic characterisation of the flow before and after the start of cavitation was carried out by Winklhofer et al [22]. As in the experiments, the injection pressure has been kept constant (10 Mpa), and the backpressure varied to get the corresponding pressure drop. Then, the model has been validated with measurements on axisymmetrical single-hole and multi-hole sac type injectors with cylindrical and tapered orifices. The effect of the geometry has been examined at maximum needle lift conditions and for different realistic engine operating conditions. To this purpose, the exact geometries of the nozzles have been reproduced in order to obtain an accurate description of the geometric details that can be determinant for the cavitation inception. Previous work about the comparison of tapered and cylindrical nozzles for a

wide range of Reynolds and cavitation numbers [23, 24, 25, 26] has revealed that there exists a correlation between cavitation and geometry. The merit of the present work is that the validation of the model is based on experimental results of mass flow rate, momentum flux at the exit of the nozzle, as well as effective injection velocity, distinguishing itself from other publications that validate mainly with flow images [27, 28]. Moreover, the results used for the model validation come from real size injector experiments.

The computational model was then used to investigate the effects of needle lift and hole geometry on flow characteristics inside the nozzle, as well as on cavitation and turbulence levels at the nozzle exit. Because of the complexity of moving mesh calculations of real size injectors, the nozzle flow is often studied at full needle lift only or by quasi-steady state fixed needle lift calculations, so that little is known about the transient phase of the needle opening/closing. In [29], Roth et al. compare results of a small number of constant needle positions, and in [30] Masuda et al. present results related to the development of the cavitation pattern. Yet, it is important to characterize precisely the flow at the nozzle exit, also in function of the needle lift position, since the exit flow conditions influence significantly the spray evolution in the engine. In this study, CFD calculations have been carried out with both fixed and moving mesh and the effect of the needle position on the cavitation pattern and the nozzle exit conditions was analysed. In addition, results of the fixed and moving mesh approaches are compared to evaluate the limits of validity of the much simpler fixed needle lift approach.

With the study presented in this thesis, valuable insight into the cavitation evolution inside real-size injector nozzles should be gained. It is expected that the CFD model will eventually allow improving designs of multi-hole Diesel nozzles, capable of producing well atomized sprays. To attain this objective,

additional work will be required, and this will be discussed in detail in the future work section.

### 1.3 Thesis Outline

The present thesis consists of eight chapters including the introductory *Chapter 1*, where the motivation and contribution of this research work is outlined. Additionally, an overview of the cavitation phenomenon is presented, together with the basic physical principles dictating its onset and development during the injection process.

*Chapter 2* reviews relevant publications of experimental and numerical investigations on cavitation occurring in both enlarged orifices and realistic injectors. Particular emphasis is given on reviews related with the effect of needle position on nozzle flow.

In *Chapter 3* a brief description of the experimental facilities including the internal geometry characterisation, as well as a description of the CFD models used in the simulations is reported.

In *Chapter 4* the cavitation model is validated for an injector-like academic geometry. The experimental data published by Winklhofer et al. [21] has been used in this work to validate the CFD model. The predicted results are compared with the measurements of the vapour field distribution, pressure field and velocity profiles. As in the experiments, the injection pressure has been kept constant (10 Mpa), and the backpressure varied to get the corresponding pressure drop. Under these conditions, the effect of various numerical parameters on the flow characteristics are investigated in order to

subsequently apply the results of this study to analyse the flow in real Diesel injectors operating conditions (above 10 Mpa).

In *Chapter 5* the model is validated for real-size geometries of single- and multi-hole sac type injectors with both tapered and cylindrical orifices at fully opened needle lift. Under these conditions, available in-house experimental data is used for the validation. The predicted results of injection rate, momentum flux at the exit, as well as effective injection velocity data are compared with experimental measurements in the form of non-dimensional flow coefficients defined in this chapter. Then, a full analysis of the predicted cavitation flow as a function of geometry and pressure conditions is presented.

In *Chapter 6* the effect of nozzle geometry and needle movement on the onset and development of the inner cavitating flow is analysed, based on moving mesh calculations. In this study, the geometries of single- and multi-hole injector have been considered, with both cylindrical and tapered orifices. Initially, the general methodology for the moving mesh generation and approach is presented. Then, a full analysis of the flow results is presented, including a dynamic picture of the developing pattern during the whole transient of the injection. The CFD analysis includes a study of the effect of cavitation on turbulent kinetic energy and velocity profiles.

*Chapter 7* commences with an extensive visualisation of the internal flow at different needle lifts positions obtained with quasi-steady state fixed needle lift calculations. Results of multi-hole nozzles with cylindrical and tapered holes in a comparative form will be examined, including the simulated results of the whole injector (360° sector). Then, comparison of the predicted flow structure at different needle positions obtained by simulations with different fixed and

moving mesh needle lift is performed (60° sector, multi-hole nozzle). With this work, the results of the much simpler fixed needle lift calculations are evaluated.

*Chapter 8* concludes the thesis with the summary of the major results. Recommendations for further work in the area of cavitation modelling are also given in the same chapter.

## **CHAPTER 2.**

### **LITERATURE SURVEY**

#### **2.1 Introduction**

Numerous literature reviews provide excellent work on the topic of cavitation in injector nozzles and fuel atomization investigated, experimentally and numerically. Dumont et al. [31] presented a description of the phenomena that occur in the injector and concluded that the transient behaviour of the exit velocity due to pressure fluctuations and cavitation is the main factor acting on the primary break-up of sprays. They analyzed the existing cavitation numerical models, emphasizing that the cavitation physics have to be clearly understood in order to take it into account in the simulation process. Arcoumanis and Gavaises [32] concluded, after discussing a large amount of experimental and modelling investigations, that although several theoretical efforts have been made to simulate the flow inside the nozzle holes of Diesel injectors, there is still a need to develop a method which can predict most of the characteristics of cavitation more accurately. The literature review of Schmidt et al. [33] provides excellent review and evaluation of the different modelling approaches. From this concluded that analytical models work very well for the steady state behaviour of axisymmetric models, and multi-dimensional models have been proved to be useful for more general geometries. Additionally, concluded that there is currently no consensus on

the basic physics behind the multi-dimensional models. Despite this controversy, there are several models available that have succeeded in predicting gross cavitation behaviour.

In this chapter are discussed important findings on the topic of cavitation, which serve as an introduction to many aspects regarding cavitation studied in the present work. It is attempted to present and discuss the key issues concerning a range of experimental studies conducted with large and real scale injectors with the aim of highlighting the key physical phenomena that need to be reproduced by the simulations. All these experiments show the need to understand the nature of cavitation. Additionally, the types of modelling strategies found in the literature are discussed together with some numerical results. Lastly, some research results concerning the effect of the needle position on cavitation characteristics will be presented. Some of the research reviewed, particularly relevant to the current work will be discussed in more detail.

## **2.2 Experimental Observations in Cavitating Nozzles**

Several experiments have shown that the presence of cavitation in the automotive injector nozzles may be a dominant factor on the atomization of the Diesel spray. This review will examine important historical investigations of injector nozzle flow, as well as recent results. The discussion covers issues like the clarification of the scale effects in cavitating flows in enlarged and realistic nozzles, the effect of cavitation on the exit flow and the spray formation and the identification of cavitation patterns.

Historically, the connection between Diesel fuel injection and cavitation was discussed by Bergwerk [11]. Based on his experimental work with simplified

large-scale and real-size single-hole injectors, Bergwerk was able to make important observations concerning the difference in cavitation flows in large- and real-size nozzles. For large-scale nozzles he observed a transition into a 'hydraulic flip' state with increasing cavitation number, which means that the spray could emerge very smoothly, taking a glass-like appearance, whereas for real-size nozzles, which may have minute imperfections, he noticed a more ruffled spray with increasing cavitation number. Moreover, in cavitating flow regime he reported the dependence of the discharge coefficient on the cavitation number, and its independence of the Reynolds number. Following the publication, however, there was certain confusion regarding cavitation and hydraulic flip and the difference in behaviour between simplified and real size nozzles. Indeed, cavitation was considered the same thing as hydraulic flip and it was recommended to be avoided.

In the same historical framework, Spikes and Pennington [34] studied also the effect of the hole geometry in conjunction with the cavitation number and Reynolds number. They measured discharge coefficients of partly transparent small submerged orifices used in fuel system units. It was shown that the effects of cavitation could be important and could cause variations in the discharge coefficients, greater than those associated with the Reynolds numbers when the flow is turbulent. Orifices with a length half of the diameter were found to have the most unstable behaviour.

More recently, in a similar study to the above, Nurick [35] explained the discharge coefficient behaviour by performing experiments with enlarged transparent nozzles. He tested both circular and rectangular sharp-edged orifices and observed the cavitating flow and hydraulic flip by varying the cavitation number, the entrance radius and length-to-hole diameter  $L/D$  ratios. He developed a phenomenological model in good agreement with

experimental data, which yielded an interesting view to detect cavitation inception.

Hiroyasu et al. [36] took photographs of low speed cavitating nozzle flow and observed a very significant correlation between the nozzle flow and the downstream spray. They used transparent large-scale nozzles to observe the presence of cavitation. The spray angle was found to increase significantly and the jet breakup length to shorten in the presence of cavitation. This correlation established the importance of understanding the flow in the nozzle, and particularly the cavitation, to predict spray break-up. This experimental study also showed that the nozzle length did not have any significant effect on the discharge coefficient.

Much information has been gained over the years through experimental studies on enlarged transparent Diesel nozzles. Real-size production nozzles have very small dimensions and operate at very high injection pressure over very short time periods. It is, therefore, very difficult to visualize the internal flow. Hence, most of these studies were performed on large-scale transparent models with the aim of visualizing the cavitation structure within the nozzles and linking it with the spray characteristics.

The work of Soteriou et al. [10, 37] was among the first in using large-scale transparent Diesel injector nozzles to understand the different flow states which exist inside the nozzle holes and how they affect the spray characteristics and flow rate. For this, steady state flow tests have been carried out to study the flow on real-size simple geometry nozzles consisting of circular orifices, multi-hole sac type nozzles, sac type nozzles with only one hole at different angles, and standard VCO nozzles. Some transient flow tests have also been carried out on standard sac type multi-hole and also VCO

nozzles. In addition to the real-sized equipment, large acrylic models of 20 times normal sizes have been used running under steady state conditions. They considered injection into oil, as well as into gas, in order to clarify the behaviour of the flow. The results were presented in the form of photographs of the cavitating flow inside the large-scale nozzles and of the spray behaviour emerging from both real-size and large-scale nozzles. Additionally, pressure and mass flow rate measurements were performed in order to calculate the discharge coefficients of each nozzle.

The discharge coefficients resulting from the large models were in good agreement with those from the real sized models. The transition between the different flow states occurred at the same cavitation numbers on both the large and the real sized nozzles. This result was significant since it established a macroscopic link between large-scale and real-size nozzle cavitation. Another interesting finding was that in the case of a simple submerged orifice, choking would occur once the cavitation had filled the entire cross section of the hole, whereas with flow discharging into gas, transition into hydraulic flip would result and no choking; the latter transition in the case of the real-size orifice was not quite clear due to the unavoidable asymmetries and other imperfections in the geometry of the equipment. The effect of turbulence and geometric asymmetries was identified in the experiments with a multi-hole nozzle. The presence of the needle increases the turbulence in the sac and prevents hydraulic flip in the holes of a standard nozzle. On the contrary, when the needle is removed and with increasing cavitation number, a hydraulic flipped state may occur. However, partial hydraulic flip could happen in multi-hole VCO nozzles, and it was found that it produced asymmetric sprays. Finally, it is important to mention the authors' finding that cavitation in the nozzle hole causes atomization of the jet immediately on exit and is entirely beneficial.

In order to gain more insight into internal flow characteristics in nozzles, Soteriou et al. [38, 39] used laser light sheet illumination to study the onset and development of cavitation in a scaled-up plain orifice nozzle. In addition, measurements were taken using Laser Droplet Velocimetry (LDV) and the refractive index matching technique in order to establish the velocity profiles within the orifice under non-cavitating conditions. The injection was considered into liquid and gas.

This flow visualization technique allowed the identification of new details in the cavitating flow characteristics. Flow conditions were obtained in which the cavitation produced an opaque mass of small bubbles, and other conditions in which large transparent vapor pockets were produced. Cavitation inception was found to take place in the hole entrance, in the mainstream flow close to locations of peak velocity, and within the attached boundary layer located downstream of the separated one. Formation of “plug-cavitation” appeared with an increase of the cavitation number, which means that the bubble clouds became more opaque and individual bubbles could not be distinguished anymore. This was much denser and turbulent compared with the structures that had been identified up to that transition. With increasing cavitation number, the plug was found to propagate towards the hole exit, causing a significant increase in the spray angle, and the spray appeared bushy and atomized right at the hole exit. This state of the spray did not last for very long though, as there was a transition to hydraulic flip subsequently. Another important observation made in this study was that for a low Reynolds number of 2000 and increasing cavitation number a transparent gas void was created and started to grow. The authors also observed that the emerging spray became slightly bushy and its angle increased due to cavitation.

Concentrating now on the cavitating flow, clarification of the structure of cavitation flows in real scale nozzles was achieved as a result of the study by Bode [40]. He observed temporal variations in the cavitation pattern and cavitation films that would stretch out from the hole entrance. The location of these films seemed to be related to surface irregularities, because the location of the films did not change in repeated tests with the same nozzle. He also noted that the development of the cavitation pattern varied with the upstream pressure.

Chaves et al. [20] extended this work and used transparent nozzles of the same size as in Diesel injectors to study hole cavitation. The nozzles used were made of a glass that had almost the same index of refraction as Diesel fuel. This allowed observing the flow within the nozzle hole even though the hole was cylindrical. In a steady flow rig, short exposure video pictures of the flow were made at injection pressures up to 100 MPa. Discharge measurements and a measurement of the flow velocity in the nozzle hole using a modified laser-two-focus-velocimeter completed the picture of the flow. Contrary to the observations of Soteriou et al. [10], the authors concluded that in high injection pressure conditions, it was difficult to identify the structure of the cavitating flow, and to determine whether it was a rough vapour film or foam of small bubbles. They speculated that the bubbles have their own length scale and thus do not scale up in large models. Despite these differences, the authors showed that the coefficient of discharge is independent of the model scale. From this comparison it could only be concluded that some information could be obtained from scaled-up nozzles and other information may not. In addition, they did observe that with increasing injection pressure the cavitation reached the nozzle exit (supercavitation). They noted that supercavitation was accompanied by a dramatic increase in the spray angle produced by the nozzle.

Arcoumanis et al. [41] compared cavitation images obtained in a real-size nozzle with those obtained in an enlarged fully transparent acrylic nozzle replica. A comparison of the measured discharge coefficients showed that for high needle lift there is a better agreement between them. It also confirmed that, for the real-scale nozzle, the discharge coefficient drops asymptotically with increasing cavitation number after the onset of cavitation. Also the authors found that the Reynolds number did not play any significant role in cavitating conditions. Another important finding was that string cavitation was observed in the real-size nozzle, but only at high needle lifts. This kind of cavitation is very similar to the vortex cavitation observed in propeller flows, and it is formed with the interaction of hole cavitation and sac vortices. Visual comparison of the various flow regimes in the real-size and large-scale nozzles showed similarities but also important differences. The effect of increasing the cavitation number was significant in both cases. However, in the real-scale nozzle the observed structures collapsed inside the hole for low Reynolds and cavitation numbers, while in large-scale nozzle case, the cavitation structures always exited the hole. They found that cavitation in scaled-up experiments appeared in the form of foamy clouds of bubbles. In real-scale experiments, however, there were clear voids, similar to those seen also by Chaves et al. [20]. These dissimilarities seem to indicate that cavitation is a phenomenon that cannot be scaled.

The study of Roth et al. [3] was focused on the dynamic behaviour of incipient and developed cavitation. In this work a digital high-speed video camera was employed to visualize the flow in the transparent enlarged models of various injection nozzles of the mini-sac and VCO type. A refractive index matching flow rig described previously by Arcoumanis et al [42], was used under steady and quasi-transient flow conditions with fixed needle position. The LDV

technique was also applied for taking detailed velocity measurements inside the enlarged mini-sac nozzle in single-phase and cavitating conditions. The following observations were reported in this study: a vortex structure was formed between the needle, needle seat and two adjacent holes in both the mini-sac and the VCO type nozzles for the high needle lift positions. They claimed that this was a prerequisite for string cavitation to occur. Hole-connecting strings could be seen for both high and low needle lifts in the mini-sac case, whereas for the VCO they could only be seen for high lifts. The fluid flow entering the injection hole from the side of the injection holes created recirculation zones and low pressure regions, which were identified as possible zones for cavitation initiation. From the LDV measurements it was concluded that turbulence levels increased in the lower part of the injection hole as the cavitation number was increased. Nevertheless, close to the hole exit the averaged turbulent kinetic energy for all cavitation conditions decreased asymptotically to the turbulence level of the non-cavitating flow.

Roth et al. [29] also studied the effect of multiple-injection strategy on nozzle hole cavitation, both experimentally and numerically. A real common-rail Diesel injection system was employed with a double-shutter CCD camera in order to visualise cavitation inside a submerged and optically accessible real-size VCO nozzle (one out of the six holes). Initially, the cavitation development was investigated for single injection events, followed by flow images obtained during multiple injections consisting of a pilot and a main injection pulse. In order to identify the effect of pilot injection on cavitation development during the main injection, the dwell time between the injection events was varied between 1.5-5 ms for different pilot injection quantities. The extensive test matrix included injection pressures of 400 and 800 bar and back pressures ranging from 2.4 up to 41 bar. The results confirmed that cavitation patterns of the pilot injection are very similar to those of the main

injection. The flow inside the VCO nozzle was also simulated using a CFD model which took into account the movement of the needle. Moving needle simulations showed that cavitation inception was very fast and synchronous for both the pilot and the main injection events, while its intensity in the sense of spatial extent appeared to peak at relatively low needle lifts (60  $\mu\text{m}$ ).

Gavaises and Andriotis [43] investigated the cavitating flow characteristics inside multi-hole injectors for large Diesel engines. In this work, transparent nozzle replicas, two high speed cameras, various illumination light sources and computational fluid dynamics were used. Flow imaging showed that cavitation was formed not only at the hole entrance due to the local pressure drop induced by the nozzle inlet geometry, but also inside the volume below the needle and just upstream of the injection holes. CFD calculations of the internal flow showed that cavitation strings were formed in the areas where large vortical structures were present. Simultaneous imaging of the flow inside the nozzle, the injection holes and the near-nozzle spray structure revealed the effect of string cavitation on the hole flow structure and the consequent effect on spray cone and deflection angle. These were found to vary considerably and in a transient mode in the presence of a string inside the hole. The authors concluded that string cavitation was a source of cycle-to-cycle and spray-to-spray variation in Diesel fuel injectors.

Gilles-Birth et al. [44] investigated in-nozzle flow characteristics of a VCO type injector. A transparent real-size single hole injector was developed and adapted to a pressure chamber. A series of experiments for the visualisation of the onset and development of cavitation inside the nozzle and the initial fuel break up process were conducted applying the back light illumination method. They detected that different types of cavitation took place in the nozzle hole over the whole operating range of injectors for gasoline direct

injection. According to the authors, the cavitation occurring within small holes could be divided into three categories. Homogeneous (bubble) cavitation occurs due to temporary microscopic voids that can constitute the nuclei necessary for the transformation of macroscopic bubbles. Heterogeneous (film) cavitation in which the surface roughness of the nozzle hole walls can act as a nuclei reservoir in areas of local pressure below the critical pressure. This cavitation type occurs mainly at the inlet of the nozzle hole resulting in cavitation films and due to dynamic processes, bubbles separate and flush away. The cavitation film can grow up to the nozzle outlet, which is then called supercavitation. Moreover, if very strong vorticities occur in the flow field the pressure within the centre of the vortex can fall below the critical vapour pressure. This results in string shaped cavitation structures. It was shown that the in-nozzle flow characteristic has an effect on the spray shape and atomisation of the spray. However, due to the experimental set-up constraints, the authors investigated relatively low injection pressures.

Reid et al. [45] studied also string cavitation in an optical automotive multi-hole fuel injector with true-scale geometry at injection pressures of up to 2050 bar. The authors observed the hole-to-hole vortex interaction and, in particular, that of a bridging vortex in the sac region between the holes. A dependency on Reynolds number was observed in the formation of the visible, vapor filled vortex cores. Above a threshold Reynolds value, they observed that changes to fuel injection pressure had no observable influence on their formation and appearance, as well as the appearance of the cavitation strings, demonstrating independence of cavitation number and fuel injection pressure across the experimental range. Thus, it was surmised that only the initial formation of cavitation strings is influenced by vortex intensity.

Focusing now on the internal flow and cavitation characteristics, Kato et al. [46] used an enlarged model to analyse theoretically supercavitation conditions (flow conditions in which cavitation reaches the hole exit). They measured the mass flow rate from each hole and also the pressure head at different points between the needle and the nozzle body. The authors found that the cavitation, which occurred at the inlet of the hole, was affected by the configuration of the sac and injection hole and that the cavitation had a direct effect on the contraction of flow at the inlet of holes and its recovery. They proposed for future research to apply the results as input boundary and initial conditions for CFD calculations.

Another study on scaled-up simplified nozzles was performed by Henry and Collicot [47], who visualized cavitation inside a slot orifice with a minimum dimension ranging from 0.127 to 1.525. The visualization of the flow showed that the cavitation region was formed by a conglomeration of tiny bubbles; this finding supports the validity of numerical models based on the assumption that cavitation is a phenomenon initiated by the presence of nuclei which grow. The liquid-vapor interface was found to vary significantly with the slot geometry and local surface conditions at the inlet corner. It was observed that cavitation in certain orifices experienced a complex, and apparently cyclical, growth and disintegration process. This finding is important since it supports the evidence of the highly transient nature of cavitation even in simplified geometries.

Matsumura et al. [48] made visual analyses of the fuel flow inside the nozzle using enlarged acrylic slit nozzles. The results demonstrated that vortices that are formed within the nozzle sac are continuously propagated in a periodic manner within the sac and that they influence the streamline of fuel flow from the sac to the slit. It was also demonstrated that the smaller the vortices that

formed in the sac, the thinner the liquid film that formed at the edge of the slit. The authors claimed that this enlarged the region of the central portion of the slit in which cavitation occurred, thereby improving atomization of the fuel spray.

As fuel atomization just outside of the nozzle is of primary interest in engine combustion research, Zhen et al. [49] investigated the atomization process of a steady spray of fuel containing dissolved gas; they used Diesel fuel containing dissolved CO<sub>2</sub> and air in order to study the effects of the concentration of the dissolved gas, the injection pressure, and the nozzle L/D ratio. The experiments were performed under atmospheric conditions with simple and Diesel-like simplified nozzles. The atomization process and spray characteristics were observed and measured by instantaneous shadowgraphy and a particle size analyser, respectively. The authors concluded from their experiments that the Injection of Fuel containing a small Concentration of Dissolved Gas (IFCDG) can greatly improve the atomization and produce a parabolic-shaped spray, since the SMD of the spray would increase. It was found though that there exists a concentration threshold for the gas concentration, below which, increase of the injection pressure would improve spray atomization, and above which, any injection pressure increase did not have any further effect on the spray. Finally, the L/D ratio in the simple nozzle was found to be significant, with larger nozzle ratios obtaining the beneficial effect of IFCDG.

Studies to connect the nozzle flow to the downstream spray behaviour was published by Tamaki et al. [50, 51]. They performed experiments under conditions ranging from decompression to high ambient pressures by using acrylic nozzles with various L/D ratios and different inlet shapes of the nozzle hole, similar to the hole of an actual nozzle. In conclusion of this study, it was

determined that the primary factor in the atomization of the liquid jet was the disturbance of the liquid flow resulting from the cavitation phenomena.

Another study concerning the influence of cavitation on spray characteristics was performed by Badock et al. [52]. They used laser light sheet and shadowgraphy techniques to investigate cavitation in the nozzle of a real-size single-hole injector and on the spray break-up at the hole exit. The experiments were performed with a Bosch Common Rail system capable of generating unsteady injection conditions with rail pressures up to 60 Mpa. The nozzle was modified in order to replace the metal tip with a transparent one made of acrylic glass. The Diesel-like test oil was injected into a chamber which could be pressurized up to 1.5 MPa. The authors of this study concluded that the scattering of the images was too important to be useful for quantitative measurements of the cavitation film thickness. The multiple scattering caused the formation of a milky cloud in front of the observing plane and for this reason only the near exit part of the spray could be visualized. Nevertheless, the images obtained allowed visualizing the various stages of cavitation development; at the beginning of the injection, large gas bubbles could be observed in the sac hole, which remained in the orifice during the time between injections. At the beginning of the injection additional air was sucked into the spray hole. Afterwards these large air bubbles were flushed out of the nozzle with liquid. Another observation was that even in the case when the cavitation films reached the nozzle exit an intact liquid core surrounded by cavitation was visible. At different times of the injection process, single cavitation bubbles or disruptions from cavitation films were observed, but no foam or any accumulation of small bubbles. The closing process of the needle produced similar images as the opening phase. The authors concluded that for all rail pressures the films have similar dimensions. Regarding the link between internal flow and spray structure, it was observed

that the bubbles which survived after the closing of the needle, visible in the hole and the sac caused mushroom-like structures or a pre-jet during the early stage of injection. Additionally, with the same experimental set up, Badock et al. [53] investigated the effect of hydrogrinding on cavitation development and spray break-up. However, in this experiment Badock et al. did not find any significant influence of cavitation on the spray characteristics, contrary to previous reports by other researchers.

More recently, Ochoterena et al. [54] also conducted experiments with scaled-up, optically transparent nozzles, to analyse the influence of cavitation and turbulence on atomization. They promoted cavitation inside the nozzle by modifying the temperature and consequently the vapour pressure of the injected liquid. The results showed that cavitation length could be correlated to atomization regardless of the fluid temperature, flow regime or pressure drop in the nozzle. In addition, it was shown that an increase in cavitation inside the nozzle increased the spray angles. However, the authors concluded that it was not possible to separate the sole effect that cavitation or turbulence had on atomization due to the fact that these experiments were conducted at high Reynolds numbers where turbulence was present.

It is evident from the aforementioned studies that cavitation in the injector nozzle may be causing significant disturbances in the exiting jet and that turbulence is somehow linked with cavitation. He and Ruiz [4] performed an experimental study on how cavitation affects the characteristics of turbulence inside a nozzle. Their test-rig comprised a relatively large-scale channel, which was used to reproduce the flow pattern in a square-edged Diesel injector orifice by dynamic similarity. Water was the working fluid, and by using a vacuum pump, dynamic similarity was attained between the experiment conditions and those found in a real-size Diesel nozzle. Both

cavitating and non cavitating flows were measured by using a LDV technique. The authors found that turbulence in the cavitating flow is higher and decays more slowly than in the non cavitating flow. They claimed that this could explain the sudden increase in spray angle observed in Diesel fuel injectors at the onset of cavitation.

Knox-Kelecy et al. [55] used a scale model of a high pressure Diesel fuel injector nozzle hole and conducted an experimental investigation of the spectral characteristics of turbulent flow. Turbulence time frequency spectra were obtained for significant locations, in order to determine how geometry affects the development of the turbulent spectra. The sharp and rounded geometries showed significantly different turbulent spectral characteristics. In addition, the holes with sharp inlets showed differing spectral characteristics for varying L/D values, contrary to holes with rounded inlets.

Chaves et al. [20] also presented another interesting observation from a nozzle with rounded inlet whose internal surface was not sufficiently smooth and had irregularities. The authors concluded that surface roughness could cause cavitation even in a nozzle with rounded inlet. The implication of this observation is that a nozzle may be cavitating, even if the nozzle inlet is rounded. They also observed the downstream spray at atmospheric pressure. When the injection pressure was high enough for the cavitation to extend to the nozzle exit (supercavitation), the downstream jet presented asymmetry and began to break up sooner.

Kim et al. [56] investigated also enlarged Diesel injection nozzles. They conducted experiments with a circular nozzle, as well as a set of nozzles of elliptical and similar cross-sectional area but with varying orifice aspect ratio in order to study the cavitation and its influence on the discharge coefficients

of the different geometries. The equipment consisted mainly of the liquid injection system, which used water at room temperature, measuring devices like flow and pressure sensors and a CCD camera for the flow visualization. They concluded that the flow rate of all type of nozzles increased with increasing injection pressure, and that the discharge coefficient decreased. The onset of cavitation appeared for the same injection pressure, regardless of the nozzle. However, the cavitation area for circular nozzles was longer than for elliptical nozzles at the same injection pressure. In the case of the elliptical nozzles, they found that the largest aspect ratio led to shorter cavitation lengths for the same injection pressure. However, the above conclusions were extracted at very low pressure operating conditions (up to 4.5 bars), and so their relevance to Diesel injectors may be limited.

The enlarged Diesel nozzles provided over the years valuable information concerning the nature of cavitation. Nonetheless, since cavitation cannot be scaled [41], real-size nozzle experiments are needed to depict the cavitating flow behaviour. Goney and Corradini [57] used realistic multi-hole Diesel injectors to examine how the characteristics of the spray are influenced by nozzle cavitation as well as ambient pressure and hole inlet geometry. In their test-rig a common-rail system, a high-pressure constant volume spray chamber, a high-speed digital camera and a Cu-vapour laser were included. They used two nozzles, one with a sharp-edged hole inlet and one with a rounded one, but the hole diameter of both nozzles was the same. The authors found that the mass flow rates of the sharp edged nozzle were independent of backpressure in cavitating conditions (similar to choking), which was not the case for rounded nozzles. They reported higher values of discharge coefficients compared with those found in the literature, and they attributed this to their use of sac instead of injection pressure, with pressure losses thus neglected, and to some uncertainty regarding their accuracy on

the sac pressure measurements. They also found that the discharge coefficient of rounded nozzles could decrease even with increasing backpressure. Under the same operating conditions, the spray SMD of the sharp edged nozzle was found to be larger than that of the rounded nozzle and it decreased with increasing backpressure.

Cavitation has been identified not only for its well-known influence on the discharge coefficient but also for its key role versus in the “coking” phenomena (fouling with solid deposits inside the hole volume or close to the hole exit). This phenomenon especially appears in small diameter holes and it is linked with the rapid losses observed in injected fuel flow rate. Argueyrolles et al. [58] described a methodology to define the minimum cavitation intensity required to avoid coking risk, given that enhanced cavitation reduces coking. For this, they realized both experimental and numerical studies to analyze the relation between various geometric parameters, cavitation and coking. A new criterion based on “cavitation intensity” was proposed to evaluate the possible coking problems and at the same time to define the minimum cavitation intensity required to avoid coking risk. The authors concluded that it was possible to optimize the nozzle geometry to achieve the best trade-off between engine performance (power and pollutant emissions) and robustness regarding coking.

Han et al. [6] presented numerical results of the internal flow and spray visualization to study the influence of the internal geometry on the primary spray breakup. They used different types of multi-hole minisac and VCO nozzles with cylindrical and tapered geometries, and different types of single-hole nozzles with defined grades of hydro grinding (HG). A commercial code was used for the CFD analysis, a high-speed drum camera to measure the global characteristics of the spray and a long-distance microscope to magnify

the Diesel spray in the nozzle hole vicinity. They predicted that the internal flow field characteristics such as the distribution of pressure, the kinetic turbulence energy, the velocity profiles and the cavitation were different in cylindrical and conical nozzles. In addition, the authors with the macroscopic observations found differences in the spray structure for single-hole versus multi-hole nozzles which were claimed to be due to the difference in cavitation and turbulence intensity of the internal flow. Indeed, the single-hole nozzle had higher liquid column prior to break-up and smaller spray angle, implying reduced atomization close to the nozzle exit.

Blessing et al. [59] also performed experiments with transparent 1-hole and 6-hole mini-sac real size nozzles under high pressure conditions. The authors made a comparison of the nozzle flows between a conventional common-rail (CR) and a Pump Line Nozzle (PLN) system. The investigations of the effects of an injection rate shaping were accomplished with Amplifier Piston Common Rail System (APCRS). A CCD camera was used to visualize the internal flow. Additionally measurements close to the nozzle exit were done with shadowgraphy images of the jet. The authors found that a rounding of the inlet edges of the hole led to a higher uniformity of the flow and thereby to a reduction of cavitation in the nozzle. Moreover, the flow in tapered nozzles with rounded edges appeared practically cavitation free. The average spray angles of the jets emerging from the high conicity holes were smaller and spray break-up and tip penetration increased. CFD calculations were also performed by the authors to reproduce the effect of the hole conicity on cavitation formation and development. The flow inside the sac volume of the nozzle connected to the 'needle-lift controlled' CR system was identified as highly turbulent and presented an uneven pressure distribution in the sac hole. Contrary to this, the flow inside the nozzle which was connected to the

'Pressure controlled' PLN system exhibited more stable flow behaviour and therefore a smaller spray angle.

Collicott and Li [60] visualised the flow inside a real scale (200  $\mu\text{m}$ ) tilted nozzle at real pressure conditions of up to 210 Mpa. It was found that surface roughness and the orifice inlet were affecting the flow. They also claimed that regardless of whether the cores of a pair of counter-rotating streamwise vortices entrain cavitation, the swirling flow in the exit plane may be of significance in droplet formation. However, the authors found poor repeatability of results.

The above-mentioned studies prove that the nozzle hole geometry greatly influences the cavitating characteristics. To confirm this, Desantes et al. [61, 62] adopted a non-destructive characterization of the internal nozzle geometry based on the microscopic visualization of silicone moulds of the nozzles [63]. This technique allows measuring with precision the orifice diameter, the radii of the orifice entrance and any existing internal geometry irregularity. The authors then measured the mass and the momentum flux of the injected spray emerging from the characterised two-hole real-size research VCO cylindrical nozzle. The injection system used was a conventional Common Rail Fuel Injection system which allowed fuel injection under high (up to 1500 bar) and relatively constant pressure. With the Spray Momentum test rig it was possible to determine the impact force of the spray, equivalent to the momentum flux of each spray. In non cavitating conditions it was found that the mass flow was proportional to the pressure difference along the nozzle and that it collapsed when cavitation would initiate. After the collapse the mass flow does not increase further when varying the backpressure. It was also observed that, contrary to the behaviour of the mass flow, the momentum flux did not collapse, but was proportional to the

pressure drop for any injection and discharge pressure, independently of the presence of cavitation or not. Also, the outlet velocity, calculated by dividing the momentum flux by the mass flux was found to increase when cavitation appeared.

Investigations with simplified geometries of Diesel nozzles have been published in the literature. In these, it was easier to do quantitative measurements and to isolate the various interacting phenomena, allowing thus safer conclusions to be drawn. Ganippa et al. [64] investigated the structure and evolution of cavitation and its effect on the spray dispersion using a simple transparent scaled-up Diesel nozzle and varying the hole inclination ( $90^\circ$ ,  $85^\circ$ ,  $80^\circ$  and  $0^\circ$  to the nozzle axis). In all the experiments, tests were done with water as the working fluid and they used high-speed motion pictures, flash photography and stroboscopic visualization. Observations revealed that at the inception stage, the cavitation bubbles were seen at different positions in all four nozzles. As the hole inclination increased the cavitation shifted to one side of the inlet corner, a tendency seen from the incipient stage. The authors also observed that the instabilities of the shear layer caused the cloud cavitation structures to break off, which subsequently led to the shedding of the cloud-like cavitation structures. Under very high pressure flow conditions the cavitation cloud could transform into a glossy sheet form. The non-symmetric distribution of cavitation within the hole resulted in a jet, only partially atomized on the side where there was more cavitation.

The above works show the difficulty in gaining quantitative information about the internal flow in real-size nozzles using the experimental facilities. Walther et al. [65] applied a Particle Image Velocimetry (PIV) measurement technique to measure the velocity field inside a real-size single hole Diesel nozzle.

Fundamental studies were carried out using a stationary pressure system generating injection pressures up to 10 MPa. Nevertheless, the authors observed that the feasibility of their technique under higher injection pressure had to be proven.

Winklhofer et al. [22] published results of extensive studies of the structure of cavitation flow in Diesel injector-like geometries (transparent nozzle of rectangular cross-section). The flow geometry of interest was eroded into 0.3 mm thick steel sheets, which were sandwiched between a pair of sapphire windows. Visualization of the vapour field distribution, of the pressure in the liquid, measurements of velocity, as well as, mass flow were reported for standardised throttle sets in stationary flow conditions at inlet pressure levels of 100 bar. The back-pressure was adjusted to provide the desired pressure drop. These experiments were performed for injection into liquid, so no hydraulic flip could occur. The results showed that the discharge coefficient was significantly affected by the cavitation level at super-cavitation flow regime, when the flow was choked and the mass flow rate became independent on the downstream pressure. According to the observations, the conicity of the orifice had no apparent effect on the variation of the discharge coefficient with the cavitation number when the flow was choked. Though, the nozzle shape was found to determine the inception and critical flow conditions.

Though experimental analysis is still unavoidable due to the complex nature of cavitation, observing the flow in Diesel injectors is very difficult, if not impossible, as they are characterized by high pressure injections through very small nozzles with diameters of around 100 microns or less. For instance, manufacturing of prescribed hole entrance radius is not possible and even precise measurement of the real-size radius is difficult task. In addition, a

decrease in pressure below a critical level leads to cavitation, which adds another level of complexity to the problem. Due to the difficulty of directly measuring the characteristics of the two-phase flow in very small orifices such as found in automotive engine applications, the use of numerical simulations is very useful in order to understand the flow features inside and at the exit of the injector nozzle, as well as to provide more realistic boundary conditions for modeling spray and atomization processes downstream the nozzle exit.

### **2.3 Cavitation-Modelling Approaches and Validation**

The presence of abrupt changes in density, typically encountered in cavitating flows, induce sharp variations in pressure gradients and hence pose a major challenge in numerical simulations. In spite of the numerical challenges, useful models predicting the flow in fuel injector nozzles have been developed. Several types of cavitation models have been reported in the literature and each model is based on different assumptions. The purpose of this chapter is to present and discuss the most important findings in the modelling of the cavitation phenomenon.

Interface tracking methods and methods that do not take into account the interface location between liquid and vapour for simulating cloud cavitation have been extensively explored by researchers. In the first category, the most used is the volume of fluid (VOF) method [66] and it usually requires the resolution of all involved length and time scales to precisely reconstruct the interface between liquid and vapour on the sub-cell level. This results in very large computational efforts. Therefore, this method is still limited to basic studies. Methods that do not take into account the interface location, however, are popular due to their computationally inexpensive nature, while retaining accuracy when compared to the interface tracking methods.

Among the methods that do not take into account the interface location, are the two-fluid models and the continuum models. In the case of the two-fluid approach [67, 68], two sets of conservation equations, one for the liquid and one for the vapor, are solved and the interaction between phases is modelled in the form of additional exchange terms. The continuum models or homogeneous equilibrium mixture (HEM) models [15, 69, 70] treat the flow as a homogeneous mixture of liquid and vapour bubbles and apply a separate transport equation for the vapour volume or mass fraction to describe the evolution of the cavitation region. The homogeneous mixture models assume both phases are uniformly mixed together and no clear two-phase structures and inter-phase boundaries can be identified in the flow, while employing a void fraction variable to quantify regions where the flow properties have been modified. The mixture density, which varies from the liquid density to the cavitation vapour density, indicates the fraction of liquid and gas in a given cell. The continuum models are the most widely used and are based on different formulations, depending on how the equation of state and pressure equations are formulated: methods based on vapour production terms, bubble dynamics equations, or barotropic equation of state.

For the purpose of the current discussion the modelling approaches are divided into two categories, namely barotropic equation approach and bubbly mixture approach. Such a classification has been previously used in the literature [71]. In the first category, heat transfer between the vapour and liquid phases in the process of bubble growth is considered and an instantaneous effect of local pressure on the density of the homogeneous mixture is assumed. In the second category, the pressure difference between the vapour and the liquid phase is considered as the driving effect for the formation and destruction of vapour.

### 2.3.1 Barotropic equation approach

Delannoy and Kueny [72] pioneered the usage of a barotropic law with a compressible mixture approach to model cavitation, which is a classical thermodynamic approach. Particularly, they proposed a formulation that strongly linked the mixture density to the static pressure: indeed, they used an equation of state which described the mixture density. Their approach consisted in modelling the cavitating liquid as a homogeneous two-phase mixture of liquid and vapour. One main assumption in this case is to neglect the possible slip between the two phases, which leads to a single-phase fluid with a density that may vary over a large range, from pure liquid to pure vapour. They neglected also viscosity effects, and so turbulence was not taken into account. Simulations of one- and two dimensional cavitation flows in a Venturi were performed. They predicted that the 2-D simulations were quite realistic, contrary to the 1-D simulations, and in agreement with the experiment, the cavitation bubble was found to separate and collapse downstream. However, the predicted detachment frequency was distinct from the experimental one. Moreover, the calculated results over-predicted by about 50% the length of the detached cavitation bubble and were not able to predict its total disappearance. Although, the approach yielded some encouraging results, it was oversimplified, since the density must be related not simply to the local pressure but also to the time-dependent bubble evolution caused by the changing pressure field. Nevertheless, this kind of model has been applied in the last decade by other researchers with different state laws.

Another similar approach to that of Delannoy and Kueny was developed by Schmidt et al. [73, 74]. The two-dimensional, transient model was developed to predict small, very fast, nozzle flows as found in Diesel fuel injectors. The two-phase sound speed was modelled using the classic HEM model [69]. The

model used a barotropic equation of state, but included the compressibility of both the liquid and the vapour phases to improve numerical stability. Although they applied their model to a variety of injector-like geometries, they reported important influence of geometric characteristics. Results of the flow for a sharp inlet corner planar cavitating nozzle with ratio length to diameter  $L/D$  of 4 were presented. The dependence of the discharge coefficient on the cavitation number was well predicted compared with results taken from the literature. Additionally, the predicted centreline velocity was in good agreement with that measured in Chaves et al. [20]. Taking this nozzle as starting point, they analysed the effect of several geometric parameters on the nozzle flow. They found that rounding of the nozzle yielded higher discharge coefficient and more uniform exit momentum profile. The nozzle length was found to have less effect on the discharge coefficient and on the flow structure. They also reported that greater entrance angle led to a higher coefficient of discharge. In addition, they presented results for a representative VCO axisymmetric nozzle at low needle lift and noted that the inclusion of the needle had a smaller influence on the outlet flux than the above mentioned parameters. The model has proven to be quite reliable and robust and has been therefore implemented in a commercial code [75]. However, this model does not take turbulence into consideration, and this means that essential flow features, as the experimentally observed vortical structure are not adequately predicted.

More recently, Xie et al. [76] reported that the model developed by Schmidt et al. [74] did not work consistently when applied to the simulation of unsteady transient cavitating flows with large vapour to liquid density ratio or under the condition of a low surrounding pressure. Accordingly, they proposed a modified Schmidt model for achieving greater robustness and consistency. They simulated several cavitating flows where analytical, experimental or numerical

results were available for comparison, and then they applied to multi-dimensional transient cavitating flows generated by underwater explosions. The authors concluded that their model could be applied to both small and large scale transient cavitating flows.

Avva et al. [77] presented an enthalpy-based model of cavitation. The authors started with an energy equation for a two-phase mixture and assumed homogenous flow, no inter-phase slip, and thermal equilibrium between liquid and vapour. They calculated thermodynamic properties of the two-phase mixture from the void fraction and from the properties of the saturated liquid and vapour. The model was tested for 2D sharp-edged orifice cases and the predicted dependence of the discharge coefficient on the cavitation number was found to be in good agreement with the measured one. Unfortunately, because of stability problems, they were not able to model the high speed nozzle flow which typifies Diesel injectors.

Dumont et al. [17] presented a simulation code based on a HEM model, using the same barotropic equation of state as the model of Schmidt et al. [74] extended to a three-dimensional version. The authors had to implement an advanced non-reflective outlet boundary condition to deal with strong pressure wave propagation at the nozzle exit. The model was validated for the bubble collapse of a well-known case; the collapse of a symmetric bubble in an infinite domain. They applied the model to 2D and 3D geometries (1 mm length, 0.2 mm diameter), and with conditions typical of Diesel injector simulations (1000/50 bar). The results predicted a recirculation zone, which was formed downstream of the sharp edge and not attached to it. Then, the cavitation extended throughout the orifice within the boundary layer and reached the exit, though without forming any vortical structures. Hence, this model predicted that cavitation was strongly present in the liquid jet leaving

the injector and entering the combustion chamber, affecting thus the exit density profiles.

Ning et al. [78] developed a three-dimensional HEM model and implemented it into the CFD code KIVA-3V. Assuming isentropic flow, an equation relating pressure with density and the speed of sound of the mixture was derived. The model was applied to simulate cavitating flow within injector nozzle passages. The flow solutions at the nozzle exit obtained from the nozzle flow simulations (velocity/density profiles) were further coupled with an Eulerian-Lagrangian Spray and Atomization (ELSA) model to investigate the effects of nozzle flow physics on the downstream spray atomization process. The known effects of nozzle passage geometry (tapered/cylindrical nozzle, sharp/rounded edge) and injection conditions on the development of cavitation zones and the nozzle discharge coefficient were well captured by the predictions, as the predicted trends were consistent with experimental observations and theoretical analysis, however, no quantitative comparison with experimental results were reported in this work. The computational results from the ELSA simulations were in reasonable agreement with experimental results, though, the authors reported that the effect of the turbulence modelling in the coupling approach was found to be important.

Recently, Peng Kärrholm et al. [79] developed a viscid model for the OpenFOAM platform, which used a barotropic equation of state and the HEM assumption and allowed both compressible liquid and vapour to be modelled. The turbulence was not modelled in this study. The mass flow and the cavitation obtained from the simulations were compared to data obtained in experiments, in which the flow through an injector-like throttle was examined. Although the model predicted the choking of the flow in the channel, it over-predicted the cavitation probability due to the value of the liquid viscosity,

according to the authors. The pressure profile from the simulation was not similar in shape or value to the experimentally derived profile. The authors also found that a vortical flow structure originated from the top and the bottom walls and by changing the boundary condition on these walls from non-slip to a slip condition, a more physical behaviour was observed. However, this led to an over-prediction of the cavitation region.

The barotropic model has been applied recently to actual Diesel fuel injector geometries. Salvador et al. [80] implemented and validated a model based on the barotropic equation of state and the HEM assumption in the OpenFOAM platform. Turbulence was equally neglected. The comparison of the numerical and experimental data was presented in terms of mass flow rate, velocity at the exit and pressure and cavitation distributions for an academic geometry, as well as for a real single-hole Diesel injector nozzle. For the academic geometry, the numerical results agreed well with the experiment in terms of mass flow and velocity at the outlet. However, the predicted cavitation propagated up to the hole exit which was not the case in the experimental reference case. For the real size injector they found reasonable agreement in terms of mass flow and momentum, with the code overestimating the results.

Marcer et al. [28, 66] developed and improved a VOF-type interface tracking method to describe numerically the onset and development of cavitation within Diesel injectors using the named EOLE code. The EOLE code uses a multiphase Navier-Stokes KMT-VOF cavitation model (Kinematics and Mass Transfer VOF model). In this model, the cavitation dynamics is solved using the kinematic properties of the VOF model, considering that the liquid/vapour interface moves with a velocity equal to the liquid velocity. An additional thermodynamic effect was introduced as a source term to characterize mass transfer processes (vaporization and condensation). The authors performed

two-dimensional simulations of Diesel injector nozzles, considering two different entrance geometries (straight and rounded) and various upstream and downstream pressure levels. This numerical approach allowed to describe the onset and development of different cavitation regimes and a good agreement with experimental results was obtained for the discharge coefficients. Encouraging results were also achieved concerning the emission frequency of the cavitation pockets at the injector exit.

To conclude with the barotropic modelling approach, Catania et al. [81] applied and assessed a model based on the barotropic equation, which included a comprehensive thermodynamic approach for the simulation of cavitation. In the pure liquid field, thermal effects associated to the fuel compressibility were computed. For the cavitation simulation, different thermodynamic evolutions of the vapour and liquid mixtures were considered. The geometry consisted of 5 holes and of a reduced sac volume. Predicted time-histories of injector needle lift and pressure at two locations, for two engine loads at the same pump speed were successfully compared to experimental results, however no visualization results of the cavitation pattern were presented.

### **2.3.2 Bubbly mixture approach**

In this section the cavitation models presented are based on the assumption that cavitation is a pressure-difference driven phenomenon. Although the treatment of pressure is an essential part of all cavitation models, in the barotropic based ones it is considered in a thermodynamic context, contrary to the models that will be presented here.

Bubble growth rates have been investigated since the beginning of the last century. The simplest but very effective description for the bubble growth rate

is the Rayleigh relation [19], which is widely used in numerical computations, and is a basis for several multi-dimensional cavitation models. Rayleigh modelled an incompressible liquid surrounding an empty, spherical, cavity. He treated the liquid using a potential flow solution, with two boundaries: the surface of the bubble and the far-field. Rayleigh assumed that the pressure at the cavity wall was zero and that the pressure at infinity was constant, and calculated how a bubble of initial radius would collapse. However, his mathematical model predicted that as the cavity collapsed, the velocity at the walls would become infinite. Rayleigh recalculated bubble collapse when the cavity was filled with a gas, which limited the collapse velocity. Plesset [82] expanded the spherical cavity model to include surface tension and vapour pressure effects. He treated vapour pressure as a constant, and allowed the far-field pressure to be a prescribed function of time.

Knapp et al. [2] expanded the mathematical model by including the effect of ideal gas in the cavity. Their study was focused in explaining that in any real liquid flow there were a variety of gas bubbles which may serve as a nucleus for the initiation of cavitation. They also noted that there was a hysteresis in the appearance and disappearance of cavitation. Indeed, the pressure of cavitation disappearance was found to be different from the pressure at which cavitation appears.

Kato et al. [83] took into account both inertial and thermal effects in order to study the growth rate of cavitation bubbles. As an example, one extreme is cavitation of cold liquids where inertial effects dominate, and the other is boiling, where thermal effects dominate. From their simulations they concluded that the Jacob number ( $Ja$ ), which is the ratio of the liquid heat capacity to the required heat for evaporation, is the non-dimensional parameter with which the relative significance of thermal and inertial effects

can be determined. At low Jacob numbers thermal effects are significant, whereas at high Jacob numbers the inertial effects dominate. However, according to this model, the bubble growth in Diesel injectors would yield bubbles of 3mm radius, i.e much larger than the radius of the nozzle. This physically impossible result suggests that actually the bubbles never attain the size limit prescribed by heat transfer. This study is quite significant, since highlights the relative importance of thermal and inertial effects in bubble collapse.

Kubota et al. [16] proposed to relate the density evolution to the motion of bubbles in the flow. A given number of bubbles are considered at the inlet, and their evolution is governed by the Rayleigh-Plesset equation according to the pressure field. This model, which was named bubble two-phase flow (BTF) model, treated the two-phase flow as continuum by regarding the cavity as a compressible viscous fluid with greatly changing density, based on a local void fraction. The vapour fraction was determined at each location by the local bubble number density and bubble radius. Neither slip between the bubbles, nor bubble coalescence or break-up was taken into account. Additionally, the number density was assumed to be constant. Kubota et al. contributed to a modification of the bubble dynamics equation by considering a sub-grid scale bubble interaction. Both experimental and numerical studies were performed in order to validate the model. They tested the algorithm for a NACA0015 hydrofoil at three angles of attack and their results matched experimental data well. This model seemed reasonable for modelling low Mach number, large scale, cavitating flows. Nonetheless, the authors reported numerical problems in some cases and to ensure stability, they had to limit both the maximum and minimum void fraction.

Chen and Heister [84] presented shortly after a pressure-based cavitation model in which cavitation was modelled as a mixture, based on hydrodynamic equilibrium between the two phases. This meant that the pressure in the cavitation region was set equal to the vapour pressure. In previous work [85] the authors found that the direct use of this condition caused numerical instabilities. Therefore, they had to enforce the pressure equal with the vapour pressure condition indirectly. The turbulence modeling was neglected. They performed calculations for external flows over axisymmetric head forms, as well as for an internal flow in a sharp-edged orifice. In the external flow calculations, the predicted data agreed well with experimental data in terms of wall pressure distribution and radial extent of the cavitation region. The largest errors occurred in the back portion of the wake region. For the internal flow calculations a strong Reynolds number effect was found, which led to unsteady, periodic shedding of cavitating regions at higher Reynolds number.

Shortly afterwards Chen and Heister [86, 87] presented another model assuming the existence of small bubble clouds on a sub-grid scale. The flow inside single hole sharp-edged and rounded plain-orifice pressure atomizers typically used in Diesel engine fuel injectors was simulated in two dimensions. Results for sharp-edged orifices indicated that partially cavitating flows were typically periodic. Reducing the orifice diameter tended to inhibit both the initiation and the overall extent of the cavitation region. Even a slight rounding of the orifice inlet lip had dramatic effects on both cavitation and orifice discharge characteristics. Indeed, rounding tended to inhibit cavitation substantially, and increased the orifice discharge coefficient under both cavitating and non cavitating conditions. Finally, the cavitation field developed quite rapidly at the initiation of the injection process [86]. Two-dimensional simulations of external flows over various axisymmetric bodies [87] yielded

encouraging agreement with experimental data in terms of the cavity extent and cavity oscillation frequency.

The above model was further validated [88] by comparing predicted unsteady cavity lengths inside slots with chamfered orifices of various dimensions with the measured ones. The effects of orifice size, pressure drop, and site density (a free variable arising in the homogeneous fluid formulation related to the number of nucleation sites in the flow field) on the length and periodicity of the cavitation region were studied. The agreement was found to be good. The model was also used for three-dimensional simulations of a plain-orifice pressure atomizer by Bunnell and Heister [89]. The presence of cavitation was found to affect the orifice discharge coefficient, while the presence of a significant cavitation zone could impede vorticity transport inside the hole, causing nearly all the fluid to be ejected through a crescent-shaped sector of the orifice exit plane.

More recently, Mulemane et al. [90] compared the barotropic modelling approach with the Bubble Two Phase (BTF) one, as both were integrated in the same commercial code [91]. In addition, the standard  $k-\epsilon$  turbulence model was used. Different Diesel fuel injector nozzle configurations (VCO/Minisac type, sharp/rounded inlet) with injection pressure of 1000 bar and a backpressure of 1 bar were used. The BTF model predicted less vapour compared with the barotropic model, which reflected also on the discharge coefficients when comparing with experimental values at full needle lift, with the Barotropic model closer to experiment. The vapour distribution predicted by the BTF model was differently spread in the flow field; the cavitation was restricted along the orifice lower regions and it was extended over a larger region, while for the barotropic case, the vapour phase was

present both in the upper and the lower regions downstream of the orifice entrance.

Although, in the current work cavitation is studied in Diesel injectors, the phenomenon is found in a wide range of engineering fields, i.e. turbomachinery and hydrodynamics. Accordingly, modelling efforts have been implemented in different geometries, mostly simplified and some of them are discussed in the next paragraphs.

The simplified bubble dynamics model by Tamura et al. [92, 93], which is an advancement of the Matsumoto et al. [94] work, has an hybrid structure of mixture and two-fluid elements. The model assumed that the liquid phase was incompressible and the gas phase compressible, consisting of spherical bubbles. The bubbles were allowed to have slip velocity so that bubble accumulation could be simulated. Two-dimensional simulations around various wing sections were performed, and the predicted drag and lift coefficients as a function of cavitation number were in qualitative agreement with the experiments. They proceeded in three-dimension simulations of the wing geometry in order to demonstrate the applicability of the model to three-dimension problems, without however proceeding to validation of the model. The authors highlighted the necessity to apply the model to more practical flow fields.

Different authors, as cited in following paragraphs, proposed more recently to consider a transport equation model for the void ratio, with vaporization/condensation source terms to control mass transfer between the two phases and governed by the difference between the local pressure in the mixture and the vapour pressure. The method avoids using quantities like bubble number density and initial bubble diameter. Also, it has the advantage

that it accounts for the time influence on the mass transfer phenomena, through empirical laws for the source term.

Kunz et al. [95] have employed different equations for the evaporation and condensation rates, which have been applied to simulate a number of high density ratio sheet- and super-cavitating flows. Two-dimensional predictions of the flow around various axisymmetric bodies showed good agreement with measured pressure distributions and drag-coefficients. Furthermore, from these two-dimensional and further three-dimensional simulations of flows about an axisymmetric ogive at angle-of-attack and a control surface interacting with a phase-separated gas-liquid stream, the ability of the model to predict the inherent physics in steady-state and transient sheet- and super-cavitating flows was verified. This model was applied to other cavitating flows subsequently [96] with quite satisfactory results. In particular, the validation results included measurements of vaporous cavity flow in a Venturi section previously reported by Stutz and Reboud and Reboud et al. [97, 98] and measurements of ventilated cavity flow over a conical forebody and cylinder and vaporous cavitating flow over a blunt cylinder previously reported by Stinebring et al [99, 100].

A similar multi-phase model for low speed gas/liquid mixtures was proposed by Ahuja et al. [101]. The rates of evaporation and condensation were both approximated as linear functions of pressure. Turbulence was modelled using the low-Reynolds number version of the  $k-\epsilon$  turbulence model, applied to the mixture. The solution procedure had an interface-capturing scheme that incorporated an additional scalar transport equation for the gas void fraction. Cavitation was modelled via a finite rate source term that initiated phase change when liquid pressure dropped below its saturation value. The rate constants were tuned in order to achieve agreement with the experimental

results in steady-state sheet cavitation for flow around cylindrical bodies [102] and NACA 66 hydrofoil [103].

Senocak and Shyy [104] presented a pressure-based algorithm for turbulent cavitating flow computations. Single-fluid Navier-Stokes equations, cast in their conservative form, along with a volume fraction transport equation were employed. The flow field was computed for both phases with the vapour pressure recovered inside the cavity via a mass transfer model. A pressure-velocity-density coupling scheme was developed to handle the large density ratio associated with cavitation. The method was assessed through simulations of cavitating flows over a cylindrical object and an airfoil. In a later study Senocak and Shyy [105, 106], proposed a cavitation model based on the analysis of interfacial dynamics (liquid-vapour interface) in an attempt to address the empiricism of existing transport-equation-based models adopted in the literature, largely determined through numerical experimentation. In the first part of the investigation they evaluated their model by comparison with existing cavitation models for flows around an axisymmetric cylindrical body and a planar hydrofoil, and through a convergent-divergent nozzle by performing steady state simulations. The authors found that, although all models provided qualitatively comparable wall pressure distributions in agreement with experimental results, there were quantitative differences in the closure region of the cavity, due to the different compressibility characteristics of each model. With the unsteady simulations performed in [106] they found better agreement of the velocity and vapour volume fraction distributions within the cavity. An important conclusion of this study is that the implication of the compressibility, reflected via the speed of sound definition, remains an open question, since each cavitation model defines a different speed of sound.

The model of Singhal et al. [107] accounted for the formation and transport of vapour bubbles, the turbulent fluctuations of pressure and velocity, and the amount of non-condensable gases, which are dissolved or ingested in the operating liquid. The phase-change rate expressions were derived from a reduced form of the Rayleigh-Plesset equation for bubble dynamics. These rates depend upon local flow conditions (pressure, velocities, turbulence) as well as fluid properties (saturation pressure, densities, and surface tension). The phase-change rate expressions employed two empirical constants, which were calibrated with experimental data covering a very wide range of flow conditions without the need of adjustments for different problems. Final validation results were presented for flows over hydrofoils, submerged cylindrical bodies, and sharp-edged orifices. The model of Singhal et al. has been implemented in commercial codes [108, 109].

Recently, cavitation models of this category have been applied to geometries typical for Diesel injector flow study. Srinivasan et al. [70] presented another pressure-based methodology employing HEM assumption for simulating high speed unsteady viscous cavitating flows. In the model, two-dimensional compressible two-phase single-fluid Navier-Stokes equations are solved. In a later study, Srinivasan et al. [110] developed a sophisticated model for predicting vapour dynamics occurring in multi-dimensional incompressible flows, which included a novel cavitation-induced momentum defect term in the liquid phase momentum equation. The results obtained by the model were in good qualitative agreement with experiments for unsteady cloud cavitation behaviour, though they were limited to planar nozzle flows.

Grogger and Alajbegovic developed a three dimensional cavitation model [111, 112, 113] that instead of treating cavitation as a single mixture, employed the two-fluid approach with consideration of bubble dynamics.

Transport equations for each phase were solved, and the exchanges of mass, momentum and turbulence between the phases were modelled. In particular, the mass exchange was approximated using a simplified Rayleigh-Plesset equation. The number density of cavitation bubbles was modelled taking into account the coalescence of bubbles at higher volume fraction levels. For turbulence closure, the standard  $k$ - $\epsilon$  model was modified by introducing an extra bubble-induced eddy viscosity. Additionally, turbulent dispersion was added to the momentum interaction terms between the two phases. The authors compared the photographs of steady-state cavitation structures in a small-scale asymmetrical planar nozzle in both steady and transient injection pressures, and they demonstrated the ability of the model to predict the cavitation development. It has to be pointed out that this model has been implemented in the commercial code FIRE [114].

Wang and Su [115] simulated cavitating flows inside a Diesel injector-like nozzle using the above two-fluid model implemented in the commercial code [114]. They evaluated the flow characteristics under constant and fluctuant inlet pressure. The numerical results showed that the appearance of supercavitation in the nozzle induced changes of the flow field structures and exit characteristics. The upstream pressure fluctuations significantly influenced the cavitation process. Hence, the authors stated the importance of studying the upstream pressure fluctuations in realistic Diesel injector cases.

The bubble model of Sou et al. [116, 117] was based on the Lagrangian frame of reference, in which they tracked each bubble separately. Constant diameter bubbles were introduced in the liquid, and when pressure reached a pre-chosen value they collapsed immediately. Large Eddy Simulation (LES) was used to predict turbulent flow. The numerical simulation of the transient

cavitating flow in an axisymmetric nozzle was conducted. They found that the calculated results of pressure distribution along the wall, the relation between injection pressure versus flow rate, and bubble distribution agreed with experimental results. Moreover, cavitation bubble clouds were periodically shed from the vena contracta, which usually formed by the coalescence of a few small bubble clouds. Finally, collapse of cavitation bubbles due to the re-entrant jet was observed in the numerical simulation.

Recently, Sou and Kinugasa [118] presented a three-dimensional LES calculation of incipient and developing cavitation with tiny bubbles and low volume fraction of cavitation in a rectangular nozzle. The growth and collapse of cavitation bubbles and nuclei was computed by Lagrangian tracking of the trajectories and by solving the Rayleigh-Plesset equation. In their experiments, the authors used discharged filtered tap water through a rectangular nozzle into ambient air. To verify the validity of the model, transient cavitation motion and turbulent velocity of the nozzle were acquired by using a high-speed camera and LDV technique. A preliminary simulation of a fully-developed turbulent flow in a channel, in which periodic boundary conditions were adopted for the inlet and exit, was carried out to generate inlet boundary conditions for the nozzle simulation. The predicted tendencies showed qualitative agreement with the experimental observations.

Shi and Arafin [119] adopted a model implemented in a commercial code [120] to study numerically the effect of fuel properties and fuel temperature changes on the cavitating flow in Diesel injector-like geometries. The liquid and the vapour phases were treated as a homogeneous mixture with a transport equation for the volume fraction of the vapour phase. The cavitation induced inter-phase mass transfer was calculated by a cavitation model based on the Rayleigh-Plesset-Equation. The model predicted significant

vortex cavitation phenomena in the throttle with strong asymmetry but unfortunately, no comparison with experimental visualization results performed. However, it was found that both the fluid viscosity and density changes had a significant effect on cavitation. In contrast, the pressure variation of the fuel saturation vapour had no significant effect, due to the very high pressure gradient caused by the flow acceleration. With all other properties kept constants, increasing the Reynolds number by increasing the density or decreasing the viscosity led to stronger flow acceleration and enhanced cavitation in a nozzle, and to a slight increase in flow efficiency in the flow regime below the critical cavitation point.

Martynov et al. [121] proposed a model based on bubble dynamics theory taking into account the bubbly nature of cavitation and assuming local homogeneity of the vapour-liquid flow. The cavitation model was built from correlations for evaporation and condensation, and an equation for the density number of cavitation bubbles, derived by assuming hydrodynamic similarity of cavitation flows. Additionally, it took into account the effect of liquid surface tension on the number density of active cavitation nuclei instead of fixing the nuclei number density. This criterion determined the onset of cavitation in the flowing liquid, and though very novel, it seems rather impractical since requires a thorough analysis of the flow to fulfill the criterion. The model applied for calculation of steady-state cavitation flows in nozzles, where the number density of cavitation bubbles was tuned in order to best fit with the cavitation patterns of available experimental results. The authors found that even by this adjustment the observed amount of vapour was difficult to be reproduced. It should be mentioned that the model was implemented into the VECTIS computational fluid dynamics code [122].

Another variant of the bubble model is the approach of Yuan et al. [123]. With respect to previous work of Sauer and Schnerr [124, 125] the turbulence was also modelled and simulations of cavitation flow on symmetric injection nozzles were performed. This approach was based on a combination of the VOF technique, originally developed for free surfaces [126] with an additional model for the growth and collapse of bubbles [19]. The vapour was assumed to consist of mini spherical bubbles with a varying radius and a constant number density with respect to the local volume of liquid phase only. From this study it was concluded that the overall extension of the cavitation region depended on the liquid quality described by the nuclei concentration and the nuclei radii, as well as the nozzle pressure difference. Higher nuclei concentration and larger nuclei radii, as well as lower pressure at the nozzle exit, caused larger overall extension of the cavitation. The study also demonstrated that the rounding of the hole entrance tended to inhibit the extension of the cavitation region and that the separation of the flow was caused by the sharpness of the entrance as well as by the cavitation process. In a later study, Yuan and Schnerr [127] studied the effect of the inlet boundary condition and demonstrated that different types of injection pressure fluctuations influenced the extension of cavitation and the phase shift between the time history of the inlet pressure and the cavitation process.

To conclude the discussion concerning this model category, Giannadakis et al. [128] developed an advanced cavitation model for automotive fuel injection systems based on an Eulerian-Lagrangian approach. In their model, the continuous phase flow was described in the Eulerian frame and the effects of the dispersed phase were taken into account. For the dispersed phase (i.e., bubbles), a bubble parcel concept was introduced to simulate the whole population of actual bubbles. Each bubble parcel had a number of non-interacting bubbles, with the same properties and experienced the same

physical processes. The detailed physical sub-processes such as bubble formation, momentum exchange between the bubbles and the liquid phase, bubble growth and collapse, bubble turbulent dispersion, bubble turbulent and hydrodynamic breakup were also incorporated into the model.

The validated model was applied to the simulation of cavitation in real size six-hole geometries, in order to identify the different patterns in these injectors. However, the calculations performed at a low injection pressure (200 bar) and unfortunately no experimental results were presented for these predictions for comparison. Firstly, the model was applied to the simulation of cavitation in a real-size six-hole gasoline nozzle, having a characteristic geometry with one hole at the centre and five side holes arranged in an asymmetric way. From the predictions it was found that the flowrate of the centre hole was higher, expecting to lead to a different spray pattern compared with the side holes. In addition, the predictions revealed a much more transient cavitation behaviour of the side holes implying a better atomising. Then, the cavitation model was employed in predicting the cavitating flow in a real-size Pintle-type piezo-driven gasoline nozzle; the calculations prompted for an inherently unsteady and periodic in the circumferential direction flow attributed to the cavitation, in conjunction with the intrinsic asymmetries of the nozzle.

## **2.4 Studies taking into account needle displacement.**

A large number of numerical and experimental studies have examined the effect of the injector needle lift and eccentricity on the cavitating flow, considered as a determinant factor in the cavitation intensity. These are presented and discussed in this chapter.

Focusing on the effect that the needle displacement has on the cavitating flow, the work of Favennec and Fruman [129] is worth mentioning. They carried out an experimental investigation in order to determine the flow coefficients of the orifices in the VCO design, as a function of the degree of cavitation and needle position. They presented results in a steady state regime for a variety of upstream and downstream pressures and seven geometric positions of the needle: without the needle and with 10, 25, 50, 100, 200 and 300  $\mu\text{m}$  needle lifts. The results show that, without the needle and whatever the upstream and the downstream pressure levels, the flow coefficient becomes function of the cavitation number only as soon as cavitation appears. It decreases regularly when cavitation is developing and reaches a near plateau when cavitation is fully developed. In agreement with reported literature, the results depended on the Reynolds number for low cavitation numbers. For the smallest needle lift, 10  $\mu\text{m}$ , the curves of the flow coefficient versus cavitation number were similar to the ones obtained without the needle when plotted for constant upstream pressures. However, a different curve was obtained for each upstream pressure. For needle lifts larger than 300  $\mu\text{m}$ , no difference could be observed compared to the case without needle.

Argueyrolles et al. [130], presented numerical results of fixed needle lift calculations at low and high lifts with the two-phase flow 3D code EOLE [66]. They investigated the behaviour of VCO and microsac nozzles, as a function of hole position, needle shape, maximum needle lift and hole exit diameter in order to explain the differences between the discharge coefficients. The most important parameter was found to be the maximum needle lift. The code predicted secondary cavitation pockets that were more frequent at low needle lift.

The effect of needle movement on cavitation was investigated also by Som et al [131], who performed simulations at different needle lift positions. A mixture based model implemented in FLUENT V6.2 software was employed for the simulations. The model predicted cavitation patterns that shifted significantly with the needle lift position during an injection event. The region of significant cavitation shifted from top to bottom of the orifice as the needle position was changed from fully open (0.275 mm) to nearly closed (0.1 mm), and this behaviour was attributed to the effect of the needle position on the flow upstream of the orifice. However, the authors performed two-dimensional calculations only, neglecting thus important characteristics of the flow.

More recently, Oda et al. [132] studied both experimentally and numerically the effects of the eccentric location of a needle on internal cavitating flow and spray cone angle of a large-scaled valve-covered-orifice (VCO) Diesel nozzle. They performed a steady-state experiment by using a 10 times large-scaled VCO nozzle. The needle was manipulated by a three-dimensional traverse with micrometers. The test liquid was water and they tested low/high needle lifts as well as different radial locations of the needle. The authors found experimentally that when the needle is perpendicularly positioned to the nozzle hole at low needle lift, four different regimes of cavitating flow appeared in the nozzle flow: upperside and lowerside sheet cavitation, upperside sheet cavitation and partial vortex, fully covered vortex cavitation, partial vortex cavitation. In the same geometric condition they observed two regimes of primary atomization, the so called “hollow cone spray” regime (increased angle) and the so called “solid cone spray” regime (lower angle). In addition, reduction of spray cone angle of the hollow cone spray was observed experimentally when atmospheric air was introduced from the hole entrance and the “air-core” was produced inside the nozzle hole. The spray cone angle was found to vary with the needle eccentricity. However, the

authors did not establish a clear relationship between the cavitation pattern and the spray cone angle. The authors compared the experimental results with CFD results of internal cavitating flow and spray cone angle. They used the code STAR-CD version 4.02 by performing fixed needle lift calculations and they incorporated the VOF model into the calculations to capture the formation of the air-core. Numerically, the authors predicted asymmetric flow between the seat and the needle by obtaining a map of streamlines, which they attributed to the needle displacement. However, they did not present any numerical results obtained with a concentric needle position. Generally, the authors claimed that the model confirmed the experimental results. However, they only presented results for low needle lift and one radial location of the needle.

The needle lift and also the eccentricity were also examined experimentally by Arcoumanis et al. [8]. In a steady state test-rig with a 20-times enlarged mini-sac acrylic multi-hole nozzle, the authors observed that the onset of cavitation occurred at almost the same cavitation number, independently of the needle lift. Furthermore, hysteresis was identified on the cavitation number of incipience (onset of cavitation bubbles) and desinense (disappearance of cavitation bubbles). In addition to hole cavitation, the authors also reported string cavitation, formed inside the sac volume. Concerning the string cavitation, it was found that its location depended on the eccentricity of the needle and its lift. However, its location and formation was found to be independent of the cavitation number. These strings seemed to develop transiently and periodically between adjacent holes and to interact with pre-existing cavitation films giving rise to significant disturbances of the flow and hole-to-hole variations, even in axisymmetric vertical multi-hole nozzles.

Masuda et al. [30] performed nozzle internal flow calculations linking the three-dimensional Eulerian internal flow calculation [113] with the Eulerian-Lagrangian spray calculation to calculate cavitation flow within real size six-hole nozzles. In the multi-fluid approach, the model equations are obtained through the ensemble averaging process [133]. In this approach, the computational domain consisted of both the nozzle injector and the spray chamber, though the spatial resolution and its effect on the results were not detailed. The needle movement during the injection period was taken into account in this calculation by imposing the needle lift law. The numerical results showed two pairs of twin vortices in the cross section near the nozzle hole inlet, which caused the cavitation bubble distribution to separate into two regions pertaining throughout the injector, towards the nozzle exit. At full needle lift, the cavitation region showed an almost steady state behaviour. The transient data of spatial distributions of velocity, turbulent kinetic energy, dissipation rate, void fraction rate, etc. at the nozzle exit were extracted. These output data was transferred to the spray calculation, in which a primary break-up model [134] was applied to the Discrete Droplet Model (DDM) [135]. The spray calculations predicted that the cone angle became large at the beginning and the end of the injection period and this was linked with predicted vortices at low needle lifts. However, it should be mentioned that the basic assumption for the approach is that there is no feedback from the flow in the spray chamber to the nozzle flow simulation [136]. Under Diesel engine like conditions this is a sufficiently good approximation as long as no backward flow from spray into a cavitation region occurs.

Later on, Du et al. [137] applied the same calculation methodology to investigate the internal flow and spray of a nozzle with orifices having different angles ( $45^\circ$  and  $90^\circ$  direction) with respect to the injector axis. The nozzle internal flow was calculated using the same Eulerian three-fluid model [113]

as Masuda et al., where Diesel fuel liquid, Diesel fuel vapour, and ambient gas were considered for a Diesel injector case. Though, the calculations performed at a low injection pressure (300 bar), since the common rail injectors operate at pressures exceeding 1300 bar. The needle valve movement during the injection period was also taken into account in the calculations, however the authors did not specify how they imposed the needle lift law. These calculations yielded as hole exit data the velocity components of the liquid phase, density of the liquid and vapour phase, turbulence kinetic energy and turbulence energy dissipation of the liquid phase and volume fraction of the vapour phase. These data were then transferred to the primary break-up model as a boundary condition. The calculation results were compared with the results of the measurement data of spray. Predicted spray morphology and penetration showed good agreement with the experimental data. From this study, it was concluded that the fuel spray from lower orifice goes faster at the beginning of the injection since the fuel pressure increases in the lower region of the sac volume firstly. At high needle lift, the fuel pressure became more uniform in the upper orifice (45° direction) which could reduce flow loss, and increase the spray penetration.

Gavaises et al. [138] used a stochastic CFD cavitation model [71] to characterize the cavitating flow distribution inside Diesel multi-hole VCO nozzles with convergent tapered holes during the transient opening/closing of the needle valve. Tapered holes were found to significantly reduce or even eliminate the formation of geometric-induced cavitation at sufficiently high needle lifts. The flow inside the tapered holes was found to be more affected by the non-uniform flow distribution developing upstream of the hole entry. This resulted in the formation of secondary vortices which were found to propagate to the nozzle hole exit; thus, according to the authors, nozzles with

tapered holes may be more sensitive to the formation of string cavitation. The motion of the needle valve affected significantly the cavitation intensity for both the cylindrical and the tapered nozzle holes.

In the work of Lee and Reitz [139] calculations with needle movement were simulated using the arbitrary Lagrangian-Eulerian (ALE) approach. For the simulation of cavitation they used HEM approach and for this, the KIVA-3V code was modified to implement a generalized equation of state. It was demonstrated that the model could predict the effect of nozzle passage geometry on the flow structure and cavitation. Special interest was focused on the transient behaviour during the nozzle closing period in single-hole nozzles and multi-hole nozzle configurations (minisac and valve-covered orifice eight-hole nozzles). The authors suggested that there is some optimum lift profile in the needle closing movement. They noted that during the nozzle closing period, the fast decrease in flow rate could increase the cavitation. In this case, the flow speed at the exit is faster than the flow speed in the middle of the nozzle, so that the average pressure inside the nozzle drops and the flow cavitates more easily. The fast closing of the needle could cause cavitation even in nozzles that do not exhibit cavitation in most conditions. In particular, it was shown that the cavitation inside the nozzle passage increased temporarily before it collapsed if the needle closing speed was relatively high (0.7 m/s). If the needle was closed slowly (0.175 m/s), the cavitation collapsed at the end-of-injection in all of the nozzles investigated in their study.

More CFD studies of the needle eccentricity have recently appeared in the literature. Chiavola et al. [67] investigated numerically a Diesel engine high pressure six-hole minisac injector in which the influence of needle motion characteristics on the internal flow was evaluated. A radial perturbation of the

axial needle motion was imposed to analyze its effect on the nozzle flow features. A comparison with a fully axial needle simulation was also performed. The model developed was based on the coupling between a 1D and a 3D code. The injector was modelled in 1D and the results obtained from the injector simulation, in terms of injection needle lift time evolution, were then used to initialize the computation within a CFD code of two-fluid approach [114] for the internal injector flow. The authors concluded that the radial component of the needle displacement was responsible for significant differences in the nozzle flow conditions since the eccentricity affected the velocity field characteristics of the annulus between the needle and the injector body and of the volume sac. In particular, they found that in the hole closest to the needle the cavitation appears on the lower half of the nozzle due to the sac flow field features. The minimum flow differences among the nozzles were observed in correspondence to the maximum needle lift. Thus, the authors deduced that without modifying the opening and closing phases, the longer is the duration of injection, the lower is the relevance of eccentricity on the flow. Unfortunately, no experimental results were presented for validation purposes.

Concluding with the needle displacement studies, Ciatti et al. [140] presented results adopting the same CFD code [114,141] in order to evaluate the flow field and cavitation. Calculations were referred to two types of VCO injectors with the same geometrical layout, but different number of holes and maximum lift value. The standard injector with 6 holes and lift of 0.43 mm was indicated as Injector1, whereas the modified injector, with 7 holes and maximum lift of 0.2 mm was called Injector2. On one hand, a comparison between the standard and the modified injector was performed for an axial needle displacement. The authors reported differences in the flow field and cavitation regions inside the holes, which were attributed as expected to the different

annulus between the seat and the needle, forcing the flow to turn roughly to enter the holes. The authors did not analyze the effect of having an additional hole. On the other hand, the response to a radial perturbation of the needle lift was evaluated for both injector layouts. One displacement was considered for injector 1 and two different displacements for injector 2. Concerning the value of eccentricity, a higher radial component resulted in a larger flow imbalance. However, the authors' main interest was focused on the macroscopic response of the flow field to the different injector layouts (especially in terms of hole to hole variations) and they did not give a detailed characterization of the cavitating phenomena.

## **2.5 Summary**

In this chapter, the literature survey has been made to review the results of experimental cavitation studies in nozzles, of numerical models developed for prediction of cavitation flows and results of studies focusing on the effect of needle displacement on cavitating flow. Some important conclusions can be drawn from this study, regarding the purpose of the present work.

There have been various experimental studies to capture the cavitation phenomenon in scaled-up transparent nozzles. It was observed that cavitation does not scale up, and therefore actual size experiments are needed to depict the cavitating flow behaviour. Nevertheless, some similarity may be noted, since in both large-scale and real-size injector nozzles the flow is highly transient and there is an inherent interaction between cavitation and turbulence. However, the real size of the nozzles and high speed of the fuel injection make direct observation difficult. Most early studies concentrated on one-hole cavitation, typically formed in the recirculation zone at the hole inlet, while recent experimental studies have revealed the presence of additional

cavitation structures in the sac volume of both valve covered orifice and sac type fuel injectors. Although experimental measurements of needle movement are becoming available, the flow in the sac volume still needs to be studied, mainly due to the extremely small geometry and very short transient time scales in real size Diesel injectors. Many irregular cavitating structures have been observed in both scaled-up and real geometries: “geometrically induced cavitation” which occurs in flow areas with sharp corners such as at the entrance into the nozzle holes, “string” or “vortex” type cavitation, which extends throughout the nozzle and is the main source of instability in the sprays exiting the nozzle holes, and “needle” cavitation which initiates in the needle seat and extends to the opposite nozzle hole when it is fully developed.

Experimental studies of cavitation flows with enlarged and real-scale nozzles have revealed that the geometry of the nozzle, needle position and operating conditions determine the pattern of the cavitation flow. They also provide useful data for testing and validating cavitation models.

Regarding the effect of orifice geometry on the injection rate in a common rail fuel injection system it was concluded that the discharge coefficient was higher for tapered nozzles than for cylindrical nozzles. Also, increasing the taper and radius of inlet curvature can hinder the appearance of cavitation, as well as increase spray tip penetration.

Concerning the influence of cavitation on the spray characteristics, it has been concluded that cavitation can improve the atomization of the emerging fuel. It was observed that as soon as cavitation appeared at the hole exit, the spray angle increased. It has been also reported that cavitation may affect the levels of flow turbulence within the nozzle and at the exit. However the

individual contribution of either cavitation or turbulence in atomization has not been clearly identified.

Various studies have appeared in the literature about the simulation of the cavitation inception and development, aiming at assessing the ability of cavitation models to predict the flow behaviour. As discussed above, the various cavitation models have been categorized into two groups, those based on the barotropic equation approach and those based on the bubbly mixture approach. In the subsequent chapters the application of a model of the second category will be presented.

Many of these models are now incorporated in commercial CFD codes. Some of them have been applied to nozzle flow simulations, and it has been demonstrated that cavitation modelling has reached a level of maturity such that it allows predicting the effects of geometry and operating conditions with reasonable accuracy. This represents a valuable contribution to the understanding of nozzle performance. However, most of the models are validated based on the comparison with flow images and at a low injection pressure, since the common rail injectors operate at pressures exceeding 1400 bar. Generally speaking, it is uncertain if cavitation models can capture the highly transient nature of the cavitating flow.

Several studies predicting the effect of needle position on nozzle internal flow in steady state regime have been presented in the past few years. Because of the complexity of moving mesh calculations of real size injectors, the nozzle flow is often studied at full needle lift only or by quasi-steady state fixed needle lift calculations, so that little is known about the transient phase of the needle opening/closing. An increased number of studies have compared the effects of steady-state and transient boundary conditions on the nozzle exit

results using fixed geometry domains. More recently, studies have been performed with moving mesh calculations in an attempt to study the effect of the transient opening/closing of the needle valve on the injector internal flow. The calculations allowed to identify the significant effect of the needle motion on the cavitation distribution and to observe complex phenomena that have to be further investigated.

## **CHAPTER 3.**

### **RESEARCH TOOLS**

#### **3.1 Introduction**

As mentioned in the introductory subsection 2.1, both experimental results and CFD calculations have been employed for analysing the flow development in the specific nozzles that will be detailed below. A brief description of the experimental facilities, as well as a description of the models implemented for the simulations is reported to help the reader to better evaluate the predicted results.

#### **3.2 Numerical Models**

In the current study, the commercial code STAR-CD based on finite volume method is used for flow and cavitation prediction. This part of the document describes the mathematical modelling practices employed in the code. The description commences with a statement of the basic differential conservation equations solved. Following this, the particular mathematical models to account for the turbulence in the calculations are presented.

### 3.2.1 Governing equations for fluid flow

The mass and momentum conservation equations solved by STAR-CD for general incompressible and compressible fluid flows are in Cartesian notation:

$$\frac{\partial \rho}{\partial t} + \frac{\partial}{\partial x_j} (\rho u_j) = s_m \quad (3.1)$$

$$\frac{\partial \rho u_i}{\partial t} + \frac{\partial}{\partial x_j} (\rho u_j u_i - \tau_{ij}) = -\frac{\partial p}{\partial x_i} + s_i \quad (3.2)$$

In general non-steady coordinates the equations take the following form [142]:

$$\frac{1}{\sqrt{g}} \frac{\partial \rho}{\partial t} (\sqrt{g} \rho) + \frac{\partial}{\partial x_j} (\rho \tilde{u}_j) = s_m \quad (3.3)$$

$$\frac{1}{\sqrt{g}} \frac{\partial}{\partial t} (\sqrt{g} \rho u_i) + \frac{\partial}{\partial x_j} (\rho \tilde{u}_j u_i - \tau_{ij}) = -\frac{\partial p}{\partial x_i} + s_i \quad (3.4)$$

Where  $t$  is time,  $x_i$  the Cartesian coordinate ( $i=1,2,3$ ),  $u_i$  the absolute fluid velocity component in direction  $x_i$ ,  $\tilde{u}_j$  the relative velocity ( $u_j - u_{cj}$ ) between the fluid and local (moving) coordinate frame that moves with velocity  $u_{cj}$ ,  $p$  the piezometric pressure,  $\rho$  the density,  $\tau_{ij}$  stress tensor components,  $s_m$  the mass source,  $s_i$  the momentum source components and  $\sqrt{g}$  is the determinant of the metric tensor.

### 3.2.2 Equations of moving mesh operations

For moving-boundary problems, an additional equation called the 'space conservation law' [143] is solved for the moving coordinate velocity components:

$$\frac{1}{\sqrt{g}} \frac{\partial \sqrt{g}}{\partial \tau} - \frac{\partial}{\partial x_i} (u_{cj}) = 0 \quad (3.5)$$

The equation relates the change in cell volume to the cell-face velocity. The satisfaction of the space conservation law together with the mass, momentum conservation equations facilitates the general moving mesh operations.

### 3.2.3 Turbulence equations

Additionally to the aforementioned conservation equations, the conventional two-equation low Reynolds number  $k$ - $\epsilon$  model has been used to simulate the effects of turbulence with transport equations as follows. The mathematical details of the model are not repeated here as they can be found elsewhere [144].

#### Turbulence kinetic energy equation

$$\frac{\partial}{\partial t}(\rho k) + \frac{\partial}{\partial x_j} \left[ \rho u_j k - \left( \mu + \frac{\mu_t}{\sigma_k} \right) \frac{\partial k}{\partial x_j} \right] = \mu_t (P + P_B) - \rho \epsilon - \frac{2}{3} \left( \mu_t \frac{\partial u_i}{\partial x_i} + \rho k \right) \frac{\partial u_i}{\partial x_i} + \mu_t P_{NL} \quad (3.6)$$

where

$$P \equiv S_{ij} \frac{\partial u_i}{\partial x_j} \quad (3.7)$$

$$P_B \equiv - \frac{g_i}{\sigma_{h,t}} \frac{1}{\rho} \frac{\partial \rho}{\partial x_i} \quad (3.8)$$

$$P_{NL} = - \frac{\rho}{\mu_t} \overline{u'_i u'_j} \frac{\partial u_i}{\partial x_j} - \left[ P - \frac{2}{3} \left( \frac{\partial u_i}{\partial x_i} + \frac{\rho k}{\mu_t} \right) \frac{\partial u_i}{\partial x_i} \right] \quad (3.9)$$

$P_{NL} = 0$  for linear models,  $\sigma_k$  is the turbulent Prandtl number and  $\mu_t$  is the turbulent viscosity. The first term on the right-hand side of equation (3.6) represents turbulent generation by shear and normal stresses and buoyancy forces, the second, viscous dissipation, and the third, amplification or attenuation due to compressibility effects.

**Turbulence dissipation rate equation**

$$\begin{aligned} \frac{\partial}{\partial t}(\rho\varepsilon) + \frac{\partial}{\partial x_j} \left[ \rho u_j \varepsilon - \left( \mu + \frac{\mu_t}{\sigma_\varepsilon} \right) \frac{\partial \varepsilon}{\partial x_j} \right] = C_{\varepsilon 1} \frac{\varepsilon}{k} \left\{ \mu_t (P + P') - \frac{2}{3} \left( \mu_t \frac{\partial u_i}{\partial x_i} + \rho k \right) \frac{\partial u_i}{\partial x_i} \right\} \\ + C_{\varepsilon 3} \frac{\varepsilon}{k} \mu_t P_B - C_{\varepsilon 2} (1 - 0.3e^{-R_t^2}) \rho \frac{\varepsilon^2}{k} + C_{\varepsilon 4} \rho \varepsilon \frac{\partial u_i}{\partial x_i} + C_{\varepsilon 1} \frac{\varepsilon}{k} \mu_t P_{NL} \end{aligned} \quad (3.10)$$

where  $\sigma_\varepsilon$  is the turbulent Prandtl number and  $C_{\varepsilon 1}$ ,  $C_{\varepsilon 2}$ ,  $C_{\varepsilon 3}$  and  $C_{\varepsilon 4}$  are coefficients whose values are kept as the defaults in the configuration of the model. The right-hand side terms represent effects analogous to those described above for the  $k$  equation. The first term on the right-hand side represents the contribution to the production of dissipation due to linear stresses and dilatation / compression effects, the second, the contribution due to buoyancy, the fourth, the contribution due to temporal mean density changes and the fifth, the contribution due to non-linear stresses. The third term in the equation accounts for the dissipation destruction. The additional term  $P'$  is given by

$$P' = 1.33 \left[ 1 - 0.3e^{-R_t^2} \right] \left[ P + 2 \frac{\mu}{\mu_t} \frac{k}{y^2} \right] e^{-0.00375 \text{Re}_y^2}$$

$\mu_t$  is defined by equation

$$\mu_t = f_\mu \frac{C_\mu \rho k^2}{\varepsilon} \quad \text{with} \quad f_\mu = \left[ 1 - e^{-0.0198 \text{Re}_y} \right] \left( 1 + \frac{5.29}{\text{Re}_y} \right) \quad \text{in which} \quad \text{Re}_y = \frac{y \sqrt{k}}{\nu}$$

where  $y$  is the normal distance to the nearest wall and  $R_t$  the turbulent Reynolds number given by

$$R_t = \frac{k^2}{\nu \varepsilon}$$

The equation for dissipation is not solved at the near-wall cell. Rather, the dissipation,  $\varepsilon_P$ , at the near-wall cell is fixed as follows:

$$\varepsilon_p = \frac{2\nu k}{y^2}$$

Where  $y^+$ , the dimensionless normal distance from the walls, (commonly used in boundary theory layer and in defining the law of the wall), should be of the order of 1.0.

### 3.2.4 Cavitation modelling

For the modelling of cavitation, the liquid and the vapour phase are treated as a mixture with a transport equation for the volume fraction of vapour phase which is computed using equation (3.11):

$$\frac{\partial a_v}{\partial t} + \nabla(a_v u) = Sa_v \quad (3.11)$$

Where subscript  $v$  denotes the vapour phase,  $u$  is the flow velocity and  $Sa_v$  is the cavitation induced mass source/sink term of volume fraction  $a_v$ , which is calculated by a model based on bubble growth theory [19]:

$$Sa_v = \frac{4\pi R^2 n_o}{1 + (4\pi R^3 / 3)n_o} \frac{dR}{dt} \quad (3.12)$$

The bubble radius  $R$  changes according to the local pressure  $p$  around the bubble, as bubbles move through the solution domain (no prescribed number of spherical bubbles of radius  $R$  within a unit volume of liquid). The rate of change of a bubble radius along its path (the bubble growth velocity) is estimated using equation (3.13) which is a simplification of the more general Rayleigh-Plesset equation.

$$\frac{dR}{dt} = \text{sign}(p_v - p) \sqrt{\frac{2|p_v - p|}{3\rho_l}} \quad (3.13)$$

where  $p_v$  is the saturation pressure and  $\rho_l$  is the liquid density. Cavitation occurs when the liquid pressure falls below a certain critical value, associated

with the saturation pressure  $p_v$ .  $P_{crit}=3000$  Pa for the studies presented in this thesis. The full Rayleigh-Plesset equation takes additionally into account inertial, surface tension and viscous effects. However, this simple but very effective description of the bubble growth (3.13) is widely accepted in the literature [123]. Recent work of cavitation takes into account the turbulent shear stress on the critical pressure [121] based on the concept of stress-induced cavitation in flows of high-viscosity fluids [145]. In his theoretical analysis, Joseph, argues that the liquid may rupture when the maximum of the principal component of the stress tensor overcomes the vapour pressure in liquid. This criterion determines the onset of cavitation in the flowing liquid. Although the approach is very novel, it seems rather impractical since it implies a stress analysis in the whole flow liquid in order to find fulfilment of the proposed criterion. The simplified equation (3.13) approximates the rates of evaporation and condensation as linear functions of pressure and neglects non-condensable gases such as air dissolved in the liquid and it does not take into account the bubble history. Its main drawback is that it does not represent bubble collapse accurately. The seed radius was set to  $1E-06$  m and the nuclear number density to  $1E+14$   $m^{-3}$ , in agreement with values proposed in the literature for real-size nozzle simulations [123, 127]. As initial condition, the solution was converged to steady-state before connecting the cavitation model and performing the corresponding calculations. Cavitating flows have to be computed in a time-marching manner, even if the final solution is steady.

The basic assumptions of the cavitation model are the following:

- There are cavitation seed bubbles present in the liquid, homogeneously distributed and of equal size; the initial seed radius is one of the model parameters and needs to be specified.

- The number of seed bubbles per unit volume of liquid is constant and is also a model parameter to be specified.
- All bubbles present in a control volume at any time are spherical and of the same size; however the bubble radius changes with time, as expressed by equation (3.13).
- Both liquid and vapour densities are constant.
- The density ratio of vapour to liquid is small,  $\ll 1$ .
- There is no slip between bubbles and liquid, i.e. vapour bubbles are treated as a component of the effective fluid.

### 3.3 Experimental Facilities

The validation of the cavitation model described in the previous section is based on the comparison of numerical solution with experimental results of mass flow rate, momentum flux at the exit of the nozzle, as well as effective injection velocity. The test rig used to obtain this data is described next, as well as the methodology adopted for the characterisation of the nozzles.

#### 3.3.1 Experimental apparatus and operating conditions

The injection system used in the experiment is a conventional Common Rail Fuel Injection system which makes it possible to reach high (up to 1400 bar) and relatively constant pressure values. A pressure regulator allows fixing the inlet pressure at a given value. The back pressure is modified by changing the effective discharge area of the vessel. The injection rate is measured by means of an injector meter. Additionally, the momentum flux of the liquid fuel leaving the nozzle hole is determined by measuring the force exercised by the spray on a pressure sensor. A detailed description of the experimental set-up has been previously presented in publications by the author's group in [146].

As has been shown in a number of studies [5, 35] the cavitation number is the main dimensionless number used to indicate the cavitation intensity. Here the cavitation number is defined as:

$$KN = \frac{P_{inj} - P_{back}}{P_{inj} - P_{vapor}} \quad (3.14)$$

It is assumed that the vapour pressure  $P_{vapor}$  is negligible as is the case for typical engine conditions.

Two types of measurements were performed: a) measurements of the injection rate and momentum flux of the single-hole and multi-hole injectors at fully opened needle lift at three values of  $\Delta p$ , and varying back-pressure (see Table 3.1) and b) measurements of the injection rate and momentum flux during the whole injection process (opening and closing of the needle) for both single and multi-hole injectors at various injection pressure conditions (see Table 3.2). These conditions presented in these tables were also simulated with the CFD code. The injection pressure ( $P_{inj}$ ) ranges from 310 to 1580 bar, while the back pressure ranges from 10 to 100 bars. The needle is not removed during the measurements.

$\Delta p$ (bar)	$P_{inj} - P_{back}$	KN	$\Delta p$ (bar)	$P_{inj} - P_{back}$	KN	$\Delta p$ (bar)	$P_{inj} - P_{back}$	KN
300	310-10	0.97	700	710-10	0.99	1400	1410-10	0.99
	320-20	0.94		720-20	0.97		1410-10	0.99
	330-30	0.91		740-40	0.95		1420-20	0.98
	340-40	0.88		750-50	0.93		1450-50	0.97
	350-50	0.86		760-60	0.92		1460-60	0.96
	360-60	0.83		770-70	0.91		1470-70	0.95
	370-70	0.81		780-80	0.90		1480-80	0.94
	380-80	0.79		800-100	0.88		1500-100	0.93
	400-100	0.75		880-180	0.80		1580-180	0.89
	480-180	0.63						

Table 3.1: Operating conditions investigated at fully opened needle

$P_{inj} - P_{back}$ (bar)	800-50	800-10	1410-10	1500-50	1500-10
KN	0.94	0.99	0.99	0.97	0.99

Table 3.2: Operating conditions investigated at different needle positions with fixed and moving mesh calculations

### 3.3.2 Internal geometry characterization

Since the injector internal geometry is known to affect significantly the flow inside the nozzle as well as at the exit, it is important to characterise well this geometry and to reproduce it as best as possible for the calculations.

The single-hole injector is of the sac type with the hole positioned coincident with the nozzle axis. This simple geometry is of interest since it helps in the clarification of the flow phenomena. It has frequently been used for spray investigations because it allows to study a single spray without any interactions of other sprays, and because the experimental procedure needed to measure is simpler (Figure 3.1 a). The multi-hole injector is also of the sac type except that there are six holes equally distributed every  $60^\circ$  around the periphery and their inclination angle is  $72.5^\circ$  with respect to the needle axis (Figure 3.1 b).

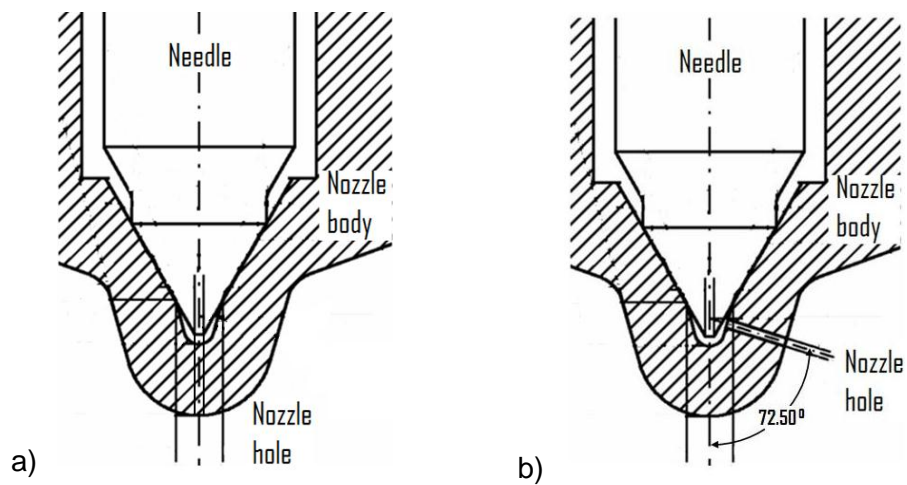


Figure 3.1: Configuration of the a) single-hole and b) multi-hole sac-type nozzle.

A silicone mould technique has been used [63] to characterise the exact geometry of the holes. The main geometric data of the nozzles is taken from the microscope images of the moulds presented in Figure 3.2, using special computer aided design software.

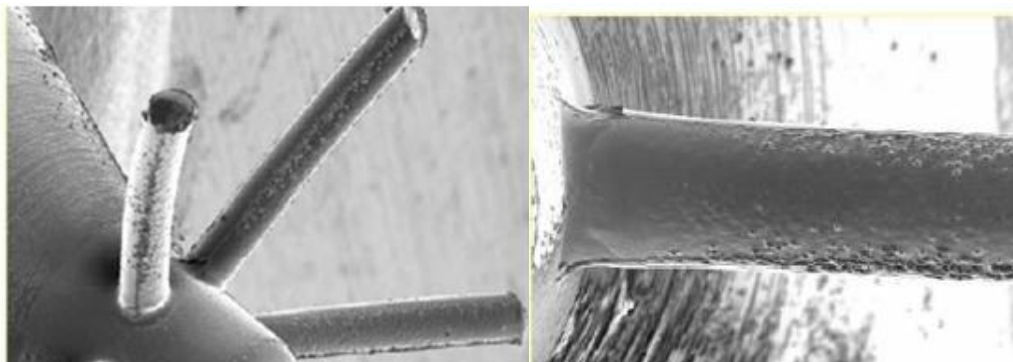


Figure 3.2: Silicone moulds characterization of the multi-hole nozzle.

Two nozzle shapes have been investigated for both the single-hole and multi-hole injectors: a cylindrical nozzle and a tapered nozzle. The dimensions for the single-hole nozzle are shown in Table 3.3. The K-factor, defined in equation 3.15 defines the exact taper of the nozzle:

$$K - factor = \frac{D_i - D_o}{10} \quad (3.15)$$

	<b>Cylindrical</b>	<b>Tapered</b>
Average diameter in the entrance of the orifice ( $\mu\text{m}$ )	157	176
Average diameter in the middle of the orifice ( $\mu\text{m}$ )	163	170
Average diameter in the outlet of the orifice ( $\mu\text{m}$ )	163	165
Orifice nozzle length ( $\mu\text{m}$ )	1000	1000
Radius of the nozzle ( $\mu\text{m}$ )	45	88
K-factor	-0.6	1.1

Table 3.3: Dimensions of the cylindrical and tapered single hole-nozzle.

The exact geometry description of the 6 nozzles of the multi-hole nozzle indicates that there are small differences in the hole shapes. The nozzle dimensions of the six holes for both the tapered and cylindrical multi-hole nozzle are shown in Table 3.4 following the nomenclature shown in Figure 3.3.

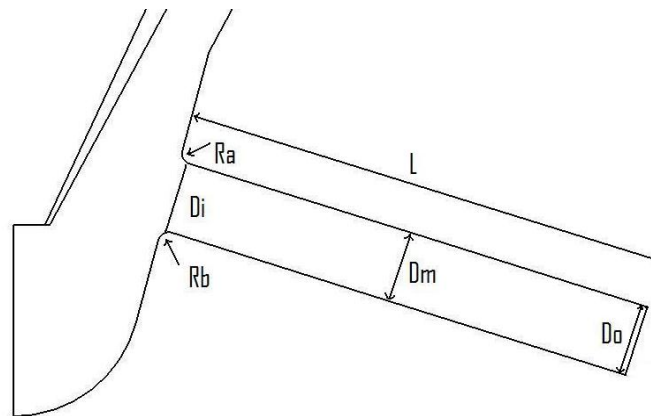


Figure 3.3: Sketch of the multi hole nozzle with main geometric parameters.

<b>Tapered Nozzle</b>	<b>R<sub>a</sub> (μm)</b>	<b>R<sub>b</sub> (μm)</b>	<b>D<sub>i</sub> (μm)</b>	<b>D<sub>m</sub> (μm)</b>	<b>D<sub>o</sub> (μm)</b>	<b>L (μm)</b>	<b>k-factor</b>
1	39	39	150	143	139	1000	1.1
2	42	42	150	144	138	1000	1.2
3	48	48	151	143	137	1000	1.4
4	35	35	151	143	139	1000	1.2
5	41	41	151	143	138	1000	1.3
6	37	37	154	144	137	1000	1.7
<b>Cylindrical Nozzle</b>	<b>R<sub>a</sub> (μm)</b>	<b>R<sub>b</sub> (μm)</b>	<b>D<sub>i</sub> (μm)</b>	<b>D<sub>m</sub> (μm)</b>	<b>D<sub>o</sub> (μm)</b>	<b>L (μm)</b>	<b>k-factor</b>
1	22	22	146	148	147	1000	-0,1
2	21	21	147	150	147	1000	0.0
3	21	21	147	148	147	1000	0.0
4	20	20	148	148	146	1000	0.2
5	20	20	146	147	149	1000	-0.3
6	24	24	149	147	148	1000	0.1

Table 3.4: Dimensions of the six holes of the cylindrical and tapered multi hole-nozzle.

### 3.4 Summary

In this chapter, the basic mathematical models that have been considered in this study for the prediction of the cavitating flow have been presented. Subsequently, the experimental facilities used to measure the flow characteristics at the nozzle exit have been briefly described. In addition, the flow conditions at which measurements and simulations were performed have been enumerated. In the next chapter, the focus is on the comprehensive model validation with an academic throttle geometry. Details of the problem configuration, model parameters and validation results, together with the predicted flow field results will be presented and discussed.

# **CHAPTER 4.**

## **VALIDATION OF THE CAVITATION MODEL WITH AN**

### **ACADEMIC STUDY**

#### **4.1 Introduction**

This chapter focuses mainly on investigating numerically the 3D flow within Diesel injector-like geometries, to subsequently apply the results of this study to analyse the flow in real Diesel injectors and pressure operating conditions (above 100 Mpa). For this, the cavitation model based on bubble growth theory [19] and described in section 3.2.4 was used, as implemented in the commercial code [18]. Numerical predictions were performed on a throttle channel at different operating conditions, with and without cavitation, and compared to available experimental measurements documented by Winklhofer et al [22]. The chapter starts with a description of the computational domain and the numerical parameters tested in the simulations. Then, the predicted results are compared with the measurements of the vapour field distribution, pressure field and velocity profiles, followed by an analysis of the flow distribution. The chapter ends with a summary of the most important conclusions.

## 4.2 Computational Domain and Grid Independence Results

For the validation and parametric studies performed within this work, the injector-like throttle channel geometry J of reference [22] was considered. Since the geometry considered is symmetric (Figure 4.1), only half of the geometry was calculated by imposing symmetry boundary conditions along the axis boundary. Constant pressure boundary conditions were set at the inlet and outlet and a no slip boundary condition was used at the wall.

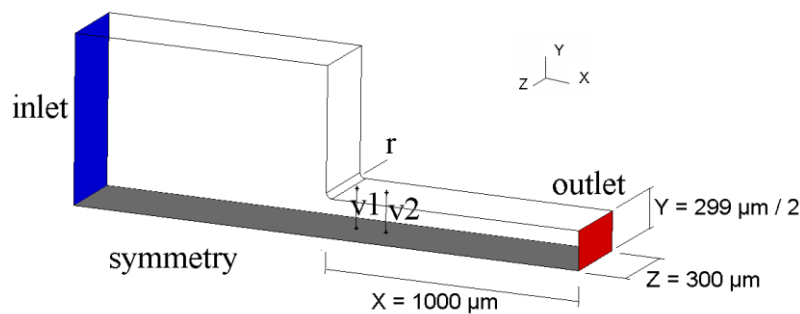


Figure 4.1: Geometry of computation domain and boundary conditions.

Although the size of the channel is substantially larger than current Diesel injector orifices, this geometry is used as a reference in the literature [119, 131] and can therefore be used to validate the model. The calculations were performed taking into account the roundness of the nozzle entrance ( $r=20\ \mu\text{m}$ ) and the three-dimensional nature of the flow. The cross-section of the nozzle is almost square (width, Y-axis =  $299\ \mu\text{m}$  and thickness, Z-axis =  $300\ \mu\text{m}$ ) and the length is  $1000\ \mu\text{m}$  (X-axis), as shown in Figure 4.1. The results of a CFD calculation are known to be affected by the resolution of the computational mesh, especially in the regions of high gradients. In order to verify the grid independence of the solution, different adaptive refinements were performed. To start with, the calculations were realised with the mesh

resolution shown in Figure 4.2 (121820 cells) with average cell size of 1-3  $\mu\text{m}$ .

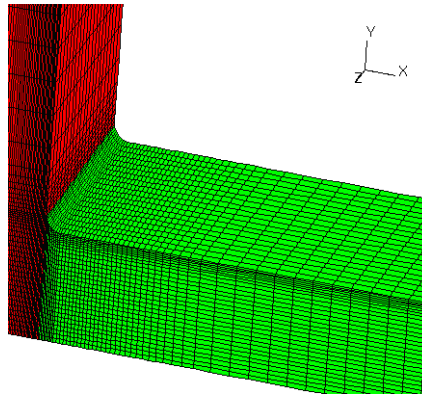


Figure 4.2: Visualization of mesh distribution.

Figure 4.3 shows the refined zones, which resulted from the refinement process based on pressure gradients and velocity magnitude gradients, respectively, yielding a total cell number of 207094.

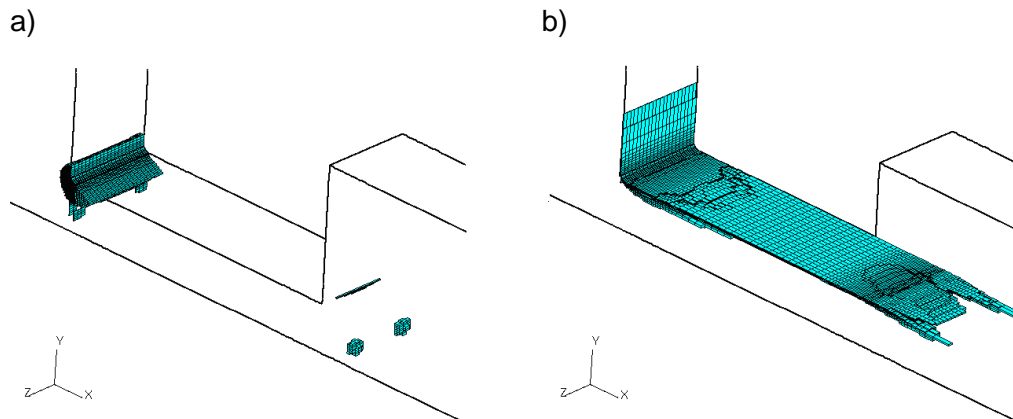


Figure 4.3: Refined locations by a) pressure, b) velocity magnitude.

It is seen that with the pressure-gradients method, the mesh was refined at the inlet corner, while with the velocity magnitude gradients it was refined in

the upper part of the nozzle. However in terms of injection rate the differences between the meshes are not significant, maximum 3% (see Table 4.1). Nevertheless, the mesh adopted for the calculations was the mesh with a local refinement at the nozzle entry to capture the large pressure and velocity gradients in this region related with the onset of cavitation.

	<b>Coarse mesh</b>	<b>Refined by pressure</b>	<b>Refined by velocity</b>
Injection rate (g/s)	8.26	8.14	8.04

Table 4.1: Injection rate results (g/s) obtained for different mesh resolutions.

### 4.3 Turbulence Modelling Study

The flow inside the injector-like nozzle considered in this work is clearly turbulent since its Reynolds number is about 12000. Hence, a turbulence model is required for the flow simulation. In this study, a reference configuration with the  $k$ - $\epsilon$ /low Reynolds/hybrid turbulence model was first defined and calculated (see Table 4.2). A turbulence model study was then performed, mainly with variants of the  $k$ - $\epsilon$  and the  $k$ - $\omega$  turbulence models to check their influence on the predicted flow field from an engineering point of view (see Table 4.2). For this study, all other parameters were kept as in the reference case.

The results obtained with the different turbulence models tested are illustrated in Figure 4.4, in terms of velocity profiles in cavitating and non cavitating conditions. These are extracted at the positions V1 and V2 inside the throttle hole (see Figure 4.1).

<b>Reference configuration used for calculations</b>				
k- $\epsilon$ /low Reynolds/hybrid	Medium time step (1.0E-06)	Conjugate Gradient	1.0E-06	1.0E+14
<b>Parameters varied (one at a time based on reference configuration)</b>				
<b>Turbulence modelling approach/ wall treatment</b>	<b>Time step (s)</b>	<b>Solution algorithm</b>	<b>Seed radius (m)</b>	<b>Nucleus number</b>
k- $\epsilon$ /high Reynolds/standard	Small time step (5.0E-07)	Algebraic Multigrid	1.0E-05	1.0E+12
k- $\omega$ SST/low Reynolds/hybrid				
k- $\omega$ SST/high Reynolds/standard	Large time step (2.0E-06)		5.0E-05	1.0E+16
k- $\omega$ standard/low Reynolds/hybrid				
k- $\omega$ standard/high Reynolds/standard				
k- $\epsilon$ RNG/standard				

Table 4.2: Reference configuration (highlighted) used as basis for parameters variation study and definition of parameters varied: turbulence model, time step, solution algorithm, seed radius, nucleus number.

It is seen that by using the different models, for a certain mesh resolution, the velocity profiles have practically identical shapes at both positions, with slight quantitative differences of about 2% maximum. It was also found that the maximum difference with the various turbulence models is about 2% in terms of injection rate, which is the key parameter for the validation.

In view of these results, it was finally decided to use the k- $\epsilon$ /low Reynolds number turbulence model with hybrid near wall treatment for closure of the equations. This model seemed the most appropriate for the range of Reynolds numbers considered, indicative of transitional rather than fully turbulent flow, as well as a good compromise between approximation to experimental results in terms of injection rate and solution cost. In addition, the hybrid near wall treatment provides valid boundary conditions for a wide range of near-wall mesh densities, which ensures independence of the  $y^+$

value, and it is better adapted to this type of flow than the standard wall function approximations, generally used for high Reynolds number models.

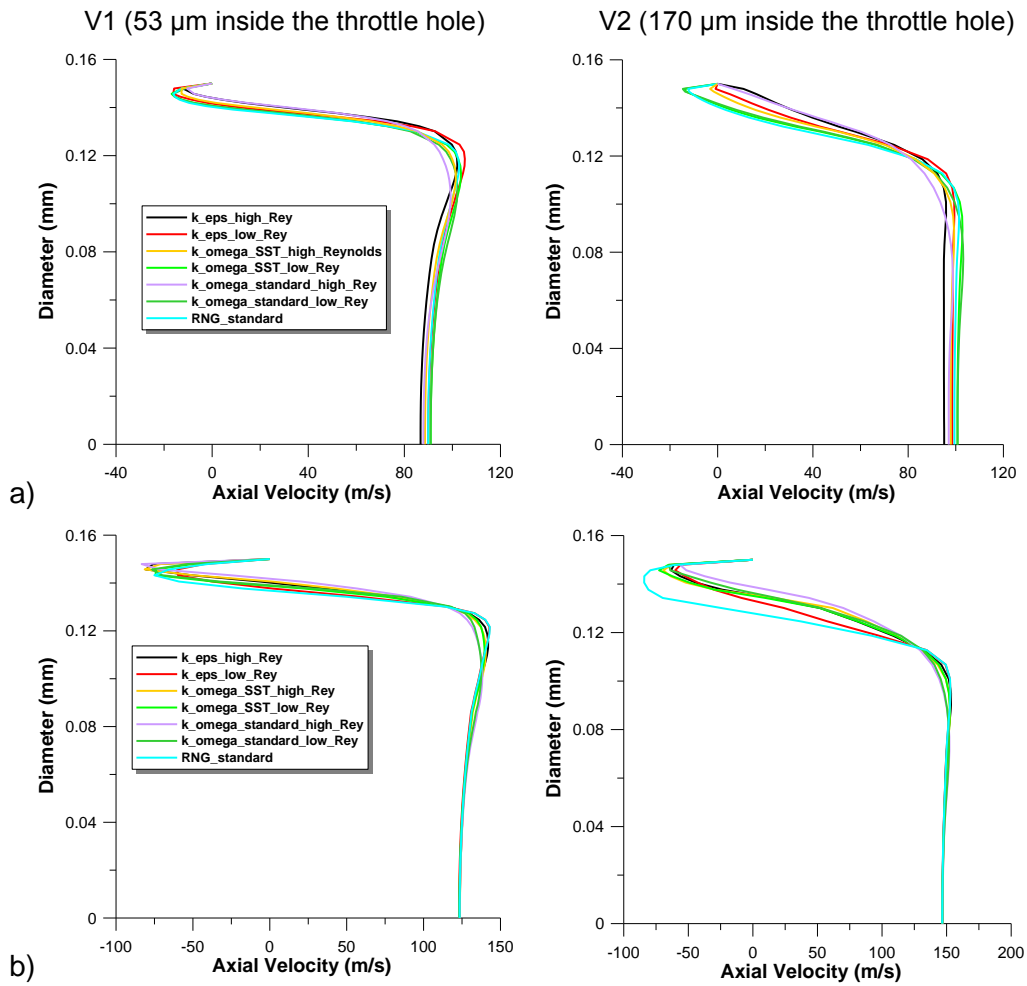


Figure 4.4: Predicted velocity profiles obtained with different turbulence models in position v1 and v2 a) at condition without cavitation ( $\Delta p=41$  bar) and b) at choked flow conditions ( $\Delta p=85$  bar).

#### 4.4 Set-up of Numerical Method

The solver is based on the finite volume approach and the iterative process has been performed with the SIMPLE algorithm [73, 147]. Although inlet and outlet pressures are constant, the modelling of the cavitation phenomenon itself is transient. The cavitating flow has to be computed in a time-marching manner, even if the final solution is steady-state. In the rest of the text, this approach will be termed “quasi-steady state” calculations. In order to accelerate convergence and ensure stability of the calculations, the solution was converged to steady state before connecting the cavitation model and performing the corresponding time-dependent calculations. To analyse the influence of the time-step on the solution, several calculations were performed, with different values of the time-step (5.0E-07; 1.0 E-06; 2.0E-06 s) and all other parameters as in the reference configuration (see Table 4.2).

For the convective flux approximation, a second order scheme (MARS) for the momentum equations and a first order scheme (UD) for the k- $\epsilon$  equations was used. The working fluid was Diesel fuel with properties as given in Table 4.3, a).

	a)		b)	
	Liquid	Vapor	Liquid	Vapor
Density (Kg/m <sup>3</sup> )	828	0.025	832	0.1361
Viscosity (kg/ms)	2.14x10 <sup>-3</sup>	1x10 <sup>-5</sup>	6.5x10 <sup>-3</sup>	5.953x10 <sup>-6</sup>

Table 4.3: a) Fluid properties used for the calculations, b) Fluid properties tested (Peng Kärholm et al., 2007).

The configuration highlighted in Table 4.2 and Table 4.4 was implemented and used as reference to obtain the results presented in this thesis.

Momentum	Turbulence	Cavitation	Injection rate (g/s)
MARS	UD	UD	8.14
MARS	CD	UD	8.20
MARS	UD	CD	8.14
UD	UD	UD	8.24
CD	UD	UD	8.16

Table 4.4: Considered combinations of discretization schemes and corresponding injection rate results (UD-upwind differencing-1<sup>st</sup> order, CD-Central Differencing-2<sup>nd</sup> order, MARS-Monotone Advection and Reconstruction Scheme-2<sup>nd</sup> order).

Some additional parameters that may influence the solution, referring to both the solver and the cavitation model itself, were each varied in turn, maintaining the others of the reference configuration constant, as shown in Table 4.2. From these parametric studies, it may be concluded on the one hand, that the effect on the injection rate of varying only the time-step or the seed radius, or changing the solution algorithm, is negligible. On the other hand, a change of the discretization scheme (see Table 4.4) or a variation of the nucleus number density (see Figure 4.5) had slightly more influence, resulting in a variation of the injection rate of up to 1.5% ( $\Delta p=85$  bar). Moreover, there is an inverse relationship between the minimum pressure and the amount of vapor predicted. Indeed, this is verified by examining the effect of nucleus number density on the minimum pressure and the injection rate (see Figure 4.5). It is seen that with decreasing minimum pressure, the injection rate decreases, which is consistent with an increase of the predicted volume fraction of vapour.

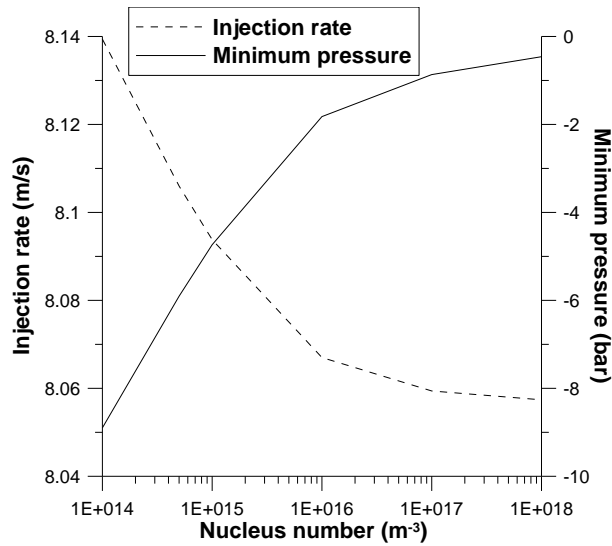


Figure 4.5: Injection rate and minimum pressure as a function of nucleus number density ( $\Delta p=85$  bar).

The computational (CPU) time of the single-phase runs to reach the steady-state calculation was of the order of 1h per calculation on a core of an Intel QuadCore Xeon CPU @ 2.00 GHZ, while the CPU cost of the quasi-steady state cavitation runs was of the order 1 min per time step and the calculations performed for 0.001 s.

#### 4.5 Validation Results

The optical and hydraulic characterization of a transparent throttle channel flow before and after the onset of cavitation carried out by Winklhofer et al. (2001) has been used in this work to validate the CFD model. As in the experiments, the injection pressure has been kept constant (100 bar), while backpressure varies to get the corresponding pressure drop.

### 4.5.1 Injection rate results

In Figure 4.6 the results of the injection rate of the test case at different pressure drops is compared with the measurements. As seen in Figure 4.6 the main deviation with respect to the experimental data is on the critical conditions, above which the mass flow becomes choked. The preliminary calculated results show that the mass flow collapses when the outlet pressure is 30 bar (i.e.  $\Delta p=70$  bar) instead of 35 bar (i.e.  $\Delta p=65$  bar) as observed experimentally. The total pressure in the simulation cases is reduced by the dynamic pressure at the inlet, which represents a pressure loss at the entrance. The pressure difference in the predicted cases is estimated by taking into account this inlet loss.

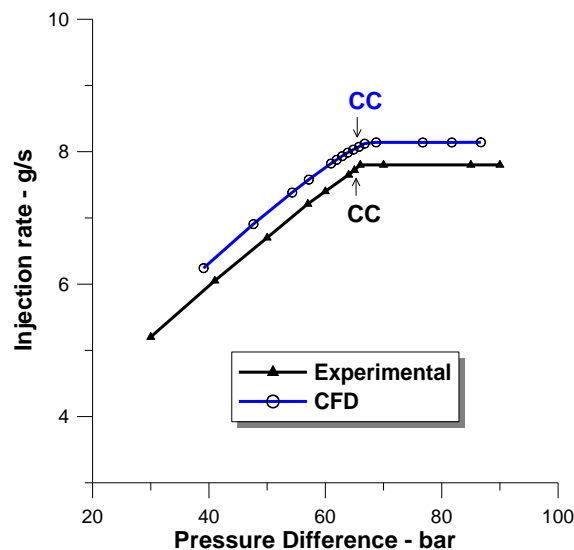


Figure 4.6: Experimental data from Winklhofer et al. (2001) and predicted injection rate plotted versus the pressure difference, where CC critical conditions.

The injection rate predicted results are systematically over-estimated by about 4%. However, this deviation is not critical for the further analysis of this

case study. The study is aimed at showing the ability of the model to describe variations in the length of the vapour region with the cavitation number, rather than at providing exact validation of the model, since this would require more specific experimental information about the cavitating flow. In fact, the slight over-prediction may be linked to the uncertainties in the values of liquid viscosity. Indeed, it was found that the effect of liquid viscosity can have a significant influence on the amount of cavitation. Considering the lack of experimental values for viscosity, calculations were made with fuel properties found in the literature [79] in order to check the effect of viscosity (see Table 4.3, b). It was observed that there was less generation of vapor with higher liquid viscosity (see Figure 4.7). Higher viscosity leads to lower dynamic pressure and thus yields higher absolute pressure values and less cavitation in accordance with [119]. As a general trend, the cavitation model predicts a reduction of the nozzle mass flow rate with increasing cavitation intensity, which is in agreement with the measurements.

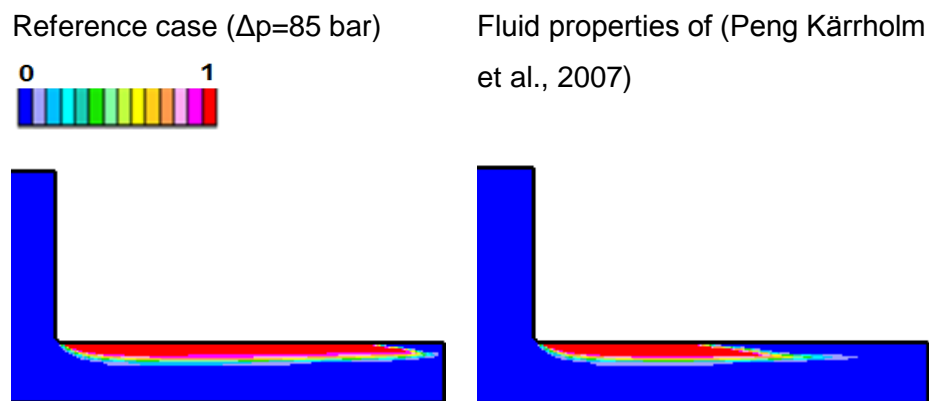


Figure 4.7: Volume fraction of vapour distribution with different fluid properties at longitudinal middle plane,  $\Delta p=85$  bar.

Cavitation appears in the nozzle hole entrance due to the abrupt change of the flow direction associated with large pressure drop and high fuel velocities.

With decreasing back pressure, the cavitation bubble expands up to the exit with maximum amount of vapour in the upper and lower part of the nozzle. Preliminary calculations using different density numbers of cavitation bubbles (Figure 4.5) have shown that even using the highest value of those recommended (in the range of  $1\text{E}+11\text{ m}^{-3}$ - $1\text{E}+14\text{ m}^{-3}$ ) for high-pressure, high-velocity systems, the amount of vapour observed in the experiments could not be predicted with accuracy. This discrepancy can be explained by the influence of the turbulence model and the fluid viscosity, as mentioned above.

Although the model under-predicted the amount of vapour, qualitative agreement has been found with the experiments. The cavitation field in the predicted cases grows significantly just by increasing the pressure drop from critical cavitation (CC) to CC + 1 bar (see Figure 4.8), as also observed in the experiment.

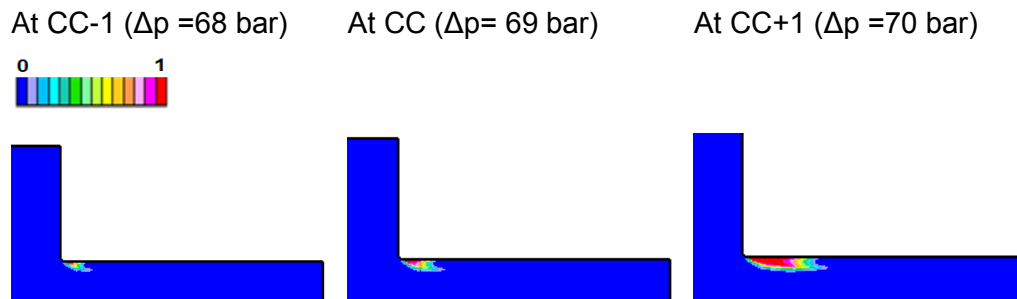


Figure 4.8: Predicted volume fraction of vapour fields around critical cavitation at longitudinal middle plane.

#### 4.5.2 Velocity profiles

Velocity profiles are shown in Figure 4.9 for operating conditions without cavitation ( $\Delta p = 41$  bar), with moderate cavitation ( $\Delta p = 70$  bar) and at choked flow conditions ( $\Delta p = 85$  bar). The velocity profiles are extracted downstream

of the throttle entrance at the position v1 (53  $\mu\text{m}$  inside the throttle hole) and v2 (170  $\mu\text{m}$  inside the throttle hole), as seen in Figure 4.1.

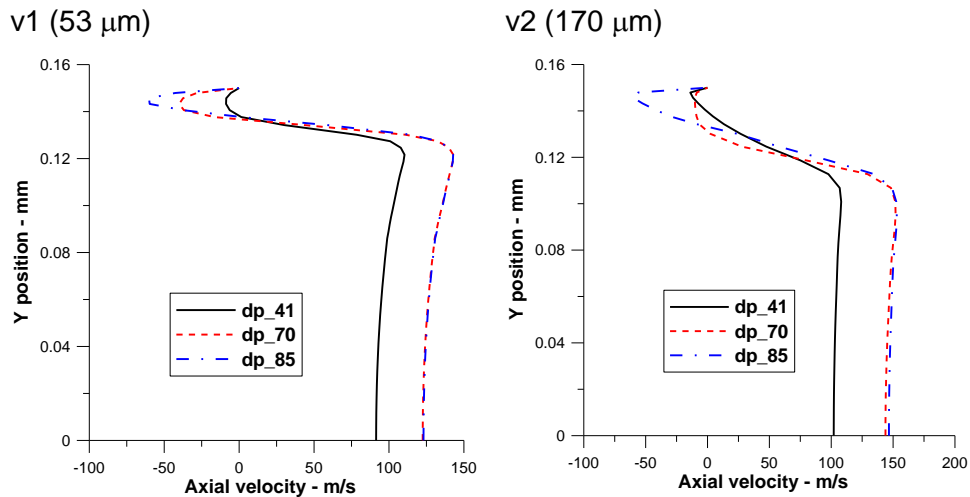


Figure 4.9: Velocity profiles in position v1 and v2 at condition without cavitation ( $\Delta p=41$  bar), with moderate cavitation ( $\Delta p=70$  bar) and at choked flow conditions ( $\Delta p=85$  bar).

The measured velocity profiles described in Winklhofer et al. (2001) refer to geometry U (301  $\mu\text{m}$  inlet and 284  $\mu\text{m}$  outlet width). Hence, only a qualitative comparison can be made with respect to geometry J, studied here. In agreement with Winklhofer et al. (2001), at position v1 the velocity peaks near the shear layer and shows a minimum in the channel center. This profile is the same at higher pressure drops where the velocity peak near the cavitation region significantly increases. According to Winklhofer et al. (2001), at position v2 the velocity profile changes with respect to that of position v1, with the maximum velocities observed near the boundary of the cavitation region and also in the channel center. The latter, however, is not observed in the calculation: the velocity profiles are flat at the center, until affected by the cavitation zone.

The velocity profiles also show the reverse flow near the wall in the hole entrance, thus indicating that the flow separates in this region. According to the observations by Winklhofer et al. (2001), at a higher pressure drop the cavitation seems to initiate in the separated shear layer. With increasing formation of cavitation, the low pressure recirculation area fills with vapour. The same is observed in the numerical solution of the nozzle flow, as confirmed in Figure 4.8: the onset of cavitation appears in the low pressure recirculation area and grows with increasing pressure drop.

### **4.5.3 Pressure profiles and fields**

In Figure 4.10 the predicted pressure fields are shown at non cavitating conditions and at critical conditions. The most relevant feature concerns the pressure gradients, which are confined to the entrance area of the nozzle independently of the pressure drop. In agreement with Winklhofer et al. (2001), the solution shows that the main pressure gradient layer covers a size of about one throttle diameter, with half of this layer extended into the upstream area in front of the throttle entrance. The images also illustrate the precise location of the low pressure recirculation zone commented before, where at increasing pressure drop cavitation is initiated. At critical conditions, the minimum pressure predicted at the entrance of the nozzle is less than the saturation pressure, which indicates that there appears cavitation in this area (Figure 4.10, b).

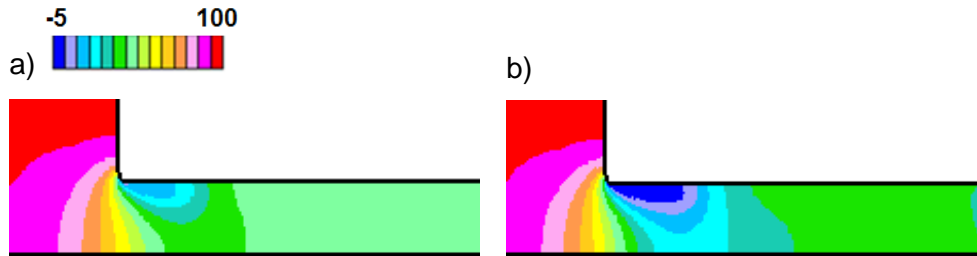


Figure 4.10: a) Pressure distribution (bar) at non cavitating conditions ( $\Delta p=58$  bar), and b) at CC ( $\Delta p=69$  bar).

Figure 4.11 illustrates the pressure profile of the simulated case at CC conditions ( $\Delta p=69$  bar) along the symmetry line of the vertical middle plane compared with the experimental one ( $\Delta p=65$  bar). As already mentioned, the predicted pressure at the inlet is lower than the experimental one due to the pressure loss calculated. Particularly, the static pressure in the simulating cases is reduced by  $0.5 \cdot \rho \cdot U^2$  in the entrance while running the calculation although it was set to 100 bar. This can be thought of as an entrance loss. Although, the minimum pressure attained in the calculations is smaller than in the experiment, due to the different critical conditions obtained, there is good qualitative agreement. It is seen that along the line the pressure minimum appears in the zone of low pressure recirculation, followed by the pressure recovery downstream of the throttle entrance.

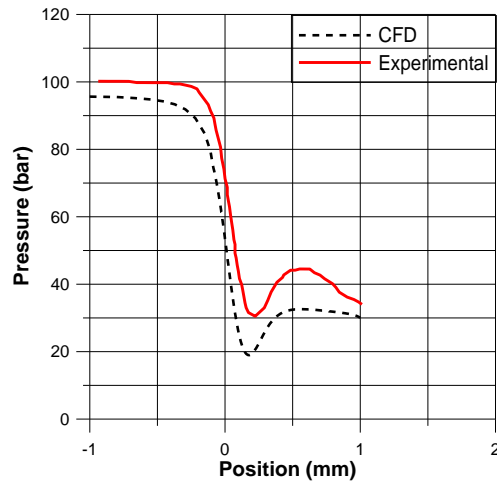


Figure 4.11: Predicted and experimental pressure profiles at CC conditions.

#### 4.6 Further Analysis of the Predicted Flow Field Results

Figure 4.12 shows contours of velocity and vapour volume fraction, illustrating a pair of vortices that appear and extend towards the exit at  $\Delta p=85$  bar.

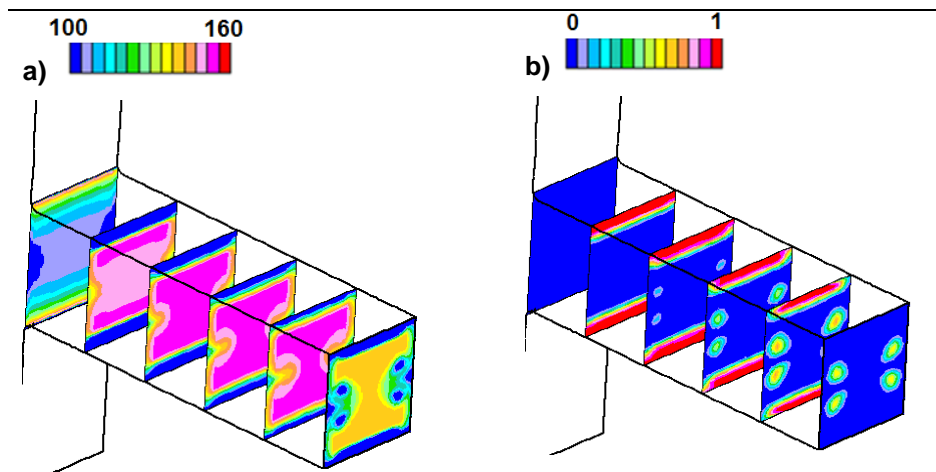


Figure 4.12: Velocity magnitude (m/s) and b) volume fraction of vapour fields in perpendicular planes to the flow direction.

These predicted vortices are also documented in references [79, 119] for this kind of Diesel injector-like geometries. As seen in Figure 4.12, the flow is accelerated in the upper and lower half of the nozzle where the inlet is rounded and vortices are formed in the interior. Calculations made with variants of the  $k-\epsilon$  and the  $k-\omega$  models at  $\Delta p=85$  bar predicted vortices of similar location and strength but their size depended on the turbulence model and treatment of the near wall flow (Figure 4.13).

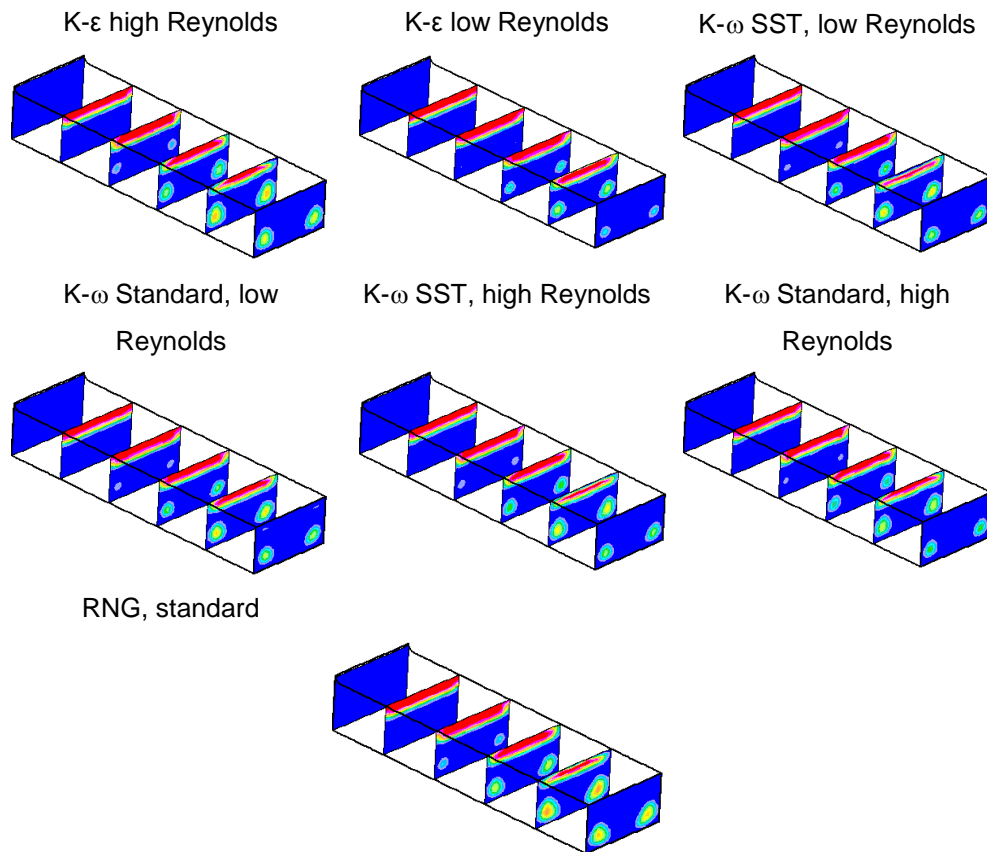


Figure 4.13: Distribution of cavitation field obtained by the different turbulence models.

Since experimental data is not available to validate the aforementioned results, it is not clear which model is more accurate. Rotational vortices and vortex induced cavitation are typical characteristics in Diesel injectors and are known to affect significantly the emerging fuel spray [3; 43].

## **4.7 Summary**

The commercial code [18] has been used in order to study cavitating flow within an injector-like geometry. The solution has been validated with experimental data documented by Winklhofer et al. [22]. It was found that the cavitation model could predict reasonably well the observed pressure field and low pressure recirculation area linked to the presence of cavitation at the nozzle entrance. Although there is a slight over-prediction of the critical conditions pressure drop, the model rendered accurately the effects of pressure drop variation in the nozzle. The amount of vapour generated in the cavitation region is under-estimated by the model. This could be due to the overestimation of the liquid viscosity, the influence of the turbulence model or of the vapour-liquid phase interactions not taken into account.

Vortices are formed inside the nozzle, resulting in localized pockets of low pressure where cavitation regions are detected. Given the insufficiently documented experimental data, the study does not allow safe conclusions to be drawn about the effectiveness of the cavitation model concerning the prediction of the cavitating vortical structures. Hence, it would be very useful to deepen the experimental studies of the flow inside injectors, to provide more precise and extensive validation of the cavitation and turbulence models. Additionally, since the final objective is to simulate Diesel injector flow, calculations with higher injection pressures will be tested in the next chapters, as Diesel injection pressures are generally over 100 Mpa. However,

the study presented here confirms that the model is sufficiently accurate and may be used to gain insight into the flow phenomena occurring within a Diesel injector.



# **CHAPTER 5.**

## **CAVITATION IN REAL SIZE INJECTORS AT FULL NEEDLE LIFT**

### **5.1 Introduction**

The purpose of the current chapter is to study the influence of real size Diesel injector geometries on the inception of cavitation and to assess the ability of computational fluid dynamics to determine cavitating flow conditions at full needle lift. For this, the exact three-dimensional internal geometries of real-size sac type Diesel injectors (tapered/cylindrical, single and multi-hole nozzles) were meshed, as described in Section 3.3.2. Since the needle is fully opened for approximately 90% of the injection duration [148], it is considered that the flow attains a quasi-steady state. The effect of needle movement on the internal flow characteristics was thus neglected. A full description of the nozzle flow characterisation is presented and the results of the CFD calculations are validated against in-house experimental data. Finally, the flow features at cavitating and non cavitating conditions as predicted by the computational model are analysed. The vapour volume fraction and velocity spatial distributions, as well as the characteristics of the flow at the nozzle exit

are presented, allowing an analysis of the cavitation pattern in function of the pressure conditions and the geometry.

## 5.2 Investigated Computational Domains

The model has been validated on the basis of comparisons with measurements on axisymmetrical single-hole and multi-hole sac type injectors with cylindrical and tapered orifices. In this series of simulations, a  $90^\circ$  sector for the single-hole and a  $60^\circ$  for the multi-hole nozzle was meshed taking into account the symmetry of the injector, in order to mitigate the computational cost. Since the six nozzles are not geometrically identical, the dimensions of one of the holes were taken as representative of the average geometry. The exact geometries of the multi-hole nozzle that were meshed are described in Table 5.1. The curvature radius along the inlet edge is not uniform in the multi-hole nozzles, as may be appreciated in the silicone moulds images (Figure 3.2) and since the variable radius was not supported by the cad software used for this geometry, it was decided to take an upper radius.

Nozzle	$R_a$ ( $\mu\text{m}$ )	$R_b$ ( $\mu\text{m}$ )	$D_i$ ( $\mu\text{m}$ )	$D_m$ ( $\mu\text{m}$ )	$D_o$ ( $\mu\text{m}$ )	$L$ ( $\mu\text{m}$ )	k-factor
Cylindrical	22	22	146	148	147	1000	-0.1
Tapered	42	42	150	144	138	1000	1.2

Table 5.1: Cylindrical and tapered nozzle dimensions.

The sectors meshed correspond to the full lift configuration ( $250 \mu\text{m}$ ). Images of the discretized geometries are shown in Figure 5.1.

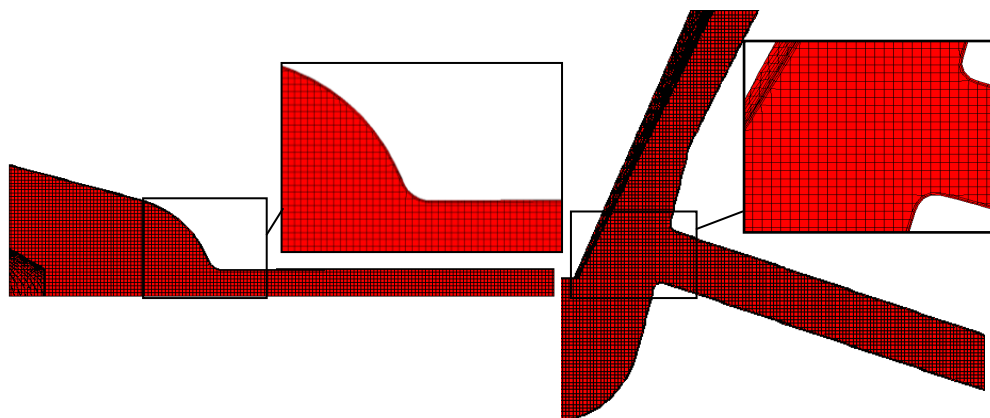


Figure 5.1: Computational mesh of the single-hole and multi-hole nozzle for the internal flow calculation.

The number of cells was approximately 80.000 for the single-hole and 600.000 for the multi-hole nozzle (cell size: 10  $\mu\text{m}$  approximately). The mesh fineness was determined on the basis of the previous grid independence study performed for the single-hole nozzle due to the high computation resources required for the multi-hole nozzles. In this study, the computational meshes (90° sector) used had different cell sizes in the axial and radial directions of the fixed part but with similar distribution, and the number of cells ranged from about 57000 to 95000 (Table 5.2). The one finally selected for the calculations (10  $\mu\text{m}$ ) was dense enough to allow grid independent results. Indeed, calculations with the finest mesh used (8.5  $\mu\text{m}$ ) yielded only about 1% difference in the injection rate (see Table 5.2).

Cell size ( $\mu\text{m}$ )	Total cell number	Injection rate (g/s)
10	57223	3.80
9.5	65491	3.84
9	83165	3.84
8.5	94748	3.84

Table 5.2: Injection rate results for different meshes for cylindrical nozzle (310/10 bar).

Periodic boundary conditions have been imposed at the geometric periodic boundaries with constant pressure boundaries prescribed at both the inlet and outlet. For the validation of the model, the simulations were performed by first obtaining a single-phase steady-state calculation of the flow and then running transient simulations with the cavitation model connected.

### 5.3 Nozzle flow characterization

To analyze the orifice flow in detail, it is necessary to define and determine characteristic flow parameters at the exit of the nozzle. Three non-dimensional coefficients  $C_d$ ,  $C_M$  and  $C_v$  are defined to compare the predicted results with the experimental measurements. These coefficients are expressed by equations (5.1), (5.3), and (5.4). The first non-dimensional parameter  $C_d$ , the discharge coefficient, is obtained by dividing the real mass flow  $\dot{m}_f$ , either measured by the rate of injection meter or calculated by the numerical method divided by the theoretical mass flow:

$$C_d = \frac{\dot{m}_f}{A_o \rho_l u_{th}} = \frac{\dot{m}_f}{A_o \sqrt{2 \rho_l \Delta p}} \quad (5.1)$$

The theoretical velocity at the outlet section,  $u_{th}$  is obtained by using Bernoulli's equation between the inlet and the outlet of the nozzle hole, and assuming that the inlet velocity is negligible:

$$u_{th} = \sqrt{\frac{2 \Delta p}{\rho_{liq}}} \quad (5.2)$$

The non-dimensional parameter  $C_M$ , the momentum coefficient is defined with the theoretical momentum flux:

$$C_M = \frac{\dot{M}_f}{A_o \rho_l u_{th}^2} = \frac{\dot{M}_f}{2 A_o \Delta p} \quad (5.3)$$

In order to describe the inner flow in more detail, the velocity coefficient  $C_v$  is defined, which takes into account losses in the velocity. Indeed,  $C_v$  defines the ratio between effective velocity and theoretical velocity:

$$C_v = \frac{\dot{M}_f}{\dot{m}_f} = \frac{u_{ef}}{u_{th}} \quad (5.4)$$

## 5.4 Validation results

### Effect of the KN

In this paragraph, the results of the calculations are compared to experimental data in terms of discharge, momentum and velocity coefficients. The operating conditions investigated are given here to remind (Table 5.3). In Figure 5.2 and Figure 5.3, the flow coefficients of single-hole and multi-hole nozzles respectively are plotted against the cavitation number KN (see equation 3.14) for each level of pressure. Both measured and predicted data of the non-dimensional coefficients  $C_d$ ,  $C_M$  and  $C_v$  are normalised with the value corresponding to the minimum KN ( $C_d$ ,  $C_M$ ,  $C_v=1$ ) They are only presented for the cylindrical nozzles. In the tapered nozzle, there is no cavitation and hence, the discharge and momentum coefficients depend only on pressure, and do not vary with KN.

$\Delta p$ (bar)	$P_{inj} - P_{back}$	KN	$\Delta p$ (bar)	$P_{inj} - P_{back}$	KN	$\Delta p$ (bar)	$P_{inj} - P_{back}$	KN
300	310-10	0.97	700	710-10	0.99	1400	1410-10	0.99
	320-20	0.94		720-20	0.97		1410-10	0.99
	330-30	0.91		740-40	0.95		1420-20	0.98
	340-40	0.88		750-50	0.93		1450-50	0.97
	350-50	0.86		760-60	0.92		1460-60	0.96
	360-60	0.83		770-70	0.91		1470-70	0.95
	370-70	0.81		780-80	0.90		1480-80	0.94
	380-80	0.79		800-100	0.88		1500-100	0.93
	400-100	0.75		880-180	0.80		1580-180	0.89
	480-180	0.63						

Table 5.3: Operating conditions investigated at fully opened needle.

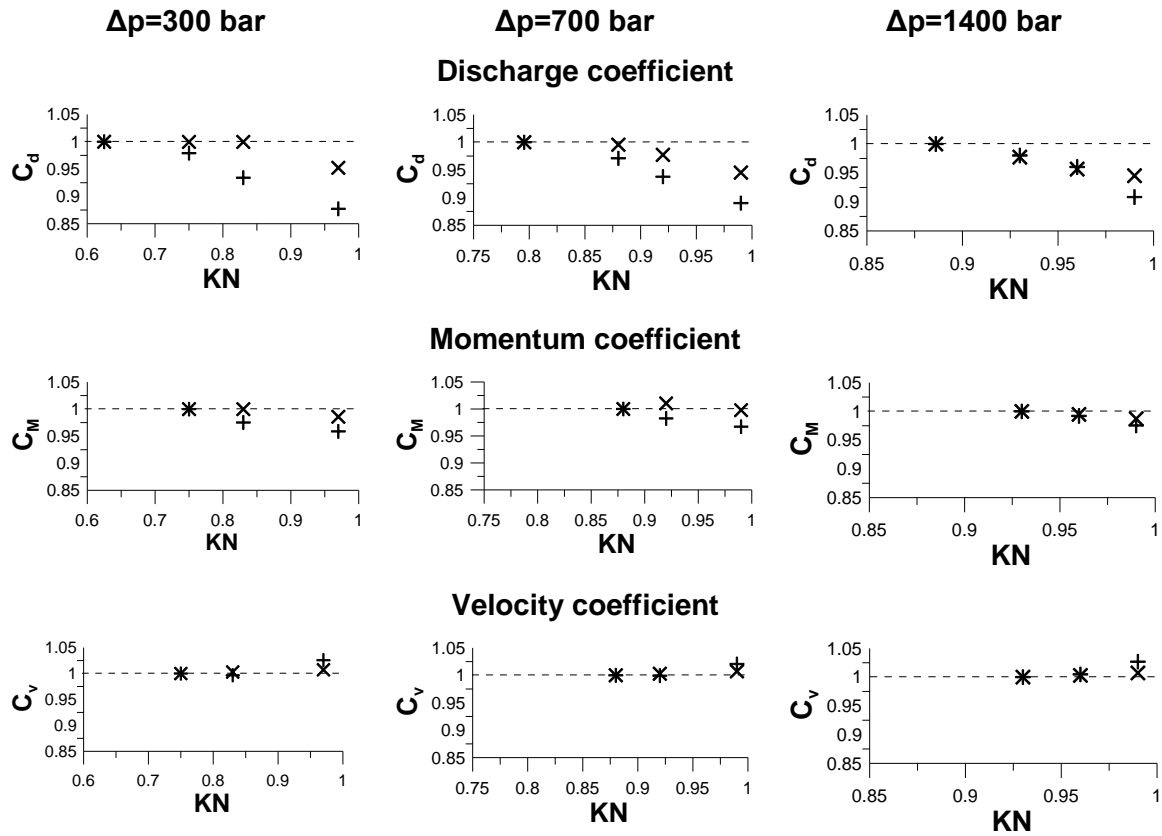


Figure 5.2: Comparison between experimental and CFD results of flow coefficients for the cylindrical single-hole nozzle (+ Experimental, × CFD).

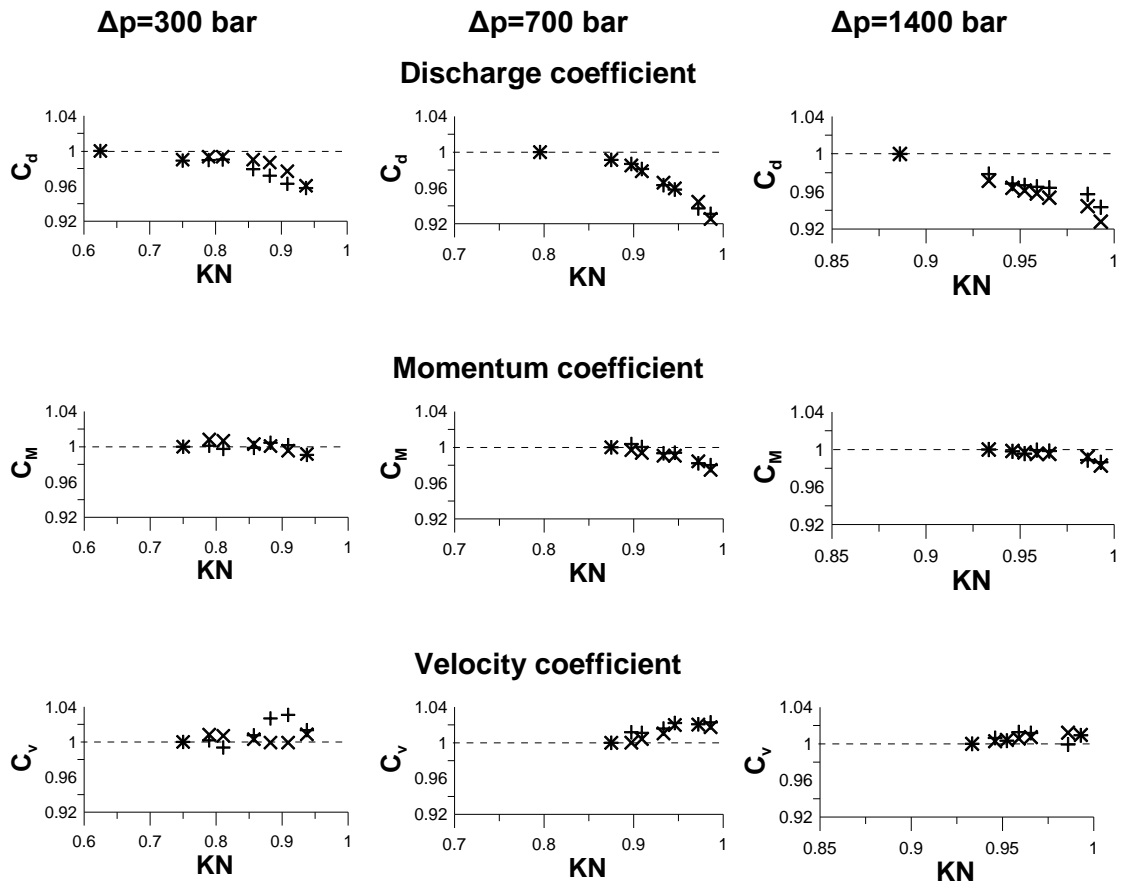


Figure 5.3: Comparison between experimental and CFD results of flow coefficients for the cylindrical multi-hole nozzle (+ Experimental, × CFD).

The model overestimates the experimental data with the highest deviation at the lower pressure drops ( $\Delta p=300$  bar), with a maximum of about 10 % for the discharge coefficient for both nozzles; however, the agreement in the tendencies is quite good. In the single-hole case, the difference between predicted and experimental results is more pronounced, mainly because the pressure boundary at the inlet was prescribed at a position quite near to the hole inlet. The percentage difference in the coefficients is mainly because the pressure was prescribed in the calculation domain at a different position from

the experimentally measured in the Common Rail; hence, the pressure loss within the injector body was not taken into account in the calculations.

For both nozzles, the values of  $C_d$  are constant as a function of KN before the onset of cavitation. This is particularly obvious for  $\Delta p=300$  bar, where the onset of cavitation occurs for  $KN=0.85$  only. When the cavitation starts there is a reduction of the mass flow rate. The calculations predict with good accuracy the critical cavitation conditions, which correspond to the pressure drop at which cavitation starts in the nozzle hole [21]. For the multi-hole case at high pressure drops ( $\Delta p=700$  bar,  $\Delta p=1400$  bar) the  $C_d$  decreases as a function of KN at all operating conditions, indicating that there is cavitation for all KN at these pressures. The momentum coefficient also has a decreasing trend in cavitating conditions but not to such degree as the discharge coefficient. The comparison of the velocity coefficients reveals that the model can capture the increase in mean velocity caused by the onset and development of cavitation. This velocity behaviour was observed previously [25, 149].

#### **Effect of the pressure drop**

Next, the effect of the pressure drop on the flow coefficients will be discussed. Figure 5.4 shows  $C_d$  and  $C_M$  results as a function of pressure drop for the single-hole and multi-hole cases. For each pressure drop a low and a high KN test case result is presented. It is observed that for the single-hole the flow coefficients are practically independent of the pressure drop. The predicted and experimental results show good agreement, with some discrepancies for the cavitating (cylindrical) nozzle.

For the multi-hole case, however, the experimental results show that the flow coefficients increase with increasing  $\Delta p$ . Comparison of the cylindrical and

tapered nozzles shows that the increasing trend does not depend on the nozzle design, nor on the presence of cavitation. However, in the tapered nozzle the  $C_d$  increases more than in the cylindrical with increasing  $\Delta p$ , as expected, due to the absence of cavitation. The  $C_M$  follows the same increasing trend. The model was not able to reproduce this increasing trend of the flow coefficients in the multi-hole nozzles, except a slight increase. This discrepancy can be related with the fact that the model overestimates the injection rate results at higher degree at low pressure drops. The pressure loss within the injector body was not taken into account when imposing the injection pressure on the calculation domain, which is expected to be more significant in the multi-hole nozzle.

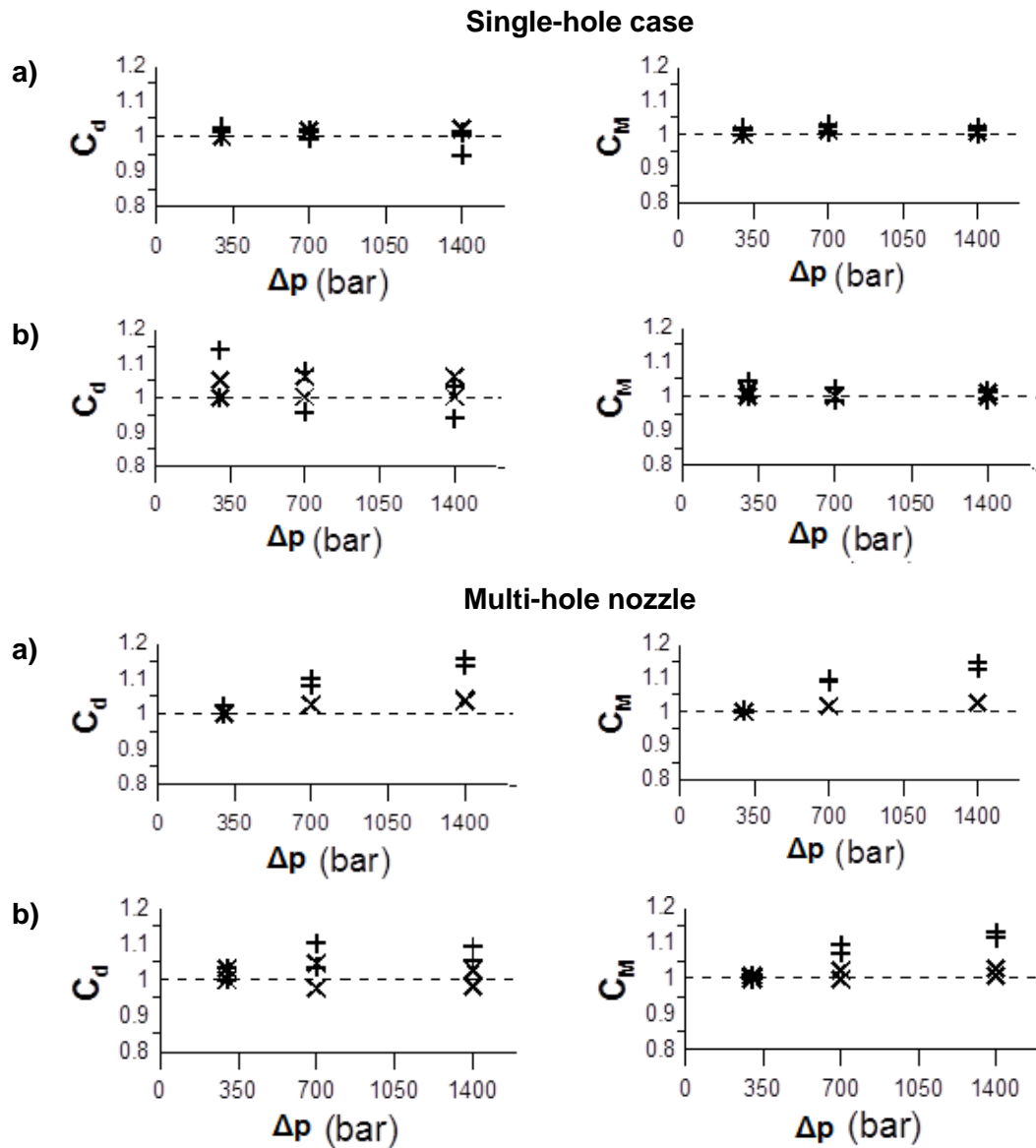


Figure 5.4: Effect of pressure drop on discharge and momentum coefficient for single-hole and multi-hole nozzle with **a)** tapered and **b)** cylindrical orifices (+ Experimental, × CFD).

## 5.5 Analysis of the Flow Cavitation Pattern

### 5.5.1 Predicted flow in single-hole Diesel injectors

#### Analysis of the internal flow distribution

In Figure 5.5, representative images of the flow in the cylindrical single-hole are presented for low and high KN cases corresponding to incipient and fully developed cavitation regime respectively. The vapour volume fraction distribution and the corresponding velocity flow field images are shown, which allow illustrating the transient nature of the cavitation. They are presented for each level of pressure at a time when the field does not evolve further. Overall, cavitation develops around the nozzle circumference, and remains confined close to the wall as also observed in [10, 71]. The results indicate that with increasing injection pressure and KN, more vapour generates, but the overall cavitation pattern does not change significantly otherwise. The influence of the backpressure is more important: its increase hinders the extension of cavitation. Indeed, at low KN the cavitation collapses downstream about half of the nozzle length, while at high KN, the cavitation region expands and fills in the whole nozzle until the exit, remaining attached to the wall.

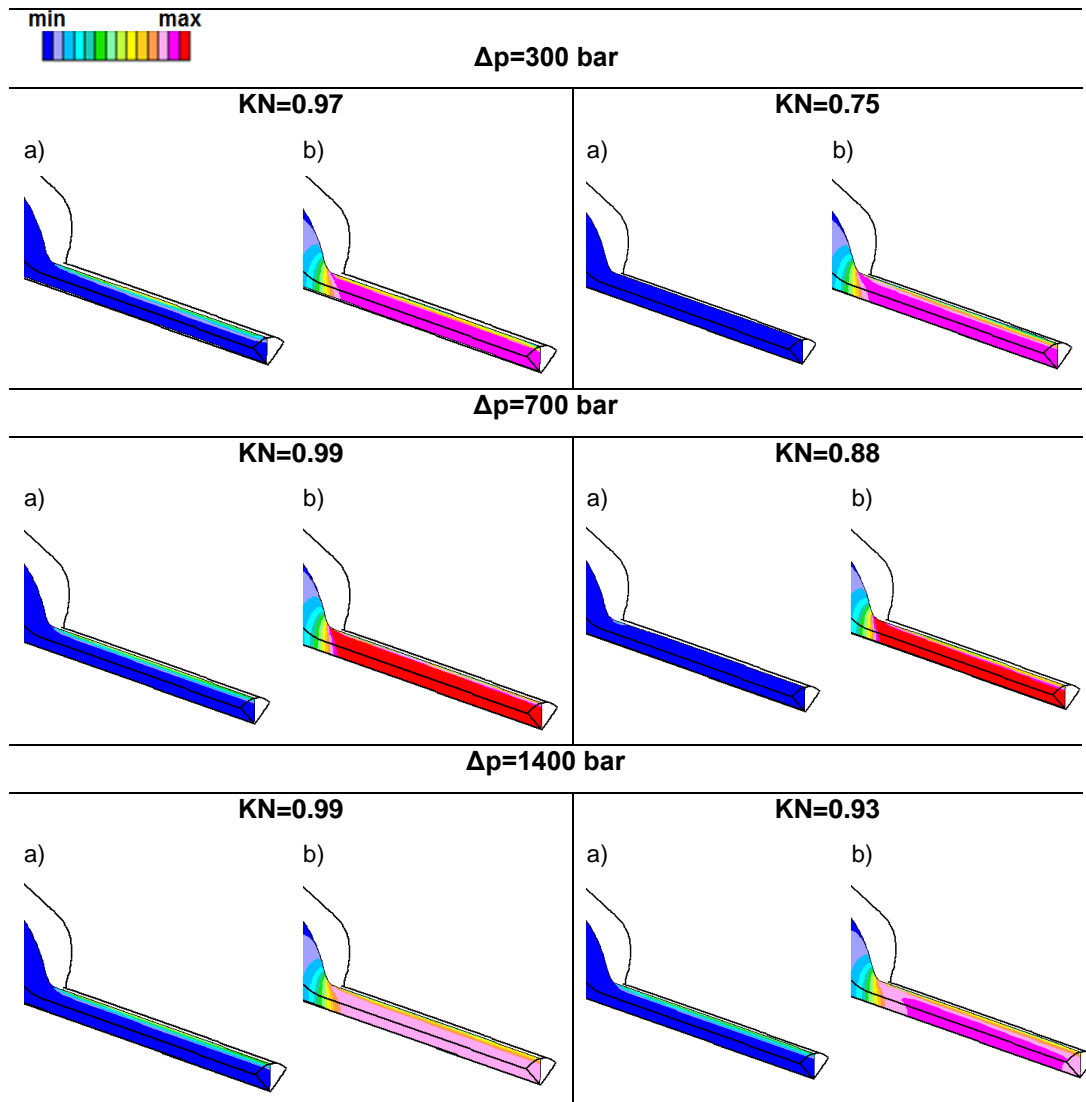


Figure 5.5: Representative a) volume fraction of vapour and b) velocity field images for different levels of pressure and KN (cylindrical nozzle). Colour scale: volume fraction of vapour: 0-1, velocity magnitude (m/s): 0-300 for  $\Delta p = 300$  bar, 0-400 for  $\Delta p = 700$  bar, 0-700 for  $\Delta p = 1400$  bar.

In Figure 5.6 the volume fraction of vapour distribution with different cell size computational domains is presented (Table 5.2). The same colour scale is used in the images (min=0, max=1). It is seen that a finer mesh can improve the spatial distribution but it does not affect significantly the flow behaviour.

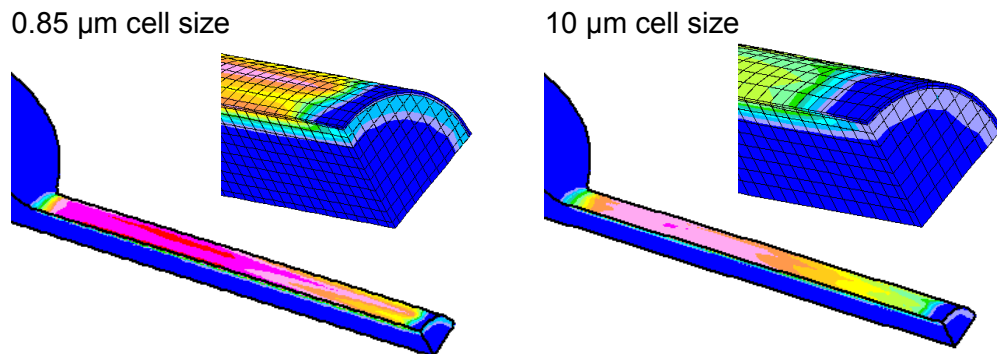


Figure 5.6: Volume fraction of vapour distribution with different mesh resolutions.

The corresponding representative images of vapour volume fraction and velocity magnitude of the tapered nozzle are presented in Figure 5.7. It is seen that this kind of nozzle does not cavitate, even for high injection pressures and high KN. A more gradual acceleration is observed compared with the cylindrical nozzle.

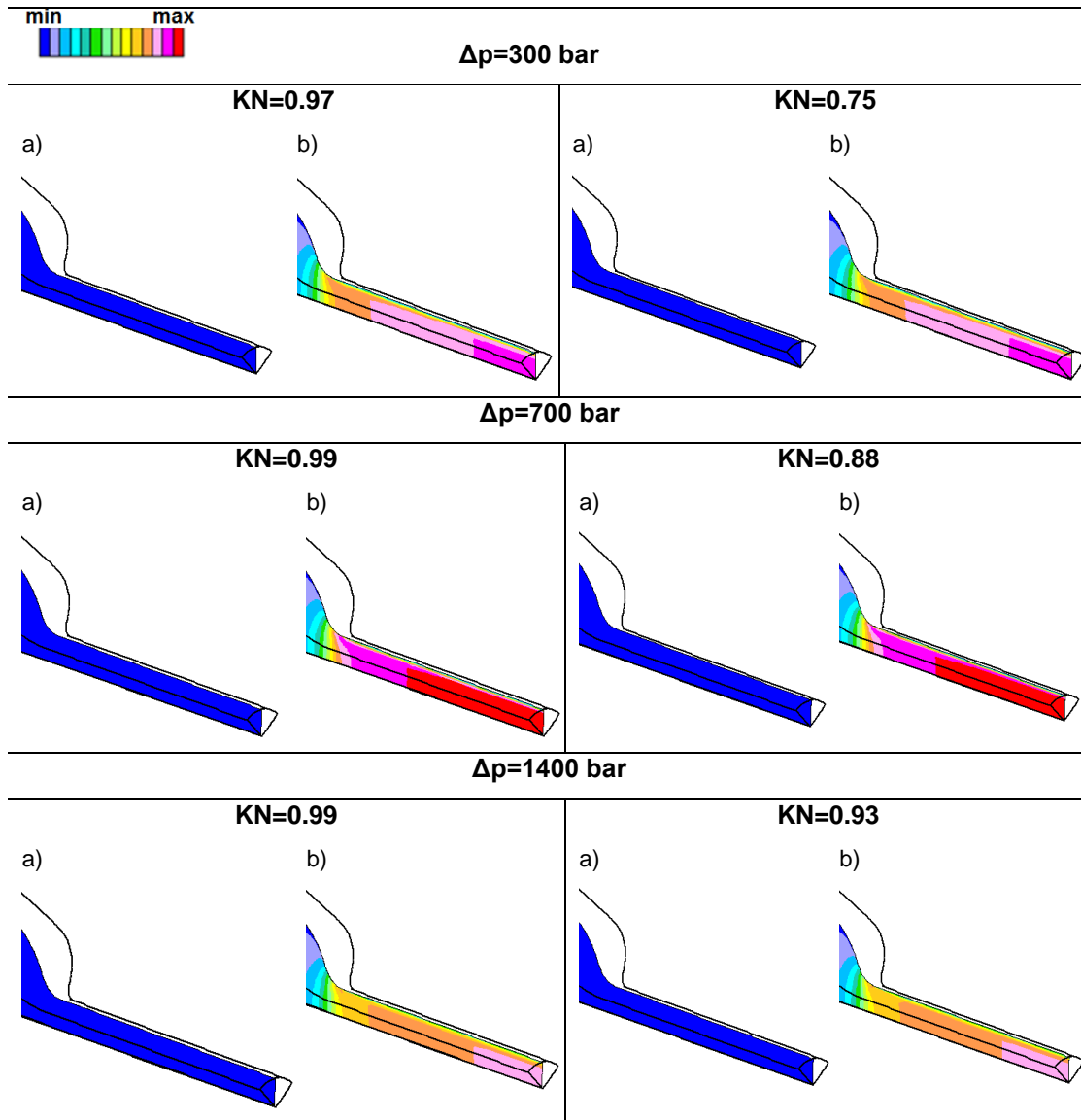


Figure 5.7: Representative a) volume fraction of vapour and b) velocity images for different level of pressures and KN (tapered nozzle). Colour scale: volume fraction of vapour: 0-1, velocity magnitude (m/s): 0-300 for  $\Delta p = 300$  bar, 0-400 for  $\Delta p = 700$  bar, 0-700 for  $\Delta p = 1400$  bar.

**Analysis of the nozzle exit characteristics**

Concentrating now on the nozzle exit, the effect that the cavitation pattern has on the outlet flow conditions is analysed. Plots of the density and axial velocity along the dimensionless radius of the nozzle are presented in Figure 5.8, for the cylindrical and tapered nozzles at the various operating conditions ( $\Delta p=300$  bar;  $\Delta p=700$  bar;  $\Delta p=1400$  bar) and varying KN; these provide a clear indication of the extent of cavitation. The positional data is referenced as follows: the value at position zero corresponds to the centre of the hole.

For the cylindrical nozzle, there is an evident decrease of density due to the presence of cavitation at the hole exit, especially for high flow rates and enhanced cavitation conditions (high KN). The profiles are asymmetrical with minimal density in the upper part of the hole, which indicates the appearance of cavitation in the upper area of the nozzle exit. In the tapered nozzle, the density profile is constant along the diameter for all KN, with the density value equal to the liquid density. This indicated clearly that there is no vapour, hence no cavitation, at the tapered nozzle exit. This is linked with the acceleration of the flow inside the nozzle. It is clear from the above remarks that the nozzle geometry and the operating conditions greatly affect the flow distribution at the nozzle exit.

Looking at the velocity profiles at the nozzle exit, they are very similar in nozzle shape in both nozzles and for all  $\Delta p$  levels. Considering that the flow in the tapered nozzle never cavitates, this shape similarly indicates that the predicted cavitation does not affect significantly the velocity profiles. However, it is worth noting that the velocity profile becomes slightly steeper near the wall (when cavitation occurs) when the flow cavitates ( $\Delta p=700$  bar). But it does not change practically with cavitation intensity, since all cavitating profiles are almost identical.

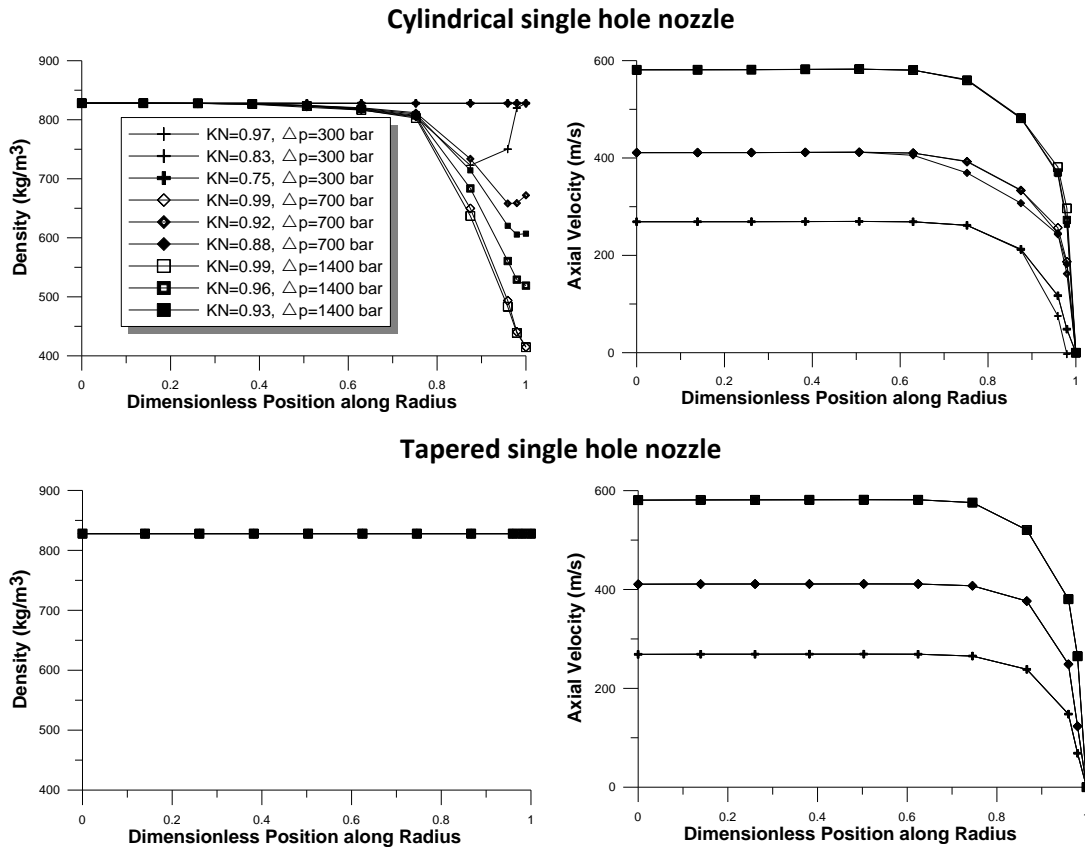


Figure 5.8: Density and axial velocity profiles at the exit of the cylindrical and tapered single hole nozzle for different pressure levels. The legend symbols are the same in all graphs.

## 5.5.2 Predicted flow in multi-hole Diesel injectors

### Analysis of the internal flow distribution

The flow pattern inside the multi-hole nozzles is described in detail in this section. Figure 5.9 illustrates the cavitation pattern along the nozzle axis, with representative vapour volume fraction images of low and high KN for each level of pressure. The images are limited to the cylindrical nozzle, since practically no cavitation appears in the tapered nozzle, except in small areas at the hole inlet and at enhanced cavitation conditions only. Except for the

cases with  $\Delta p=300$  bar and low KN, overall, cavitation appears in the upper area of the nozzle hole entrance for all  $\Delta p$  conditions, due to the abrupt change of the flow direction. It is seen that the cavitation distribution in this type of nozzle differs from the single-hole nozzle pattern. The largest quantity of vapour is concentrated at the top of the hole in the first half of the nozzle, and then expands to fill in the whole nozzle region up to the exit. In addition, the prediction shows that a kind of double vortex structure starts forming inside the nozzle and propagates downstream towards the hole exit. Similar cavitation patterns have been previously described in the literature [30, 130]. It is thought that the pressure difference between the upper and the lower side of the hole induces this vortex flow.

Overall, with increasing injection pressure and KN, more vapour generates and the intensity of the vortices grows, but the general cavitation pattern does not change significantly otherwise. The influence of the backpressure is more drastic, as its increase hinders the extension of the cavitation. Similar experimental observations are reported in reference [29].

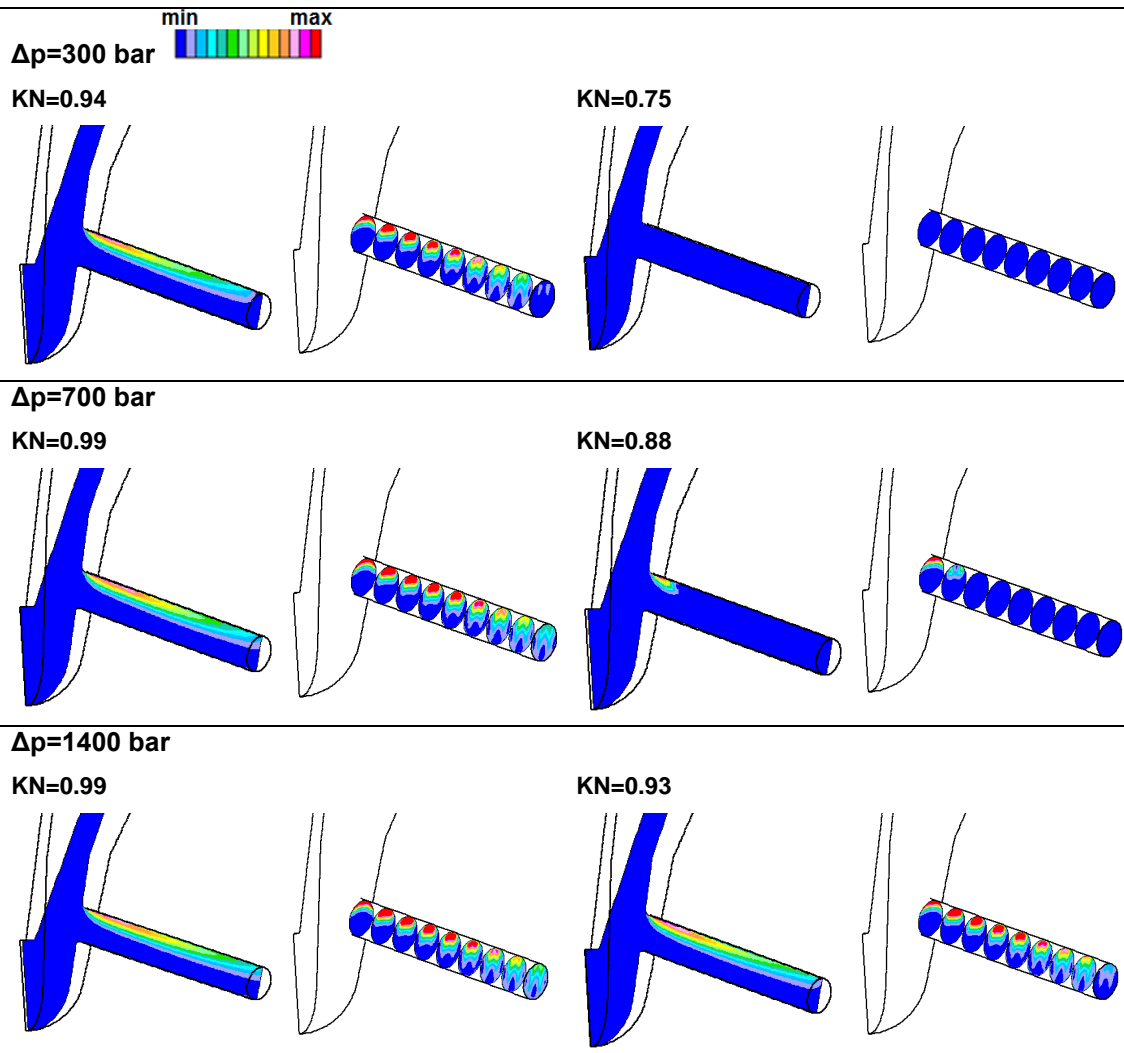


Figure 5.9: Representative volume fraction of vapour images of the cylindrical nozzle for different levels of pressure and KN (colour scale: 0-0.5 for the multiple cross-section cuts; 0-1 for the vertical cuts).

#### Analysis of the nozzle exit characteristics

Focussing now on the nozzle exit, the effect that the cavitation pattern has on the outlet flow conditions is analysed. Figure 5.10 indicates the locations at the exit of the nozzle where the CFD data of the density and velocity profiles

is extracted. The positional data is referenced as follows: the value at position zero along the vertical edge corresponds to the bottom of the hole, while along the horizontal edge the zero is located on the left hand side of the hole.

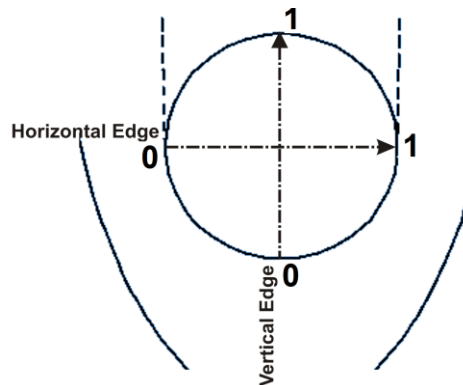


Figure 5.10: Hole outlet measurement locations for the density and velocity profiles.

Plots of the density along the vertical and horizontal axes of the nozzle are presented in Figure 5.11 for the cylindrical nozzle at the various operating conditions ( $\Delta p=300$  bar;  $\Delta p=700$  bar;  $\Delta p=1400$  bar) and for varying KN; these provide a clear indication of the extent of cavitation. For the cylindrical nozzle, there is an evident decrease of density due to the presence of cavitation at the hole exit, especially for high flow rates and enhanced cavitation conditions (high KN). The profiles of density along the horizontal edge are symmetrical with a pair of low peaks towards the centre of the hole. These peaks correspond to the appearance of the vapour vortices mentioned above, with clearly more vapour in the centre of the vortices, as seen in Figure 5.9. Along the vertical edge, the profiles are asymmetric with minimal density in the upper part of the hole, which indicates the appearance of cavitation mostly in the upper area of the nozzle exit.

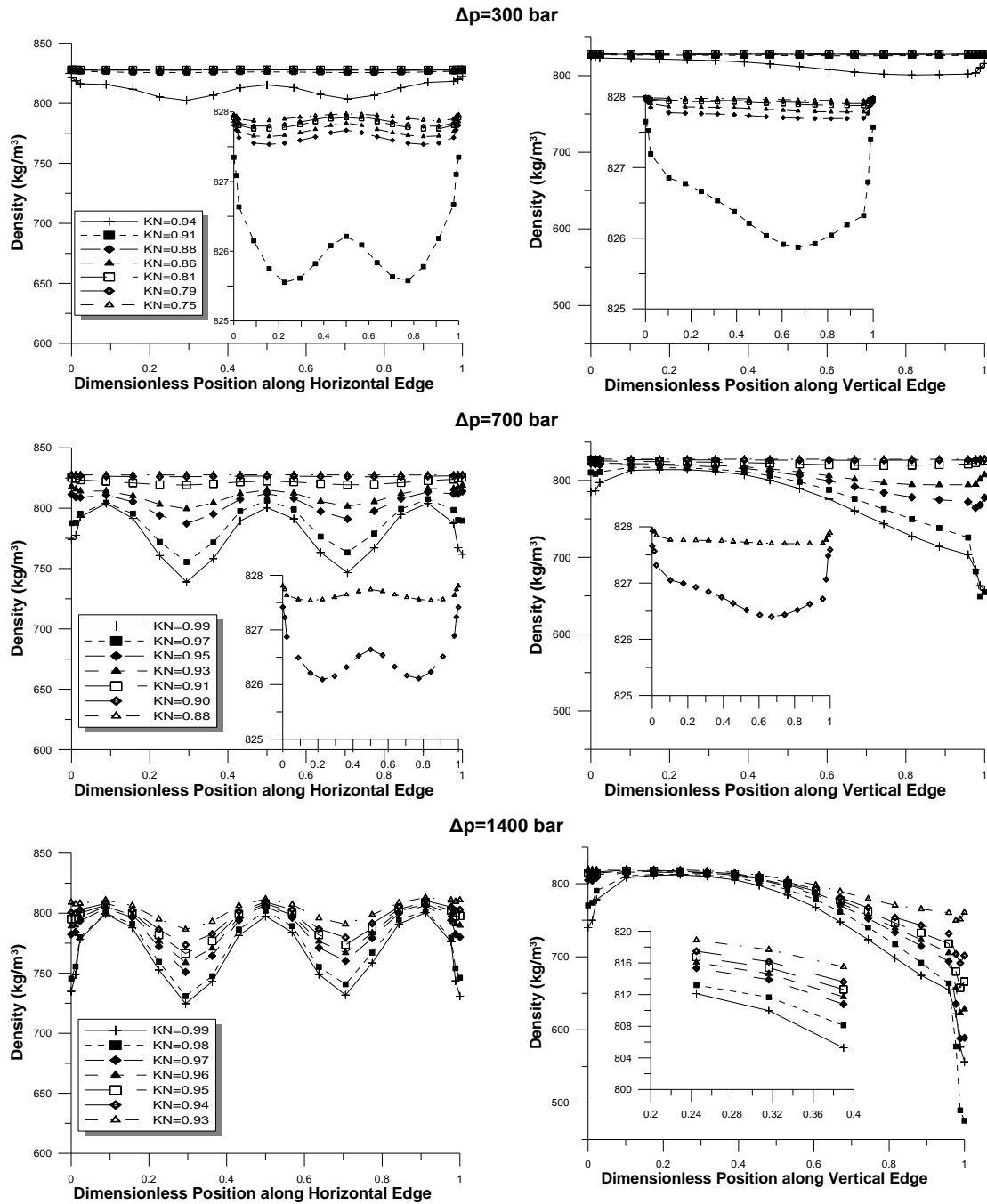


Figure 5.11: Density profiles at the exit of the cylindrical nozzle for different pressure levels

Predicted density profiles at the exit of the tapered nozzle are presented in Figure 5.12. The absence of cavitation in the tapered nozzle, linked with the acceleration of the flow inside the nozzle, observed in the single-hole case is visible in this case too. Only in severe conditions ( $\Delta p=1400$  bar,  $KN=0.99$ ) there is a decrease in density attributed to the slight vapour formation induced by the swirling flow (see density profile along the horizontal edge), as well as in the lower and upper parts of the nozzle (density profile along the vertical edge).

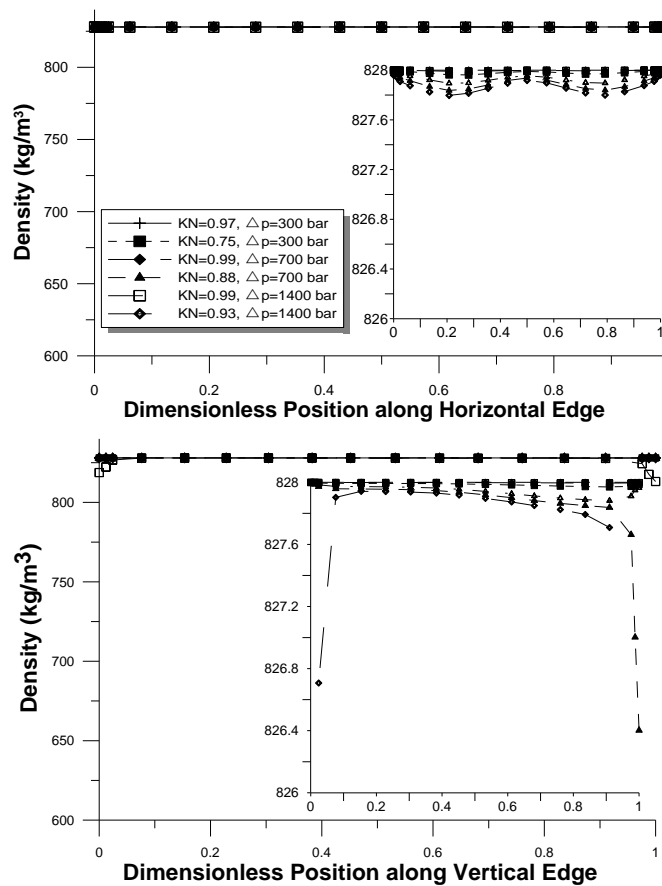


Figure 5.12: Density profiles at the exit of the tapered nozzle (the legend for top and bottom figures is the same).

In Figure 5.13, axial cut views of the velocity and vapour volume fraction are visualised for both nozzles at extreme conditions ( $\Delta p=1400$  bar,  $KN=0.99$ ). These illustrate the vortical flow pattern that appears in both cases and how the cavitation structures follow the vortical flow inside the cylindrical nozzle, with more vapour entrained by the high velocity flow at the center of these vortices.

Cylindrical multi hole nozzle  
( $\Delta p=1400$  bar,  $KN=0.99$ )

Tapered multi hole nozzle  
( $\Delta p=1400$  bar,  $KN=0.99$ )

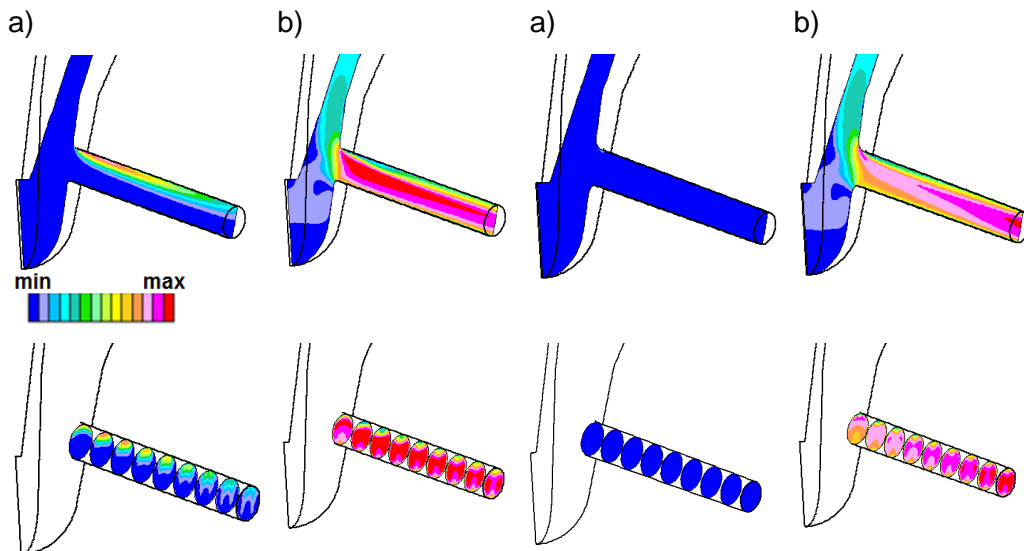


Figure 5.13: a) Volume fraction and b) velocity distribution in the cylindrical and tapered nozzles (colour scale: 0-1 for the volume fraction of vapour; 0-580 m/s for the velocity magnitude).

The axial velocity profiles for low and high cavitation numbers for each level of pressure are plotted versus the dimensionless nozzle diameter (horizontal/vertical edge) in Figure 5.14. For the cylindrical nozzle, there is no appreciable change in the velocity profile shape along the horizontal edge for different  $KN$ . This is due to the limited amount of vapour that is present along

the horizontal edge. The velocity peaks in the vorticity zones are more pronounced at enhanced cavitation conditions and higher pressure drops. Along the vertical edge the differences in the profiles for varying KN are more pronounced, due to the larger amount of vapour observed in the upper region. In this case, the velocity maximum is near the border of the cavitation cloud and is also more pronounced at enhanced cavitation conditions and higher pressure drop. Similar observations have been reported in [22] about the velocity profiles in cavitating conditions. For the tapered nozzle, the shape of the velocity profiles is very similar to that of the cylindrical nozzle, as may be seen in the bottom part of Figure 5.14. However, due to the absence of cavitation the velocity profiles are identical for varying KN and same  $\Delta p$ , and the peaks are slightly less marked than those of the cylindrical nozzle.

Globally, it seems that cavitation introduces an asymmetry in the region of cavitation which causes a displacement of maximum velocity. However, the asymmetrical profile was found also in the tapered case (vertical edge), which indicates that the velocity at the exit of the nozzle is still affected on how the flow enters on the nozzle (the flow is not stabilized yet). Indeed, for the single-hole case, it is seen that the velocity profile of the tapered is perfectly symmetric, as the flow enters symmetrically in the nozzle.

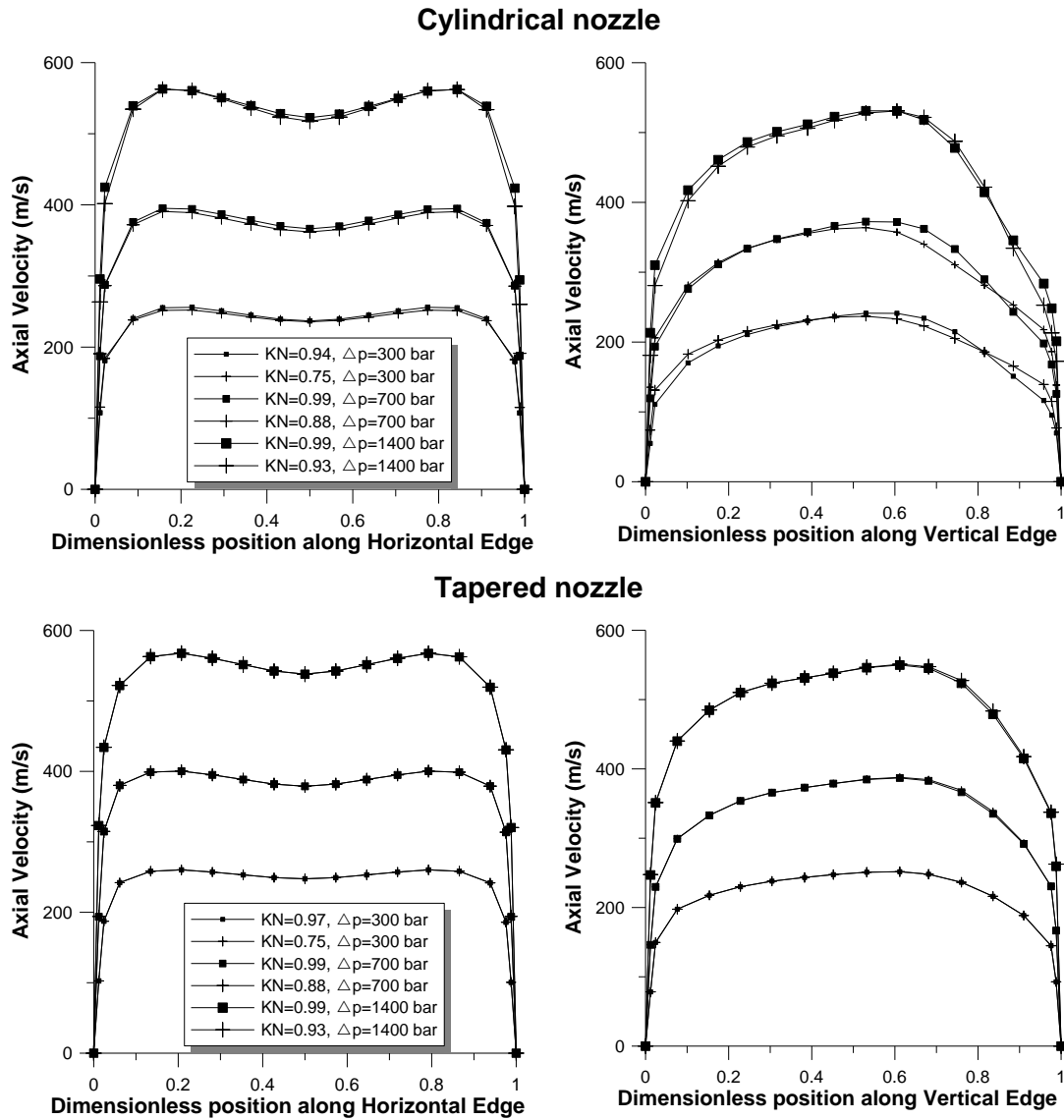


Figure 5.14: Axial velocity profiles at the exit of the tapered and the cylindrical nozzles for different levels of pressure and KN (the legend for the right hand side figures is the same as for the left hand side).

## 5.6 Summary

The predictive capability of the commercial cavitation model was assessed for single-hole and multi-hole nozzles and the cavitation pattern was analysed as a function of pressure conditions and geometry at fully opened needle lift. Predicted results were validated against available in-house experimental data by comparing the flow coefficients. The following conclusion remarks may be drawn from this study:

- Overall, the agreement of the model with the experiments at fully opened needle lift has been found to be quite satisfactory for both nozzles on a qualitative level. For both nozzles, the onset of cavitation was well predicted by CFD as observed by the discharge coefficient  $C_d$  reduction. The known effect of cavitation number has been reproduced quite faithfully by the simulations.
- Cavitation modelling has reached a level of maturity such that it allows predicting the effects of geometry and operating conditions with reasonable accuracy. This represents a valuable contribution to the understanding of nozzle performance.

Next, the effect of pressure drop on the flow coefficients was analysed for the single-hole and multi-hole nozzles:

- It has been observed experimentally that the  $C_d$  was independent of the pressure drop in the single-hole nozzle, while in multi-hole nozzle an increasing trend with increasing pressure drop pressure was observed for both the tapered and cylindrical nozzles. The CFD calculations, however, did not predict clearly this behaviour, probably due to the fact that the pressure loss within the injector body was not

taken into account when imposing the injection pressure on the calculation domain.

The influence of nozzle type on the cavitation structure present in orifices at operating conditions of low and high KN has been analysed.

- The predicted single-hole nozzle cavitation distribution was confined to the wall area, showing different extension depending on the operating conditions.
- A more complicated cavitation pattern was predicted in the multi-hole nozzles. The cavitation develops mostly in the upper part of the nozzle and follows the vortical pattern imposed by the flow velocity as evidenced in the density and velocity profiles. Low density peaks are observed at locations where there is maximum velocity, indicating that vapour bubbles are entrained by the swirling flow.
- The back pressure plays a more important role in the development of cavitation than the injection pressure. Indeed, an increase of the injection pressure does not influence significantly the cavitation pattern, while an increase of the backpressure hinders the cavitation expansion.
- The density and velocity profiles at the exit of the nozzle provide valuable information concerning the presence of cavitation at the hole exit; this is important to understand how it may affect the atomisation process of the liquid fuel jet.

## **CHAPTER 6.**

### **EFFECT OF THE NEEDLE MOVEMENT ON THE NOZZLE**

#### **FLOW**

##### **6.1 Introduction**

In this chapter, the onset and development of the inner cavitating flow is analyzed in relation with the needle movement by performing moving mesh calculations. Both single-hole and multi-hole nozzles with cylindrical and tapered orifices will be examined. Initially, the general methodology for the moving mesh generation and movement approach is presented. Subsequently, a full analysis of the flow results is presented, including a dynamic picture of the developing pattern, analysis of the nozzle exit characteristics and correlation between cavitation and turbulence.

##### **6.2 Moving mesh strategy**

In this chapter the specific approach to fully automatic three-dimensional mesh generation is presented. The approach for moving the generated mesh is also described. The ability to handle complex geometries is an important part of transient calculations of Diesel injectors; therefore, there is a demand for fully automatic mesh generation capable of dealing with such geometries.

To apply the method proposed, the fixed and the moving parts of the calculation domain have to be specified. The first step is to define the initial mesh (cut) which is not subject to motion. In this study the initial geometry was meshed by the automatic mesher of STAR-CCM+ Version 3.02.003. As long as the initial mesh remains the same, by extracting coordinate information from edge lines and defining vertices, the desired moving geometry is defined.

In this problem, the vertices that are subject to motion are those that define the bottom of the needle while the moving area is the annulus formed between the needle and the needle seat, illustrated in Figure 6.1(a). When the needle is fully closed, the annulus through which the flow enters into the injector nozzles disappears (see Figure 6.1(b)). The bottom part of the injector with 10  $\mu\text{m}$  needle lift is considered as initial mesh and is not subject to motion in this study (see Figure 6.2(a)). A low needle lift value has to be considered as the solver cannot handle meshes with size zero. The cell size of the initial mesh used is that of the fixed needle meshes.

In the moving mesh simulations presented here, a  $90^\circ$  sector for the single-hole injector and a  $60^\circ$  sector for the multi-hole injector are considered, as was the case for the full needle lift calculations.

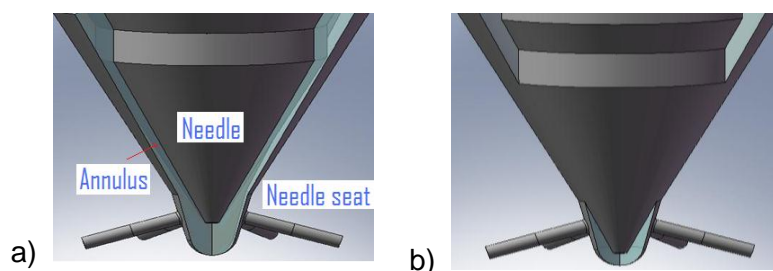


Figure 6.1: a) Needle at full lift, b) Needle at a low lift.

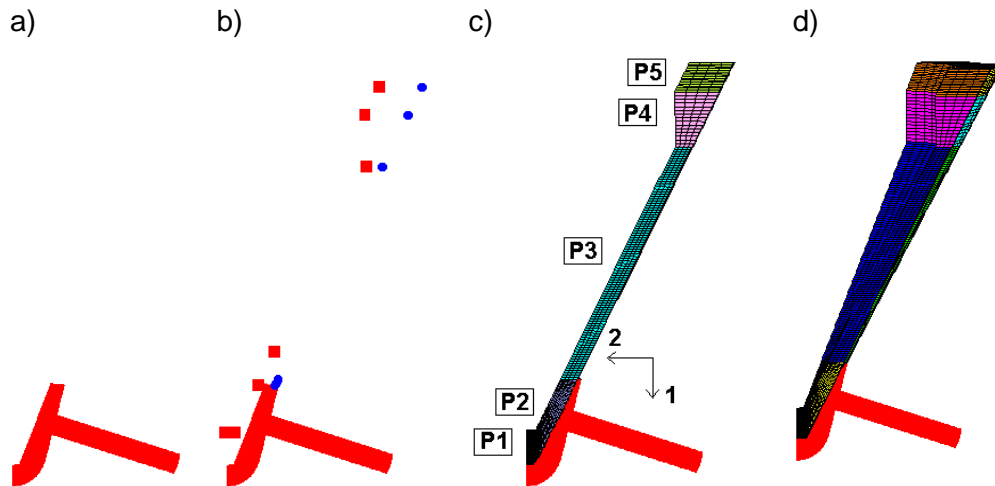


Figure 6.2: a) Initial domain at 10  $\mu\text{m}$  needle lift, b) vertices defining the contour; in squares the vertices subject to motion c) patches defined for mesh generation, d) full needle lift mesh after extrusion.

Once the initial domain is meshed, the vertices that define the contour of the geometry at full lift (250  $\mu\text{m}$ ) have to be specified (Figure 6.2(b)). The vertices will be subject to motion and also they will be used to generate the surface (patch) which maintains uniformity during mesh motion (five patches created, see Figure 6.2(c)). The patches are defined in terms of characteristic points (vertices that are not subject to motion) and derived points (vertices that are subject to motion) and then extruded along a specified direction and using a coordinate system in order to obtain the mesh corresponding to the full needle lift (Figure 6.2(d)). The extrusion consists of defining the number of cells that the mesh will have in each direction (Figure 6.3). The patch can be extruded to create a three-dimensional mesh block once the user decides on the number and distribution of the cells, depending on the geometrical complexity of the model. The meshes of the annulus between the needle and the needle seat stretch and shrink with the needle movement.

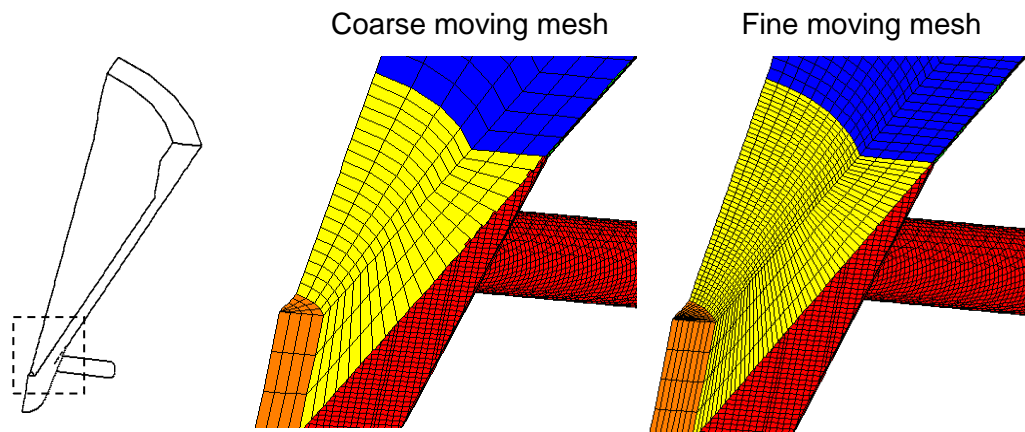


Figure 6.3: Meshes of the moving part obtained by the extrude facility.

The sac and the hole of the single- and multi-hole nozzle were meshed with the fineness resolution determined in the full needle lift calculations (cell size:  $10\ \mu\text{m}$ ); the moving mesh part (mesh between the needle and the injector body) was generated with coarser cells that expanded or contracted with the needle movement (Figure 6.4). The total number of cells was about 70.000 for the single-hole nozzle and 80.000 cells for the multi-hole nozzles.

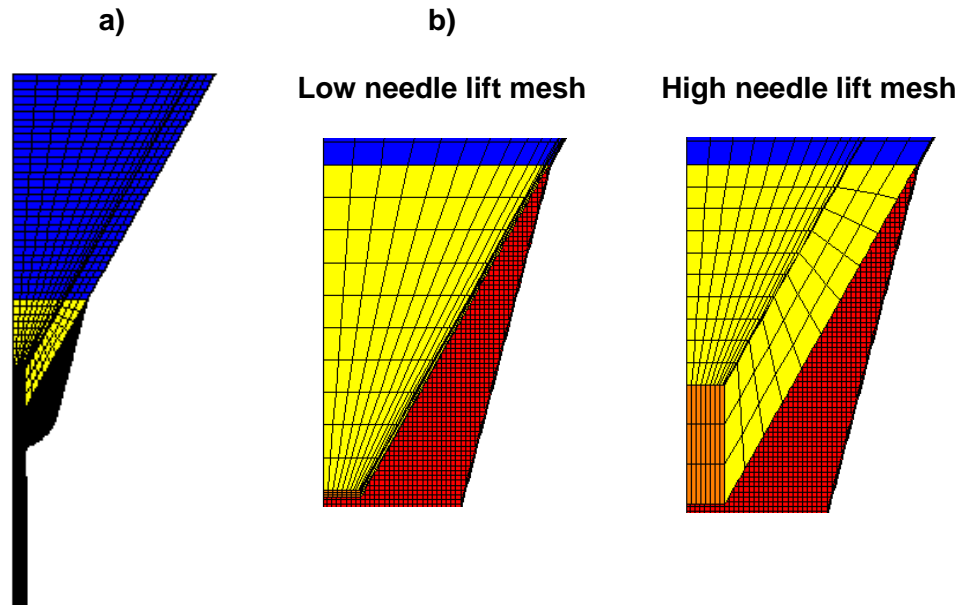


Figure 6.4: Images of the mesh used for the calculation a) general view at full lift, b) close-up at the hole entrance visualizing the coarse (moving) and fine (fixed) region mesh at low and high needle lifts.

To determine the mesh resolution of the moving part, different mesh resolutions were examined on a study performed with the multi-hole geometry. The meshes differ by the number of cells in the horizontal and vertical layer, respectively (Figure 6.5).

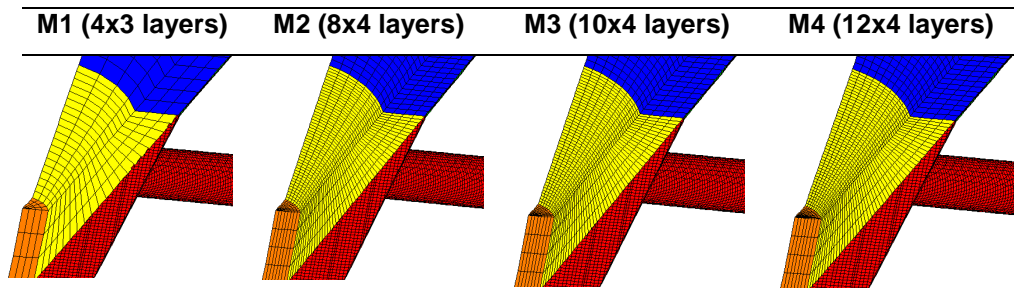


Figure 6.5: Different mesh resolutions (vertical $\times$ horizontal layers) used for the moving mesh part.

The injection rate results obtained with the different mesh resolutions are presented in Figure 6.6. As seen, meshes M3 and M4 yield the same result, while some over-prediction of the mass flow rate can be observed with M2. In the end, the M3 was selected for the multi-hole nozzle calculations to reduce the computational cost, though the accuracy may be compromised.

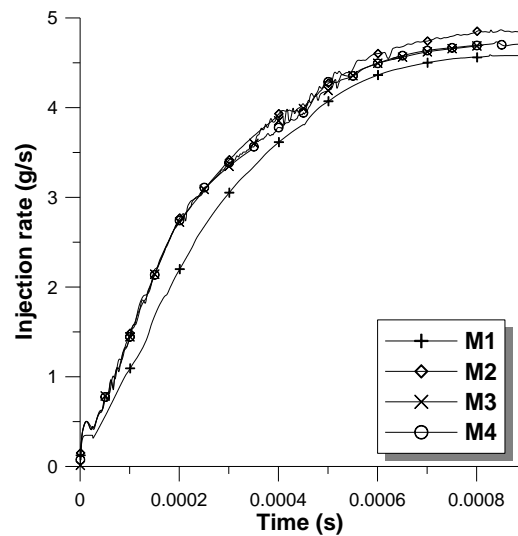


Figure 6.6: Injection rate evolution with different mesh fineness (multi-hole nozzle).

The moving mesh of the single-hole nozzle was with 10 cell layers vertically (as M3) and with 3 layers horizontally (instead of 4), since the pressure gradients were less important in this nozzle.

The final step is to define the connectivity between the fixed and the moving part of the mesh by creating couples of cells at the interfaces. This is automatically done by the code once the user supplies the appropriate commands in the set-up routine. The mesh is now complete and ready to use for calculation.

Two directions of the coordinate system are used for all calculations (single, multi-hole nozzle) in order to move the mesh, avoiding generation of negative cell volumes (badly formed) and consequently divergence of the solution. An example is given here for the multi-hole nozzle. The patch P1 is moved following direction number 1 defined in Figure 6.2, c. The distance considered for the displacement is the one directly calculated in the needle lift user subroutine, since this patch follows the lift of the needle. The other patches, P2, P3, P4, and P5 are moved following direction number 2. In order to follow the real needle valve opening, the displacement of these patches is equal to half of the calculated displacement of the needle (P1). This is allowable due to the conventional geometry of the injector considered. Indeed, the nozzle seating forms an angle of  $30^\circ$  with the axis of the nozzle, so the displacement of these patches assumes the value of (needle displacement  $\times \sin 30^\circ$ ). It is thus possible to have the true geometry displacement and also keep the mesh aspect constant, having only the cell size change. The other possibility would have been to move all the patches following direction number 2, using the displacement calculated for P1. However, the former strategy was preferred in order to avoid the deformation of the mesh during needle valve

closing. This deformation generated negative volumes for the cells on the interface between the fixed and moving parts.

### **Needle lift law**

In single nozzle holes, the same lift law (based on simple linear equations) was used for the cylindrical and tapered nozzle calculations.

In the multi-hole holes, since the needle lift law is not known and cannot be measured, the following technique was followed in order to define it. Six fixed geometry calculations were performed, each at a different needle lift: 25  $\mu\text{m}$ , 50  $\mu\text{m}$ , 75  $\mu\text{m}$ , 100  $\mu\text{m}$ , 200  $\mu\text{m}$  and 250  $\mu\text{m}$ . Thus, the curve for injection mass flow as a function of needle lift was obtained. A correspondence between this curve and the experimentally measured injection rate yields the needle lift law as a function of time (Figure 6.7, a). Between the various interpolated points, the slope was calculated and adapted to define the lift law numerically (Figure 6.7, b). Figure 6.7, c, shows the predicted injection rate with the needle lift law used, while Figure 6.7, d shows the experimental and the predicted injection rate results (normalised) obtained.

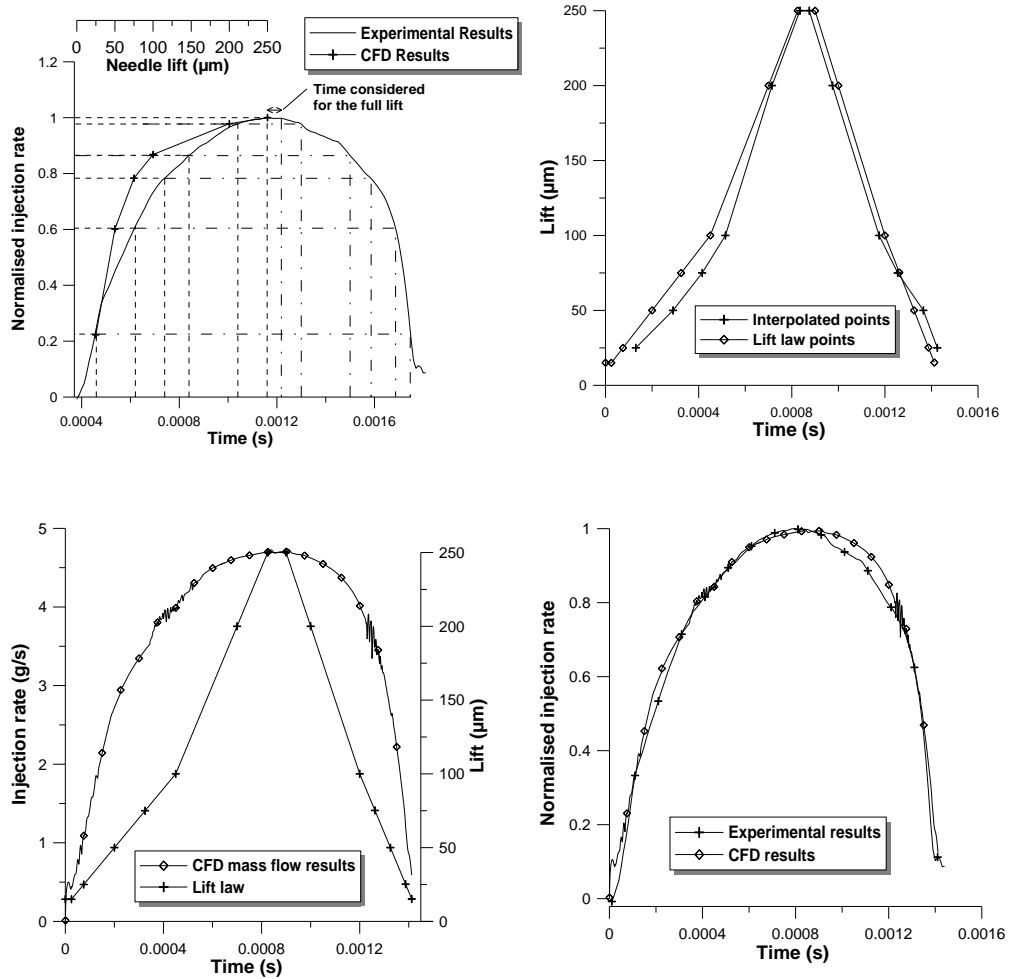


Figure 6.7: a) Mass flow interpolation between experimental and computational results at fixed needle lifts b) Interpolated points and lift law considered for the calculations versus time. c) CFD Injected mass flow and lift law considered, d) Comparison between CFD and experimental injected mass flow.

Thus, the lift was estimated as a function of time using equation (6.1) which is used to move the needle in the transient calculations.

$$l(t) = l(t_i) + \frac{dl(t)}{dt}(t - t_i) \quad (6.1)$$

where  $l(t_i = 0) = 0$  and  $t_i$  is the time corresponding to the previous lift point.

The solution needle displacement was calculated by a specific routine, which was integrated in the code, and which read at each iteration the appropriate set of commands. The procedure may be described by the following steps: 1) Start calculation at time 0. 2) Calculate displacement  $A(0)$ , where  $A(0)$  the needle lift. 3) Delete all cells. 4) Import the initial mesh. 5) According the  $A(0)$  calculate the new coordinates on the moving part that define the new surface. 6) Create the patch surface. 7) Extrude the patch creating the domain (meshed). The number of cells is defined via user commands, 8) Delete the patch, 9) Merge the double vertices, 10) Construct the connectivity between the fixed and moving part. 11) Calculate. 12) Repeat the steps 2-11 until a determinate time value is reached.

## 6.3 Results obtained by Moving Needle Simulations

### 6.3.1 Predicted flow in single-hole Diesel injectors

#### Needle motion influence on internal flow distribution

The calculations of the flow characteristics were performed at real engine operating conditions (1410/10 bar). Representative images of the predicted vapour volume fraction, the turbulence kinetic energy and the velocity field are presented in Figure 6.8 for the tapered and the cylindrical nozzle at full lift. Figure 6.8 shows that even at these critical conditions, the tapered nozzle does not cavitate as was also observed in Chapter 5 for the fixed needle lift mesh calculations. For both nozzles, when the liquid enters into the injection hole, the velocity increases rapidly due to the decrease of cross sectional area. The highest velocity gradients are confined to the entrance area of the

nozzles where the lowest pressures are also expected. The flow acceleration is more gradual in the tapered nozzle than in the cylindrical, also observed for the fixed full needle lift calculations. For both nozzles, the turbulence kinetic energy is enhanced at the hole inlet and diffuses towards the hole exit. This has also been observed in the reference [3], but has been attributed to the bubble break-up process which takes place along the hole length. However, the turbulence level in the tapered hole inlet and along the nozzle is lower. One reason for this difference may be linked to the hole inlet smoother curvature (R88 instead of R45 for the cylindrical nozzle), as well as to the greater inlet diameter of the tapered nozzle (D176 instead of D157 for the cylindrical nozzle). This was confirmed by comparing results of the two nozzles under non cavitating flow conditions (1500/100 bar). Another reason is the absence of cavitation in the tapered nozzle.

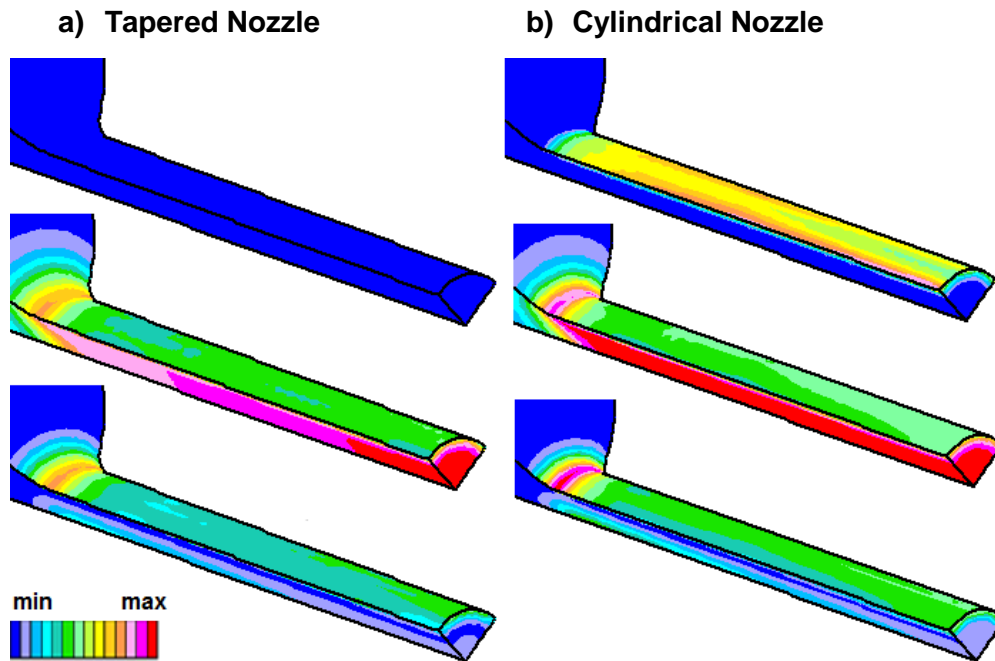


Figure 6.8: Representative images of volume fraction of vapour, velocity magnitude and TKE from top to bottom for a) tapered and b) cylindrical nozzle hole at fully opened needle lift. Color scale: fraction of vapour: 0-1, velocity magnitude (m/s): 0-600, TKE( $\text{m}^2/\text{s}^2$ ): 0-5000.

Representative images of the cavitation distribution during the needle motion are presented in Figure 6.9, limited to the cylindrical nozzle, since no cavitation appears in the tapered nozzle. They show that the cavitation at all needle lifts develops confined to the periphery of the nozzle, in agreement with observations by [10, 71]. The extension of the cavitation bubble grows with the needle lift. However, there is a kind of hysteresis between the needle valve opening and closing particularly at low needle lifts: it is clearly visible in Figure 6.9 for 25  $\mu\text{m}$  that the vapour does not reach the nozzle exit at valve opening, while it does at valve closing. This shows that the influence of the

needle lift motion on the development of cavitation is more important when the needle ascends. On the contrary, during the needle closing the cavitation seems less transient, it takes longer to recede back.

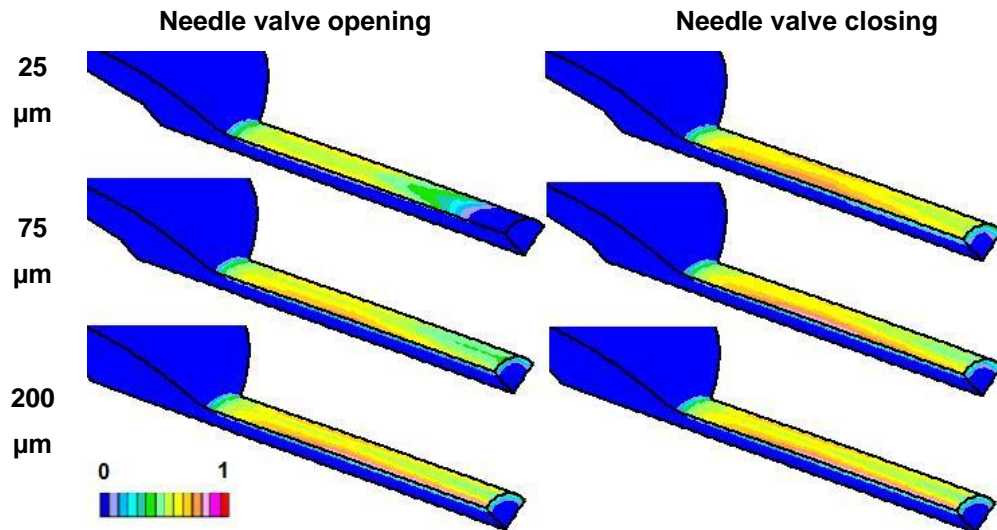


Figure 6.9: Predicted volume fraction of vapor field at different needle lifts during the needle valve opening and closing.

Figure 6.10 shows the evolution of the cavitation bubble close to the nozzle exit while the needle is descending (at about 31  $\mu\text{m}$  needle lift). It is interesting to note that the cavitation level attains its peak at 1650  $\mu\text{s}$ , and then suddenly decreases between this instant and 1660  $\mu\text{s}$ . This illustrates the fact that the cavitation cloud grows and exits the nozzle periodically, meaning that the volume fraction of vapor increases at certain instants. When it grows all the area is occupied by vapour, but just microseconds later the area is occupied mainly by liquid as the vapour cloud has been evacuated. This phenomenon may be linked to the highly transient nature of the cavitating flow.

There is some asymmetry in the cavitation pattern, especially after the evacuation is observed. This could probably be attributed to numerical differences caused by either CAD imperfections or by some inherent asymmetry of the nozzle grid [30], or by the discretization. However, it only occurs when the cavitation level is low and does not affect significantly the solution.

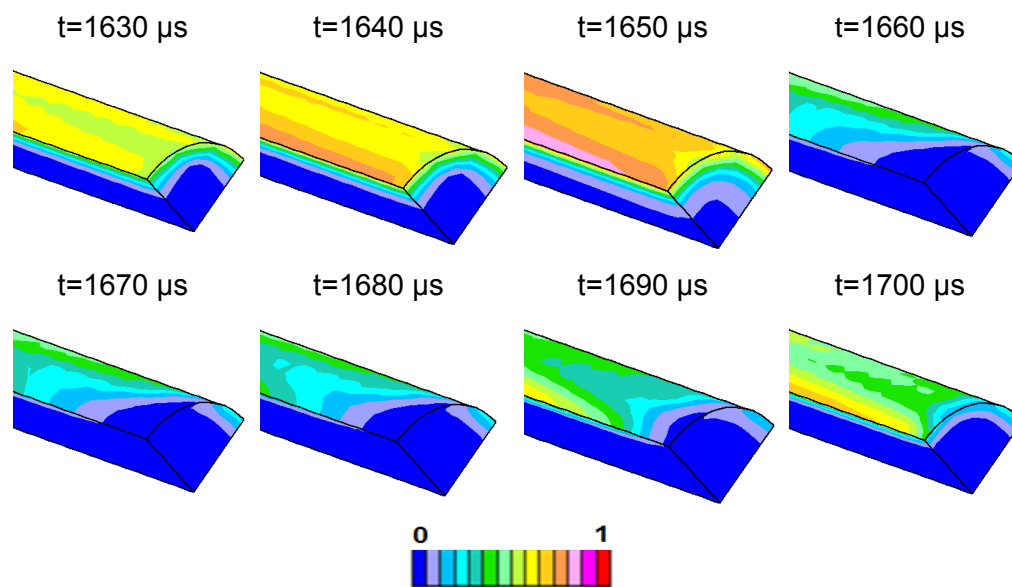


Figure 6.10: Temporal sequence of volume fraction of vapour showing the exit of cavitation cloud at needle closing for the cylindrical nozzle.

#### Needle motion influence on nozzle exit characteristics

The interest of the presented calculations and results is to derive information from the nozzle internal flow conditions for the boundary conditions of the spray calculation. Though the spray calculation itself is beyond the scope of this paper, a further analysis of the internal nozzle flow results at the exit section yields important information, in terms of injection rate, velocity, turbulence and cavitation, as shown in Figure 6.11 for both the cylindrical and

the tapered nozzles (average values over the entire cross sectional area). The same lift law based on simple linear equations was imposed for the cylindrical and tapered nozzle calculations.

As seen in Figure 6.11, top left, the quantity of injected fuel is less in the case of the cylindrical nozzle than in the tapered nozzle, due to the smaller inlet diameter and the presence of cavitation. Additionally, the cavitation has the effect of decreasing the exit area and, consequently, increasing the exit velocity (velocity magnitudes curve, top right).

In terms of evolution during the needle motion, the CFD results clearly show that the mass flow rate increases greatly with increasing needle lift until a certain value, as would be expected. However, very quickly, the mass flow rate becomes independent of the lift. This effect is also noticeable in the evolution of the velocity at the exit. It indicates that the maximum mass flow rate and velocity are limited by the nozzle inlet section conditions.

The turbulence kinetic energy, however, changes noticeably with the needle movement (Figure 6.11, bottom left). It is created at very low needle lifts ( $<50 \mu\text{m}$ ), during both opening and closing, independently of whether there is cavitation or not. This is due to the restricted area in the annulus between needle and nozzle body, so that locally the liquid accelerates, increasing the turbulence level. The TKE attains its maximum level when the mass flow rate and velocity stabilise at their maximum value (between  $50$  and  $75 \mu\text{m}$  lift). Then the turbulence level decays significantly and stabilises at high needle lifts (over  $150 \mu\text{m}$ ), and increases again when the needle descends below  $100 \mu\text{m}$ . The fast turbulence dissipation coincides with the disappearance of the mean velocity gradients and it is interesting to note that the renewed increase at needle closing (between  $150 \mu\text{m}$  and  $50 \mu\text{m}$ ) is more important in

the tapered nozzle, so that the TKE level is the same in both nozzles just before needle closing. This seems to indicate that the generation of cavitation in the cylindrical nozzle tends to absorb part of the turbulence generated during the needle motion.

However, it has to be acknowledged that although in this study the TKE level seems to depend little on the cavitation inside the nozzle, this merits further investigation. Indeed, several authors [150,151,152] have noted that there are large turbulence levels in the cavitating flow. The main reason for this discrepancy may be related to the low levels of cavitation present in the nozzles of this study.

This may be confirmed when observing the evolution of the volume fraction of vapour during lift motion (Figure 6.11, bottom right). The maximum level of TKE coincides with the onset of cavitation at approximately 50  $\mu\text{m}$  lift; then with further lift opening (50  $\mu\text{m}$  to 150  $\mu\text{m}$ ), the quantity of vapour initially oscillates and gently increases up to the moment the fully developed cavitating regime is attained, at relatively high lift (150  $\mu\text{m}$ ). Even then, it has to be noted that there is only 25% vapour, indicating the flow cavitation levels present in this study. The level of TKE decreases during this exact period, at a slightly faster rate than in the non-cavitating case. In addition, while the level of cavitation remains stable, so does the level of turbulence. Furthermore, the sudden growth of the vapour cloud observed at needle closing (1650  $\mu\text{m}$ , see Figure 6.10, and the peak of volume fraction in Figure 6.11, bottom right) just before its release coincides with the period when the needle reaches low lifts and the TKE renewed generation is lower than in the non-cavitating case.

It seems that at low needle lifts, the vapour bubble is more unstable due to the increased flow turbulence caused by the restricted flow passage. At high lifts, it is fairly stable.

Another interesting point is that there is a kind of hysteresis between needle opening and closing (Figure 6.11 bottom). The process of needle opening seems to generate more turbulence than the needle closing, and this is independent of the nozzle geometry, and of the presence of cavitation.

Moreover, the hysteresis is also visible in the cavitation evolution: there is significantly more vapour reaching the nozzle exit when the needle descends. This may be explained as follows: since at full lift, the cavitation is fully developed, the increase in turbulence caused by the closing of the needle enhances further the generation of cavitation. This seems to confirm that part of the turbulence serves to feed the generation of cavitation, when there is cavitation.

However, it is the needle motion at low lifts, which enhances the turbulence level and, the cavitation absorbs part of the turbulence kinetic energy to grow. This has to be taken into account when analyzing the flow characteristics at the nozzle exit and setting up boundary conditions for the spray calculations.

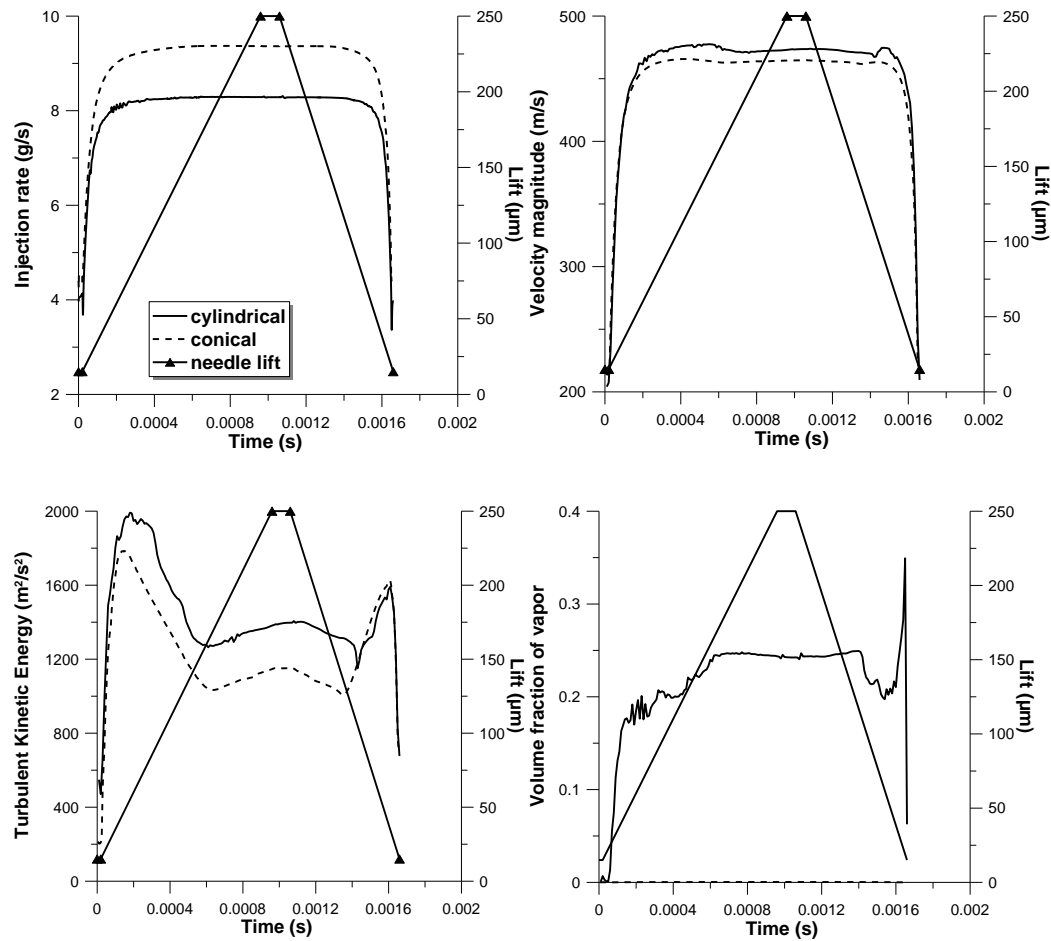


Figure 6.11: Instantaneous results of injection rate, mean velocity, TKE, and volume fraction of vapour at the exit of the nozzle during the simulated injection process.

### 6.3.2 Predicted flow of multi-hole Diesel injectors

#### Needle motion influence on internal flow distribution

The results presented here correspond to calculations made for the following pressure conditions: 800/10, 800/50, 1500/10 and 1500/50 bar. The effect of operating conditions and geometry (including needle lift) on the cavitation pattern will be analysed in this chapter. Firstly, the tapered nozzle is

examined. Practically, no cavitation appears in this type of nozzle, except at the hole entrance for higher pressure drops (1500/10 bar) and very low needle lift (about 15  $\mu\text{m}$  lift) as is seen in Figure 6.12. Cavitation also appears (similarly with the cylindrical multi-hole nozzles) at the annulus between needle and nozzle body at low needle lifts as it is seen in Figure 6.13, with more cavitation during the needle closing. Overall, it is predicted that even at large pressure drops and low needle lift this type of nozzle prevents cavitation from reaching the nozzle hole exit.

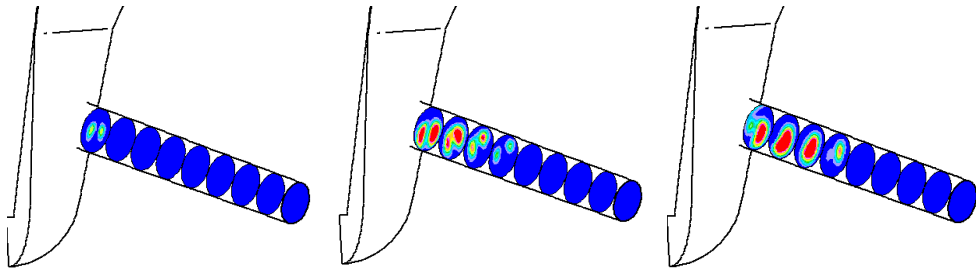


Figure 6.12: Sequence of images of predicted cavitation field for the tapered nozzle at 1500/10 bar and very low lifts (about 15  $\mu\text{m}$ ).

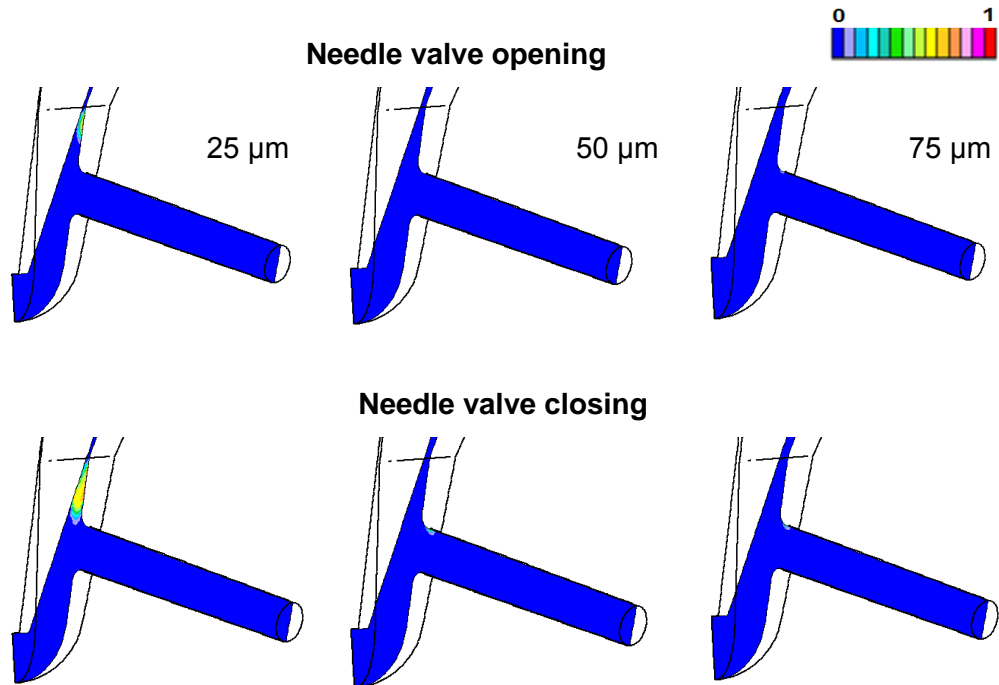


Figure 6.13: Predicted cavitation field at different needle lifts for the tapered nozzle during the needle valve opening and closing (1500/50 bar).

In Figure 6.14 are illustrated the cavitation field contours for the cylindrical nozzle at different needle lifts for the operating condition 1500/50 bar. The cavitation distribution at low needle lifts is quite different from that at high needle lifts. For lifts below 200  $\mu\text{m}$ , the cavitation region starts in the upper part of the hole inlet and, further downstream, it tends to be distributed along two main vortices that reach the hole exit. For all investigated conditions, it seems that with low needle lift the cavitation structures are more unstable, as already observed for the single-hole case. This is due to the increased flow turbulence caused by the restricted passage of the flow in the region between needle seat and nozzle, which affects the levels of turbulence at the hole entrance [3].

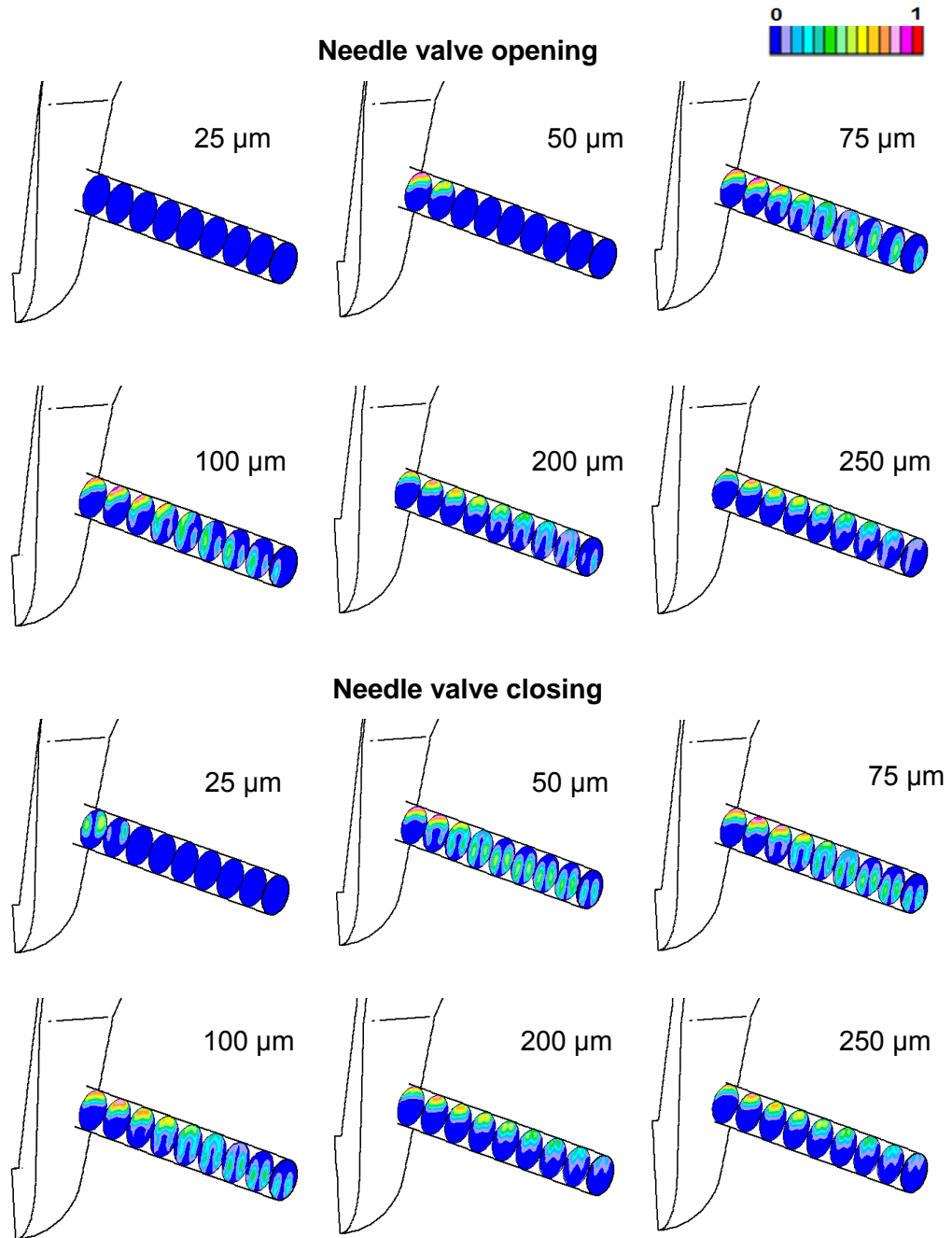


Figure 6.14: Predicted cavitation field at different needle lifts for the cylindrical nozzle during the needle valve opening and closing (1500/50 bar).

As lift increases to full lift, the cavitation field evolves from the two vortices that collapse into a single one which occupies the upper half of the nozzle. Also, some asymmetry is observed with respect to a longitudinal cross section passing through the nozzle axis is observed. However, it could also have physical meaning, since it has been experimentally observed that the injector geometry is not perfectly symmetric [63].

The turbulence level is highly increased at the hole entrance, especially at low needle lift independently of the nozzle hole and diffuses along the nozzle hole. This is illustrated in Figure 6.16 where, the instantaneous TKE results (available at 800/50 bar), not only at the exit but also at different cross sections along the nozzle hole (Figure 6.15) of both tapered and cylindrical multi-hole are presented. Further details and analysis of the turbulence distribution and velocity field for this kind of injector will be presented in Chapter 7.

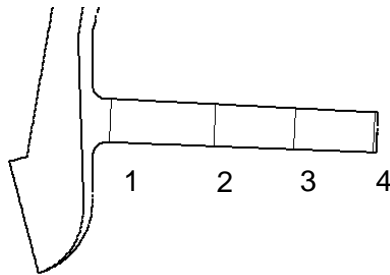


Figure 6.15: Location of nozzle cross-section considered for post-processing in this study.

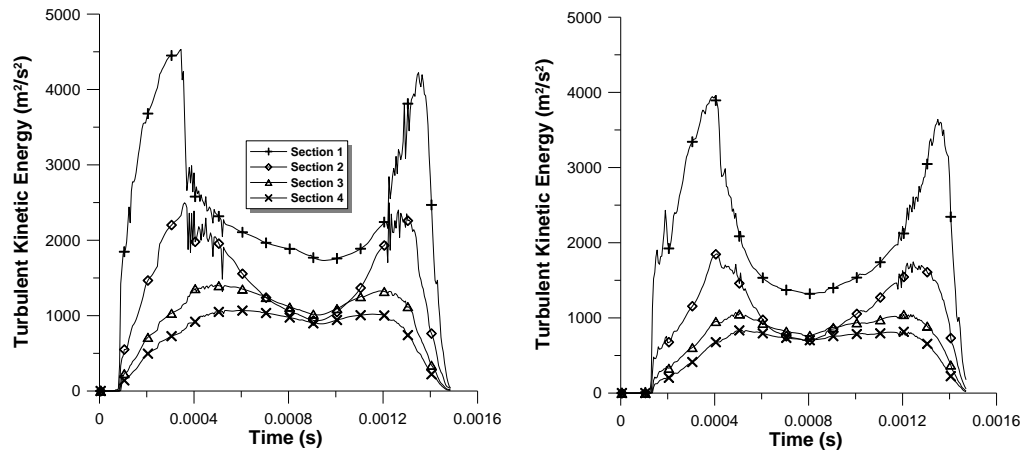


Figure 6.16: Instantaneous results of multi-hole nozzle at different section along the nozzle hole for a) cylindrical and b) tapered nozzle (800/50 bar).

Representative images of the flow streamlines in the volume sac and inside the holes (tapered and cylindrical), obtained with the moving mesh are presented in Figure 6.17. It is observed that at low needle lifts the flow inside the sac volume is highly rotating, noticeably so at the nozzle inlet. This can be related to the appearance of the side corner recirculation and cavitation at the nozzle inlet. After rotating in the sac volume the flow turns and enters from the lower part of the nozzle. At high needle lifts the recirculation zone at the entrance of the nozzle is less intense.

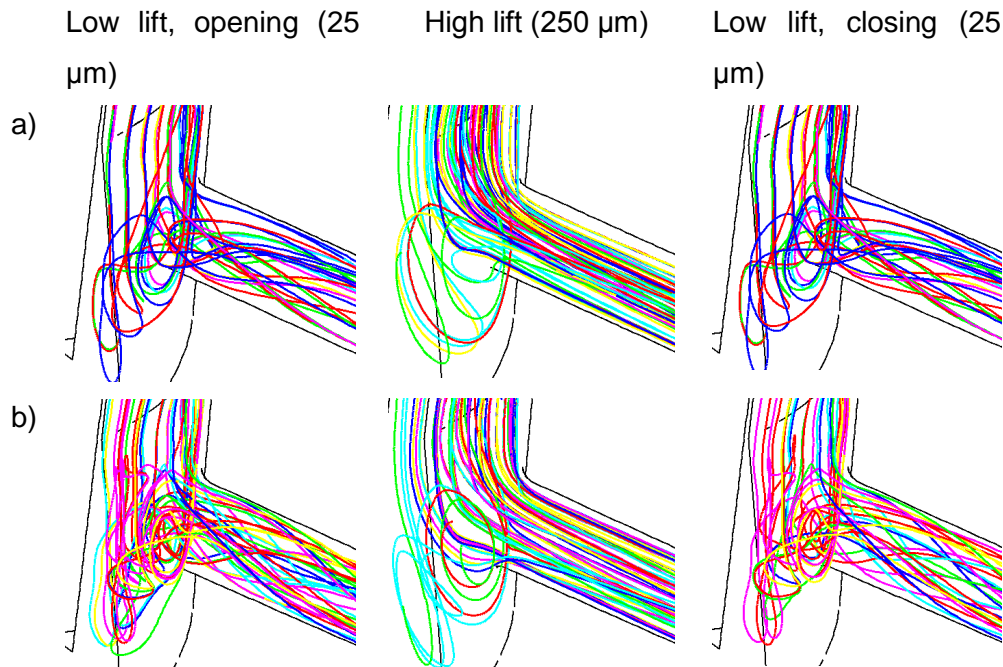


Figure 6.17: Streamlines of the internal flow of a) cylindrical and b) tapered nozzle at low and high lifts (1500/50 bar).

#### Needle motion influence on nozzle exit characteristics

In Figure 6.18 the temporal evolution of the cavitation intensity is presented by the percentage of area occupied by vapour at the exit of the cylindrical nozzle. Here the area of all cells containing at least 5% of vapour is represented. No cavitation was observed at the exit of the tapered nozzle. Indeed, post processing of the results showed that the cavitation region completely disappears in this nozzle at high needle lifts in agreement with [3]. Only a very small region in the nozzle inlet area exists at low needle lifts that and does not reach the exit (1500/10 bar). For the cylindrical nozzle it is observed (Figure 6.18) that for the case 800/50 bar some vapour reaches the hole outlet at low lifts, whereas none is seen at high lifts. For 800/10, 1500/50 and 1500/10 bar the cavitation does reach the exit even at full lift but tends to decrease while the needle remains at full lift. The strong oscillations observed

in this figure are linked to pressure oscillations in the flow field, which may be due to the highly transient character of the flow physics.

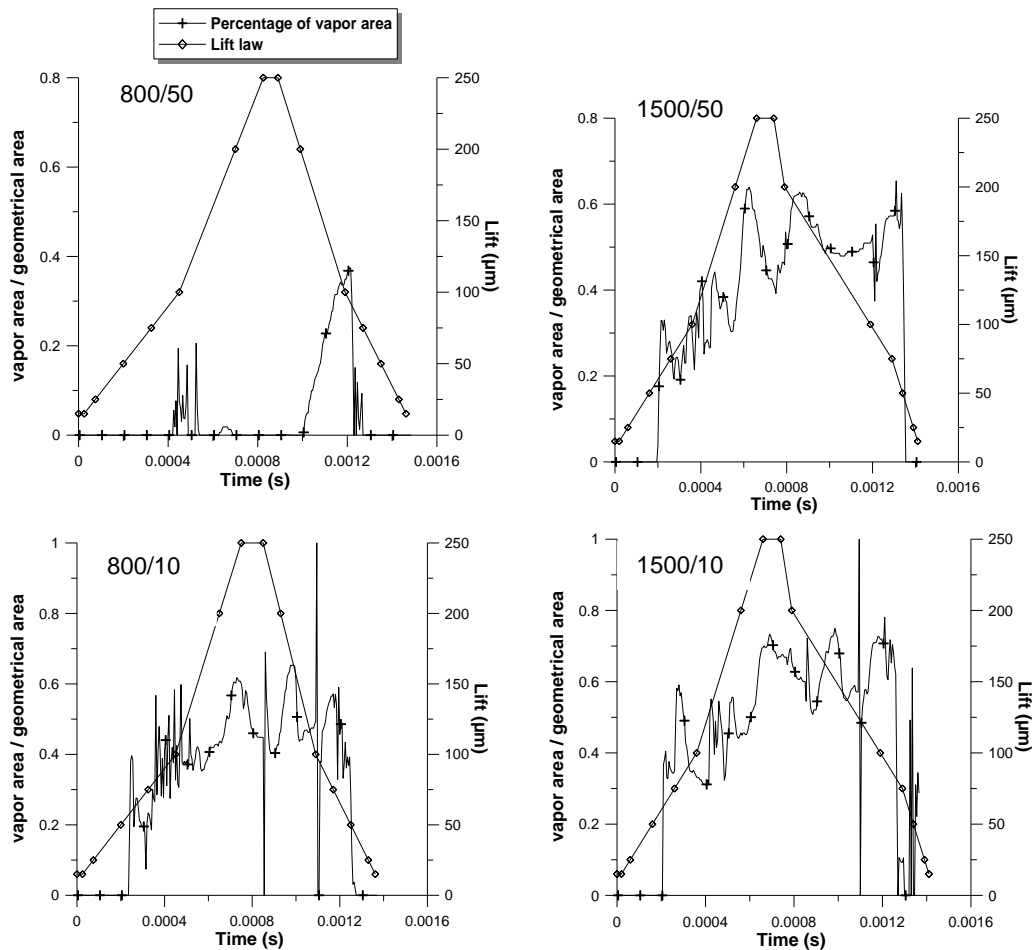


Figure 6.18: Lift curve and % exit area occupied with some vapour (volume fraction of vapour between 0.06 and 1 considered) as a function of time for the cylindrical nozzle.

Another interesting point is that for all operating conditions, the phenomenon of hysteresis is present at low needle lifts between the needle valve opening

and closing (Figure 6.18) as was also observed for the single-hole injector. More vapour reaches the nozzle exit during needle closing than during needle opening. This is also clearly visible in Figure 6.14.

Also, at low lift during closing and particularly for the cases 800/10 bar and 1500/10 bar there appears some peaks in the vapour area curves of Figure 6.18, that can be explained by the fact that at certain times the cavitation cloud grows and exits from the nozzle, as is illustrated in Figure 6.19. The same was also observed for the single-hole injector.

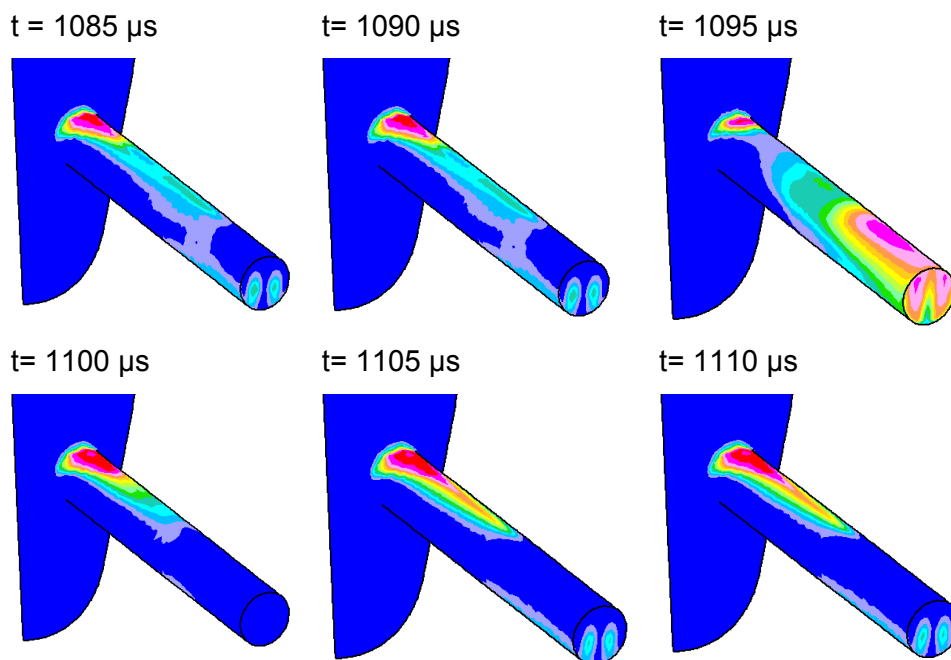


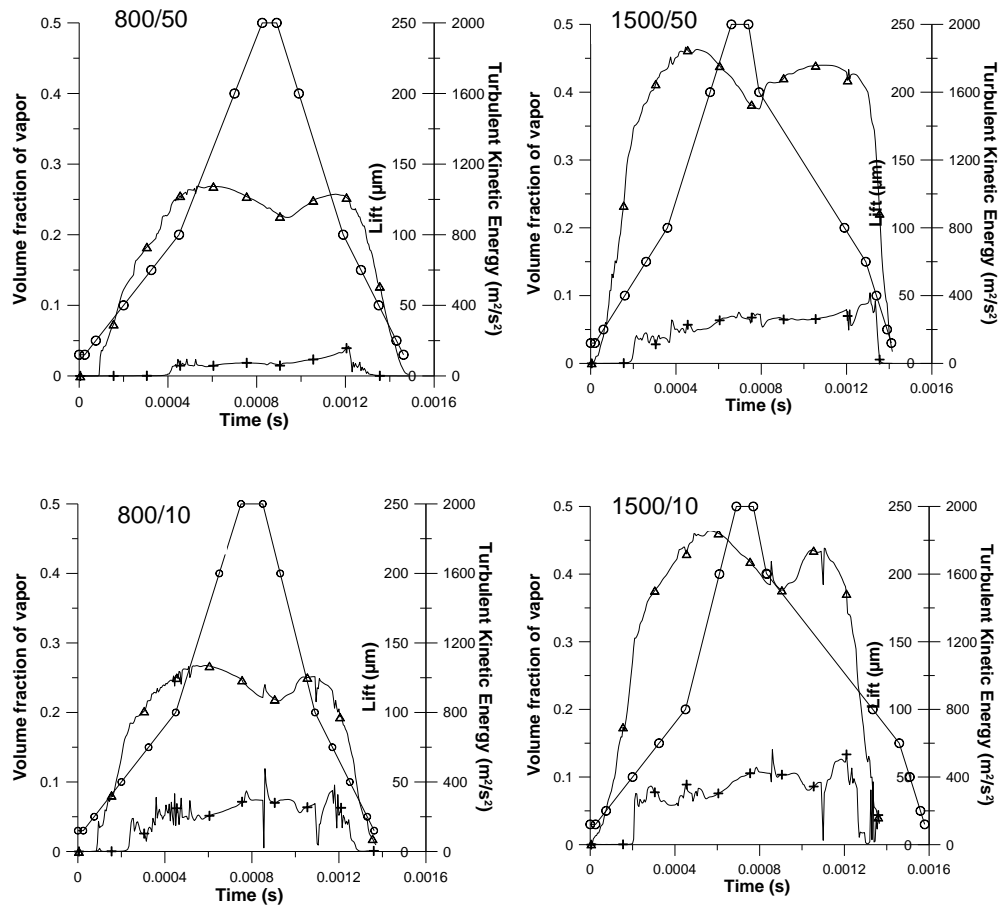
Figure 6.19: Temporal sequence of volume fraction of vapour showing the exit of cavitation cloud at needle closing for the cylindrical nozzle (1500/10 bar).

Figure 6.20 presents results for the cylindrical nozzle at all operating points in terms of turbulent kinetic energy and average volume fraction of vapour at the hole exit. The following observations confirm the points made for the single-hole injector:

- The hysteresis between needle opening and closing is also visible in the levels of TKE and volume fraction of vapour at all cases, more pronounced for the high pressure injection cases.
- The maximum creation of TKE is linked to the needle initial phase opening and its decay to the final phase of closing, and hence to the acceleration/deceleration of the flow at the entrance of the nozzle when the lift is relatively low (constricted passage of the flow). It is worth noting that the maximum level of TKE is attained earlier (around 100  $\mu\text{m}$  lift) for the high back-pressure cases (50 bar) than for the 10 bar back-pressure cases (between 125 and 200  $\mu\text{m}$  lift).
- The level of TKE is higher for the high injection pressure cases (1500 bar), as would be expected, and does not depend on the pressure drop in the nozzle. This tends to confirm that the generation of turbulence in the nozzle is linked to the needle movement, rather than to the flow acceleration within the nozzle.
- In addition, these results confirm that the generation of high turbulence is not directly linked to incipient cavitation. The TKE maxima appear generally at a later stage than the onset of cavitation. However, the TKE creation is slower as soon as cavitation becomes significant, as indicated by the smoother slope of TKE once cavitation has settled in.
- Clearly also, the turbulence level decay with growing cavitation, as was also observed for the single-hole nozzle, at least during the needle opening. The TKE plateau observed at high lift in the single

hole case (see Figure 6.11 bottom left) is not visible for the multi-hole case, but the minimum TKE level at high lifts is attained at a full lift also. This is a clear indication that the generation of cavitation seems to absorb part of the turbulence kinetic energy, but not significantly so. Indeed, the maximum cavitation level occurs generally when the TKE level is increasing again, due to the closing motion of the needle.

- The general TKE level does not depend on the quantity of cavitation present in the nozzle. This can be clearly seen when comparing the results at different operating conditions. There is clearly more cavitation in the 800/10 bar than in the 800/50 bar case, yet the level of TKE is practically the same in both cases. The same may be observed for the 1500/10 bar and 1500/50 bar cases. However, this conclusion must be regarded with care, since in all cases, the level of cavitation is relatively low.



legend: in + the volume fraction of vapour, in ▲ the TKE, in ○ the lift law

Figure 6.20: Instantaneous results of average TKE and volume fraction of vapour at the exit of the cylindrical nozzle.

The effect that the presence of cavitation has on the velocity profiles at the nozzle exit at different needle lifts (25, 50, 75, 100, 200, 250  $\mu\text{m}$ ) is presented in Figure 6.21 which shows the axial velocity versus the dimensionless nozzle diameter of the cylindrical nozzle along horizontal/vertical edges (as in Figure 5.10, chapter 5.5.2) for the 1500/50 bar case. The velocity increases with

increased needle lift as expected. For the cylindrical, there is no appreciable change in the velocity profile shape along the horizontal edge for the needle opening and closing. This is due to the limited amount of vapour that is present along the horizontal edge. However, the phenomenon of hysteresis is also reflected on the velocity profiles, mainly on the middle needle lifts (50-100  $\mu\text{m}$ ). The velocity peaks in the vorticity zones are higher with increasing needle lift.

Along the vertical edge the differences in the profiles between opening and closing are more pronounced, with higher velocities during needle closing due to the higher amount of cavitation (hysteresis). Overall, the profiles are asymmetrical at all needle lifts due to the higher amount of cavitation on the top of the nozzle, with the velocity maximum more pronounced at high needle lifts due to the extension of cavitation at the nozzle exit.

Plots of the axial velocity versus the dimensionless nozzle diameter of the tapered nozzle (horizontal/vertical edge) are presented in Figure 6.22. Similar observations can be made for the tapered nozzle, though the velocity peaks at high lifts are not so pronounced due to the absence of cavitation at the nozzle exit. The needle movement seems to have a determinant influence on the velocity profile shape, indeed, important differences on the velocity profiles have been observed between opening and closing mainly at low needle lifts.

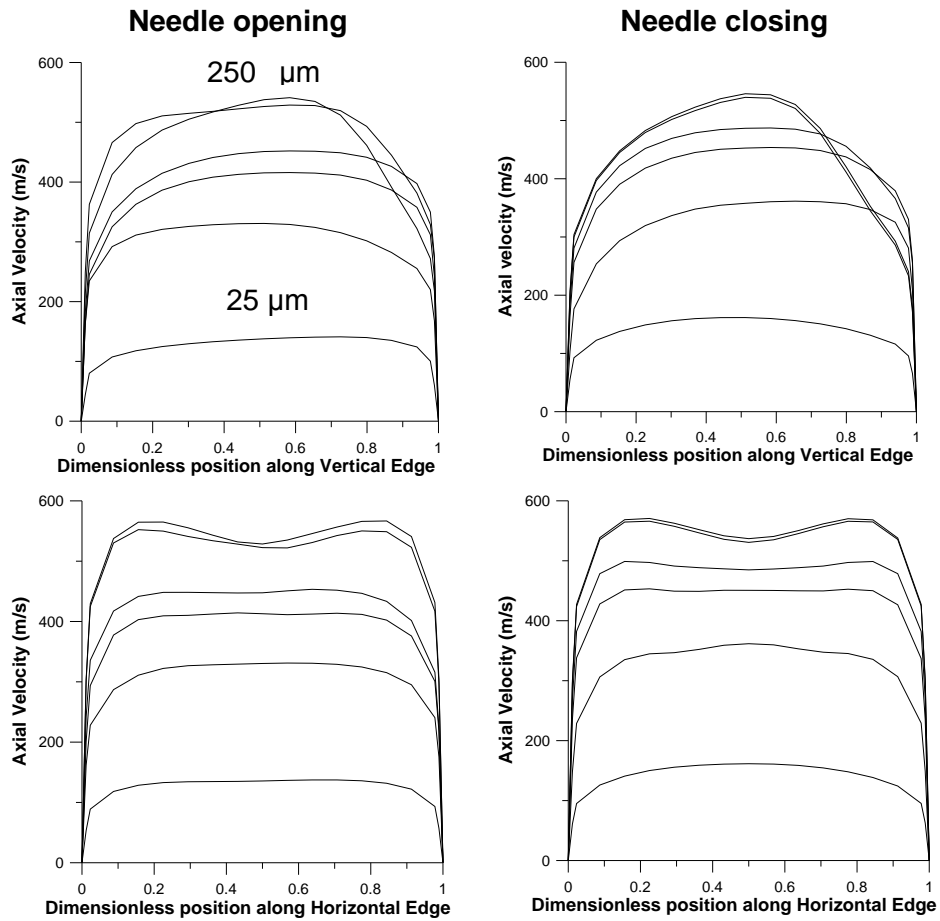


Figure 6.21: Axial profiles at the examined lifts along a vertical and a horizontal edge for the cylindrical nozzle during the needle opening and closing (1500/50 bar, lifts: 25, 50, 75, 100, 200, 250  $\mu\text{m}$ ).

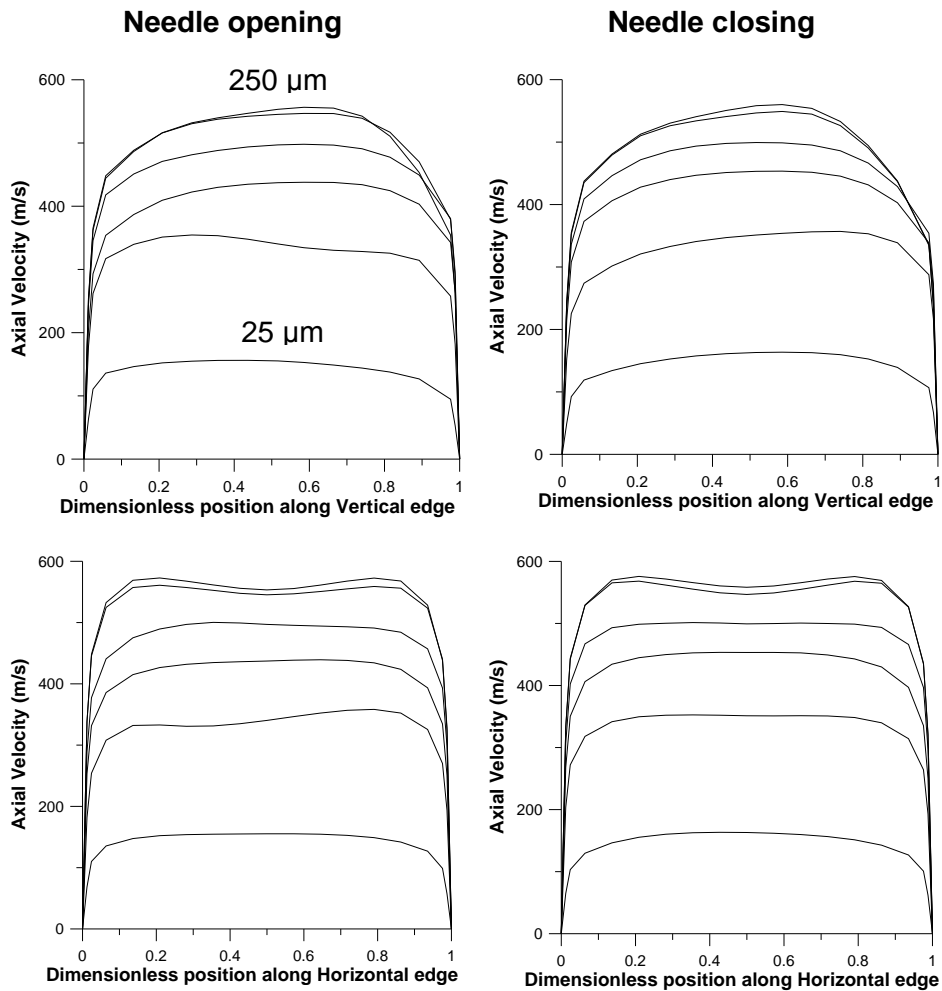


Figure 6.22: Axial profiles at the examined lifts along a vertical and a horizontal edge for the tapered nozzle during the needle opening and closing (1500/50 bar, lifts: 25, 50, 75, 100, 200, 250  $\mu\text{m}$ ).

## 6.4 Summary

In this chapter, it was intended to gain knowledge about the influence of nozzle geometry and needle lift on the inception and development of

cavitation, as well as on the characteristics of the flow at the exit of the nozzle, in order to provide information for spray calculations. Both single- and multi-hole injectors, with tapered and cylindrical orifices have been modelled. The needle lift motion was taken into account using CFD moving mesh calculations. A simple moving mesh strategy was developed for the multi-hole nozzle calculations which required an interpolation between the experimental results and the results with calculations at fixed needle lifts. The main conclusion remarks are noted below:

- As is already known, the shape of the nozzle greatly affects the onset of cavitation. The convergent shape towards the exit greatly modifies the pressure distribution in the nozzles and thus the cavitation formation. Indeed, no cavitation appears in the single-hole tapered nozzle, independently of the needle movement. The cavitation is significantly reduced also in the multi-hole tapered nozzle, as some vapour appears only in the restricted area between the needle and injector body at low needle lift or at the hole entrance at high pressure drops and very low needle lift.
- In the cylindrical single-hole nozzle, the cavitation develops attached to the wall and its extension varies depending on the needle lift. In the cylindrical multi-hole nozzle, the cavitation tends to follow a vortical structure which is more enhanced at low needle lifts.
- The model predicts clouds of cavitation growing and evacuating the nozzle at low needle lifts, which is in accordance with the highly transient nature of the flow during needle motion and shows that cavitation regime is much more transient than at high needle lifts.
- The turbulence kinetic energy is mainly created in the first stages of needle opening and in the last stage of closing, independently of whether there is cavitation or not. This is probably due to the local

acceleration of the flow at the nozzle inlet caused by the restricted passage.

- The needle motion creates a kind of hysteresis, which is visible in the turbulence kinetic energy evolution, independently of the presence of cavitation, as well as in the development of cavitation.
- It is seen that the form of the velocity profiles of the multi-hole nozzle change with increasing needle lift, as well as between the opening and closing phase of the needle, independently of the presence of cavitation. The hysteresis is also reflected on the velocity profiles during the needle motion. The peaks of velocity profiles of cylindrical nozzle are more marked at full needle lift due to the amount of vapour reaching the exit, though the asymmetry is present at all needle lifts. Comparing the two holes (tapered, cylindrical), it is seen that in the tapered nozzle the peaks are less pronounced especially at high lifts, though quite similar with the cylindrical nozzle at all needle lifts, as the vortical flow pattern appears in both nozzles. The flow visualization for the tapered nozzle shows that the flow is generally asymmetrical at the nozzle exit, but the asymmetry is less marked compared with the cylindrical case. This confirms that cavitation (present in the cylindrical nozzles) affects the symmetry of the flow.

In conclusion, it is important to take into account the needle motion, since its effect is determinant to characterise the flow at the nozzle exit and provide boundary conditions information for spray calculations.

The needle motion is mainly responsible for the creation of the turbulence kinetic energy that reaches the nozzle exit. In fact, at low lifts, during opening and closing, turbulence is enhanced; at high lifts, it decays. This is always the case, whether there is cavitation or not.

Furthermore, the development of cavitation seems to be linked somehow to the turbulence level. Indeed, it seems that part of the turbulence kinetic energy is being absorbed during the growth of the cavitation bubble. This information is valuable when considering boundary conditions for the spray calculations. It is generally assumed that cavitation enhances the turbulence, since it reduces the outlet effective area. However, the study presented here tends to prove that cavitation growth absorbs part of the turbulence kinetic energy generated during the needle motion. It may be inferred that at higher cavitation levels, when the bubble growth is more important, the process may absorb more turbulence kinetic energy.



# **CHAPTER 7.**

## **COMPARATIVE STUDY OF QUASI-STEADY AND MOVING MESH SIMULATIONS**

### **7.1 Introduction**

The purpose of this chapter is to study the influence of real size Diesel injector needle position and movement on the inception and development of cavitation. In general in order to simplify the problem, CFD calculations are made either at fixed needle lift position or without the needle. However, the cavitation phenomenon is highly unsteady and it is important to know whether needle dynamics may also cause or influence cavitation.

Hence, in this chapter, a comparison between the “traditional” “quasi-steady approach”, i.e at fixed needle lift, and the moving mesh approach is made, in order to evaluate the validity of the “quasi-steady” approach. For this, an extensive analysis of the needle position effect on the internal flow characteristics and exit characteristics will be performed with fixed needle lift calculations.

## Chapter 7 Comparative Study of Quasi-steady and Moving Mesh Simulations

It was seen in Chapter 5 that the flow distribution in multi-hole nozzles is very different from the single-hole nozzle pattern at fully opened needle lift. In this chapter the complicated cavitation pattern predicted at different needle lifts in the multi-hole nozzles is further investigated (1500/50, 1500/10, 800/50, 800/10 bar). Results of multi-hole nozzles with cylindrical and tapered holes will be examined, including results obtained with the whole injector (360° sector, 1410/10 bar). Then, the flow features at different needle lifts as predicted by both methodological approaches are analysed and compared using a 60° computational domain (symmetry of the 6-hole injector), to finally conclude about the limits of validity of each approach.

### **7.2 Fixed needle lift strategy**

The moving mesh strategy was extensively elaborated in Chapter 6.2. For the numerical analysis of the flow at different fixed needle lifts, quasi-steady state computations were performed for the entire range; the needle was initially set at the smallest opening value (25 µm) and the unsteady calculation performed until the solution no longer evolved. For all other values of needle lift, the calculations were started from the previous lift solution (e.g. for 50 µm, the run was started from the solution obtained for 25 µm). The time step for these calculations was 1E-06 s.

In this section only results of the multi-hole injector will be presented, since this case illustrates better the diverse cavitation patterns predicted at different needle lifts. Both computational domains of one hole (symmetry of the injector) and six holes (whole injector) will be examined. The latest geometry was used to examine the flow within the sac volume and how it affects the flow characteristics at the different holes. The cell size (3 dimensions) inside

the holes was 10  $\mu\text{m}$  approximately in all calculations as determined in the full needle lift calculations.

### **7.3 Results obtained by Fixed Needle Lift Simulations**

#### **7.3.1 Predicted flow of multi-hole Diesel injectors (symmetry of the injector)**

##### **Injection rate comparison between the cylindrical and tapered nozzles**

At fixed calculations the needle was positioned at six different lifts: 25, 50, 75, 100, 200, 250  $\mu\text{m}$  and the predicted injection rate results for these calculations are shown in Figure 7.1, where the injection rate results are compared for the cylindrical and tapered nozzles ( $\Delta t=1\text{E-}06$  s). Though, the experimental injection rate is available only at full lift due to the difficulty in performing experiments at different fixed needle lifts. The computational results show that the injection rate increases asymptotically with needle lift. As may be seen, at low lifts the mass flow rate is quite the same in both the cylindrical and the tapered nozzles, while at higher lifts, there are slight differences due to the appearance of cavitation at the hole exit.

## Chapter 7 Comparative Study of Quasi-steady and Moving Mesh Simulations

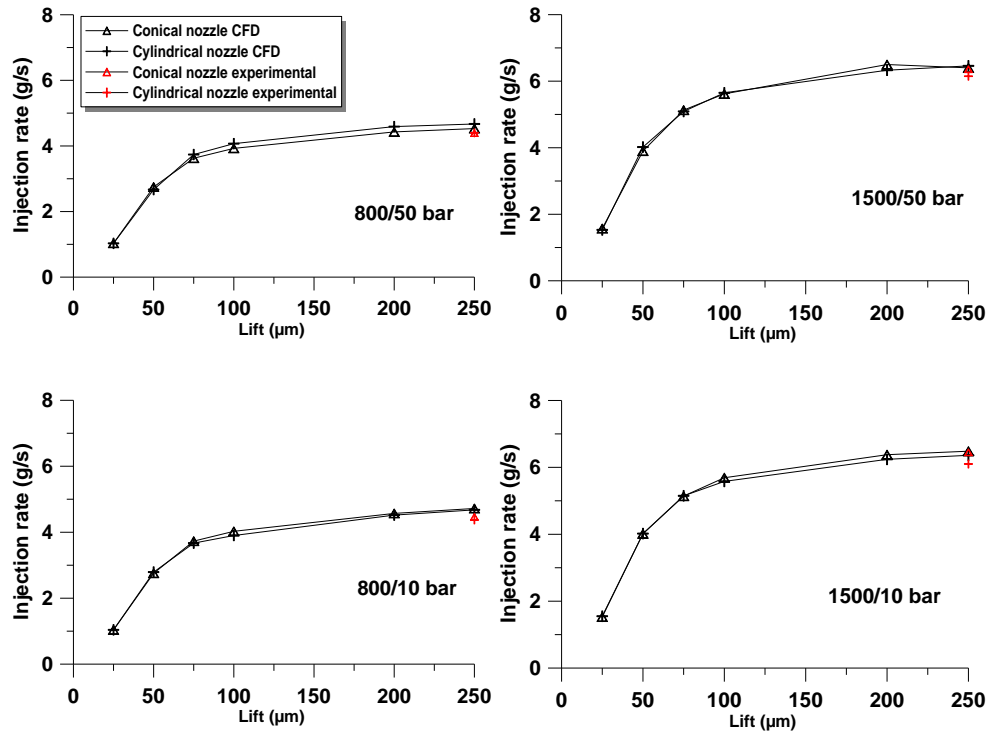


Figure 7.1: Injection rate results as a function of lift for the cylindrical and the tapered nozzles in the investigated operating conditions.

Indeed, at high lifts (100-250 μm) the cylindrical nozzle injection rate is less than that of the tapered nozzle in the operating conditions 1500/50, 1500/10 and 800/10 bar due to the vapour bubble that reaches the exit, as has been seen in section 5.5.2. On the contrary, in the operating condition 800/50 bar the mass flow of the cylindrical nozzle is greater than that of the tapered nozzle: in this case there is no cavitation at the cylindrical nozzle exit and so there is no area reduction due to cavitation. Moreover, this tendency is verified by the experimental results, the injection rate at full lift for the tapered nozzle is greater than for the cylindrical nozzle for 1500/10, 1500/50 and 800/10 bar cases, and both are equal for 800/50 bar case.

## Chapter 7 Comparative Study of Quasi-steady and Moving Mesh Simulations

Figure 7.2 shows the correlation between the flow discharge coefficient of the nozzles in function of pressure drop and needle lift. For the operating conditions examined here (800/10, 800/50, 1500/10, 1500/50) the discharge coefficient  $C_d$  of the tapered nozzle (defined in section 5.3) is higher than that of the cylindrical nozzle, as expected. This is also confirmed by the experimental values obtained at full lift. Furthermore, there is good agreement between predicted and experimental discharge coefficient values at full needle lift. For both nozzles,  $C_d$  varies slightly with increasing pressure drop and significantly with needle opening. It is interesting to note that at minimum lift, the tapered and cylindrical nozzles have similar  $C_d$ , but that very quickly at 50  $\mu\text{m}$  lift, the values are significantly different, more so at high lifts. This is due to the presence of cavitation bubbles at the exit of the cylindrical nozzle, as will be commented in the next section.

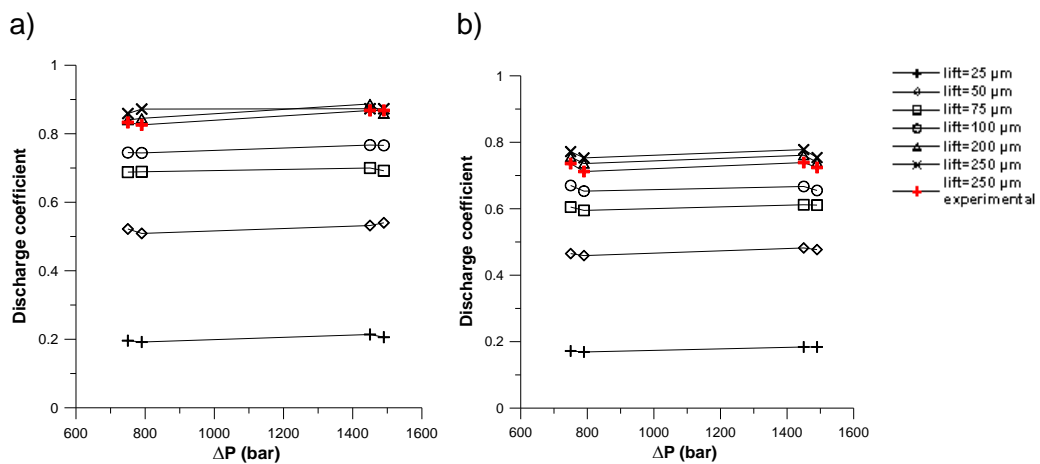


Figure 7.2: Evolution of  $C_d$  in function of pressure drop at different needle lifts for a) tapered and b) cylindrical nozzle.

**Cavitation pattern comparison between the cylindrical and tapered nozzles**

In Figure 7.3 representative images of the volume fraction of vapour of tapered multi-hole nozzle at different needle positions are presented, as obtained by the fixed needle lift calculations (1500/10 bar). It ought to be mentioned at this point that although a “quasi-steady state” is reached at the end of each fixed needle simulation, there is a fluctuating behaviour in the flow distribution. It should be clarified that the images presented are part of a transient timeline, in which for some time instances the flow pattern becomes momentarily slightly different; for this reason the selected images are representative of the average flow observed. The same colour scale has been used as much as possible to make the comparison between the different operating points easier. The images are extracted at the mid-plane of the nozzle and at the exit of the nozzle. These views were selected to better illustrate the extension of cavitation and its effect on the nozzle exit characteristics.

The flow visualization in terms of volume fraction of vapour shows that no cavitation is present at the hole exit for any lift of the tapered nozzle cases. However, at low lift values, a cavitation bubble appears in the needle seat in all operating conditions, which extends beyond the nozzle bend for the low back-pressure cases (1500/10, 800/10 bar). This vapour region disappears quickly, already at 50  $\mu\text{m}$  lift, so that there is only liquid at medium to high lift values. It was thus found that the reduction of backpressure favours the extension of cavitation independently of the needle lift. The needle seat cavitation seems to appear mostly at very low lift and even in those cases where the initial vapour region extends beyond the nozzle bend, it remains very unsteady and the bubble implodes between 25 and 50  $\mu\text{m}$  lift.

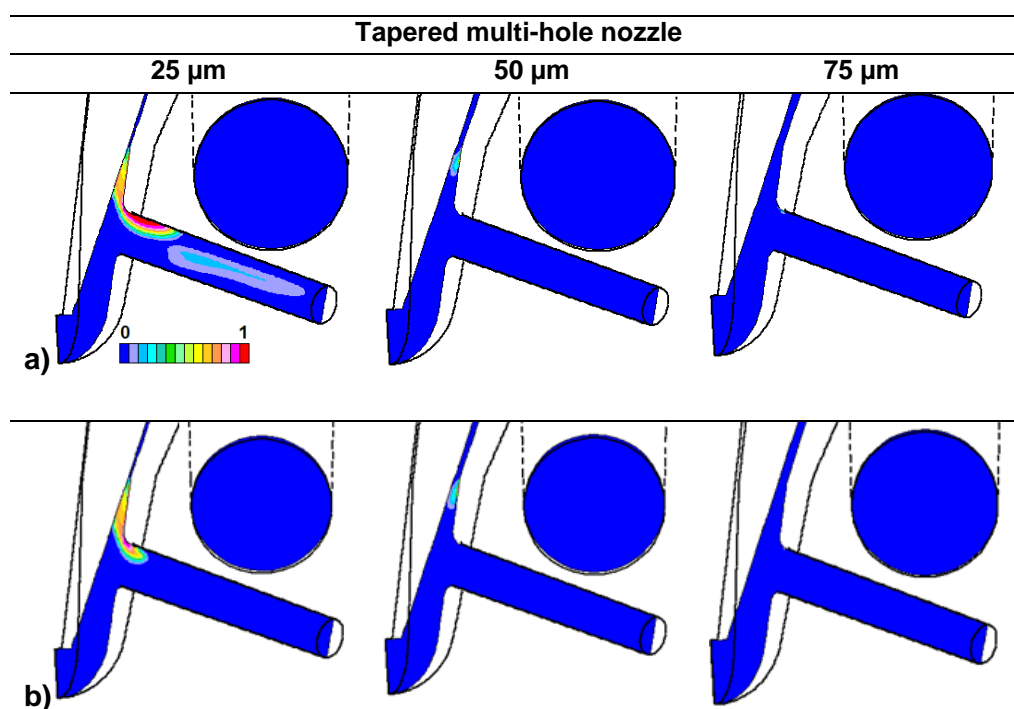


Figure 7.3: Representative images of volume fraction of vapour of tapered multi-hole nozzles at different needle positions at a) 1500/10 bar, b) 800/10 bar.

Comparing Figure 7.3 and Figure 7.4 it may be seen that the cavitation intensity and pattern is significantly different for tapered and cylindrical nozzles. This is also reflected in the discharge coefficient (Figure 7.2), but not on the injection rate values (Figure 7.1). It is clear that the cavitation pattern at the nozzle exit will affect significantly the emerging fuel jet. The post processing has shown that there is a cavitation bubble in the needle seat for 25  $\mu\text{m}$  lift, which tends to disappear at 75  $\mu\text{m}$  (Figure 7.4).

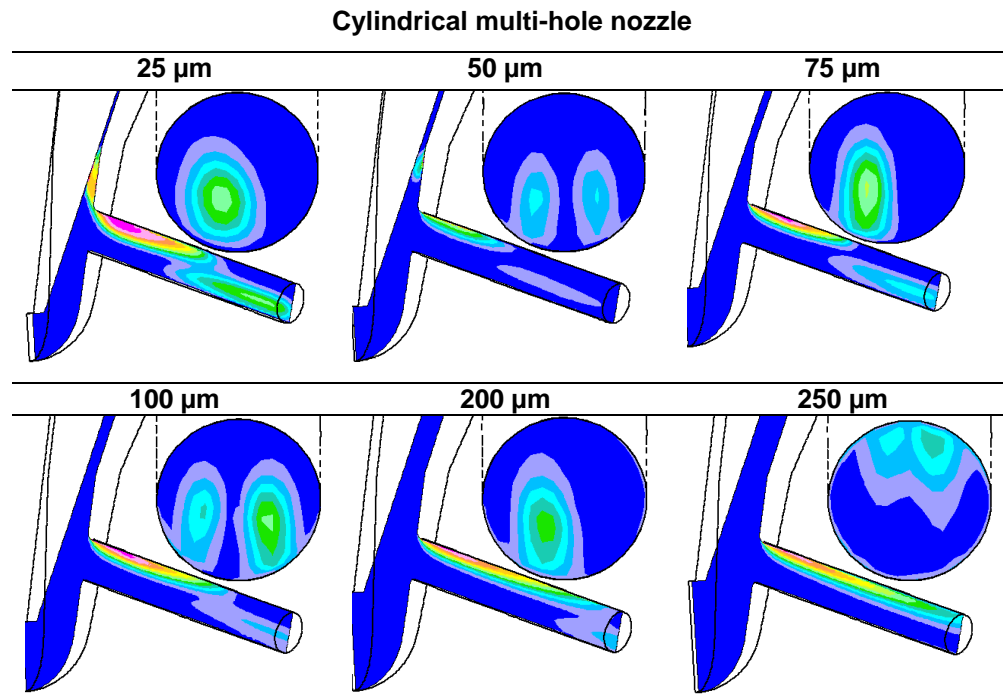


Figure 7.4: Representative images of volume fraction of vapour of cylindrical multi-hole nozzles at different needle positions (1500/10 bar). Same color scale as in Figure 7.3.

It was found that in the operating conditions of 10 bar back-pressure (800/10, 1500/10 bar), these bubbles extend downstream along the nozzle inlet bend, and seem to separate in two smaller bubbles at 50 μm lift (Figure 7.5). In all cases, there is a cavitation bubble at the nozzle inner bend from 50 μm lift onwards, either as the remains of the previous needle seat bubble, or as newly generated (800/50, 1500/50 bar). The cavitation bubble grows in extension along the upper part of the nozzle in all cases, and reaches the nozzle exit except in the 800/50 bar case. Overall, the cavitation pattern is very unsteady as a function of the vortical flow structure caused by the acceleration of the flow through the constriction caused by the needle lift position. Its structure is more stable with increasing needle lift.

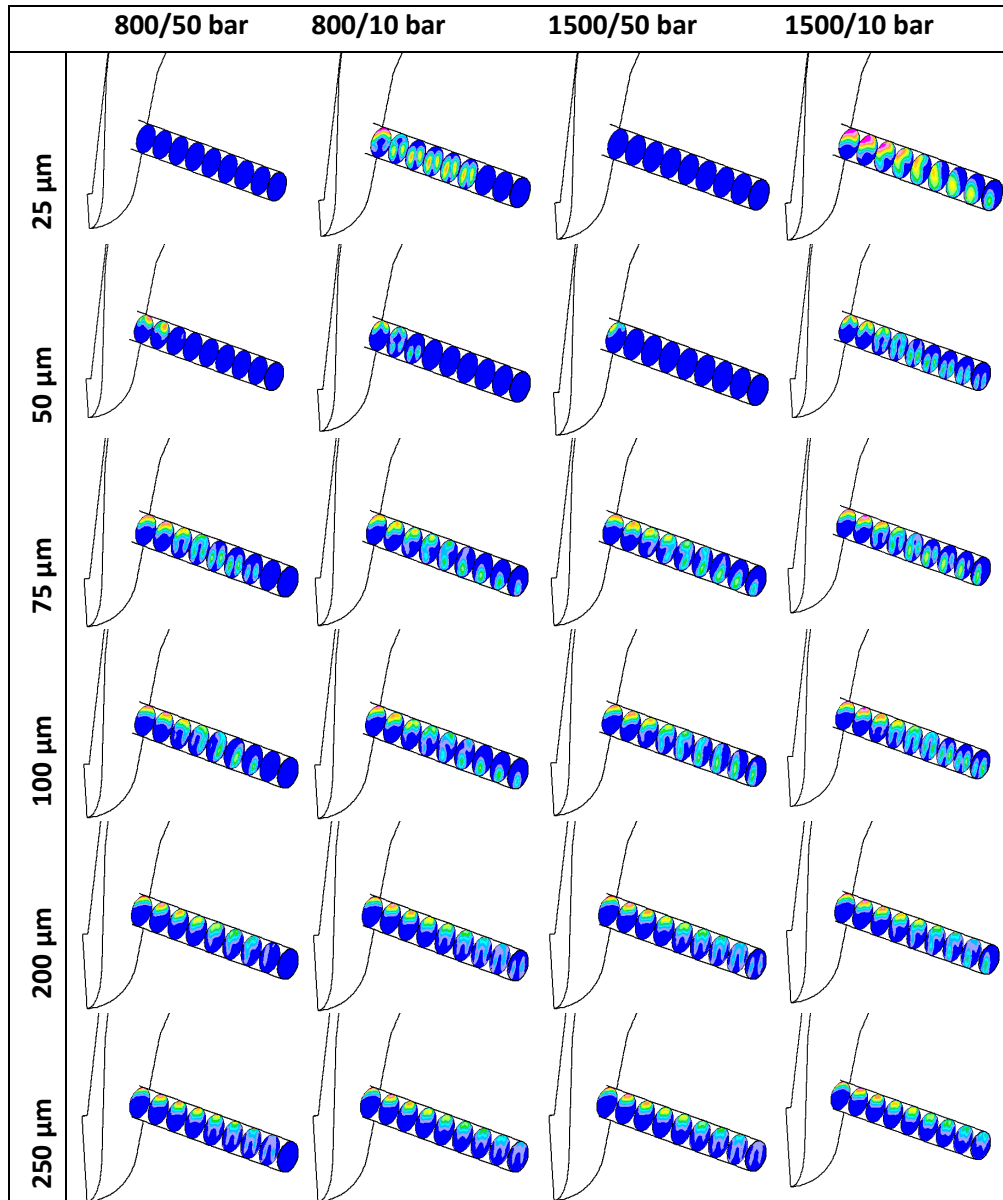


Figure 7.5: Representative images of volume fraction of vapour of cylindrical multi-hole nozzles at different needle lifts and operating conditions.

Additionally at low needle lifts ( $25\ \mu\text{m}$ ) and low bar back pressure (800/10, 1500/10 bar), a fluctuating injection rate was obtained. An example is given in

## Chapter 7 Comparative Study of Quasi-steady and Moving Mesh Simulations

Figure 7.6 for 25  $\mu\text{m}$  needle lift (800/10 bar) and as is seen, no stable injection rate has been obtained with the same time step used in the calculations of other needle positions ( $\Delta t=1\text{E}-06$  s); the fluctuation is 7% which may be significant.

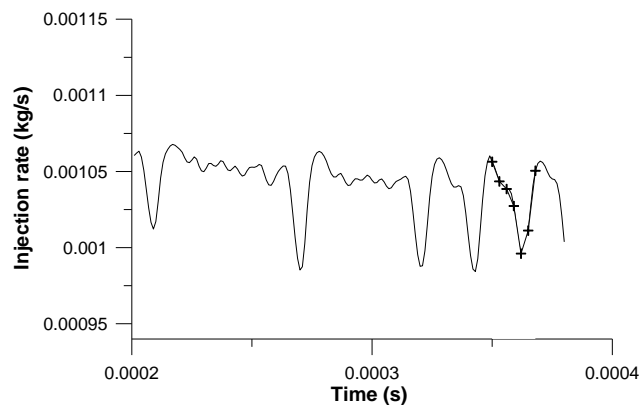


Figure 7.6: Injection rate as a function of time at 25  $\mu\text{m}$  needle lift, in crosses time instances at which the flow field examined (800/10 bar).

To explain the fluctuations observed, a post-processing of the flow at the different instants of Figure 7.6 is presented in Figure 7.7, in terms of volume fraction of vapour and velocity magnitude fields. This figure illustrates the highly transient nature of the cavitation phenomena. Indeed, it shows how the cavitation bubble first grows, to then diminish again. This in turn affects the velocity flow field and generates the fluctuations of flow rate.

In fact, the solution of this quasi-steady calculation obtained at fixed needle position of 25  $\mu\text{m}$ , is quite different from that of the moving mesh calculation even using the same time step, as will be seen later. A new calculation was performed with a smaller time step ( $\Delta t=0.5\text{E}-06$  s) so as to check for numerical instabilities due to the time-step, but there were no significant changes in the injection rate and the consequent cavitation field observed.

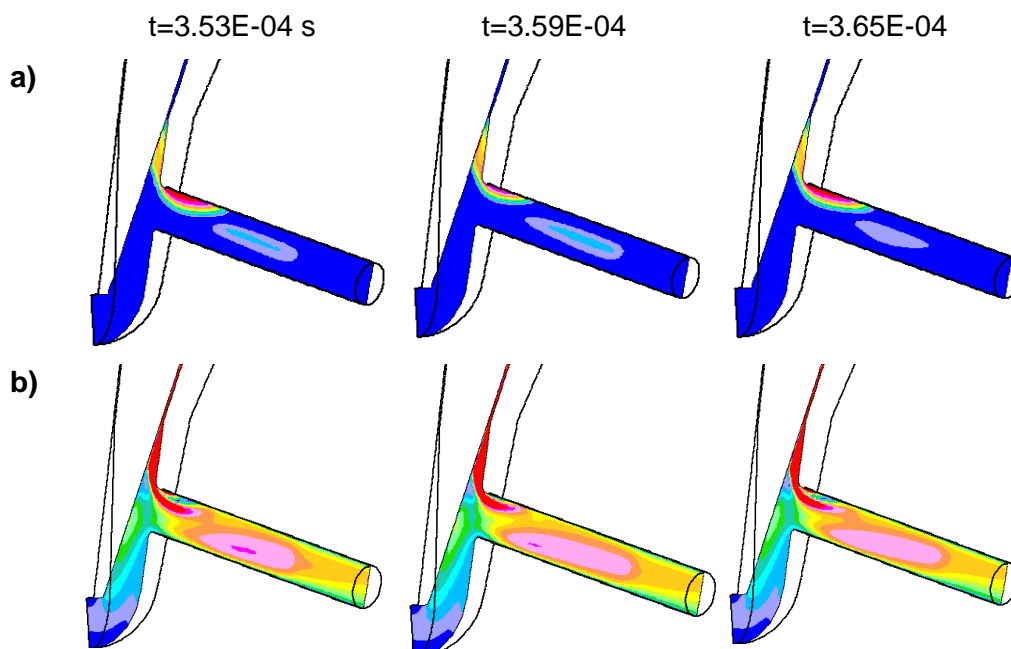


Figure 7.7: a) volume fraction of vapour and the corresponding b) velocity magnitude fields at different time instances.

### **Velocity magnitude comparison between the cylindrical and tapered nozzles**

A brief summary of the main conclusions that can be extracted from the visualisations of the velocity field is given here. These observations are true for all operating conditions investigated, though obviously the velocity levels are much higher in the high injection pressure cases (1500 bar).

Figure 7.8 shows representative images of the velocity magnitude in the tapered and cylindrical multi-hole nozzles at different needle positions (1500/10 bar). The views selected are the same as those defined for Figure 7.3.

## Chapter 7 Comparative Study of Quasi-steady and Moving Mesh Simulations

In the mid-plane view along the nozzle axis, it is seen that the flow field in the annulus between the needle and the nozzle body is similar for both nozzles at all needle lifts as expected. Below 50  $\mu\text{m}$  needle lift, the velocity is highly accelerated due to the restricted area, while it decelerates as the needle opens further. However, the more gradual acceleration of the flow along the hole in the tapered nozzle is obvious for all needle lifts.

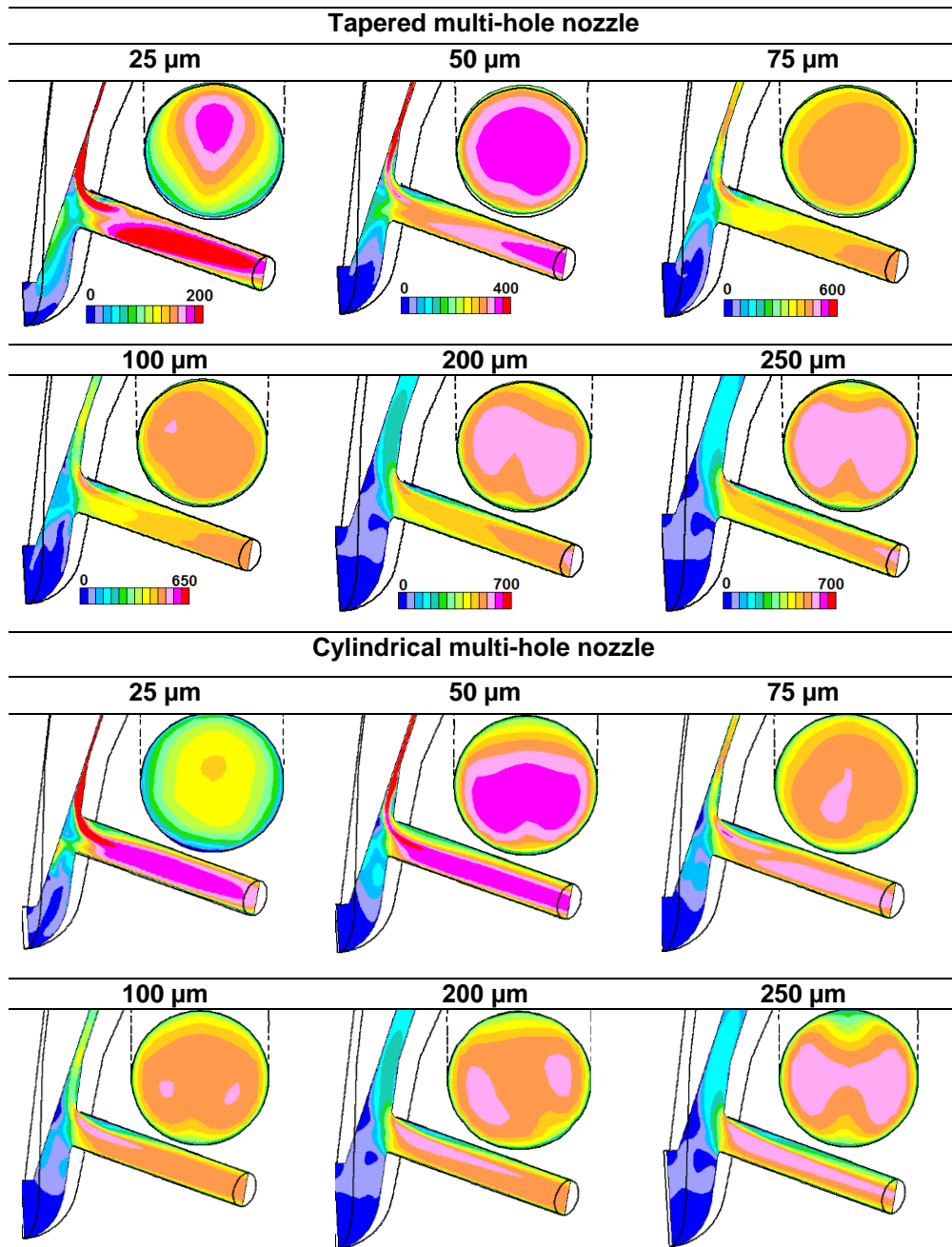


Figure 7.8: Representative images of velocity magnitude of tapered and cylindrical multi-hole nozzles at different needle positions (1500/10 bar).

## Chapter 7 Comparative Study of Quasi-steady and Moving Mesh Simulations

In both nozzles, the velocity field is clearly non homogeneous at the hole exit for all operating points. There are also clear differences in the organisation of the flow pattern at different lifts. In all pressure cases, at low to medium lifts (25  $\mu\text{m}$  to 75 or 100  $\mu\text{m}$ ) the flow at the nozzle exit is organised around a central core of higher velocity, while at higher lifts (100  $\mu\text{m}$  to 250  $\mu\text{m}$ ), there are two parallel cores of higher velocity. In the tapered nozzle, the velocity field is more homogeneous than in the cylindrical nozzle and in all cases, it is organised around a central core. At high lifts the central core tends to divide in two, in the second half of the nozzle. The analysis above permits concluding that at all needle lifts, and in both nozzles, there is a clear vortical structure of the internal flow. And, as seen in Figure 7.5 for the cylindrical nozzle, where there are enhanced cavitation conditions, the cavitation bubble follows this same vortical structure, probably entrained by the velocity field.

By analysing further the flow along the nozzle, it is obvious that for both nozzles the flow pattern is quite different at very low lift at the entry of the nozzle. The high velocity gradients that appear shortly before the nozzle bend, extend beyond the hole entrance up to 75  $\mu\text{m}$  lift. For higher lifts, the gradients are confined to the nozzle entrance. In the cylindrical nozzle this high velocity area in the entrance can be related to the secondary flow that is created downstream of the hole entrance in the second half of the nozzle hole and causes the cavitation to have a continuous pattern. However, the flow at the nozzle exit is not significantly different between the two nozzles.

Since the velocity flow distribution is similar at the nozzle exit of both nozzles the velocity profiles at the exit of the nozzle are not expected to be very different. This is confirmed by the averaged velocity magnitude profiles at the exit of the cylindrical and tapered holes illustrated in Figure 7.9 at all lifts investigated (1500/50 bar). As seen, the shapes of the curves for the velocity

## Chapter 7 Comparative Study of Quasi-steady and Moving Mesh Simulations

magnitude are for both nozzles quite similar. At low needle lifts the profiles have a more uniform shape than at full needle lift, independently of the nozzle shape. Indeed, at high lift, the velocity profiles along the horizontal axis show two peaks, as well as some asymmetry, independently of the nozzle shape, related to the vortical structure commented above.

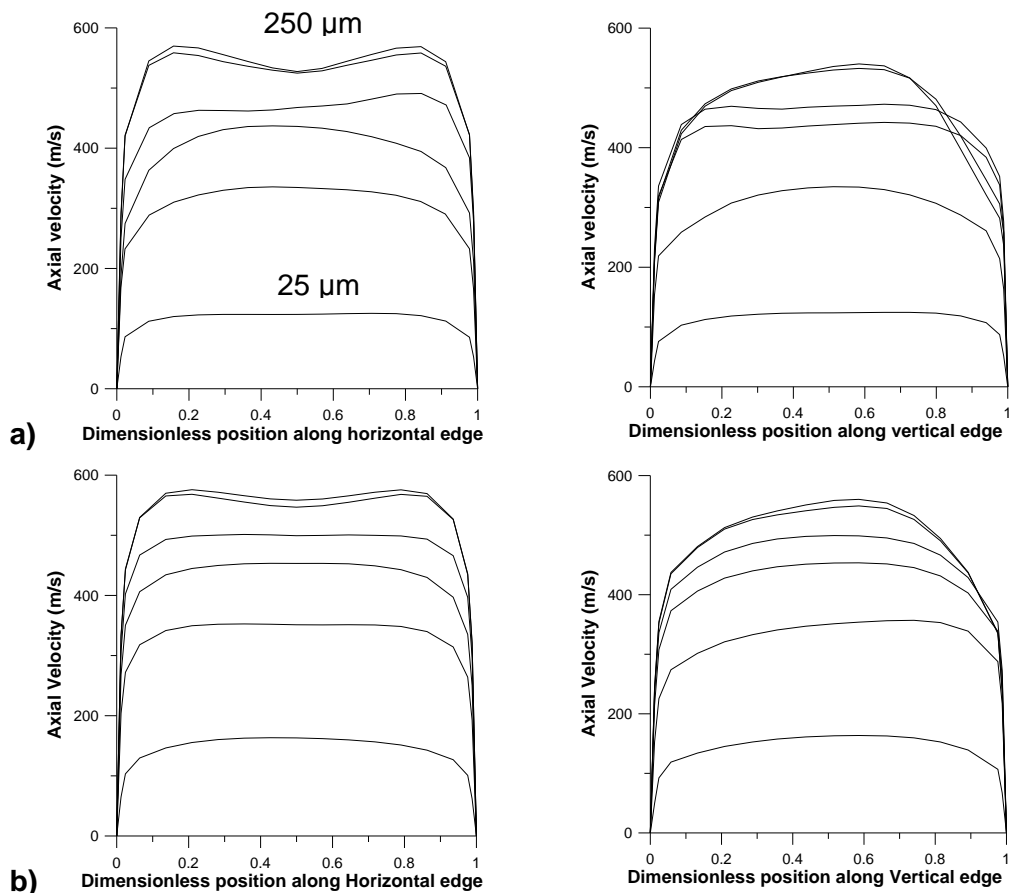


Figure 7.9: Representative axial velocity profiles of all lifts along the central horizontal and vertical edges for a) the cylindrical nozzle and b) the tapered nozzle (1500/50 bar).

## Chapter 7 Comparative Study of Quasi-steady and Moving Mesh Simulations

The presence of cavitation at the cylindrical nozzle exit does not seem to affect significantly the velocity profiles shapes. In fact, the needle position seems to have a much more determinant influence on the velocity profile shape for the nozzles and operating conditions investigated.

The averaged outlet velocity magnitude in function of lift is presented in Figure 7.10 for all operating points and both nozzles. As expected, the velocity is higher for the high injection pressure cases (1500 bar). It increases very quickly until 75  $\mu\text{m}$  lift and then stabilizes asymptotically to its maximum value.

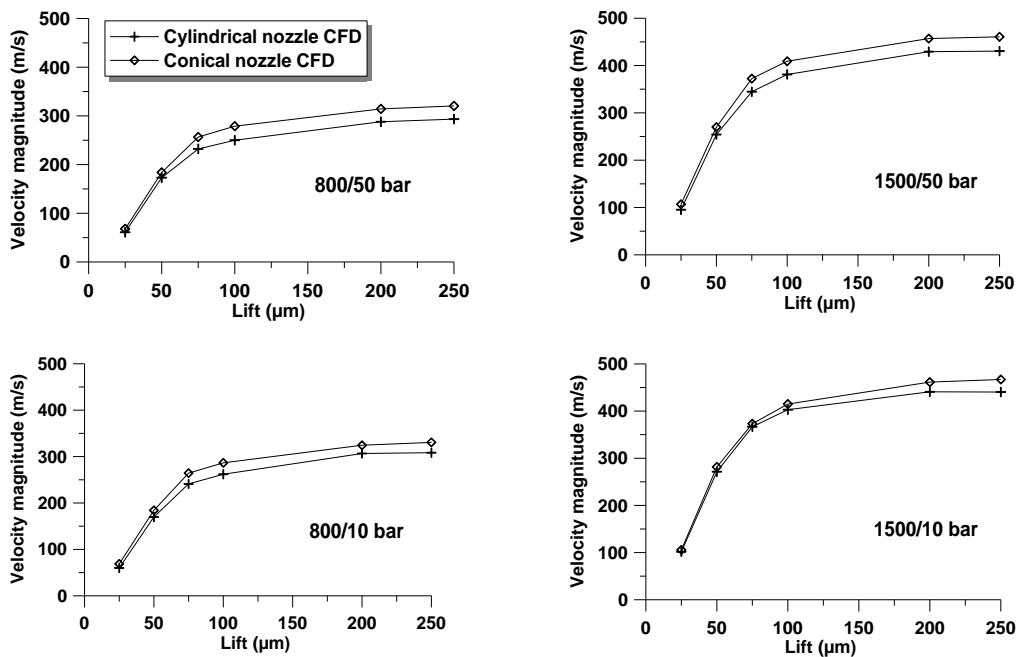


Figure 7.10: Outlet velocity evolution (area averaged values) as a function of lift for the cylindrical and the tapered nozzles in the investigated operating conditions.

**Turbulence comparison between the cylindrical and tapered nozzles**

The images of TKE field in the tapered and cylindrical multi-hole nozzles at different needle positions (1500/10 bar) are shown in Figure 7.11 with different colour scale at each lift in order to illustrate the gradients, but with the same colour scale between the two nozzles in order to compare them.

In the mid-plane view along the nozzle axis, it is seen that, as for the velocity flow field the TKE in the annulus between the needle and the nozzle body is similar for both nozzles at all needle lifts. It is to be noted that the inlet radius of the tapered nozzle is smoother and the inlet diameter larger, so that the change of the flow in the hole entrance is less abrupt (see Table 7.1, which is here to remind).

Nozzle	R <sub>a</sub> ( $\mu\text{m}$ )	R <sub>b</sub> ( $\mu\text{m}$ )	D <sub>i</sub> ( $\mu\text{m}$ )	D <sub>m</sub> ( $\mu\text{m}$ )	D <sub>o</sub> ( $\mu\text{m}$ )	L ( $\mu\text{m}$ )	k-factor
Cylindrical	22	22	146	148	147	1000	-0.1
Tapered	42	42	150	144	138	1000	1.2

Table 7.1: Cylindrical and tapered nozzle dimensions.

At low needle lifts the gradients of TKE are located mainly at the hole entrance and are shifted towards the lower part of the hole entry with increasing needle lift. For all cases however, the TKE diffuses along the nozzle hole and its level increases significantly with needle lift.

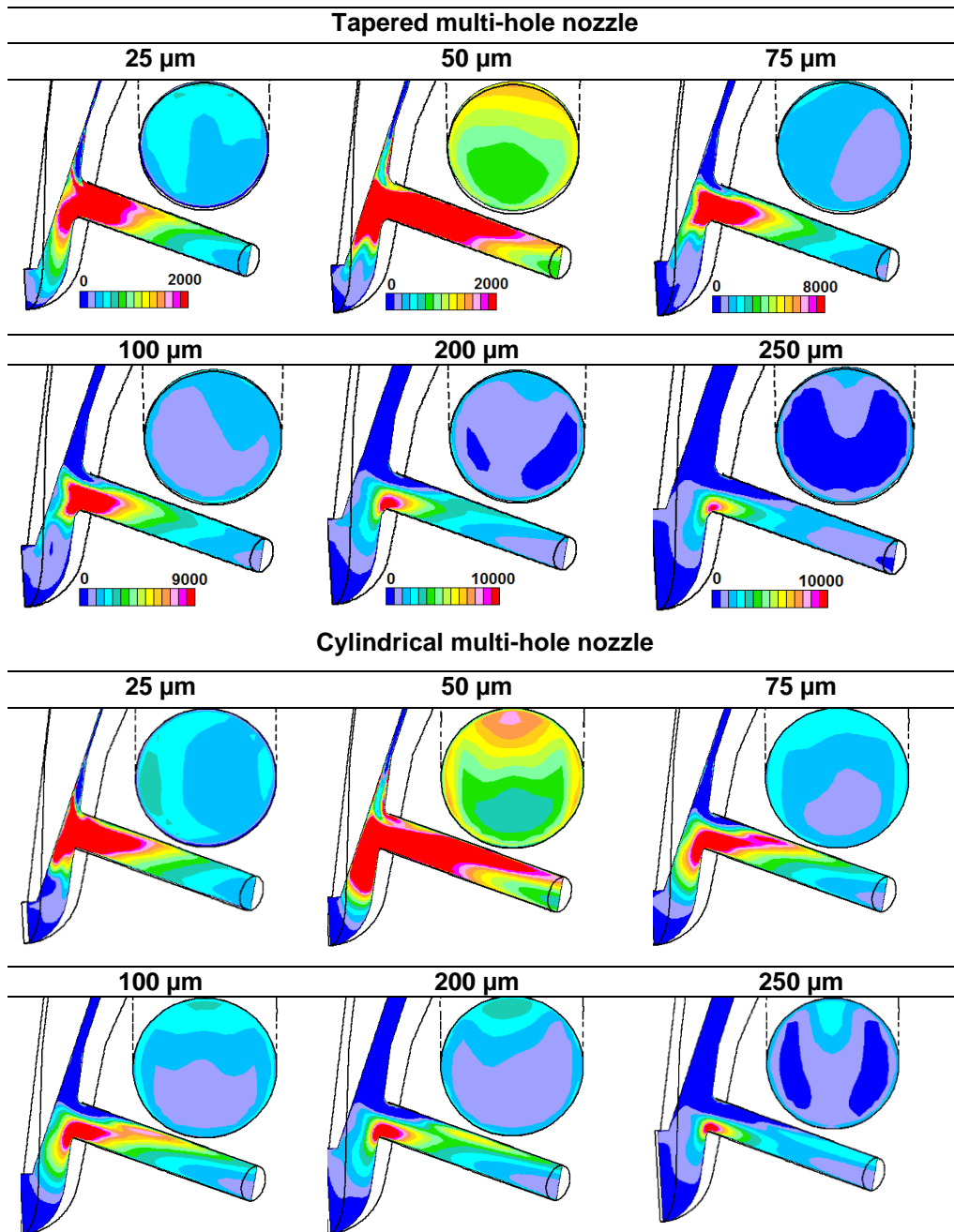


Figure 7.11: Representative images of TKE of tapered and cylindrical multi-hole nozzles at different needle positions (1500/10 bar).

## Chapter 7 Comparative Study of Quasi-steady and Moving Mesh Simulations

In Figure 7.12 the turbulence evolution as a function of needle lift is given in terms of kinetic energy and kinetic energy coefficient at the nozzles exit for the studied operating conditions. The turbulent kinetic energy is normalized by the square of the velocity magnitude, thus defining the following coefficient:

$$C_k = \frac{k}{V^2} \quad (7.1)$$

The TKE curves show that the turbulence is higher for the cylindrical nozzles, and that it depends highly on the injection pressure. Indeed, it is about double as high for the 1500 bar cases. For both nozzles, it is clear that, the turbulence kinetic energy level increases significantly in all the operating conditions for needle lifts up to 100  $\mu\text{m}$  and then stabilizes and hardly changes until full opening. For the tapered nozzle, the TKE level tends to decrease slowly after that until full opening. For the cylindrical nozzle, the level of turbulence remains approximately constant after 75-100  $\mu\text{m}$  lift, in spite of the increasing development of the cavitation along the nozzle. It seems that most of the turbulence is generated at low lift, when there is only cavitation at the needle seat or right at the nozzle entry, and the flow velocity gradients are high. A slight decrease is even observed in the last stage of opening. Since the cavitation at the needle seat disappears after 75  $\mu\text{m}$  lift, it confirms that the turbulence level created initially at low lift is generally upheld, but not increased by the cavitation within the nozzle.

A slight difference in the TKE's maxima in function of injection pressure is observed when comparing both nozzles. Indeed, in the case of the tapered nozzle, the TKE maximum is attained at 75  $\mu\text{m}$  lift for 800 bar pressure injection, while for 1500 bar, it is attained at 100  $\mu\text{m}$  lift. In the case of the cylindrical nozzle, the maximum is attained at 100  $\mu\text{m}$  lift, independently of the needle lift.

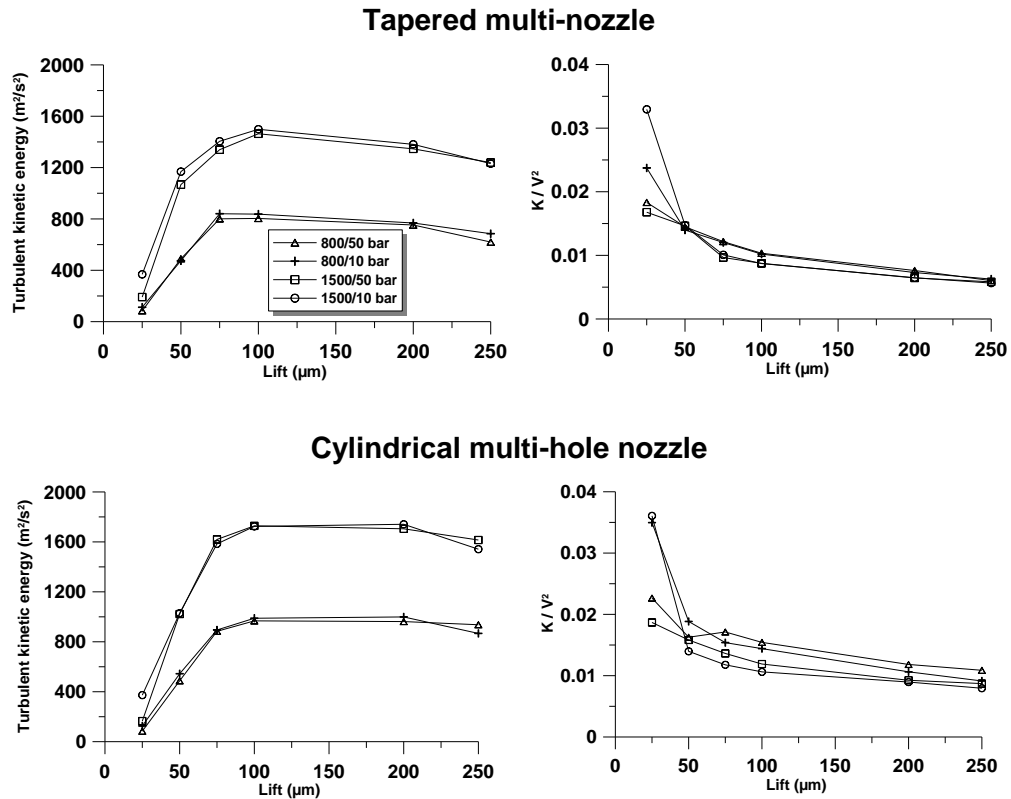


Figure 7.12: Turbulent kinetic energy and turbulent kinetic energy coefficients for the tapered and the cylindrical nozzle.

The normalized turbulent kinetic energy  $C_k$ , however, shows some differences depending on the back-pressure. For both nozzles, the two curves representing the cases of 10 bar back pressure behave similarly, with an important decrease of the coefficient up to 75  $\mu\text{m}$  lift, followed by a slower decreasing slope. For the 50 bar back-pressure cases (see Figure 7.12), the evolution of  $C_k$  is monotonically asymptotic and smoother.

In the cylindrical nozzle, the slope of the curve for the case 1500/50 bar is smoother overall, while that of 800/50 bar shows an initial decrease, followed by an uncharacteristic growing tendency between 50 and 75  $\mu\text{m}$ , to then

## Chapter 7 Comparative Study of Quasi-steady and Moving Mesh Simulations

decrease asymptotically. By linking these observations with the post processing visualization (Figure 7.5) of the volume fraction of vapour, it would seem these differences may be linked to the appearance of cavitation at the hole inlet. Indeed, for the 800/50 bar case at 25  $\mu\text{m}$  there is some cavitation in the needle seat area, but not at the hole inlet. At 50  $\mu\text{m}$  the velocity gradient increases suddenly due to the vapour generation at the hole inlet; at 75  $\mu\text{m}$  the cavitation is already developed and the turbulence coefficient shows an asymptotic evolution from then on. For the 1500/50 bar the initial fall and raise behaviour at needle opening (25-50  $\mu\text{m}$  lift) is not observed, probably due to the fact that the cavitation bubble generated at the hole inlet is very small. For the other operating conditions (800/10 bar, 1500/10 bar) cavitation is generated from the beginning at 25  $\mu\text{m}$  lift in the area of the needle seat, and also in the hole inlet.

It is interesting to further compare the cylindrical and the tapered solutions in order to try and correlate the differences observed with the presence of cavitation, and to explain some of the oddities observed, in particular in the 800/50 bar cylindrical case.

As a next step, a comparison is made between the variation of TKE and that of the velocity magnitude in function of lift (Figure 7.13), in order to correlate them. The percentage of increase in TKE and velocity magnitude in Figure 7.13 is calculated starting from 50  $\mu\text{m}$  and with respect to the previous lift. It is seen that for all the operating conditions the rate of change of velocity from lift to lift at the exit of the nozzle is the same for both nozzles.

This is not the case for the rate of change of TKE: For all cases except 1500/10 bar, at low lifts, the TKE rate of change increases over twice as much as that of velocity. At 1500/10 bar the TKE increases at the same rate

## Chapter 7 Comparative Study of Quasi-steady and Moving Mesh Simulations

as the velocity does. In all cases, when the velocity at the hole exit stabilizes at its asymptotic value, so does the TKE. This indicates that the turbulence level at the hole exit is directly linked to the flow velocity, but that it is also influenced by some other parameter at low lifts. However, the rate of change of TKE does not seem to be related to the cavitation level at the nozzle exit, since in the 1500/10 bar case, there is practically no cavitation in the tapered nozzle after 25  $\mu\text{m}$  lift whereas cavitation is fully developed in the cylindrical nozzle. It could be related to the onset of cavitation though.

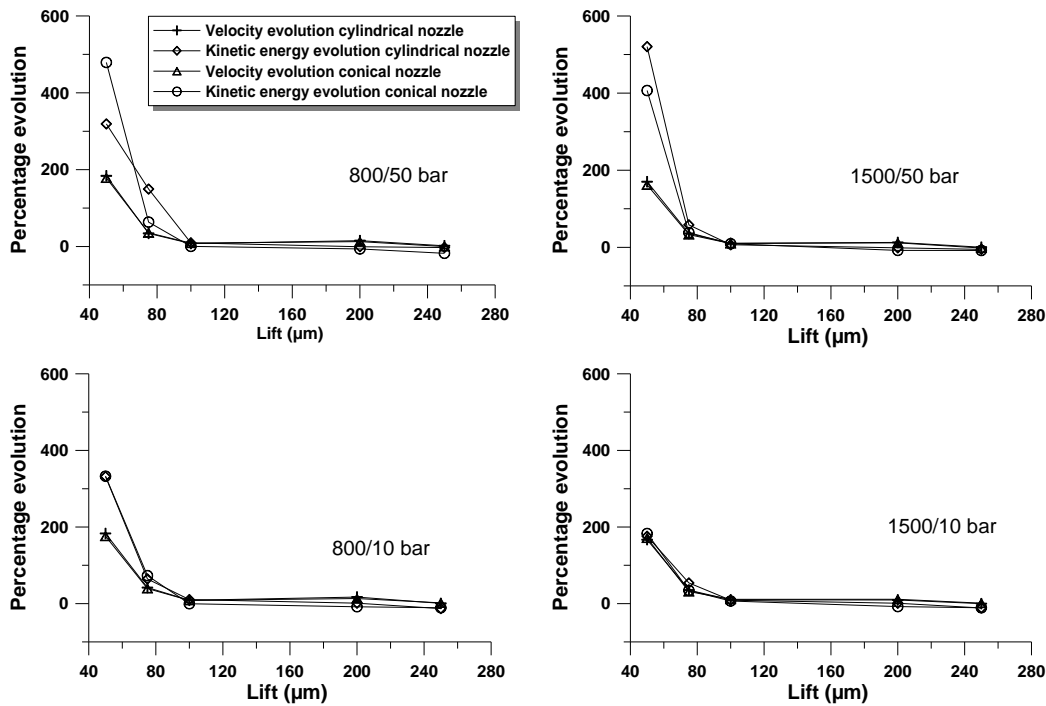


Figure 7.13: Rate of change of velocity and TKE in function of lift at the exit of the nozzles.

In order to study the effect of the onset of cavitation on the TKE level, an analysis of both TKE and volume fraction of vapour is performed at four different sections along the nozzle, as indicated in Figure 7.14. The evolution

## Chapter 7 Comparative Study of Quasi-steady and Moving Mesh Simulations

of TKE, volume fraction of vapour and velocity magnitude along both nozzles and for all lifts is represented in Figure 7.15 for the 800/50 bar case. This case has been chosen, because no cavitation reaches the exit.

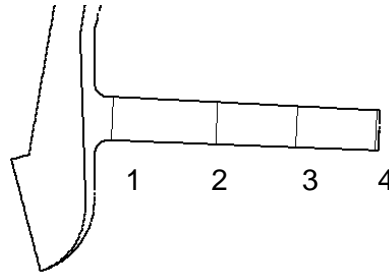


Figure 7.14: Location of nozzle hole considered for post-processing in this study.

It can be shown from Figure 7.15 that the turbulence level falls asymptotically along the hole in both nozzles as the TKE diffuses along the nozzle hole. Close to the hole exit the averaged turbulent kinetic energy in the cylindrical nozzle decreases to the same turbulence level of the non-cavitating flow (tapered nozzle). At 75 and 100  $\mu\text{m}$  lifts high levels of turbulence as that appear in the first half of the nozzle length which cannot be related with the flow velocity. This happens independently of the nozzle geometry, possibly due to the secondary flow effect and thus cannot be related directly with the presence of cavitation since indeed, there is no cavitation in the tapered nozzle. However, overall, the turbulence level along the hole is slightly higher in the cylindrical (cavitating) nozzle than in the tapered one.

Additionally, the effect of cavitation on the velocity along the nozzle hole may be deduced from Figure 7.15. In the tapered nozzle, at high needle lift, the velocity increases along the nozzle. This is expected as there is no cavitation and, since the nozzle is convergent, the flow accelerates. On the contrary, in

## Chapter 7 Comparative Study of Quasi-steady and Moving Mesh Simulations

the cylindrical nozzle, the velocity decreases along the nozzle, as the cavitation does not reach the exit for this operating condition. Particularly, above 50  $\mu\text{m}$  needle lift, the velocity level is higher in the cylindrical nozzle than in the tapered at the first half of the nozzle. It then decreases until the exit where it takes smaller values than the in tapered nozzle.

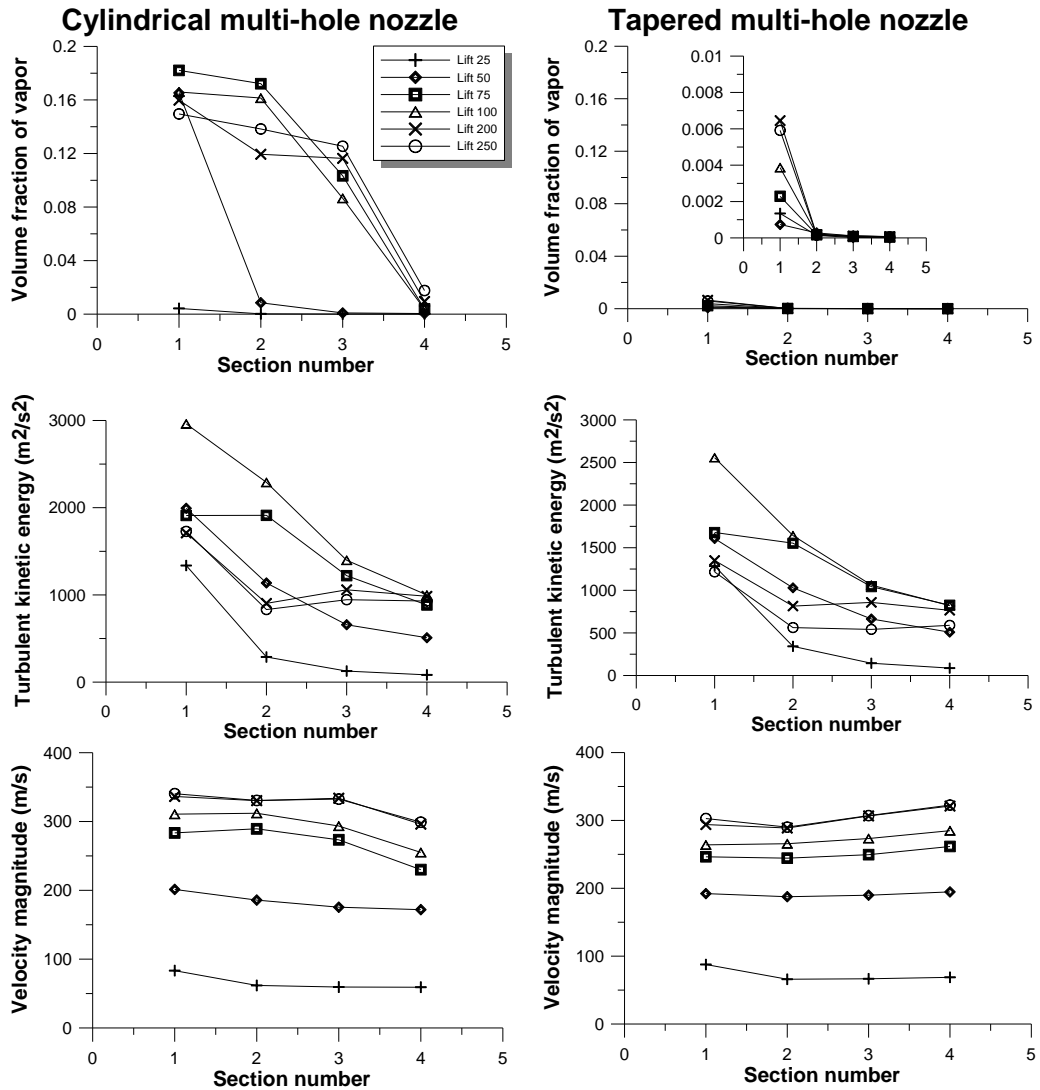


Figure 7.15: Volume fraction of vapour, TKE, and velocity along the nozzle hole in different lifts (800/50 bar).

### 7.3.2 Predicted flow of multi-hole Diesel injectors (whole injector)

The aim of this section is to determine the influence of the needle position on the flow structure of the sac volume and the injection holes of a multi-hole Diesel injector. In the previous chapters, predicted results were presented for

## Chapter 7 Comparative Study of Quasi-steady and Moving Mesh Simulations

a mesh sector of 60° (symmetry of the injector) and hence one of the six holes was chosen as being representative of all. In this study, the investigation goes into more depth by simulating the entire 360° sector (entire nozzle). Axial displacement of the needle (symmetrical geometry) was considered. The needle was positioned at two different lifts: 25 μm (low lift) and 250 μm (high lift). The two real six-hole injector geometries were considered, one with cylindrical nozzles, the other with tapered nozzles to study the effect of cavitation at 1410/10 bar. In order to meet the mentioned goals two series of calculations were performed. In the first series of calculations, nozzle holes of the same dimensions were considered (highlighted nozzle holes in Table 7.2). The same dimensions were also considered when simulated the 60° degree sector. This configuration was taken into account as reference geometry. In the second series, predictions using different hole size matching the actual hole sizes of the real-size nozzle were performed and the results compared of those of reference geometry.

Nozzle hole	Cylindrical Nozzle					Tapered Nozzle				
	R (μm)	D <sub>i</sub> (μm)	D <sub>m</sub> (μm)	D <sub>o</sub> (μm)	k-factor	R (μm)	D <sub>i</sub> (μm)	D <sub>m</sub> (μm)	D <sub>o</sub> (μm)	k-factor
1	22	146	148	147	-0,1	39	150	143	139	1.1
2	21	147	150	147	0.0	42	150	144	138	1.3
3	21	147	148	147	0.0	48	151	143	137	1.4
4	20	148	148	146	0.2	35	151	143	139	1.2
5	20	146	147	149	-0.3	41	151	143	138	1.3
6	24	149	147	148	0.1	37	154	144	137	1.7

Table 7.2: Dimensional characterization for cylindrical and tapered nozzle holes.

A representative image of the mesh is shown in Figure 7.16. The cells were non-uniformly distributed in the simulation domain. The sac and the hole were

## Chapter 7 Comparative Study of Quasi-steady and Moving Mesh Simulations

meshed with a fine mesh (cell size: 10  $\mu\text{m}$ ). The mesh between the needle and the injector body was formed by coarser cells in order to reduce the computational cost (cell size: up to 50  $\mu\text{m}$ ). The mesh had about 400.000 cells for the low lift and about 550.000 for the high lift geometries.



Figure 7.16: Image of the mesh used for the calculations at full lift.

Before the presentation of the predicted results with real size dimensions, it was considered useful to perform a first series of calculations with all holes having the same dimensions as mentioned above. These series of calculation (symmetric geometry) performed for comparison reasons in order to safer conclude results concerning the asymmetry of the flow when using asymmetry geometry in the second series of calculation.

In Figure 7.17 iso-surfaces of volume fraction of vapor are presented to show the extension of cavitation. The cavitation images are illustrated for both cylindrical and tapered nozzles at low and high needle lifts. Despite the fact that the dimensions of the holes in this series of calculations correspond to a symmetrical design, it was found that the flow develops differently from hole to hole at a certain instant.

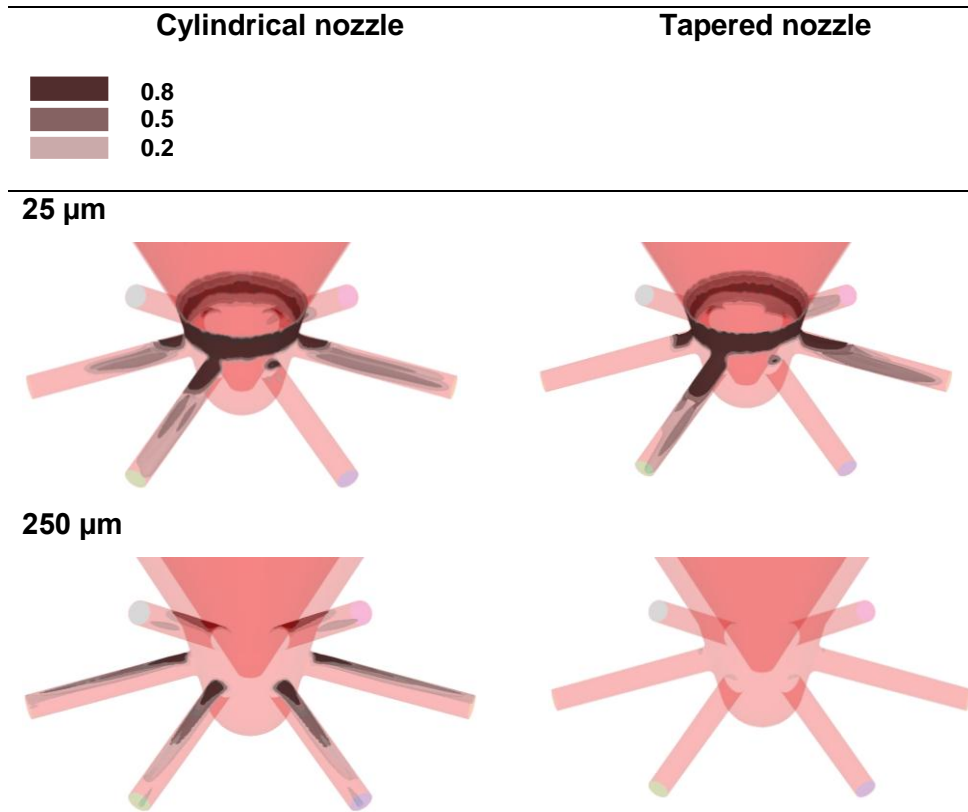


Figure 7.17: Iso-surfaces of volume fraction of vapour in cylindrical and tapered nozzles at low and high needle lift.

It is evident that the simple axial displacement cannot induce flow imbalances between the nozzles [67]. One reason for the difference in the cavitation pattern between the various holes may be due to the structure of the computational mesh and/or the solution algorithm. Particularly, while meshing, in order to substantially reduce effort and time, the surface topography and some control parameters were specified and the  $360^\circ$  sector geometry was filled with cells by the code auto-mesh module.

## Chapter 7 Comparative Study of Quasi-steady and Moving Mesh Simulations

Although flow structure variations probably due to numerical reasons are present, important conclusions may be drawn about the effect of nozzle geometry and needle lift on the development of cavitation. In the cylindrical nozzles, the cavitation distribution at low needle lifts is quite different from that at high needle lifts. For 25  $\mu\text{m}$  needle lift, cavitation is concentrated at the top of the hole in the first half of the nozzle and in the needle seat close to the holes entrance and a double vortex structure starts forming inside the nozzle, with different extension to each nozzle. As lift increases to full lift, the cavitation field evolves differently: the needle seat cavitation disappears and the cavitation mainly occupies the upper half of the nozzle. In the tapered nozzles, the cavitation distribution at low needle lift is quite similar to that of the cylindrical nozzles. However, at high needle lift, practically no cavitation appears in the tapered nozzle.

Additionally, as may be appreciated in Figure 7.17, the asymmetry in the cavitation flow pattern is much more pronounced at low needle lifts. It ought to be mentioned at this point that although a "pseudo-steady" condition is reached at the end of each fixed needle simulation, there is a fluctuating behavior in the flow distribution. It should be clarified that the above presented images are part of a transient timeline, in which for some time instances of the converged "quasi-steady state" solution the flow pattern becomes momentarily slightly different. This is clearly seen in Figure 7.18 where the cavitation pattern at a cut of the geometry for two different times of the "quasi-steady state" solution is presented. Overall, it was found that at low needle lifts the cavitation fluctuated more, and this fluctuation can be linked to the increased flow turbulence caused by the restricted passage of the flow in the region between needle seat and nozzle.

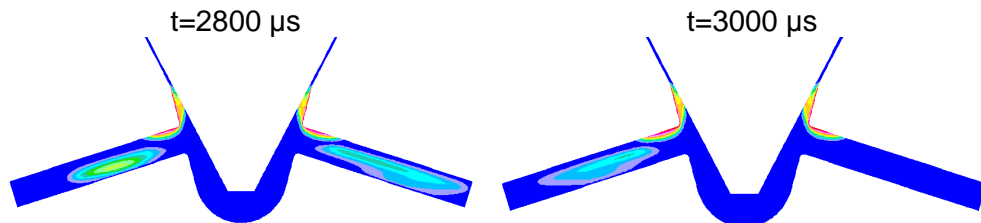


Figure 7.18: Cavitation pattern at a vertical cut for two different times, (cylindrical nozzle, 25  $\mu\text{m}$  needle lift).

Additionally, it was found that there is a link between the injection rate fluctuations of the opposite holes. When the cavitation increases in a hole, hence the injection rate decreases, the cavitation in the opposite hole decreases. This is clearly shown in Figure 7.19 where the injection rate in the opposite holes is plotted. It can be inferred that this difference in phase of the injection rate fluctuations, may produce different spray patterns of the emerging spray.

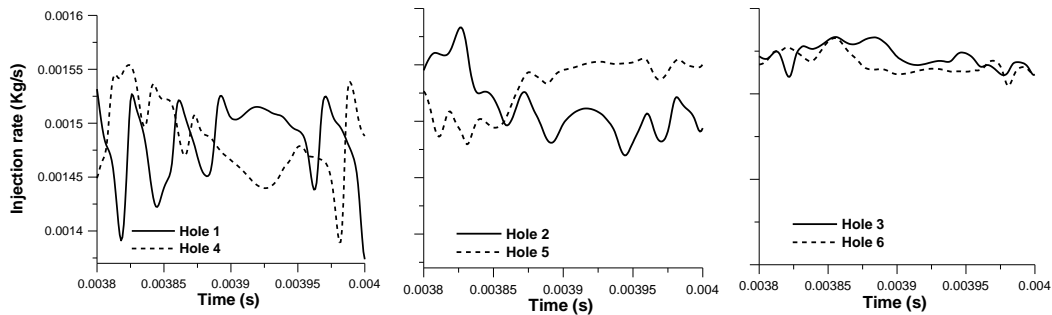


Figure 7.19: Injection rate fluctuation in opposite holes (same scale was used in the vertical axis).

Furthermore, in Figure 7.20 representative images of the streamlines are presented in order to reveal how the flow enters the hole at high and low lifts

## Chapter 7 Comparative Study of Quasi-steady and Moving Mesh Simulations

in both injectors. As has been seen in Chapter 6.3.2, that at low needle lift the flow inside the sac volume is highly rotating, noticeably so at the nozzle inlet, with the intensity of the rotating vortices increasing with decreasing needle lift. In this study where the entire geometry is simulated, the effect that the rotating flow of the sac volume and its transient nature has on each hole individually is illustrated. As can be seen, the liquid can either be delivered directly through the injection holes, or flow first inside the sac volume before entering into the injection holes. The flow coming from the annulus on one side may even deviate towards a hole on the opposite side. And streamlines descending between two holes flow towards the sac directly or tend to deviate towards the opposite nozzle. The behavior of the streamlines showing the various forms of delivering the flow through the holes seems to be independent of the nozzle shape and needle lift.

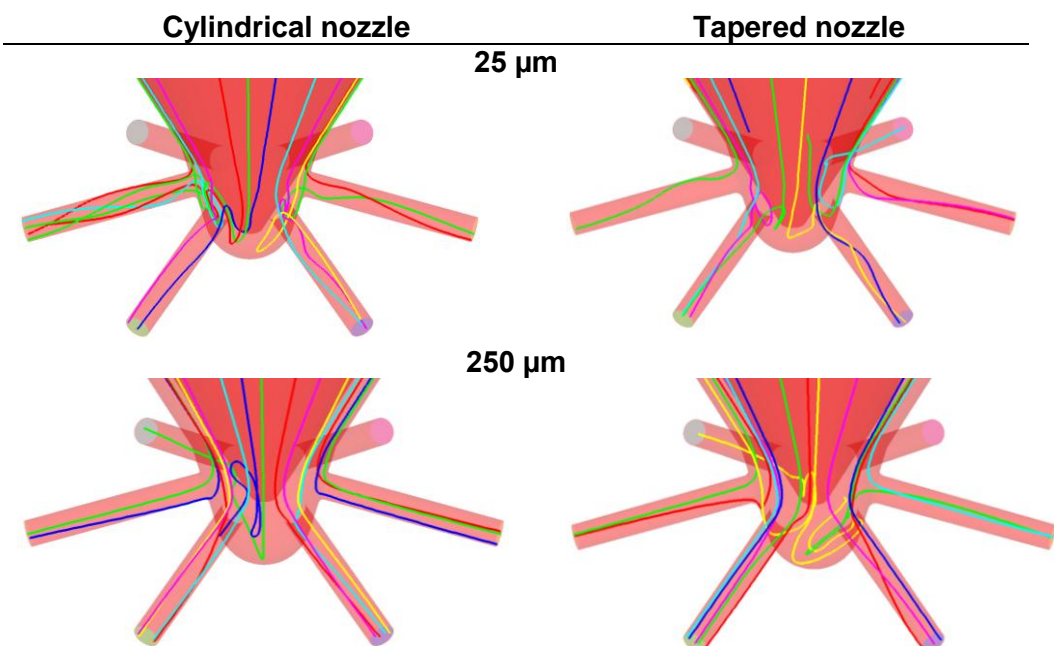


Figure 7.20: Particle tracks of cylindrical and tapered nozzles at low and high needle lift.

## Chapter 7 Comparative Study of Quasi-steady and Moving Mesh Simulations

In Figure 7.21 selected particle trajectories at different time instances for both nozzles and lift are presented. A transient flow pattern was observed in the sac volume. At different time instants, the trajectories can change completely. It should be noted that also the transient nature of the particle trajectories was found to be independent of lift position and nozzle shape. But it seems to induce higher flow imbalances in the nozzle holes at low needle lifts. It may be deduced that the way of delivering and the transient nature of the particle tracks are associated with the asymmetry of the cavitation pattern and the fluctuating nature of the cavitation inside the nozzle holes.

Having identified the basic flow trajectories within the sac volume and the nozzle holes of the symmetric injector geometries, the results for the injectors with the real dimensions of each hole are now presented.

Chapter 7 Comparative Study of Quasi-steady and Moving Mesh Simulations

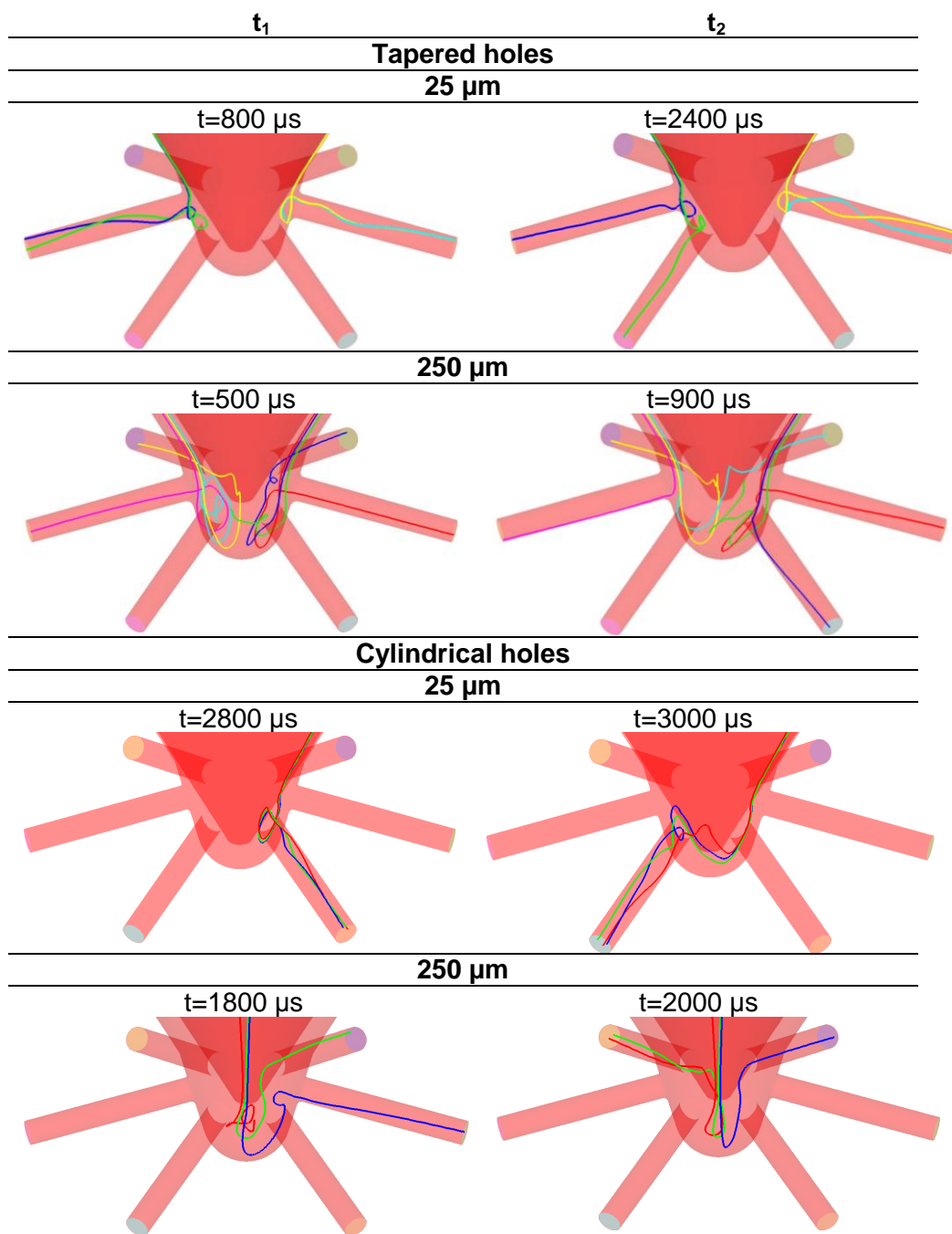


Figure 7.21: Particle tracks at two different instants of the “quasi-steady state” solution.

## Chapter 7 Comparative Study of Quasi-steady and Moving Mesh Simulations

In this section the effect of the hole geometry variations on the flow structure is studied. For this, the solution of the real geometry is compared to the symmetric geometry. In Figure 7.22 a comparison of the predicted flow rates exiting from the individual injection holes for both series of calculations are presented, where  $\Delta_m$  is the variation of the injection rate between maximum and minimum value of injection rate found. The study is aimed at showing qualitative comparison, rather than at providing exact mass flow results, since this would require more specific experimental information. From the graphs the aforementioned asymmetry on the mass flow rates is clearly illustrated. Overall, it was found that both the mean mass flow rate and its variation increase with decreasing needle lift, especially in the asymmetric geometry. It may be inferred that with higher geometrical asymmetry, the difference would be even more.

It should be noted that at low needle lift position both cylindrical and tapered nozzle are cavitating, though the mass flow of the real cylindrical holes, varies more than the corresponding tapered. The holes show major flow variation when the rotating recirculation zone is more extended towards the nozzle exit and shows a fluctuating behavior. When the needle position is at full lift, the flow is less transient. At this position the flow enters the hole more homogeneously as the annulus between needle and nozzle body is greater. Particularly, for the tapered nozzle, the mass flow is more stable as the nozzle does not cavitate at this position. This means that at high needle lift, the simplification of the real size dimensions (i.e hole entry radius) can be more valid for the mass flow prediction.

Comparing now the results of the individual holes of the two series of calculations, the influence of the geometrical parameters (i.e hole entrance

## Chapter 7 Comparative Study of Quasi-steady and Moving Mesh Simulations

radius, diameter, taper) on the injection rate is rather difficult to assess quantitatively when simulating a 360° section. As is seen in Figure 7.22, although in both series of calculations, the hole 1 for the cylindrical nozzle and the hole 2 for the tapered nozzles was with the same dimensions (see Table 7.2), the mass flows results are different. This means that the nozzle flow is affected not only by the hole geometry but also by the way that the flow enters the nozzle. Under this context, is rather difficult to assess the influence of some geometrical parameters on the mass flow when simulating the entire injector.

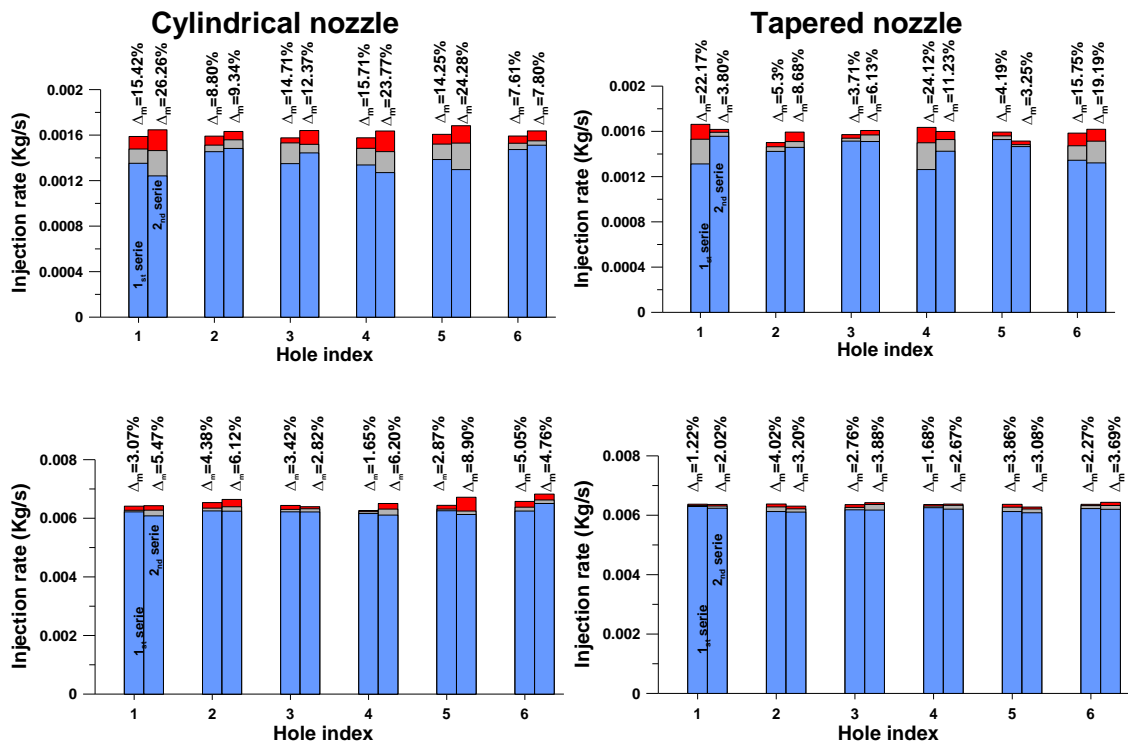


Figure 7.22: Variation of the injection rate between the various injection holes at different needle positions for the two series of calculations.

#### **7.4 Comparative Analysis of the Cavitating Flow with Fixed and Moving Needle Lift Simulations**

For Diesel engines, the determination of the exit conditions of the injector nozzle flow is of great importance because it greatly influences the spray development inside the combustion chamber and hence the combustion process. Since the possibility of experimentally observing and measuring the flow inside real size Diesel injectors is very limited, CFD calculations are generally used to obtain the relevant information. Because of the complexity of moving mesh calculations of real size injectors, the nozzle flow is often studied at full needle lift only or by quasi-steady state fixed needle lift calculations, so that little is known about the transient phase of the needle opening/closing. The aim of this section is to evaluate the two methodological approaches, comparing predicted results obtained by simulations with fixed and moving mesh needle lift. It should be noted that in these calculations, even the quasi-steady state calculations are time dependent due to the transience of the cavitation model. Since the real lift law is not known, the results presented here are of a qualitative nature, but nevertheless useful to understand the implications of using simplified approximations. At fixed calculations, the needle was positioned at 25, 50, 75, 100, 200, 250  $\mu\text{m}$ , while in the moving mesh calculations a range from 15-250  $\mu\text{m}$  was covered, simulating both the opening and closing of the needle. The operating conditions 800/10, 800/50, 1500/10, 1500/50 bar were studied. A full comparison of the predicted results in terms of volume fraction of vapour, turbulence intensity, injection rates and velocity profiles are given for the duration of the injection.

### **7.4.1 Comparative study of internal flow distribution**

It has been observed that the cavitation intensity depends strongly on the needle lift due to the effect of turbulence and vortices present in the nozzle hole. In Figure 7.23 predicted TKE distributions with fixed and moving mesh calculations for the cylindrical nozzle are compared (1500/50 bar). For each lift the colour scale is the same for both kinds of calculations. As is seen in the images, the turbulence intensity appears mainly in the hole inlet and dissipates along the nozzle hole. The fixed needle calculations can predict the increased flow turbulence caused by the restricted passage of the flow in the region between needle seat and nozzle. In the moving mesh calculations, at low needle lifts ( $<100\ \mu\text{m}$ ) the hysteresis mentioned in chapter 6.3.1 between the needle valve opening and closing is clearly seen in the images. On contrary, at high needle lifts the difference of TKE between valve opening and closing decreases. This implies that the fixed needle lift calculations can be adopted for simulating the flow field at this position.

In Figure 7.24 distributions of the predicted volume fraction of vapour are shown. As it is seen, both calculation approaches predict at certain lifts (above  $25\ \mu\text{m}$ ) a swirling cavitating flow which propagates up to the nozzle exit. The moving mesh calculations reveal that the hysteresis is also present for the cavitation field, and that the cavitation development is more pronounced at needle closing. It is seen that the fields of fixed needle calculations are more representative of those at needle opening. However, at high needle lifts, there is less hysteresis between needle lift opening and closing, so that the fixed needle lift calculations is representative of the real moving mesh calculation. This is probably due to the fact that the cavitation phenomenon at high needle lift is more stable, less transient. Additionally, the fixed needle lift calculation adequately predicted the secondary vortex structure at low needle lifts and the more stable cavitation structure at high

## Chapter 7 Comparative Study of Quasi-steady and Moving Mesh Simulations

needle lifts as is seen in Figure 7.24. But the advantage of the moving mesh calculation is that it can provide additional information about the generation process of cavitation during opening and closing of the needle.

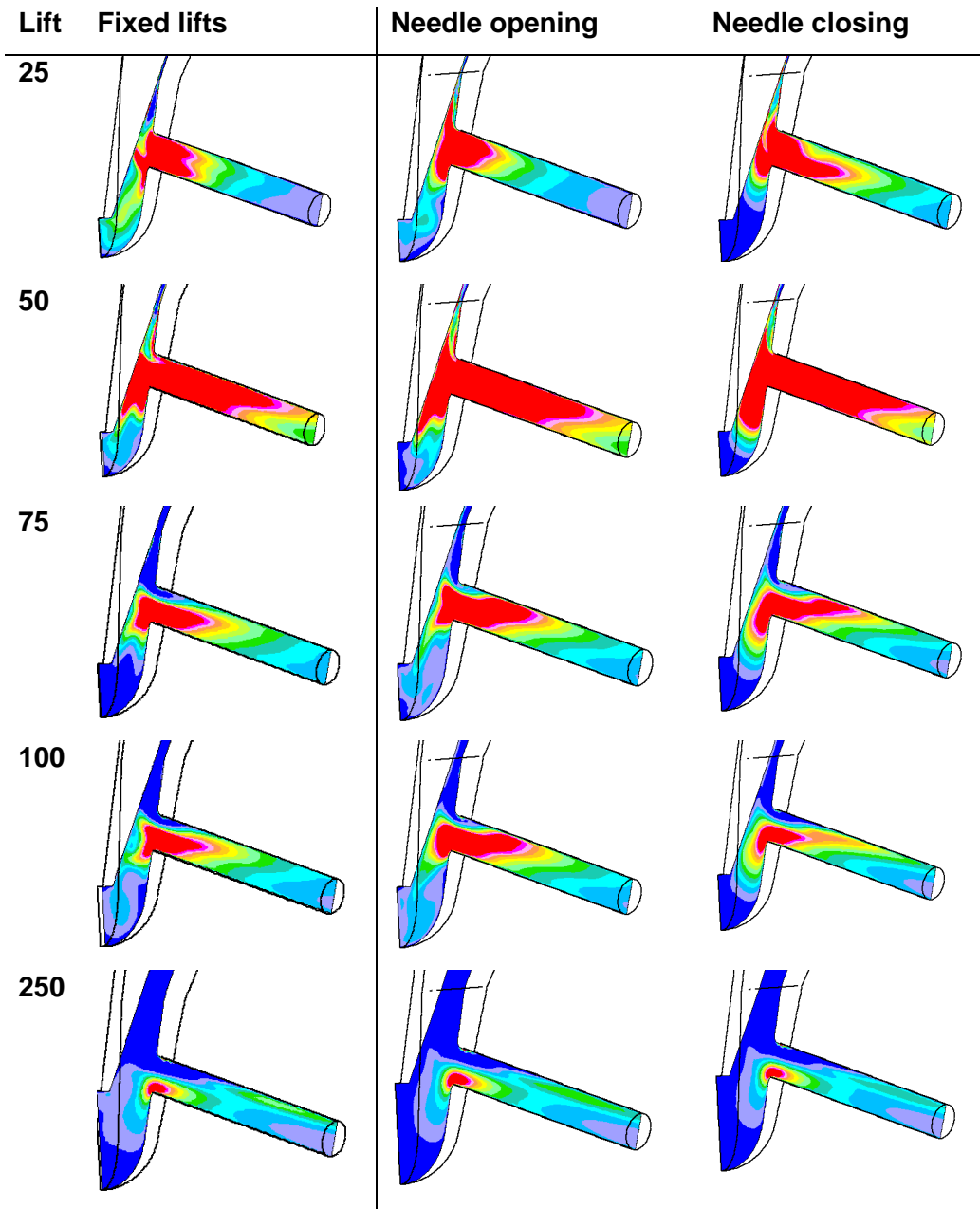


Figure 7.23: Comparative view of TKE ( $\text{m}^2/\text{s}^2$ ) at different needle lifts for fixed and transient needle lift analyses, 1500/50 bar (the colour scale is the same in both calculation methods of each lift).

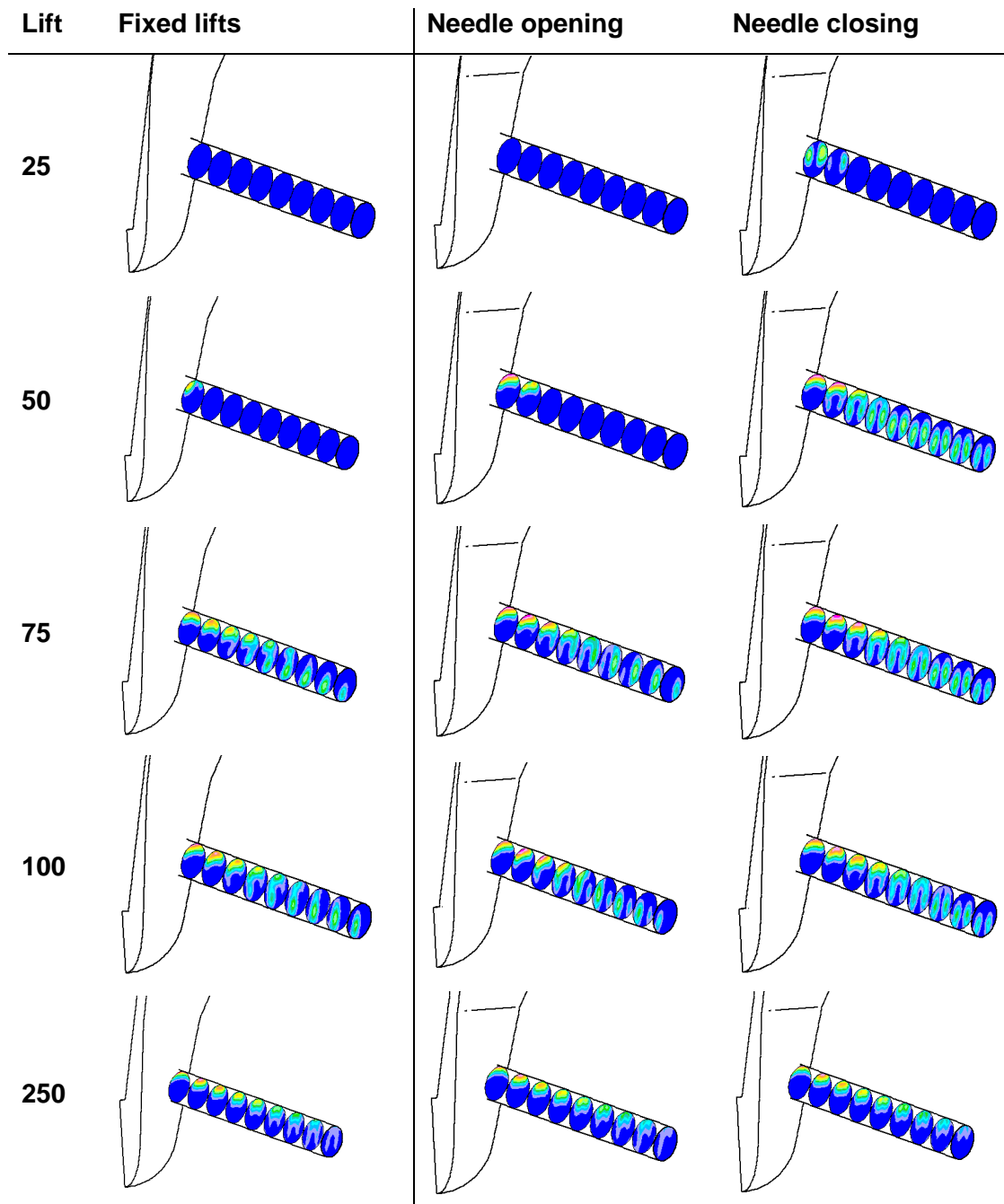


Figure 7.24: Comparative view of volume fraction of vapour at different needle lifts for fixed and transient needle lift analyses, 1500/50 bar (colour scale: 0-1).

### 7.4.2 Comparative study of nozzle exit characteristics

In this section, the focus is put on the nozzle exit flow characteristics, analysed with both the fixed and moving mesh calculations. The area averaged volume fraction of vapour and turbulence intensity at the exit of the nozzle (1500/50 bar) are represented in Figure 7.25, as calculated with the moving mesh. The instantaneous evolution of these values shows the highly transient nature of the flow, raising the question of whether fixed needle lift simulations can accurately predict the effect of the opening and closing phases on the flow characteristics.

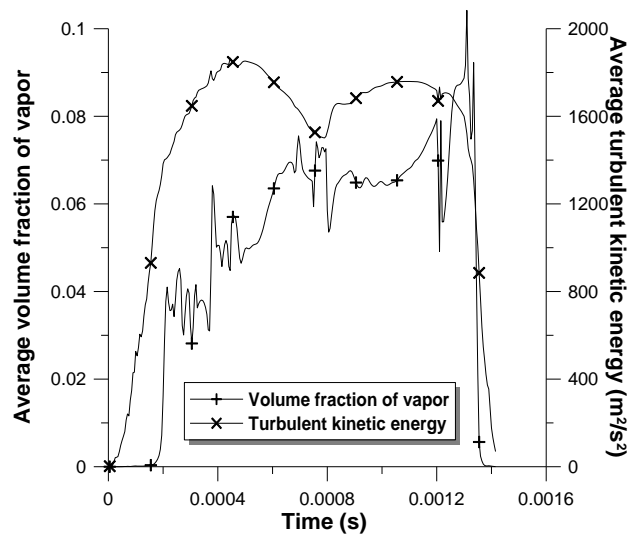


Figure 7.25: Average instantaneous TKE and volume fraction of vapour at the exit of the nozzle (1500/50 bar), calculated with moving mesh.

In Figure 7.25, the hysteresis between the needle valve opening and closing for volume fraction of vapour and TKE instantaneous values is clearly visible. As already mentioned, more vapour reaches the nozzle exit during needle closing than during needle opening. On the contrary, the turbulence intensity reaches higher levels during the nozzle opening. Although the turbulence

## Chapter 7 Comparative Study of Quasi-steady and Moving Mesh Simulations

dissipates along the nozzle, as was mentioned above, its effect is still noticeable at the nozzle exit. It is worth noting that for the calculations performed at different operating conditions, with different nozzle shapes (tapered-cylindrical), different nozzle types (single-hole, six-hole nozzles) as well as different lift curves, the phenomenon of hysteresis was present in all cases. This characteristic could not be detected with fixed mesh calculations. In Figure 7.26 are seen the results of average value of volume fraction of vapour and injection rate at the exit of the nozzle obtained with two different lift curves. The choice of needle lift law can affect greatly the injection rate since the injection rate does not become independent of the lift in contrast with the single-hole nozzle as confirmed by the injection rate measurements. However the characteristics of the internal flow described above, including the transient nature of cavitation and the hysteresis phenomena, are independent of the needle lift law. As seen by the volume fraction of vapour graphs, in both cases the hysteresis phenomenon is predicted. Concerning the injection rate, a 10% difference of injection rate is observed during the needle lift opening when used the here called “square lift law” since the lift is higher during most of the time of the opening, indeed for the needle closing the difference is less important.

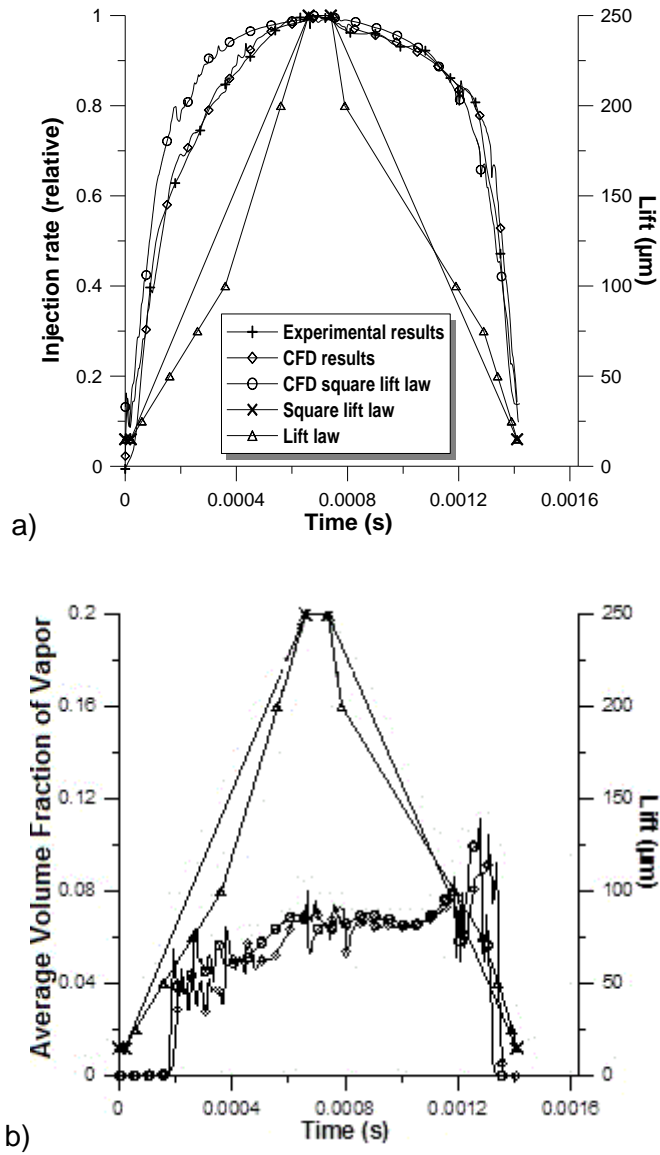


Figure 7.26: a) Injection rate at the exit of the nozzle obtained and b) average volume fraction of vapour with different needle lift laws, 1500/50 bar.

Another characteristic of the flow that was observed in the moving mesh solution is an increase in cavitation intensity at low lifts when the needle closes, represented by the volume fraction of vapour intense peak near

## Chapter 7 Comparative Study of Quasi-steady and Moving Mesh Simulations

closing (Figure 7.25). At certain instants the cavitation cloud grows and exits from the nozzle as was shown in section 6.3.2, Figure 6.19. Similar observations detecting an increase in the cavitation intensity when the needle starts to close have been published in [153]. However, at low needle lifts, the fixed calculations did not show similar clouds exiting the nozzle.

Additionally, as seen in Figure 7.25, a decrease in cavitation intensity is predicted by the moving mesh approach when the needle is fully opened. Decrease in cavitation intensity at full load has been found also in the reference [154]. The results of the fixed needle calculations are close to the transient values, but are not able to capture the decrease in vapour at full load as will be illustrated in Figure 7.28.

An attempt was made to quantify the difference of the turbulence results obtained by the both approaches at certain lifts. In Figure 7.27, the values of TKE at the exit of the nozzle of the moving mesh calculations are compared with the time averaged values of the fixed calculations. Results of both nozzles (tapered/ cylindrical) and two operating conditions (800/50 bar, 1500/50 bar) were selected for presentation here in order to see the effect of geometry and injection pressure. Due to hysteresis at low lifts the needle closing values (obtained by the moving mesh calculations) are in most cases higher than the other values (fixed, opening). For higher lifts (above 100  $\mu\text{m}$  approximately) the needle opening values are higher. This difference between opening and closing values increases when the pressure drop increases (1500/50 bar) in both nozzles. Additionally, the difference is larger for medium to high lifts (100 a 200  $\mu\text{m}$ ). The results for the fixed lift calculation lie between the needle opening and the needle closing values, representing an average value. At full lift, the difference between the opening and closing values tends to decrease. These observations seem to be independent of the

## Chapter 7 Comparative Study of Quasi-steady and Moving Mesh Simulations

nozzle geometry, as, indeed, the tapered geometry (non cavitating nozzle) shows similar tendencies.

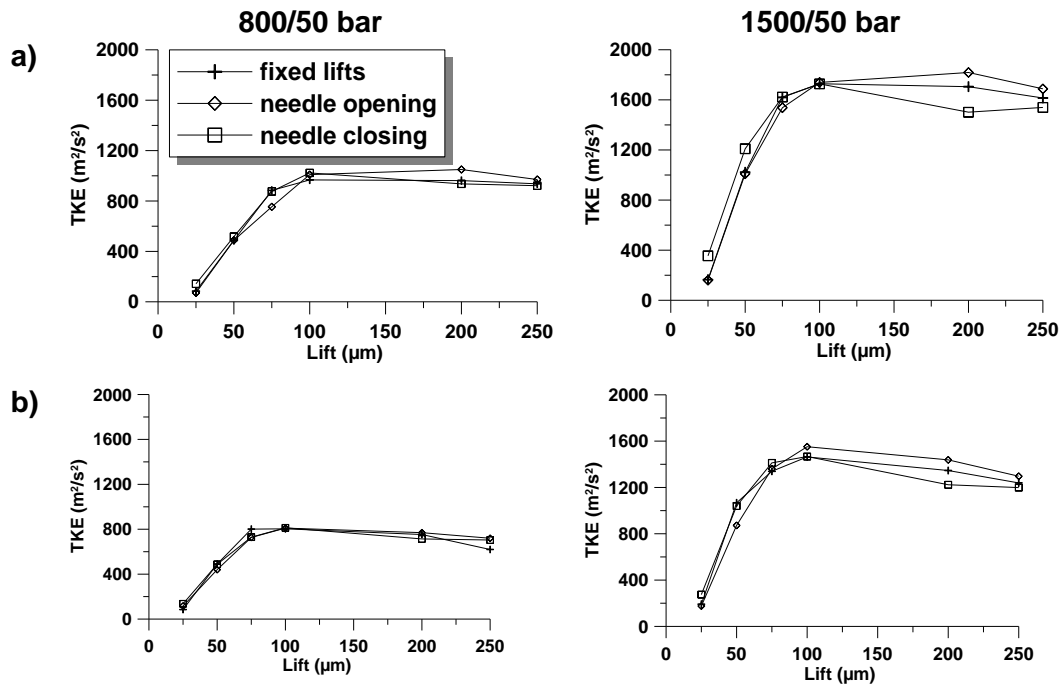


Figure 7.27: TKE at different lifts with fixed and moving mesh calculations at 800/50 and 1500/50 bar for a) cylindrical and b) tapered nozzle.

However, the outlet values predicted by the fixed needle approach, match qualitatively, with the moving mesh results. The solutions of both approaches clearly show that the TKE values significantly increase with increasing needle lift until a maximum is attained at medium lift. Beyond that, it is less sensitive to further lift increase. The turbulence level attained at high lifts depends on the injection pressure and is approximately double for the 1500 bar cases. The results also show that there is a drop in turbulence level at full lift (full load) in the needle opening phase. This drop continues during the first instants of needle closing (see 200  $\mu m$  needle lift of closing moving mesh phase). The fixed needle results cannot capture this phenomenon: in all

## Chapter 7 Comparative Study of Quasi-steady and Moving Mesh Simulations

cases, they predict a similar behaviour to needle opening, with larger TKE values at 200  $\mu\text{m}$ .

Figure 7.28 presents the percentage of area occupied by vapour at the exit of the nozzle as a function of lift for both the fixed and moving mesh calculations for four different operating conditions. The area of all cells containing at least 5% of vapour is represented. Only the results from the cylindrical (cavitating) nozzle are presented. The aim is to analyse whether the vapour quantity (represented by the mean vapour volume of fraction) present at the exit of the nozzle is accurately predicted by the fixed mesh calculations, compared with the moving mesh results. As mentioned above, although the needle is fixed, the modelling of the cavitation phenomenon itself is transient. Therefore, there is a deviation of the mean value of volume fraction of vapour due to the fluctuating mass flow, and represented on the graphs by the vertical double arrows. Clearly, the quantity of vapour present at the hole exit at a determined lift is not adequately predicted by the fixed needle lift calculations. Indeed, no clear trend can be observed when comparing the results of the fixed lift calculations and of the transient calculations. The standard deviation of the volume fraction of vapour is larger for the lifts in which the vortex structure propagates downstream from the hole entrance to the exit. Overall, at low lifts, the fixed needle lift calculations seem to under predict the quantity of vapour at the exit during needle opening, and over-predict that during needle closing. At high lifts, however, they clearly over-predict the amount of vapour at the exit. These results seem to indicate that the fixed needle lift calculations cannot properly represent the highly transient nature on the cavitation during opening and closing of the needle. This can only be captured by a full simulation of the needle movement.

Chapter 7 Comparative Study of Quasi-steady and Moving Mesh Simulations

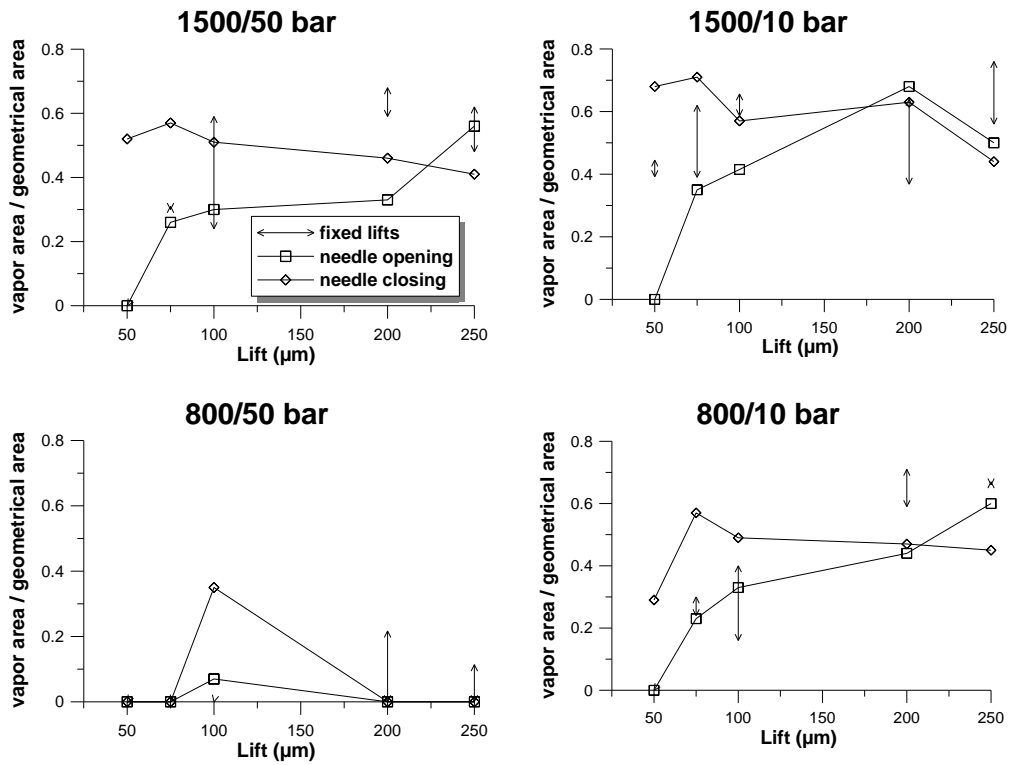


Figure 7.28: Percentage of area occupied by vapour at the nozzle exit as a function of lift with fixed and moving mesh calculations for different operating conditions.

In Figure 7.29, the injection rate obtained with the fixed and moving mesh calculations is compared. From this comparison it can be deduced that although the detailed features of the cavitating flow due to its transient nature are not adequately represented by fixed needle lift calculations, the averaged characteristics of the flow, such as the flow rate, can be predicted with good accuracy. This is very important from an engineering point of view if only the injection rate results need to be obtained.

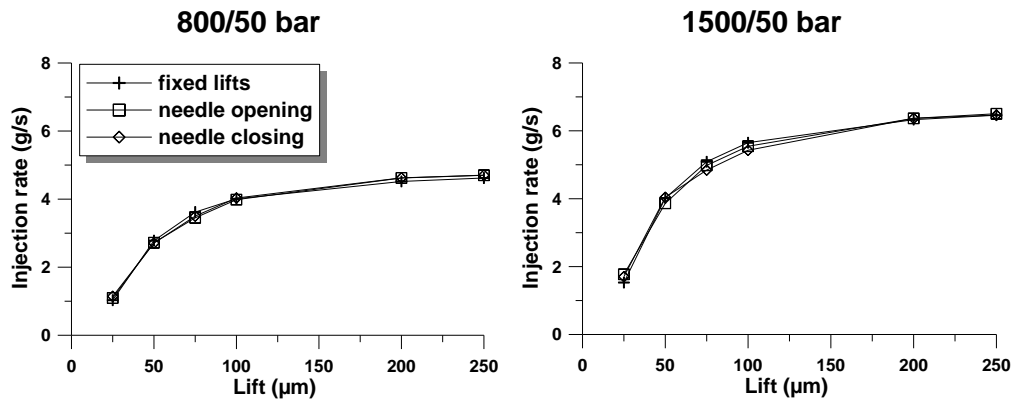


Figure 7.29: Injection rate at different lifts with fixed and moving mesh calculations at 800/50 and 1500/50 bar for cylindrical nozzle.

The velocity profiles obtained by the two approaches along the horizontal and the vertical edges (defined in Figure 5.10) are presented in Figure 7.30 and in Figure 7.31 for both nozzles and two operating conditions. The lower velocity values correspond to the 25 µm lift, the upper to the 250 µm and the legend is the same for all plots. It is seen that the velocity profiles are more sensitive to the methodological approaches. Along the vertical edge the differences in the profiles for all lifts, pressure conditions and geometries may be important. As seen, the asymmetry of the profiles at high lift is not accurately predicted by the fixed needle lift calculation. And, at low lift, the axial velocity is under/over-predicted with the fixed calculations up to 15-20%.

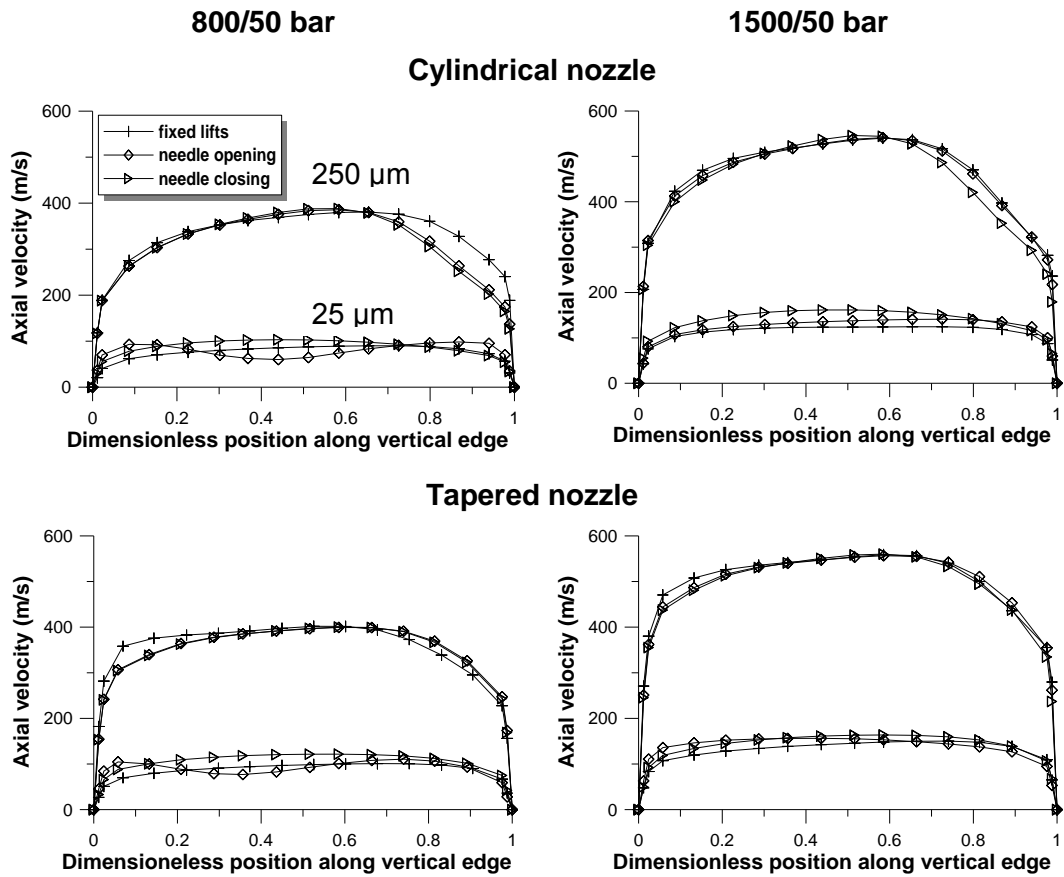


Figure 7.30: Comparison of axial velocity profiles at the exit of the nozzles along a vertical edge obtained by fixed and moving mesh calculations at 25 and 250  $\mu\text{m}$  lift.

For both nozzles, the axial velocity profiles along the horizontal axis obtained with both approaches are very similar at high lift, when the flow conditions are more stable. At low lift, the transient nature of cavitation affects more the velocity profiles (hysteresis between opening and closing) and the fixed calculation under/over predicts the axial velocity profile about 10-15%, though the profile shape is accurate enough.

## Chapter 7 Comparative Study of Quasi-steady and Moving Mesh Simulations

In summary, the fixed needle lift calculations are reasonable accurate at high lift, provided there are no pronounced flow asymmetries in the flow generated by the needle movement. However, the results at low lift, when the transient character of the flow is more pronounced, have to be considered with care, since the inaccuracies may be significant.

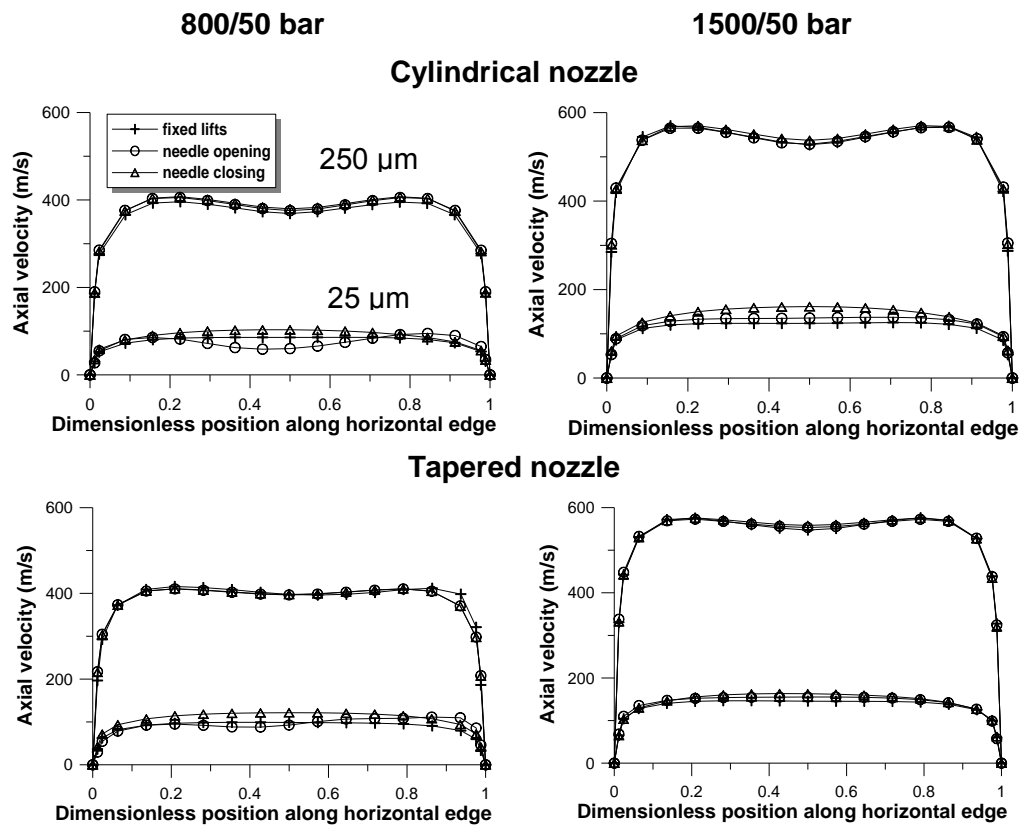


Figure 7.31: Comparison of axial velocity profiles at the exit of the nozzles along a horizontal edge obtained by fixed and moving mesh calculations at 25 and 250  $\mu\text{m}$  lift.

## **7.5 Summary**

Fixed needle lift calculations for a multi-hole injector at different needle lifts have been presented, first for a 60° sector and then for the complete injector (six holes).

- The fixed needle simulations captured the nature of the nozzle hole cavitation phenomenon at high and low needle lifts, for both the tapered and cylindrical nozzles. For the cylindrical nozzle, at low lifts, the simulations qualitatively predicted the vortex flow and the unsteady nature of the cavitating flow. At high needle lifts, a more stable cavitation pattern attached mainly to the upper part of the nozzle was predicted. Additionally, they predicted that the needle position has a more determinant influence on the velocity profiles than the presence of cavitation. Concerning the TKE intensity, they provided some basic flow characteristics such as the enhanced turbulence in the nozzle hole and the decrease of turbulence intensity at full lift.

The whole geometry of a Diesel injector was simulated by CFD calculations and important flow characteristics were identified that could not be seen clearly when assuming symmetry of the computational domain. The study was focused on investigating the flow distribution within the sac volume and the injection holes and how it is affected by the needle position and geometrical modifications of the holes. Although limitations due to theoretical and numerical simplifications are present, important conclusions for the transient behavior of cavitation can be drawn for realistic injection conditions.

## Chapter 7 Comparative Study of Quasi-steady and Moving Mesh Simulations

- From the same dimension nozzle hole simulations, that were used as initial reference, it can be deduced that the nozzle flow develops differently from hole to hole at a certain instants, especially at low needle lifts. Visualization of simulated particle tracks have shown crossing trajectories revealing the transient nature of the flow formed inside the sac volume, whereby some particles, crossover the sac region and impact on the opposite nozzle hole. The way of delivering and the transient nature of the particle tracks are deduced to be linked with the asymmetry of cavitation pattern and its fluctuatory nature inside the nozzle holes. Additionally, it was found that there is a link of the cavitation fluctuatory pattern of the opposite holes.
- Comparison between same and different dimension nozzle hole simulations has shown that overall, both the mean mass flow rate and variation increases with real size (asymmetry) geometry, as expected, but mostly on low needle lifts. It may be inferred that with higher geometrical asymmetries the, the flow between the different nozzle holes may be even more distinct. At high needle lift, the radius is less determinate due to the wider area in the annulus between needle and nozzle body which allow the flow to enter the hole entry in a less abrupt way.

From the comparison of fixed and moving mesh calculation (a 60° sector was simulated to save computational cost) it was seen that the transient moving mesh analysis additionally provided a number of flow characteristics concerning the effects of the needle position in time.

- Specifically, the results of transient analysis captured the hysteresis of vapour formation and turbulence intensity, the decrease of volume fraction of vapour at full load and peaks of vapour formation at certain

## Chapter 7 Comparative Study of Quasi-steady and Moving Mesh Simulations

times. Moreover it was established the link between the levels of turbulence with the needle motion. Although the steady simulation captured the basic flow structure inside the hole at high and low lifts, it did not capture the time dependent flow characteristics mentioned above. The two methodologies provide different nozzle exit results, especially for low needle lifts, while the percentage difference changes depending on the lift and the operating conditions. Hence, the calculations with moving mesh boundaries provide information about the transient phase of injection that may not be neglected.

## Chapter 7 Comparative Study of Quasi-steady and Moving Mesh Simulations

## **CHAPTER 8.**

### **CONCLUSIONS & RECOMMENDATIONS FOR FUTURE**

#### **WORK**

##### **8.1 Overview**

The research work presented in this thesis has focused on the analysis of cavitating flow in automotive injector nozzles using a commercial CFD code; the cavitation model is based on the bubble growth theory and the assumption that cavitation is formed by seeds. With the present model, the structure inside various types of injectors at full needle lift and at various needle lifts was investigated numerically. Initially, the cavitation model was validated with results found in the literature for an injector-like geometry. Then, the model was applied to the simulation of real size injection nozzles, both single-hole and multi-hole nozzles with cylindrical and tapered holes. For this, comparison with in-house experimental data in terms of coefficients was made at fully opened needle lift. Then, the model was used for the prediction of cavitating flow at different needle lifts. Both fixed needle lift and moving mesh calculations were performed and the two methodological approaches were compared.

In what follows, the main conclusions from the validation process are presented, together with the conclusions from the cavitating flow analysis. Subsequently, the recommended future work will be discussed in detail.

## 8.2 Conclusions

Before proceeding to the simulation of real size Diesel injectors, the model was validated against measurements found in the literature for an injector-like nozzle. The main conclusions from this validation process are:

- Comparison of calculations with experimental data showed that there was good qualitative agreement between simulation and experiment in terms of injection rate. Furthermore, relatively good agreement was found between the experimental and the predicted velocities and pressure profiles. Also, the cavitation model predicted reasonably well the observed pressure field and low pressure recirculation zone linked to the cavitation onset. Further analysis of the flow showed a vortical structure of the cavitation along the nozzle, related with the vortical velocity.
- The possible sources of discrepancy were identified and discussed; these were attributed mainly to the overestimation of the liquid viscosity, uncertainties linked to the turbulence model and the vapour-liquid phase interactions not taken into account. The identified differences between the predictions and the experiment in these cases establish a threshold level of accuracy for the subsequent cavitation model validation.

Subsequently, the model was validated against in-house experimental data of real size single-hole and multi-hole Diesel injectors at fully opened needle lift. These calculations provided then a full description of the nozzle flow characterisation.

- Overall, the agreement of the model with the experiment at fully opened needle has been found to be quite satisfactory for both cylindrical and tapered nozzles on a qualitative level. The known effect of pressure drop and taper has been reproduced quite faithfully by the simulations. The model predicted the experimentally observed increase of velocity at the nozzle exit in cavitating conditions. With the above, it is seen that cavitation modelling has reached a level of maturity such that it allows predicting the effects of geometry and operating conditions with reasonable accuracy. This represents a valuable contribution to the understanding of nozzle performance.
- It was seen that experimentally the  $C_d$  was independent of the pressure drop in the single-hole nozzles, while in the multi-hole nozzles an increasing trend with increasing pressure drop pressure was observed for both tapered and cylindrical nozzles. The predicted results did not agree with this tendency probably due to the fact that the pressure loss within the injector body was not taken into account when imposing the injection pressure on the calculation domain.
- The predicted single-hole nozzle cavitation distribution was confined to the wall, showing major extension at enhanced cavitation conditions. The backpressure plays a more important role in the development of cavitation than the injection pressure. Indeed, an increase of the injection pressure does not influence significantly the cavitation pattern, while an increase of the backpressure delays the cavitation expansion. A more complicated cavitation pattern was predicted in the

multi-hole nozzles. The cavitation develops mostly in the upper part of the nozzle and follows the vortical pattern imposed by the flow velocity.

After the end of the validation process and analysis of the cavitating flow at fully opened needle lift, simulations were made to analyse the flow during the whole transient injection process with moving mesh calculations. Both single-hole and multi-hole nozzles with cylindrical and tapered orifices has been examined. In single nozzle holes, the same lift law (based on simple linear equations) was used for the cylindrical and tapered nozzle calculations. A simple moving mesh strategy was developed for the multi-hole nozzle calculations which required an interpolation between the experimental results and the results with calculations at fixed needle lifts. The main conclusion remarks are noted below:

- The convergent shape towards the exit greatly modifies the pressure distribution during the injection process in both types of nozzles and thus the cavitation formation. Indeed, no cavitation appears in the single-hole tapered nozzle, independently of the needle movement. The cavitation is significantly reduced also in the multi-hole tapered nozzle, as only some vapour appears at low needle lift, in the restricted area between the needle and needle seat or at the hole entrance under enhanced cavitating conditions without though reaching the nozzle hole exit.
- In the cylindrical single-hole nozzle, the cavitation develops attached to the wall as was the case at full needle lift and its extension varies depending on the needle lift. In cylindrical multi-hole nozzle, the cavitation tends to follow the vortical structure observed at full needle lift, but much more enhanced when the needle descends.

- The model predicts clouds of cavitation growing and evacuating the nozzles (both single- and multi- hole) at low needle lifts, which is in accordance with the highly transient nature of the flow during needle motion. The results show also that the cavitation regime is much more transient at low than at high needle lifts.
- The turbulence kinetic energy is mainly created in the first stages of needle opening and in the last stages of closing, independently of whether there is cavitation or not. This is probably due to the local acceleration of the flow at the nozzle inlet caused by the restricted passage. Furthermore, the development of cavitation influences somehow the turbulence level. Indeed, it seems that part of the turbulence kinetic energy is being absorbed during the growth of the cavitation bubble.
- The needle motion creates a kind of flow hysteresis, which is visible in the turbulence kinetic energy evolution, independently of the presence of cavitation, as well in the development of cavitation. Indeed, at a same low needle lift, the flow pattern differs if it is in the opening or closing phase.
- It is seen that the velocity profiles in the multi-hole nozzle change greatly with increasing needle lift, as well as between the opening and closing phase of the needle, independently of the presence of cavitation. The hysteresis is also reflected on the velocity profiles during the needle motion. The peaks of the velocity profiles of cylindrical nozzle are more marked at full needle lift due to the amount of vapour reaching the exit, though the asymmetry is present at all needle lifts. Comparing the flow in both nozzles, it is seen that in the tapered nozzle the peaks of the velocity profiles are less pronounced especially at high lifts, though quite similar with the cylindrical nozzle at all needle lifts as the vortical flow pattern appears in both nozzles.

The flow visualization for the tapered nozzle shows that the flow is generally asymmetrical at the nozzle exit, but the asymmetry is less marked compared with the cylindrical case. This confirms that cavitation present mostly in the cylindrical nozzles affects the symmetry of the flow.

The whole geometry (360<sup>0</sup> degree) of a Diesel injector was then simulated by CFD fixed needle lift calculations at full needle lift (250  $\mu\text{m}$ ), as well as at low needle lift (25  $\mu\text{m}$ ). Though the computational cost was higher, important flow characteristics were identified that could not be seen clearly when assuming symmetry of the computational domain. The study was focused on investigating the flow distribution within the sac volume and the injection holes and how it is affected by the needle position and geometrical modifications of the holes. For this, two series of calculations were performed. In the first series of calculations, nozzle holes of the same dimensions were considered. This configuration was taken into account as reference geometry. In the second series, predictions using different hole size matching the actual hole sizes of the real-size nozzle were performed and the results compared of those of reference geometry. Although limitations due to theoretical and numerical simplifications are present, important conclusions for the transient behavior of cavitation can be drawn out under realistic injection conditions.

- From the same dimension nozzle hole simulations, that were used as initial reference, it can be deduced that the nozzle flow develops differently from hole to hole, especially at low needle lifts. Visualization of simulated particle tracks have shown crossing trajectories, whereby some particles flow across the sac region and impact on the opposite nozzle hole. The way of delivering and the disorderly of the particle tracks are linked with the asymmetry of the cavitation pattern and its

fluctuating nature inside the nozzle holes. Additionally, it was found that there is a link of the cavitation fluctuatory pattern of the opposite holes. Indeed, when the cavitation increases in a hole, hence the injection rate decreases, the cavitation in the opposite hole decreases.

- Comparison between same and different dimension nozzle hole simulations has shown that overall, both the mean mass flow rate and variation increases with real size (asymmetry) geometry, as expected, but mostly on low needle lifts. It may be inferred that with larger geometrical asymmetries the, the flow between the different nozzle holes may be even more distinct. At high needle lift, the inlet radius is less determinate due to the wider area in the annulus between needle and nozzle body which allow the flow to enter the hole entry in a less abrupt way.

The transient calculation with needle motion allowed obtaining a full description of the transient flow in the nozzles. Since in most cases found in the published literature, the flow inside the nozzles is studied without taking into account the needle movement, the next step in this thesis was to compare the two approaches. For this, fixed needle lift calculations of the multi-hole nozzle were performed for different needle lifts, using a 60° computational domain (symmetry of the 6-hole injector) in order to mitigate the computation cost. The main conclusions drawn from the comparison between both approaches are the following:

- The fixed needle simulations captured the nature of the nozzle hole cavitation phenomenon at high and low needle lifts, for both the tapered and cylindrical nozzles. For the cylindrical nozzle, at low lifts, the simulations qualitatively predicted the vortical flow and the unsteady nature of the cavitating flow. At high needle lifts, a more

stable cavitation pattern attached mainly to the upper part of the nozzle was predicted, in agreement with the moving mesh calculations. Additionally, they predicted that the needle position had a more determinant influence on the velocity profiles than the presence of cavitation. Concerning the TKE intensity, the fixed needle lift calculations provided some basic flow characteristics, such as the enhanced turbulence level at medium needle lift and the decrease of turbulence intensity at full lift. However, the relationship between the turbulence level and volume fraction of vapour is more difficult to establish with this approach, as it was clear from the needle movement calculations, that the turbulent level was very much related to the needle movement.

- The transient moving mesh analysis additionally provided a number of flow characteristics concerning the effects of the needle position in time. Specifically, the results of transient analysis captured the hysteresis of vapour formation and turbulence intensity, the decrease of vapour at full lift and peaks of vapour formation at certain times. From the above it is deduced that is very important to take into account the transient phase of injection.

From the above, as a general conclusion it may be stated that both the simulation of the whole injector, as well as the fully transient movement of the needle, despite their computation cost, provide valuable information of the internal flow and the hole exit characteristics, especially at low needle lift, where the cavitation is present even for the tapered holes, that may cannot be captured by simplifying the problem (symmetry of the geometry, fixed needle lift calculations). Though, this modeling approach can be quite expensive either in pre/post-processing or in computational resources, thus for an engineering purposes approach, it may be opted for the simplification of the

case. In addition, since the eventual purpose is to provide information for the spray calculation, the approach may be determined by the numerical method adopted for the spray modeling.

### 8.3 Recommendations

In the remaining part of this chapter the most important recommendations for a future work on the extension and improvement of the current work are presented:

- To describe the cavitation flow, the concept of a locally homogeneous liquid vapour mixture was applied. To calculate the evaporation and condensation flow rates, the transport equation for the volume fraction of vapour phase based on a simplification of the more general Rayleigh-Plesset equation for bubble growth and collapse, was adopted. This equation was derived under assumption that cavitation starts to develop from seed bubbles and can be described locally for cavitation bubbles of the same size. A more sophisticated model based on experimental evidence could be used, i.e. using a user-specified cavitation model, saturated vapour pressure defined through user subroutine and not as a constant.
- It is well known that the details of the internal nozzle flow influence considerably the spray formation and its characteristics, especially when cavitation occurs inside the nozzle. The numerical simulation of this flow could provide the “realistic” conditions to initialize ELSA (Eulerian-Lagrangian Spray Atomization) simulation and so, take into account the velocity and turbulence distribution at the nozzle exit section, as well as their temporal evolution during injection. The post-processing results (velocity, kinetic turbulent energy, its dissipation

rate and volume fraction of vapour at the injector's outlet section) at fully opened needle lift, as well as during the whole transient of the injection process at the exit of the nozzle could be used to study the impact of the internal nozzle flow (geometry, cavitation formation) on the spray and its characteristics. The fulfilment of the coupled simulation and the study of the internal flow influence on the spray formation could be the next phase of the present work.

- Subsequent work could continue with a radial perturbation of the needle motion and its effect on the flow characteristics.
- Some directions for experimental studies are also proposed. The effect of pressure drop on the flow coefficients at fully opened needle lift calculations could be examined more in detail numerically but also experimentally. This would bring some insight to explain why the model was not able to reproduce the increasing trend of the flow coefficients in the multi-hole nozzles observed experimentally. Experimentally the injection rate of each orifice in the multi-hole injection could be measured in order to quantify the differences of the emerging fuel flow rate. More experimental data concerning the visualization of the internal flow would be of great help in order to better validate the model.

## REFERENCES

---

- [1] Brennen C.E. *Cavitation and Bubble Dynamics*. New York; Oxford: Oxford University Press. 1995.
- [2] Knapp R.T., Daily J.W., Hammit F.G. *Cavitation*. New York; London: McGraw-Hill. 1970.
- [3] Roth H., Gavaises M., Arcoumanis C. *Cavitation initiation, its development and link with flow turbulence in Diesel injector nozzles*. SAE paper 2002-01-0214, 2002.
- [4] He L., Ruiz F. *Effect of cavitation on flow and turbulence in plain orifices for high-speed atomization*. *Atomization and Sprays* 1995;5(6):569-584.
- [5] Soteriou C., Andrews R.J., Torres N., Smith M., Kunkulagunta R. *Through the Diesel Nozzle Hole - A journey of discovery II*. ILASS-Europe, Zurich, 2001.
- [6] Han J.S., Lu P.H., Xie X.B., Lai M.C., Henein A. *Investigation of Diesel spray primary break-up and development for different nozzle geometries*. SAE paper 2002-01-2775, 2002.
- [7] Kim J-H, Nishida K., Yoshizaki T., Hiroyasu H. *Characterization of flows in the sac chamber and the discharge hole of a D.I. Diesel Injection nozzle by using a transparent model nozzle*. SAE paper 972942, 1997.
- [8] Arcoumanis C., Flora H., Gavaises M., Kampanis N. *Investigation of cavitation in a vertical multi-hole injector*. SAE paper 1999-01-0524, 1999.
- [9] Ganippa L.C., Andersson S., Chomiak J. *The structure of cavitation and its effect on the spray pattern in a single-hole Diesel nozzle*. SAE paper 2001-01-2008, 2001.
- [10] Soteriou C., Andrews R., Smith M. *Direct injection Diesel sprays and the effects of cavitation and hydraulic flip on atomization*. SAE paper 950080, 1995.

## References

---

- [11] Bergwerk W. *Flow pattern in Diesel nozzle spray holes*. Proc. Inst. Mech. Engrs 1959;173:665-660.
- [12] Sazhin S.S, Feng G, Heikal M.R. *A model for fuel spray penetration*. Fuel 2001; 80:2171-80.
- [13] Giannadakis E., Papoulias D., Gavaises M., Arcoumanis C., Soteriou C., Tang W. *Evaluation of the predictive capability of Diesel nozzle cavitation models*. SAE paper 2007-01-0245, 2007.
- [14] Aleiferis P.G., Hardalupas Y., Kolokotronis D., Taylor A.M.K.P, Kimura T. *Investigation of the internal flow field of a Diesel model injector using particle image velocimetry and CFD*. SAE paper 2007-01-1897, 2007.
- [15] Kubo M., Araki T., Kimura S. *Internal flow analysis of nozzles for DI Diesel engines using cavitation model*. JSAE Review 2003;24:255-256.
- [16] Kubota M., Kato H., Yamaguchi H. *A new modelling of cavitation flows: a numerical study of cavitation on a hydrofoil section*. Journal of Fluids Mechanics 1992;240:59-96.
- [17] Dumont N., Simonin O., Habchi C. *Numerical simulations of cavitating flows in Diesel injectors by a homogeneous equilibrium modelling approach*. 4th International Symposium on Cavitation. Pasadena, California, USA, 2001.
- [18] STAR-CD Methodology, version 4.06, CD adapco, 2008
- [19] Rayleigh L. *On the pressure developed in a liquid during the collapse of a spherical cavity*. Phil. Mag. 1917;34:94-98.
- [20] Chaves H., Knapp M., Kubitzek A., Obermeier F. *Experimental Study of Cavitation in the Nozzle Hole of Diesel Injectors Using Transparent Nozzles*. SAE paper 950290, 1995.
- [21] Payri F., Bermúdez V., Payri R., Salvador F.J. *The influence of cavitation on the internal flow and the spray characteristics in Diesel injection nozzles*. Fuel 2004; 83:419-31.
- [22] Winklhofer E, Kull E, Kelz E, Morozov A. *Comprehensive hydraulic and flow field documentation in model throttle experiments under cavitation conditions*. ILASS-EUROPE, Zurich, Switzerland. 2001.

## References

---

- [23] Sarre von Kuensberg C., Kong S.C., Reitz R. D. *Modelling the effects of injector nozzle geometry on Diesel sprays*. SAE paper 1999-01-0912, 1999.
- [24] Macián V., Payri R., Margot X., Salvador F.J. *A CFD Analysis of the influence of Diesel nozzle on the inception of cavitation*. *Atomization and sprays* 2003;13:579-604.
- [25] Payri F., Arregle J., Lopez J. J, Hermens S. *Effect of cavitation on the nozzle outlet flow, spray and flame formation in a Diesel engine*. SAE paper 2006-01-1391, 2006.
- [26] Payri R., Margot X., Salvador F.J. *A Numerical Study of the Influence of the Diesel nozzle geometry on the inner cavitating flow*. SAE paper 2002-01-0215, 2002.
- [27] Schmidt D.P., Rutland C.J, Corradini M.L, Roosen P, Genge O. *Cavitation in two-dimensional asymmetric nozzles*. SAE paper 1999-01-0518, 1999.
- [28] Marcer R., Le Cottier P., Chaves H., Argueyrolles B., Habchi C., Barbeau B. *A validated numerical simulation of Diesel injector flow using a VOF method*. SAE paper 2000-01-2932, 2000.
- [29] Roth H., Giannadakis E., Gavaises M., Arcoumanis C., Omae K., Sakata M., Nakamura M., Yanagihara H. *Effect of Multi-Injection Strategy on Cavitation Development in Diesel Injector Nozzle Holes*. SAE paper 2005-01-1237, 2005.
- [30] Masuda R., Fuyuto T., Nagaota M., Von Berg E., Tatschl R. *Validation of Diesel Fuel Spray and Mixture Formation from Nozzle Internal Flow Calculation*. SAE paper 2005-01-2098, 2005.
- [31] Dumont, N., O. Simonin, and C. Habchi. *Cavitating Flow in Diesel Injectors and Atomization - A Bibliographical Review*. in Proc. ICLASS. Pasadena, CA, USA. 2000.
- [32] Arcoumanis, C. and M. Gavaises. *Cavitation in Diesel Injectors: Modelling and Experiments*. ICLASS-EUROPE. Manchester, UK. 1998.
- [33] Schmidt D., Corradini M. L. *The Internal Flow of Fuel Injector Nozzles: A Review*. *International Journal of Engine Research* 2001; v.2, n.1.

## References

---

- [34] Spikes R.H. Pennington G.A. *Discharge coefficient of small submerged orifices*. Proceedings of the Institution of Mechanical Engineers 1959;173(25):661-665
- [35] Nurick, W.H. *Orifice Cavitation and its effects on spray mixing*. Journal of Fluids Engineering 1976; 98: 681-687.
- [36] Hiroyasu H., Arai M. Shimizu M. *Break-up length of a liquid spray and internal flow in a nozzle*. ICLASS-91, Gaithersburg, Maryland, July, 1991.
- [37] Soteriou C., Smith M., Andrews R.J. *Cavitation hydraulic flip and atomization in direct injection Diesel sprays*. IMechE Paper C465/051/93, 1993.
- [38] Soteriou C., Andrews R., Smith M. *Further studies of cavitation and atomization in Diesel injection*. SAE paper 1999-01-1486, 1999.
- [39] Soteriou, C., Smith M., Andrews R.J. *Diesel injection - laser light sheet illumination of the development of cavitation in orifices*. IMechE Paper C529/018/98, 1998.
- [40] Bode J. *Zum kavitationseinfluss auf den zerfall von flüssigkeitsfreistrahlen*. Max-Planck-Institut für Strömungsforschung, March, 1991.
- [41] Arcoumanis C., Badami M., Flora H. *Gavaises M. Cavitation in real-size multi-hole Diesel injector nozzles*. SAE paper 2000-01-1249, 2000.
- [42] Arcoumanis C., Nouri J.M., Andrews R.J. *Application of Refractive Index Matching to a Diesel Nozzle Internal Flow*. in Proc. IMechE Seminar on Diesel Fuel Injection Systems. 1992, April 14-15. London, UK.
- [43] Gavaises M., Andriotis A. *Cavitation inside multi-hole injectors for large Diesel engines and its effect on the near-nozzle spray structure*. SAE paper 2006-01-1114, 2006.
- [44] Gilles-Birth I., Bernhardt S., Spicher U., Rechs M. *A study of the in-nozzle flow characteristic of valve covered orifice nozzles for gasoline direct injection*. SAE paper 2005-01-3684, 2005.

## References

---

- [45] Reid B. A., Hargrave G. K., Garner, C. P., Wigley, G. *An investigation of string cavitation in a true-scale fuel injector flow geometry at high pressure.* Physics of Fluids 2010; 22, 031703, doi: 10.1063/1.3372174.
- [46] Kato M., Kano H., Date K., Oya T., Niizuma K. *Flow Analysis in Nozzle Hole in Consideration of Cavitation.* SAE paper 970052, 1997.
- [47] Henry, M.E. and S.H. Collicott, *Visualization of internal flow in a cavitating slot orifice.* Atomization and Sprays 2000;10(6):545-563.
- [48] Matsumura E., Sugimoto T., Kanda M., Senda J. *Analysis of fuel flow and spray atomization in slit nozzle for direct injection SI gasoline engines.* SAE paper 2006-01-1000, 2006.
- [49] Zhen H., Yiming S., Shiga S., Nakamura H., Karasawa T. *Atomization behaviour of fuel containing dissolved gas.* Atomization and Sprays 1994;4:253-262.
- [50] Tamaki N., Shimizu M., Nishida K., Hiroyasu H. *Effects of cavitation and internal flow on atomization of a liquid jet.* Atomization and Sprays 1998;8(2):179-197.
- [51] Tamaki N., Shimizu M., Hiroyasu H. *Enhancement of the atomization of a liquid jet by cavitation in a nozzle hole.* Atomization and Sprays 2001;11(2):125-137.
- [52] Badock C., Wirth R., Fath A., Leipertz A. *Investigation of cavitation in real size Diesel injection nozzles.* International Journal of Heat and Fluid Flow, 1999; 20(5): 538-544.
- [53] Badock C., Wirth R., Tropea C. *The influence of hydro grinding on cavitation inside a Diesel injection nozzle and primary break-up under unsteady pressure conditions.* ILASS-EUROPE. Toulouse, France. 1999.
- [54] Ochoterena R., Li P., Vera-Hernández M., Andersson S. *Influence of cavitation on atomisation at low pressures using up-scaled and transparent nozzles.* ILASS-Europe, Brno, Czech Republic, 2010.
- [55] Knox-Kelecy A.L., Farrell P.C. *Spectral characteristics of turbulent flow in a scale model of a Diesel fuel injector nozzle.* SAE paper 930924, 1993.

## References

---

- [56] Kim S-R., Ku K-W, Hong J-G, Lee C-W. *An experimental investigation of discharge coefficient and cavitation length in the elliptical nozzles*. ILASS-Europe, Brno, Czech Republic, 2010.
- [57] Goney K.H. Corradini M.L. *Isolated effects of ambient pressure, nozzle cavitation and hole inlet geometry on Diesel injection spray characteristics*. SAE paper 2000-01-2043, 2000.
- [58] Argueyrolles B, Dehoux S., Gastaldi P., Grosjean L. Levy F. Michel A., Passerel D. *Influence of injector nozzle design and cavitation on coking phenomenon*. SAE paper 2007-01-1896, 2007.
- [59] Blessing, M., König G., Krüger C., Michels U., Schwarz V. *Analysis of Flow and Cavitation Phenomena in Diesel Injection Nozzles and its Effect on Spray and Mixture Formation*. SAE Paper 2003-01-1358, 2003.
- [60] Collicot S.H., Li H. *True-scale true-pressure internal flow visualization for Diesel injectors*. SAE paper 2006-01-0890, 2006.
- [61] Desantes J. M., Payri R., Salvador F.J., Gimeno J. *Measurements of spray momentum for the study of cavitation in Diesel injector nozzles*. SAE paper 2003-01-0703, 2003.
- [62] Desantes J. M., Payri R., Pastor J.M, Gimeno J. *Experimental characterization of internal nozzle flow and Diesel spray behaviour*. Part I. Non evaporative conditions, 2004.
- [63] Macián V, Bemudez V, Payri R, Gimeno J. *New technique for the determination of the internal geometry of Diesel nozzle with the use of silicone methodology*. *Experimental Techniques* 2003;27:39-43.
- [64] Ganippa L.C., Bark G., Andersson S., Chomiak J. *Comparison of cavitation phenomenon in transparent scaled-up single-hole Diesel nozzles*. Proceedings of the Fourth International Symposium on cavitation, California Institute of technology, Pasadena, CA, USA, June 20-23, 2001.
- [65] Walther J., Schaller J.K., Wirth R., Tropea C. *Investigation of internal flow in transparent Diesel injection nozzles using fluorescent particle image velocimetry (FPIV)*. Proc. ICLASS. Pasadena, CA, USA. 2000.

## References

---

- [66] Marcer R., LeGouez J.M. *Simulation of unsteady cavitating flows in Diesel injector with an improved VOF method*. ILASS-EUROPE. Zurich, Switzerland. 2001.
- [67] Chiavola O, Palmieri F. *Modelling needle motion influence on nozzle flow in high pressure injection system*. SAE paper 2007-01-0250, 2007.
- [68] Von Berg E, Edelbauer W, Alajbegovic A, et al. *Coupled simulations of nozzle flow, primary fuel jet breakup, and spray formation*. J Eng for Gas Turbines Power, 2005: 127(4): 897-908
- [69] Wallis G.B. *One-dimensional two-phase flow*. McGraw-Hill. p.143. 1969.
- [70] Srinivasan V., Salazar A.J., Saito K. *Computational prediction of the flow inside cavitating injectors by Supplementing a Homogeneous Equilibrium Model (HEM) with a pressure equation*. in Proc. ICLASS. Japan, Kyoto. 2006.
- [71] Giannadakis E., Gavaises M., Roth H., Arcoumanis C. *Cavitation modelling in single-hole Diesel injector based on eulerian-lagrangian approach*. in Proc. THIESEL 2004 Conference on Thermo and Fluid Dynamic Processes in Diesel Engines, Valencia, 2004.
- [72] Delannoy Y., Kueny J. L. *Two phase flow approach in unsteady cavitation modelling*. Cavitation and Multiphase Flow Forum 98, ASME FED, 1990.
- [73] Schmidt D.P., Rutland C.J., Corradini M.L. *A numerical study of cavitating flow through various nozzle shapes*. SAE Paper 971597, 1997.
- [74] Schmidt D.P., Rutland C.J., Corradini M.L. *A fully compressible, two-dimensional model of small, high-speed, cavitating nozzles*. Atomization and Sprays 1999; 9(3): 255-276.
- [75] CD Adapco Group, STAR-CD v3.15 Methodology, 2001.
- [76] Xie W.F., Liu T.G., Khoo B.C. *Application of a one-fluid model for large scale homogeneous unsteady cavitation: the modified Schmidt model*. Comput. Fluids 2006; 35: 1177-1192.
- [77] Avva R.K., Singhal A., Gibson D.H. *An enthalpy based model of cavitation*. in Cavitation and Multiphase Flow Forum, ASME FED. 1995.

## References

---

- [78] Ning W., Reitz R. D., Diwakar R., Lippert A. M. *A numerical Investigation of nozzle geometry and injection condition effects on Diesel fuel injector flow physics*. SAE paper 2008-01-0936, 2008.
- [79] Peng Kärholm F, Weller H, Nordin N. *Modelling injector flow including cavitation effects for Diesel applications*. 5th Joint ASME/JSME Fluids Engineering Conference, San Diego, California USA, 2007.
- [80] Salvador F. J., Romero J. V., Rosello M. D, Martinez-Lopez J. *Validation of a code for modelling cavitation phenomena in Diesel injector nozzles*. Mathematical and Computer Modelling 2010; 52: 1123-1132.
- [81] Catania A.E., Ferrari A., Manno M., Spessa E. *Thermal effect simulation in high-pressure injection system transient flows*. SAE paper 2004-01-0532, 2004.
- [82] Plesset M.S. *The dynamics of cavitation bubbles*. Trans. ASME, J. Applied Mechanics, 1949; 16: 228-231.
- [83] Kato H., Kayano H., Kageyama, Y. *A consideration of thermal effect on cavitation bubble growth*. In cavitation and multiphase flow, ASME FED 1994; 194 (American Society of Mechanical Engineers, New York).
- [84] Chen Y.L., Heister S.D. *Two-Phase modelling of cavitating flows*. Computers & Fluids 1995; 24(7): 799-809.
- [85] Chen Y.L., Heister S.D. *A numerical treatment for attached cavitation*. Journal of Fluids Engineering-Transactions of the ASME 1994; 116(3): 613-618.
- [86] Chen Y.L., Heister S.D. *Modelling cavitating flows in Diesel injectors*. Atomization and Sprays 1996; 6(6): 709-726.
- [87] Chen, Y.L., Heister S.D. *Modelling hydrodynamic non-equilibrium in cavitating flows*. Journal of Fluids Engineering-Transactions of the ASME 1996; 118(1): 172-178.
- [88] Bunnell R.A., Heister S.D., Yen C., Collicott S.H. *Cavitating injector flows: Validation of numerical models and simulations of pressure atomizers*. Atomization and Sprays 1999; 9(5): 445-465.

## References

---

- [89] Bunnell R.A., Heister S.D. *Three-dimensional unsteady simulation of cavitating flows in injector passages*. Journal of Fluids Engineering-Transactions of the ASME 2000; 122(4): 791-797.
- [90] Mulemane A., Subramaniyan S., Lu P.H. Han J.S., Lai M.C., Poola R. *Comparing cavitation in Diesel injectors based on different modelling approaches*. SAE paper 2004-01-0027, 2004.
- [91] STAR-CD Methodology, version 3.150A, CD adapco, 1999
- [92] Tamura Y., Sugiyama K., Matsumoto Y. *Cavitating flow simulations based on the bubble dynamics*. in Proc. CAV2001, Fourth International Symposium on Cavitation. Pasadena, California, USA. 2001.
- [93] Tamura Y., Sugiyama K., Matsumoto Y. *Physical modelling and solution algorithm for cavitating flow simulations*. AIAA Paper 2001-2652, 2001.
- [94] Matsumoto Y., Kanbara T., Sugiyama K., Tamura Y. *Numerical study of cavitating flow structure on a hydrofoil*. in Proc. 4th KSME-JSME Fluids Engineering Conference. Haeundae, Pusan, Korea. 1998.
- [95] Kunz R.F., Boger D.A., Stinebring D.R., Chyczewski T.S., Lindau J.W., Gibeling H.J., Venkateswaran S., Govindan T.R. *A preconditioned Navier- Stokes method for two-phase flows with application to cavitation prediction*. Computers & Fluids 2000; 29(8): 849-875.
- [96] Lindau J.W., Kunz R.F., Venkateswaran S., Boger D.A. *Application of preconditioned, multiple-species, Navier-Stokes models to cavitating flows*. In Proc. CAV2001, Fourth International Symposium on Cavitation. Pasadena, California, USA. 2001.
- [97] Stutz B., Reboud J.L. *Two-phase flow structure of sheet cavitation*. Physics of Fluids 1997; 9(12): 3678-3686.
- [98] Reboud J.L., Stutz B., Coutier-Delgosha O. *Two phase flow structure of cavitation; experiment and modelling of unsteady effects*. in Proc. Third International Symposium on Cavitation. Grenoble, France. 1998.
- [99] Stinebring D.R., Holl J.W. *Water tunnel simulation study of the later stages of water entry of conical head bodies: Phase II - Effect of the afterbody on steady state ventilated cavities*. TM 79-206, The Pennsylvania State University, Applied Research Laboratory, 1979.

## References

---

- [100] Stinebring D.R., Billet M.L., Holl J.W. *An investigation of cavity cycling for ventilated and natural cavities*. TM 83-13, The Pennsylvania State University Applied Research Laboratory, 1983.
- [101] Ahuja V., Hosangadi A., Arunajatesan S. *Simulations of cavitating flows using hybrid unstructured meshes*. Journal of Fluids Engineering-Transactions of the ASME 2001; 123(2): 331-340.
- [102] Rouse H., McNown, J.S. *Cavitation and pressure distribution, head forms at zero angle of yaw*. Report of the State Univ. of Iowa, 1948.
- [103] Shen Y.T., Dimotakis P.E. *Viscous and nuclei effects on hydrodynamic loadings and cavitation of a NACA 66 (MOD) foil section*. J. Fluids Eng. 1989; 111: 306-316.
- [104] Senocak I., Shyy W. *Numerical simulation of turbulent flows with sheet cavitation*. in Proc. CAV2001, Fourth International Symposium on Cavitation. Pasadena, California, USA. 2001.
- [105] Senocak I., Shyy W. *Interfacial dynamics-based modelling of turbulent cavitating flows, Part-1: Model development and steady-state computations*. International Journal for Numerical Methods in Fluids 2004; 44(9): 975-995.
- [106] Senocak I., Shyy W. *Interfacial dynamics-based modelling of turbulent cavitating flows, Part-2: Time-dependent computations*. International Journal for Numerical Methods in Fluids 2004; 44(9): 997-1016.
- [107] Singhal A.K., Athavale M.M., Li H.Y., Jiang Y. *Mathematical basis and validation of the full cavitation model*. Journal of Fluids Engineering-Transactions of the ASME, 2002;124(3):617-624.
- [108] CFD Research Corporation, CFD-ACE Modules v6.6, July 2001.
- [109] FLUENT INC., FLUENT 6.2 User's Guide, January 2003.
- [110] Srinivasan V, Salazar A. J., Saito K. *Numerical simulation of cavitation dynamics using a cavitation-induced-momentum-defect (CIMD) correction approach*. Applied Mathematical Modelling 2009; 33 : 1529-1559.
- [111] Alajbegovic A., Grogger H.A., Philipp H. *Calculation of cavitation in nozzles using the two-fluid model*. in Proc. 7th Annual Conference

## References

---

Computational Fluid Dynamics Society of Canada. Halifax, Nova Scotia, Canada. 1999.

[112] Alajbegovic A., Grogger H.A., Philipp H. *Calculation of transient cavitation in nozzle using the two-fluid model*. in Proc. 12th Annual Conference on Liquid Atomization and Spray Systems. Indianapolis, Indiana, USA. 1999.

[113] Alajbegovic A. *Three-dimensional cavitation calculations in nozzles*. in Proc. Second Annual Meeting Institute for Multifluid Science and Technology. Santa Barbara, California, USA. 1999.

[114] AVL, FIRE 8.2 Manual - Spray, July 2003.

[115] Wang X., Su W.H. *A numerical study of cavitating flows in high-pressure Diesel injection nozzle holes using a two-fluid model*. Science China Press 2009; 54: 1655-1662.

[116] Sou A., Masaki Y., Nanajima T. *Numerical simulation of transient cavitating flow in a spray nozzle*. ILASS-Asia. Busan, Korea. 2001.

[117] Sou A., Nitta S., Nakajima T. *Bubble tracking simulation of cavitating flow in an atomization nozzle*. in Proc. of FEDSM'02 - 2002 ASME Fluid Engineering Division Summer Meeting. Montreal, Quebec, Canada. 2002.

[118] Sou A., Kinugasa T. *Numerical simulation of developing cavitation flow in a nozzle of pressure atomizer*. in Proc. THIESEL 2010 Conference on Thermo-and Fluid Dynamic Processes in Diesel Engines, Valencia, 2010.

[119] Shi J-M., Arafin M. *CFD investigation of fuel property effect on cavitating flow in generic nozzle geometries*. ILASS-Europe, Brno, Czech Republic, 2010.

[120] ANSYS CFX version 11.

[121] Martynov S. B., Mason D.J, Heikal M.R. *Numerical Simulation of two-phase flow in injection nozzles: interaction of cavitation and external jet formation*. Journal of fluids Engineering 2006; 7: 283-296.

[122] Ricardo Software VECTIS CFD, Version 3.8, User's manual, 2004 (Ricardo UK Ltd, Shoreham-by-Sea, West Sussex).

## References

---

- [123] Yuan W., Sauer J., Schnerr G.H. *Modelling and computation of unsteady cavitation flows in injection nozzles*. in 1st International Colloquium on Microhydrodynamics. Paris, France. 2000.
- [124] Sauer J., Schnerr G.H. *Unsteady cavitating flow-A new cavitation model based on a modified front capturing method and bubble dynamics*. in Proc. of FEDSM'00 - 2000 ASME Fluid Engineering Division Summer Meeting. Boston, Massachusetts, USA. 2000.
- [125] Schnerr G.H., Sauer J. *Physical and numerical modelling of unsteady cavitation dynamics*. in Proc. ICMF 2001, Fourth International Conference on Multiphase Flows. New Orleans, USA. 2001.
- [126] Hirt C. W., Nickols B. D. *Volume of fluid (VOF) method for the dynamics of free boundaries*. Journal of Computational Physics 1981; 39: 201-225.
- [127] Yuan W., Schnerr G.H. *Cavitation in injection nozzles - Effect of Injection Pressure Fluctuations*. in Proc. CAV2001, Fourth International Symposium on Cavitation. Pasadena, California, USA. 2001.
- [128] Giannadakis M, PhD Thesis, Imperial College, 2005
- [129] Favennec A-G., Fruman D.H. *Effect of the needle position on the cavitation of Diesel injectors*. In Proc of the 3<sup>rd</sup> ASME/JSME Joint Fluids Engineering Conference, July 18-23, San Francisco, California, 1999.
- [130] Argueyrolles B, Passerel D, Maligne D. *Influence of the nozzle geometry on Diesel injector internal flow: a computational approach*. in Proc. THIESEL 2004 Conference on Thermo and Fluid Dynamic Processes in Diesel Engines, Valencia, 2004.
- [131] Som S., Aggarwal S.K., El-Hannouny, E. M., Longman, D. E. *Investigation of nozzle flow and cavitation characteristics in a Diesel injector*. J. Eng. Gas Turbines Power 2010;132, 042802.
- [132] Oda T., Hiratsuka M., Goda Y. Kanaike S., Ohsawa K. *Experimental and numerical investigation about internal cavitating flow and primary atomization of a large-scaled VCO Diesel injector with eccentric needle*. ILASS-Europe, Brno, Czech Republic, 2010.

## References

---

- [133] Drew D. A. *Mathematical modelling of two-phase flow*. Annual Review Fluid Mechanics 1983;15:261-291.
- [134] Tatschl R., von Künsberg Sarre C., Alajbegovic A., Winklhofer, E. *Diesel Spray Modelling Including Multidimensional Cavitating Nozzle Flow Effects*. ILASS-Europe 2000, 2000.
- [135] Dukowicz, J.K. *A Particle-Fluid Numerical Model for Liquid Sprays*. J. Comp. Physics 1980; 35: 229253.
- [136] Kadocsa A, PhD thesis, Boudapest University of Technilogy and Economics, 2007.
- [137] Du H., Liu J., Tang J. *A CFD investigation on the nozzle of orifices distributing in different space layers*. SAE paper 2008-01-0948, 2008.
- [138] Gavaises M., Papoulias D., Giannadakis E., Andriotis A., Mitroglou M., Theodorakakos A. *Comparison of cavitation formation and development in Diesel VCO nozzles with cylindrical and converging tapered holes*. in Proc THIESEL 2008 Conference on Thermo- and Fluid-Dynamic Processes in Diesel Engines, Valencia, 2008.
- [139] Lee W. G., Reitz R.D. *A Numerical investigation of transient flow and cavitation within minisac and valve-covered orifice Diesel injector nozzles*. J. Eng. Gas Turbines Power 2010;133, 052802.
- [140] Chiatti G., Chiavola O. Palmieri F. *Flow Features in reduced dwell time Diesel injector*. SAE paper 2008-01-0927, 2008.
- [141] Tatschl R., von Künsberg-Sarre C., Alajbegovic A., Winklhofer, E. *Diesel spray modelling including multidimensional cavitation nozzle flow effects*. ILASS Europe, Darmstadt, Germany, 2000.
- [142] Warsi, Z.V.A. *Conservation form of the Navier-Stokes equations in general nonsteady coordinates*, AIAA Journal 1981; 19: 240-242.
- [143] Demirdzic I., Peric M., *Space conservation law in finite volume calculations of fluid flow*. Int. J. Numer. Methods in Fluids 1988; 8: 1037-1050.
- [144] STAR-CD Methodology, v4.06, CD adapco, 2008.

## References

---

- [145] Joseph D.D. *Cavitation and the state of stress in a flowing liquid*. Journal of Fluid Mechanics 1998;366:367-378.
- [146] Payri R., Garcia J.M., Salvador F.J., Gimeno J. *Using spray momentum flux measurement. to understand the influence of Diesel nozzle geometry on spray characteristics*. Fuel 2005;84:551-561.
- [147] Patankar S.V., Spalding D.B. *A calculation procedure for heat, mass and momentum transfer in three-dimensional parabolic flows*. Int. J. Heat Mass Transfer 1972;15:1787-1806.
- [148] Mulemane A., Han J. S., Lu P. H., Yoon S. J., Lai, M. C. *Modelling dynamic behaviour of Diesel fuel Injection systems*. SAE paper 2004-01-0536, 2004.
- [149] Chaves H., Knapp M, Kubitzek A. *Experimental study of cavitation in the nozzle hole of Diesel injectors using transparent nozzles*. SAE paper 950080, 1995.
- [150] Tamaki N., Nishida K., Hiroyasu H., Shimizu, M. *Effects of the internal flow in a nozzle hole on the breakup processes of a liquid jet*. Int. J. Fluid Mech. 1997; 24: 461-470.
- [151] Oda T., Yasuda Y. *Experimental investigation on structure of cavitating flow and velocity field inside a 2D hole nozzle*. Proc. of Annual International Conference on Liquid Atomization and Spray Systems. in Proc. ICLASS03-1205 (2003).
- [152] Sou A., Hosokawa S., Tomiyama, A. *Effects of cavitation in a nozzle on liquid jet atomization*. Int. J. Heat Mass Transfer 2007;50:3575-3582.
- [153] Papoulias D., Giannadakis E., Mitroglou N., Gavaises M., Theodorakakos A. *Cavitation in fuel injection systems for spray-guided direct injection gasoline engines*. SAE paper 2007-01-1418, 2007.
- [154] Mercer R. *A CFD code for Diesel direct injection simulation*. in Proc. ICLASS, Sorrento Italy (2003).